Ultrasonic technique for chemical process control

Chuangnan Wang

Submitted in August 2014
for the degree of Doctor of Philosophy

Centre for Ultrasonic Engineering
Department of Electronic and Electrical Engineering
University of Strathclyde
204 George Street, Glasgow,
G1 1XW, Scotland, UK

Content

Acknowledgements

I would like to thank my supervisors, Dr. Anthony Gachagan and Dr. Richard O'Leary, who have provided the invaluable guidance, technical knowledge and grammatical superiority throughout this project. This thesis would not have been possible without their support.

I also wish to thank colleagues in Centre for Ultrasonic Engineering (CUE) especially, Tapiwa Matasa, Kornpatsitt Promasa, Jerzy Dziewierz and the others for their good friendships and assistance. My sincere thanks are due to staff in Centre for Ultrasonic Engineering (CUE) for their good friendships and their excellent support. I would like to thank Tommy McCunnie, Grant Smillie and their team for their manufacturing skill and expertise and for developing transducers.

I would like to thanks University of Strathclyde for awarding me this scholarship and all the support during my PhD. I also want to thanks my friends in Glasgow for their friendly help, and sharing happiness and distress. Especially, I would like to thank my girlfriend, YanSheng Zhang, I hope that my completion of this thesis will give her courage and determination to finish her own studies.

Finally, I would like to bring my sincerely thanks to my family, for their patience, encouragement and support during my stay in Scotland.

Abstract

Ultrasound has found application in chemical processing control using both low power, high frequency monitoring techniques and high power, low frequency process enhancement approaches. In many cases, standard ultrasonic systems are retrofitted to a process and while these produce efficiency improvements, the design of bespoke systems may offer more potential. In particular, this Thesis has considered two techniques used in the biomedical field; harmonic imaging and high intensity focused ultrasound (HIFU) and has translated these into ultrasonic transducers for use in an industrial process control system.

Traditional ultrasound monitoring techniques are based on operation in the linear domain and are used to monitor chemical processes by measurement of material acoustic velocity, attenuation or based on spectral analysis. Both active and passive methods have been reported for application in this industrial sector. One issue is the presence of multiple reflections in the received ultrasonic signal which can mask the signals of interest from the load medium. This Thesis has considered a new ultrasonic monitoring approach using a combination of both linear and nonlinear spectral components. This was applied to high-throughput products and a dual frequency transducer designed and fabricated to acquire the ultrasonic backscattered signals in both the fundamental and second harmonic frequency regimes. The additional information provided by the harmonic device enabled discrimination between shampoo and conditioner products with the same density, but different molecular weights.

HIFU transducer array designs are then considered for high power, low frequency chemical process enhancement applications. Typical applications of high power ultrasound use single or multiple discrete transducers to insonify a process. These are effective, but inflexible in the delivery of the ultrasonic field. The application of a HIFU array would provide control of the high power focal region in the load medium, which offer advantages to industry. Two transducer array approaches have been considered in this Thesis based on piezoelectric composite configurations. Three HIFU arrays based on

the 1-3 piezocomposite have been fabricated to operate between 200-400kHz and fully characterised to evaluate their high power performance. A second transducer configuration was based on a novel 2-2 piezocomposite with a 2 layer stacked configuration. Simulation of this transducer design illustrated its potential for high power applications, although a number of fabrication issues resulted in the manufactured array not operating at full capacity. Importantly, the transducer configurations developed in this Thesis are shown to induce cavitation through the standard aluminium foil test.

List of Figures

List of Tables

List of symbols

Symbol	Definition	Unit
A	Signal amplitude	Volt
A_{Sn}	scattering coefficients of the n^{th} reflection of ultrasound waves	
B	Magnetic induction	Telsa
B/A	Second order nonlinear coefficient	
C_P	Specific heat at constant pressure	$Cal/(C^0kg)$
c	Acoustic velocity	m/Sec
D	Sound transmitting distance	meter
D_E	Electric charge density displacement	C/m^2
D_L	Diameter of lens	meter
D_r	Diameter	meter
D/Dt	material derivative	
d_{PE}	Direct piezoelectric coefficient	
d_{PE}^t	Converse piezoelectric coefficient	
d_{PM}	Direct piezomagnetic coefficient	
d_{PM}^t	Converse piezomagnetic coefficient	
E	Electrical field strength	V/m
e	Euler's number	
exp	Exponential function	
f	Frequency	Hertz
F	Force	Newton
G	Gain	
H	Magnetic field strength	A/m
i	Imaginary unit	
I	Signal intensity	Volt
k	Complex propagation constant of continuous phase	
k_W	Wave number	
L_F	Focusing length	meter
L	Discontinuity distance for acoustic wave propagation	meter
n_v	Unit vector normal to surface	
M	Acoustic match number	
N_F	Near field length	meter
N_P	Number of particle per unit volume	
P	Pressure	N/m^2
P_T	Stress of the transmitted wave	N/m^2
P_I	Stress of the incident wave	N/m^2
R	Radius	meter
R_C	Reflection coefficient	
S	Strain of material	
s^H	Elastic compliance under constant magnetic field	m^2/N
s^E	Elastic compliance under constant electrical field	m^2/N
S_A	Surface area	m^2
t	Time	Second

T	Absolute temperature	Kelvin
T_S	Stress	N/m^2
W	Energy density	W/m^2
Z_A	Acoustic impedance	Rayl
α	Attenuation coefficient	
β	Volume coefficient of thermal expansion	
β_T	Isothermal compressibility	m^2/N
γ	Ratio of specific heats of gas	
ε^T	Permittivity under constant stress	F/m
η	Viscosity coefficient	m·s/kg
λ	Wavelength	meter
μ^T	Permeability coefficient under constant stress	H/m
$\overline{\Pi}$	Time-averaged momentum flux density tensor	
ρ	Density	kg/m^3
σ	Surface tension	N/m^2
φ	Disperse phase volume fraction	
ω	Angular frequency	rad/sec
ψ	Aperture angle	
∇	Hamiltonian	
Δ	Laplacian	

Chapter 1

Introduction

1.1 Background

Ultrasonic technology applied in chemical processing can mainly be sorted in two categories: low power high frequency ultrasonics for chemical processing monitoring and control and high power low frequency applications for chemical processing enhancement. Examples of high power and low power ultrasonic systems utilised for industrial process control at Strathclyde are presented in Figure 1.1. Figure 1.1(a) illustrates three high power transducers incorporated into a reactor cell to induce a high power field in the central axis of the vessel. Whereas, Figure 1.1(b) illustrates an ultrasonic transducer bonded onto the outer wall of a glass reactor and used to detect acoustic emission events originating from within the reaction.

(a) high power ultrasound reaction vessel for process enhancement

(b) passive ultrasonic monitoring applied in the pharmaceutical industry

Figure 1.1 *Examples of ultrasound application in chemical process control*

This Thesis will take inspiration from the medical domain and describe the design process to translate two techniques utilised in the ultrasonic medical field into transducer solutions suitable for use in Sonochemistry applications. The concept of utilising ultrasound in Sonochemistry applications is not new, with the new techniques described herein intended to expand the applicability of ultrasonic systems within this industrial sector.

Low power ultrasonics has been applied in the chemical industry from early last century for the liquid level measurement. However, it has developed slowly until recently. In chemical processing control, the ultrasonic properties of samples, such as velocity, attenuation, and frequency spectrum, are employed to determine liquid level [1], flow rate [2, 3] and particle size [4-6]. The ultrasonics techniques are widely applied for their low expense and non-invasive nature, which is important in the pharmaceutical and cosmetic industries that require high hygiene standards. In a typical chemical processing control system, the combination of ultrasonic monitoring and spectroscopy techniques can be applied, because of the complementary of these two techniques. The spectroscopy technique [7] is mainly used to analyse samples' molecular structure. However, spectroscopy techniques are expensive, and incapable of on-line operation through opaque chemical products. Therefore, ultrasonic systems that can be employed to monitor and/or characterize the reaction, particularly for opaque material, are of interest to industry. Moreover, ultrasound can provide real-time monitoring/control information, especially if this technique is based on a chemical formulation differences for the product, rather than differences in physical properties.

Within the medical ultrasound field several imaging modes are used to maximise the information extracted from the ultrasonic echo signals [8]. In recent years, one important technique that was developed is the use of harmonic imaging [8-10]. In this technique, the ultrasonic system injects high frequency sound at a desired frequency, but the reception system is tuned to monitor returning energy at a frequency equal to double the initial excitation frequency. This is termed second harmonic imaging. Importantly, the received signals are tuned to contain only the energy of interest which has originated when a desired transition from the linear domain into a nonlinear signal that manifests itself at double the original frequency. Typically, in order to achieve this ultrasound contrast agents are utilised to facilitate this transition [11]. Importantly, the technique can demonstrate a higher contrast when compared to standard linear based imaging approaches as shown in Figure 1.2.

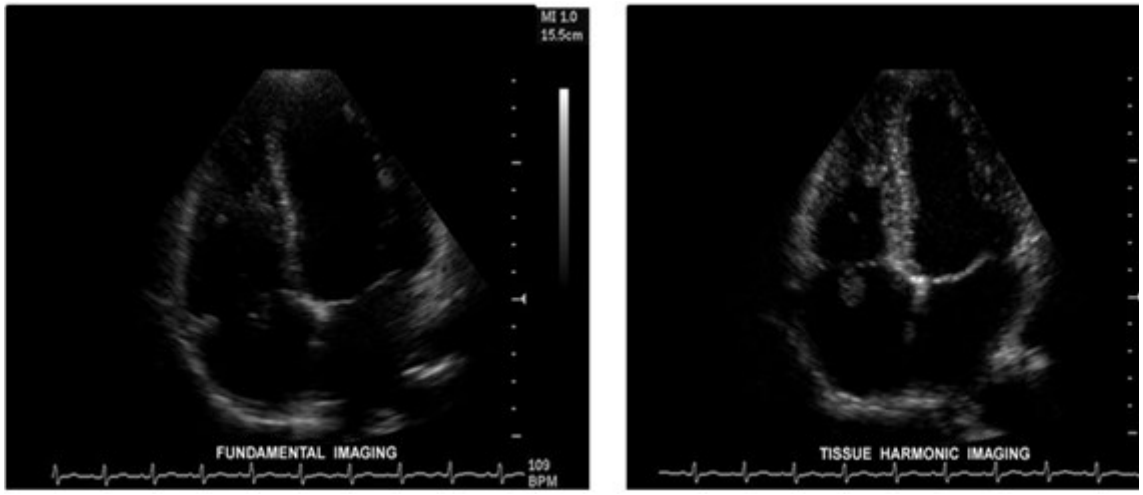

(a) Linear imaging approach (b) Harmonic imaging approach

Figure 1.2 *Comparison between linear and harmonic imaging of endocar[12]*

High power ultrasound, producing cavitation is a phenomenon accompanied with enormous heat release and shock wave emission. This has been employed as a catalyst in chemical processes since the 1980s [13, 14]. In Sonochemistry, most high power ultrasonic systems that are used to enhance the chemical reaction [15-18] are composed of a number of single element transducers, which operate at a single frequency without phase control, and in many cases insufficient energy management. Recently, systems containing several operating frequencies and basic phase control have been developed [19]. However, the multi-frequency and phase control features increase the complexity of the reactor design and subsequent power excitation electronics. It is also difficult to adapt one transducer arrangement from one reactor design to another. Therefore, a high power, low frequency phased array transducer design offers more flexible operation in terms of beam forming and energy focusing. Through beam forming, the ultrasonic energy can be focused to produce high intensity and scanned electronically to cover a large volume of reactor vessel. Moreover, through energy focusing, a low intensity near field is achieved, which prevents the generation of near field cavitation, which is a key requirement for industrial scale up of the reactor vessel. It is therefore proposed that HIFU can be considered as an alternative technique for use in Sonochemistry applications.

High intensity focused ultrasound (HIFU) [20-23] is one of the potential techniques to improve the current performance of Sonochemical reaction systems. HIFU was initially

investigated in the medical regime in the 1950s and recently applied in surgical operation for prostate cancer, with research related to HIFU radiation therapy for cancers being carried out. By intricate phase control of the excitation signal for each element, HIFU array transducer [20, 21, 23] is capable of focusing the ultrasonic energy in a specified area, then killing the cancerous cells associated with a tumour by rising the tissue temperature without damage to surrounding healthy tissue areas. High power ultrasound used to be avoided in medical surgery, but the application of HIFU array technology and focussed HIFU arrays, as depicted in Figure 1.3, has demonstrated successful application from relatively low intensity and high frequency (1MHz) ultrasound devices [24-26].

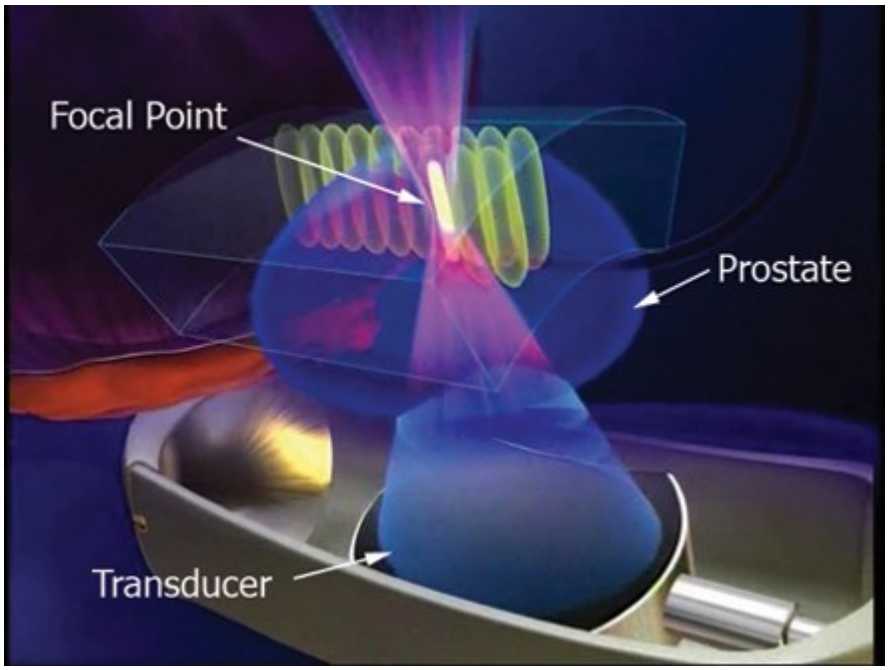

Figure 1.3 *Example of HIFU transducer and its application in clinical treatment [27]*

The frequency of ultrasound applied in Sonochemistry is typically less than 100 kHz [15]. However, the low frequency array designs for application in an industrial plant can result in manufacturing complexity and a large transducer aperture. The objective in utilising HIFU in medical clinical applications was aided by the concept that linear array transducers with relatively high centre frequencies (~MHz) could be used. By using such frequencies, it is possible to reduce the array transducer's size and hence reduce the

manufacturing complexity. Moreover, it should be able to provide a tighter focal region and increased beam steering capability.

Applications of ultrasonic techniques, in both low and high power regimes, for chemical process control applications can lead to benefits to the pharmaceutical industry:

Product quality improvement: ultrasonic monitoring systems enable on line monitoring of opaque chemical processes [28], which can enhance product consistency and produce high quality products.

Cost reduction: in monitoring systems for chemical process control, ultrasound is relatively low cost compared with spectroscopy techniques. Moreover, when applied as a chemical reaction catalyst, high power ultrasound can also be considered as an inexpensive technique and is relatively easy to implement.

Production efficiency improvement: high power ultrasound when used as a catalyst [15] can increase the chemical reaction production rate significantly, which reduces the processing time and ultimately improves efficiency. Also, the online operation of an ultrasonic monitoring system can analyse the sample without sample preparation, and again significantly improve operational efficiency.

New product development: cavitation, which is generated by high power ultrasound, may initiate certain chemical reactions that traditionally needed extreme conditions, such as high pressure and high temperature. This potential can be used to develop new products [29, 30].

It is therefore apparent that ultrasound offers significant potential in the field of Sonochemistry for both process control and process enhancement across a wide range of applications [13, 31, 32]. Moreover, ultrasonic monitoring systems can be passive or active, with the latter the focus of the work described in this Thesis [2, 3, 33]. In particular, this Thesis will describe research conducted in investigating new ultrasonic transduction approaches in both monitoring and intensification of chemical processes.

In the first part of the Thesis, ultrasonic monitoring of chemical processes using a combination of linear and harmonic frequency regimes will be investigated. Traditionally,

ultrasonic monitoring systems are used in the linear regime and interaction of the propagating ultrasonic energy with the load medium under investigation is conducted at the resonant frequency of the transducer [8]. This can work effectively, but it some cases it is difficult to separate reflections from the reactor from signals of interest from the system itself. This work concerns the application of active ultrasonic monitoring for high throughput technologies (HTT) materials, like shampoo and conditioner products. Moreover, this work investigates the potential of using active ultrasound in both through transmission and backscattering configurations for the on-line characterization of HTT products to provide valuable information on the quality and consistency of the product in the manufacturing process. Moreover, the received signals will be analysed in both the linear and second harmonic regimes to determine if additional information on the load medium can be ascertained.

In this second part of the Thesis, the HIFU transducer array concept will be investigated to produce a flexible ultrasonic delivery system for use in Sonochemistry applications. Here, the design incorporated piezoelectric ceramic composite configurations, with both 1-3 and 2-2 connectivity composites investigated. A 1-D, linear array transducer configuration was adopted and designed to operate in the frequency range of 200-400 kHz.

Prototype transducers for both low and high power operating regimes have been produced and are described in the relevant Chapters. Thus the Thesis describes the design process through to realization of a practical system. This can introduce deviation from the desired system operation through manufacturing errors and issues in the practical deployment of ultrasonic systems. These issues are analysed and fully explored where appropriate in the Thesis. Overall, the work described in this Thesis provides the initial evaluation of harmonic monitoring and HIFU techniques in the Sonochemistry field. Hence, the future work section describes how this work can be taken forward and to move closer to a practical realization of these new ultrasonic transduction approaches.

1.2 Aims and contributions of the Thesis

1.2.1 Aims of the Thesis

Provide a detailed literature review on a range of ultrasonics monitoring techniques, including passive, active ultrasonic monitoring and nonlinear ultrasound; high power ultrasonic techniques including the HIFU approach; and the field of Sonochemistry, including physical phenomenon and standard equipment. This will provide the framework for the research developed in the Thesis.

Develop an ultrasonics monitoring system for HTT product characterization based on the concept of harmonic imaging. The concept will be to utilise conventional monitoring frequencies in the MHz regime at higher power levels to induce a nonlinear response from the chemical product under investigation. This system should be able to be used as an online operation and to detect inconsistency of HTT products associated with the chemical formulations.

Develop a Finite Element modelling strategy for rapid virtual prototyping design methods to support high power focusing ultrasonic array transducer design. Importantly, this simulation methodology should provide a reliable basis for the optimization of array transducer.

Design and evaluate array transducer configurations for HIFU application in Sonochemistry. This device will operate in direct contact with the liquid load medium. The key performance criteria will be beam steering capability, generation of a tight focal region, ultrasonic efficiency, manufacturability and durability during high power operation.

1.2.2 Contributions to the field of Ultrasonics

The research work contained in this Thesis has focussed on two distinct applications of ultrasonic technology in the industrial process control field. Importantly, new ultrasonic transduction approaches have been developed and initial practical trials conducted.

- The concept of utilising nonlinear ultrasonic techniques to monitor chemical reactions has been investigated. An experimental procedure to analyse such a non-invasive ultrasound monitoring technique is described and implemented. This technique is based on the active ultrasound technique using a backscattering approach as the source of the received ultrasonic signals. Importantly, this methodology collects both fundamental and second harmonic signals, which are analysed in the frequency domain. Such an approach is widely applied in medical diagnosis, but has not been applied in industry applications to date.

- Linear chirp excitation has been utilised to facilitate extraction of the second harmonic signals using matched filtering signal processing techniques. These are typically not used in standard industrial ultrasonic equipment and have potential for application in HTT product characterization.

- A dual frequency transducer was designed and fabricated to facilitate the simultaneous acquisition of both the fundamental and second harmonic ultrasonic signals. This improved the repeatability of the data collection and represents a possible practical solution for implementation in an industrial process.

- A Finite Element Modelling methodology for simulating HIFU piezocomposite array transducers has been developed. The model features accurate representations of array transducer characteristics, such as, electrical impedance spectrum, bandwidth, cross-talk, and pressure field characteristic, from the point of view of high power applications. This modelling enables rapid virtual prototype and is an effective support tool in transducer design process.

- HIFU array transducer designs have been developed for operation in the frequency range 200-400 kHz. Here, the design criteria focussed on high intensity operation rather than the traditional imaging performance considered for typical low power array applications.

- A 1-3 connectivity piezocomposite was used as the active material in a HIFU array. Simulation was used to select an appropriate design which was manufactured to operate at a frequency of 400kHz. The key performance characteristics were evaluated and importantly, the array was shown to operate efficiently and generate a high power cavitating field. This was demonstrated through a standard aluminium foil test and moreover, confirmed the durability of the array which was used continuously for a one hour period.

- A novel 2-2 connectivity stacked array configuration was also simulated, fabricated and evaluated for application as a HIFU transducer. Unfortunately, the predicted performance was not realised due to manufacturing issues degrading the array operation. Nevertheless, the concept of using such an array configuration has been clearly demonstrated for high power applications.

1.2.3 Publications to date arising of as a result of this Thesis

C. Wang, A. Gachagan, A. Nordon, A. Robin, & D. Littlejohn 'The Characterization of HTT Products Using a Combination Linear and Non-linear Ultrasonic Techniques' 2010 IEEE International Ultrasonic Symposium, San Diego, pp. 1160-1163.

C. Wang, A. Gachagan & R.L. O'Leary 'High Intensity Focused Ultrasound Array Transducers for Sonochemistry Applications' 2011 IEEE International Ultrasonic Symposium, Orlando, pp. 2329-2332.

C. Wang, A. Gachagan, R. O'Leary, & J. Mackersie 'High Intensity Focused Ultrasound Array Transducers Using 2-2 Stacked Piezoelectric Composite Appropriate for Sonochemistry application' 2012 IEEE International Ultrasonic Symposium, Dresden, pp. 2497-2500.

1.3 Overview of Thesis Chapters

Chapter 2: Ultrasonic Techniques for Chemical Processing Control and Biomedical Diagnostics

This Chapter presents a review of ultrasonic monitoring techniques applied in chemical process control. High frequency, low power ultrasonic monitoring techniques in both active and passive methodology are described. Nonlinear ultrasound theory and its application are also reviewed. Furthermore, signals processing techniques appropriate for both monitoring in chemical processing control applications and for nonlinear ultrasound applications are described to provide background for the methodologies utilised later in the Thesis. Specific industrial applications of ultrasound monitoring techniques for chemical processing control are also discussed.

Chapter 3: Characterization of HTT Hair Conditioner and Shampoo Product Using Ultrasonic Technique

In this Chapter, an experimental setup for characterization of HTT hair conditioner and shampoo products are described. It includes the properties of the examined samples, the backscatter configuration specifically applied in this experiment and the procedure of data processing. A dual mode transducer was designed and manufactured to collect the signals in both fundamental and second harmonic frequency regimes. Experimental results are presented and show the potential of the described ultrasonic monitoring technique.

Chapter 4: High Intensity Ultrasound and Sonochemistry

This Chapter reviews high intensity ultrasound behaviours in liquid. The cavitation theory and its experimental observation, and other phenomena are described. A brief review of Sonochemistry is also presented. The interaction between high intensity ultrasound and a chemical reaction are described. In addition, high power ultrasound devices and ultrasonic reaction vessels are also reviewed.

Chapter 5: High Intensity Focused Ultrasound and Its Application

In this Chapter, a brief review of high intensity focused ultrasound and its application is presented. Several configuration of HIFU transducer are introduced. The configuration and application of HIFU phased array transducer are also discussed. HIFU has been applied in the medical field for many years in a high frequency regime, between 1MHz to 5MHz, to reduce risk of cavitation. The Chapter will relate the current state-of-art in medical HIFU devices to how this can be exploited in an industrial Sonochemistry application.

Chapter 6: Design, Simulation and Manufacture of 1-3 Composite Transducer for HIFU Application in Sonochemistry

In this Chapter, three 1-D phased array transducers, using the 1-3 configuration piezoelectric ceramic composite, for high intensity focused ultrasound application are presented. The procedure of simulation, design and manufacture of the transducer is described. Also, the calibration of the manufactured transducer, in electrical impedance spectrum, pressure field, and aluminium foil tests was carried out. The calibrated results demonstrate the potential in cavitation generation, beam steering ability and hence the possibility of application in Sonochemistry for these transducers.

Chapter 7: Design, Simulation and Manufacture of 2-2 Composite Transducer for HIFU Application in Sonochemistry

This Chapter presents a 1-D phased array transducer with a 2-2 connectivity configuration piezoelectric ceramic composite for high intensity focused ultrasound applications. A detailed description of the simulation and design process is presented. The transducer manufacture and calibration results also show good consistency with the simulation results and demonstrate the potential of this transducer in the application in Sonochemistry application.

Chapter 8: Conclusions and Future Work

The Thesis ends with an overview of the key technical points from the two transducer development aspects of the research. Suggestions for how to progress these described ultrasonic techniques further are then provided.

Chapter 2

Ultrasonic techniques in chemical processing control and biomedical diagnosis

2.1 Introduction

Chemical process control is a statistical and engineering discipline that deals with the architecture, mechanisms and algorithms for maintaining the output of a chemical process within a desired range. During the 1900s, the development of piezoelectric materials enabled wider applications of ultrasound techniques, such as fluid level testing, flow rate measurement and temperature measurement. In recent years, due to the advancements in computing, in terms of both speed and scale, it is possible to carry out data analysis on large datasets and this has enabled particle size measurement, based on ultrasound spectrum analysis, to be conducted.

Ultrasound monitoring techniques applied in chemical process control can be divided into 2 categories. One is the active ultrasound technique in which the ultrasound source is external to the chemical reaction. The other is the passive ultrasound technique in which the ultrasound source is from the chemical process itself, such as cavitation and particle collisions. Both techniques are described extensively in Section 2.2 and Section 2.3, respectively.

Usually, ultrasonic techniques use the fundamental frequency signal during the entire excitation, reception and signal processing stages. However, Burns discovered that analysing the second harmonic signals led to 30dB higher signal to noise ratio (SNR) when applied to an ultrasound contrast agent in 1994[11]. This discovery provoked great interest in research on the utilization of nonlinear ultrasound and harmonic imaging within the medical community. Hence, nonlinear ultrasound has been widely investigated and applied in the biomedical regime, but has not been fully explored in the chemical process control field.

2.2 Active ultrasonic excitation and receive configurations

An active ultrasonic monitoring system generally consists of an ultrasonic excitation system and a receiving system. By varying the transmitting and receiving strategies, the active ultrasonic monitoring is defined into 3 main categories: pitch-catch, pulse echo and backscattering configurations. By analysis of the received data, it is possible to measure the material acoustic properties, like acoustic velocity, attenuation constant, and frequency response characteristic.

2.2.1 Through transmission configuration

For this Thesis, the pitch-catch configuration of interest is through transmission. In this arrangement, the analysed sample is inserted in between two transducers. The transmitting signals are excited in one transducer and received by another transducer in the same axis, which is shown in Figure 2.1. In the Figure, and subsequent Figures, *G* represents the generating or transmission transducer and *R* the reception device. In this configuration, velocity and attenuation can be measured.

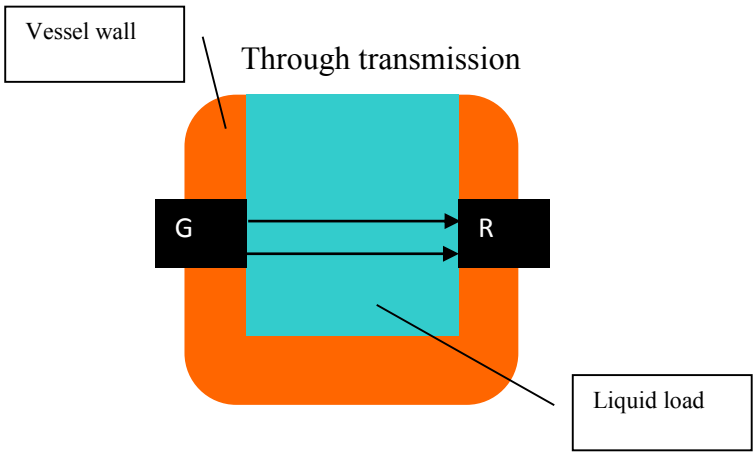

Figure 2.1 *Through transmission configuration*

The propagation time of ultrasound between two transducers is measured, and then velocity *c* is calculated by:

$$\boldsymbol{c = \frac{d}{t}} \tag{2.1}$$

where *c* is the sound speed in sample, d is the transmitting distance and t is the transit time.

Attenuation is determined by comparison of the amplitude of the sending signal and receiving signals. The attenuation factor α is calculated by:

$$\boldsymbol{\alpha = In\left(\frac{A_S}{A_R}\right)/d} \tag{2.2}$$

where A_S is the sending signals amplitude and A_R is the receiving signals amplitude.

For attenuation measurements, electrical circuits at the excitation and receiving stages will result in an error in the operation, due to the imperfect matching to the transducer and energy dissipation on the circuits. To avoid this error, at least two measurements at different distances away from the excitation transducer should be taken and then calculated by Equation 2.3.

$$\boldsymbol{\alpha = In\left(\frac{A_{L1}}{A_{L2}}\right)/\Delta L} \tag{2.3}$$

Where A_{L1} and A_{L2} are the amplitude of the measurement signals at distance *L1* and *L2* respectively, Δ*L* is the distance between *L1* and *L2*.

The experimental principle of the through transmission technique is simple, but in practice, there are several factors that need to be considered in experimental design to avoid inaccurate measurement, such as temperature variation, reverberation of ultrasonic pulses in vessel walls, transducer bandwidth, diffraction effects and phase cancellation due to non-parallel walls.

In the through transmission configuration, the system can analyse received data in the time or frequency domains. Moreover, there are a large number of excitation schemes that can be implemented. As an example, both wideband and narrowband excitation

signals are discussed: a broadband pulse, see Figure 2.2, and a tone burst, illustrated in Figure 2.3. In both of these idealised signal representations, the excitation pulse is fired into the sample, and then the signals, after interaction with the sample, are received in the opposite transducer. The received signal contains information on the transmitting time t and the received amplitude A, which are dependent on the characteristics of the material under investigation. The broadband pulse approach provides a short time duration ultrasonic signal, as shown in Figure 2.2, which is important if high resolution discrimination between features in the load medium is of interest. It is also appropriate to convert the time domain response into the frequency domain and consider the wideband received spectrum for additional information on the load material. Importantly, the energy contained in the pulse is limited due to the short time duration of the signal. Tone burst excitation is defined as a finite number of cycles of a sinusoidal signal, with a rectangular window function shown in Figure 2.3. Here, the centre frequency of the signal is typically chosen to match the ultrasonic transmitter to maximise the efficiency of the transducer operation. As the signal frequency matches the operational frequency of the transducer and the time duration is long, the energy contained in this excitation scheme is significantly higher than in the broadband pulse case. However, this frequency needs to be chosen carefully to avoid significant nonlinear effects. Importantly, use of the tone burst scheme restricts the receive signal analysis to the time domain only. Another important factor for the tone burst excitation scheme is use of a windowing function, which enables peak value detection and simplifies temporal measurements. Typically, the choice of excitation scheme depends on the application.

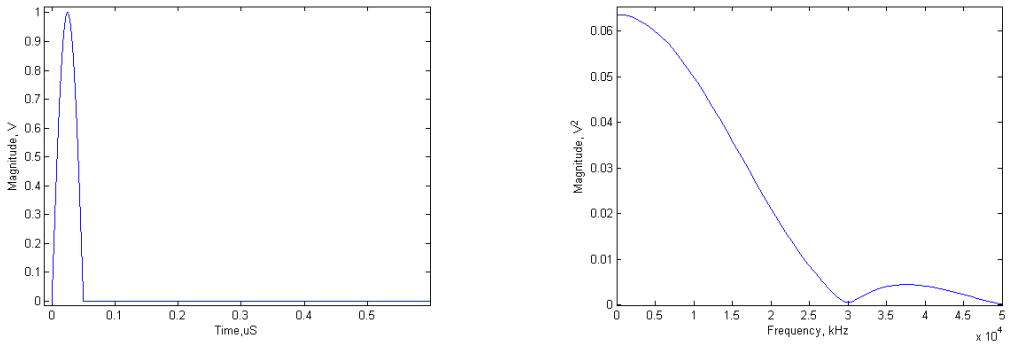

(a) (b)

Figure 2.2 *Broad band pulse signal, (a) time domain, (b) frequency domain*

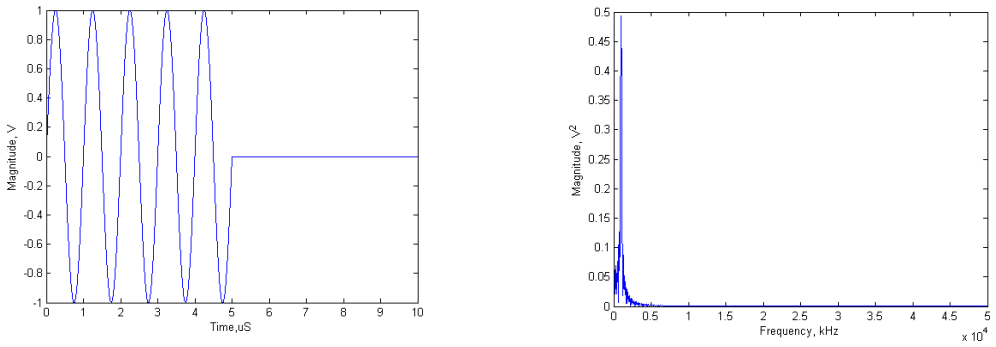

(a) (b)

Figure 2.3 *Tone burst pulse signal (a) time domain, (b) frequency domain*

2.2.2 Pulse echo configuration

Pulse echo operation is a configuration which is similar to the through transmission approach. Both velocity and attenuation are the main material properties of interest and measured using the same approach as described in Section 2.2.1. The difference between the pulse echo and through transmission configurations is that only a single transducer is employed in generating and receiving of signals. Figure 2.4 shows that the ultrasound signal is sent into the sample, and then the signal is reflected from a reflector and received by the same transducer. In this case the transducer is identified as *G/R*. When calculating the velocity and attenuation parameters, it is important to note that the transmitting distance is doubled compared to the through transmission configuration.

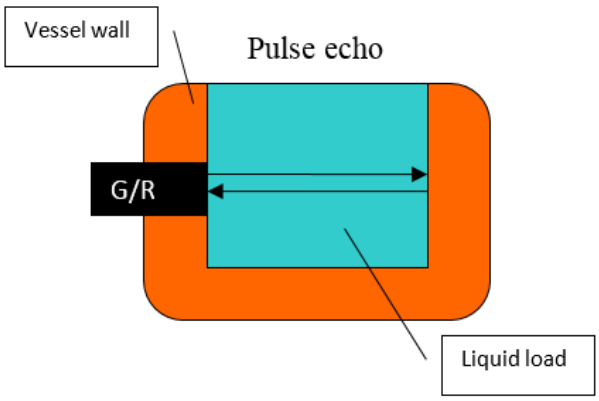

Figure 2.4 *Pulse echo configuration*

2.2.3 Backscattering approach

The backscattering configuration is when an ultrasound pulse is fired into a heterogeneous media, and the received signals are generated by the microstructure of the load medium. This has a similar arrangement to the pulse-echo case, but for this work the reception transducer will be orientated at an angle of 90º relative to the excitation axis. This is illustrated in Figure 2.5.

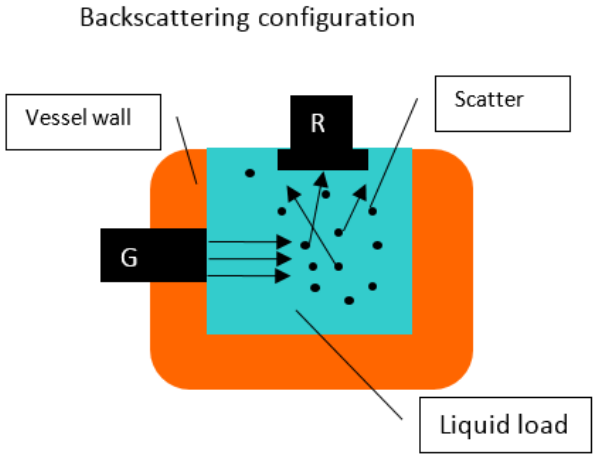

Figure 2.5 *Backscattering configuration*

When an ultrasound pulse propagates through a heterogeneous media, there are several kinds of interaction which take place, such as intrinsic absorption, visco-inertial absorption, thermal absorption and scattering [34]. In particular, scattering can take the form of particle pulsation or particle oscillation. Both of these relate to the particle size and the different acoustic properties between particles and their surroundings. Particle pulsation occurs in the ultrasound pressure field due to differences in the adiabatic compressibility and/or thermal properties of the particle and surrounding liquid. It is a phenomenon that occurs when an ultrasonic wave propagating in a material, causes periodic fluctuations in the local pressure and temperature as the material expands and contracts. In the long wavelength regime, in which particle size is much smaller than the wavelength, the pressure and temperature of the particles are similar to the surrounding liquid, and hence this regime is not able to generate significant pulsation scattering.

Particle oscillation is caused by density differences between the particle and the surrounding liquid. When the particle interacts with the ultrasound wave, it can oscillate backwards and forwards. As the particle has different inertia compared with the surrounding liquid, it generates a scattering wave which is emitted at a different propagation direction to the original transmitting ultrasound wave [35].

Great effort has been conducted in the investigation of the interaction between ultrasound and particles. Single scattering in dilute systems, in which each wave is only scattering by a single particle, is well understood mathematically and reasonable agreement has been achieved between the mathematical modelling and experiment results [5, 36, 37]. Multiple scattering is defined as that in concentrated systems, where a wave might be scattered by a number of different particles. This condition is much more difficult to analyse; nevertheless, significant progresses has been achieved since the 1950s. Several models were proposed by Epstein and Carhart 1953 [38], Waterman and Truell 1961 [39] and Allegra and Hawley 1972 [40]. The most comprehensive and widely used model is from Waterman and Truell. In this model, the particles are spherical, do not physically interact with each other, and are randomly distributed in space. The ultrasonic property of the ensemble of scatterers is represented by the complex propagation constant:

$$\boldsymbol{k = \frac{\omega}{c} + i\alpha} \tag{2.4}$$

where c is ultrasonic velocity, ω is the angular frequency and α is attenuation coefficient.

This can be used to determine $f(0)$ and $f(\pi)$, the far field scattering amplitudes of the waves scattered from the individual particles,

$$\boldsymbol{(\frac{k}{k_0})^2 = 1 + \frac{4\pi N_P f(0)}{k_0^2} + \frac{4\pi^2 {N_P}^2}{k_0^4}[f^2(0) - f^2(\pi)]} \tag{2.5}$$

$$\boldsymbol{f(0) = \frac{1}{ik_0}\sum_{n=0}^{\infty}(2n+1)A_{Sn}} \tag{2.6}$$

$$\boldsymbol{f(\pi) = \frac{1}{ik_0}\sum_{n=0}^{\infty}(-1)^n(2n+1)A_{Sn}} \tag{2.7}$$

where k_0 is the initial complex propagation constant of the continuous phase,

N_P is the number of particle per unit volume, $\phi = 4\pi r^3 NP/3$,

ϕ is the disperse phase volume fraction,

ω is the angular frequency,

i is imaginary unit,

r is the particle size,

A_{Sn} is the scattering coefficients of the nth reflection of ultrasound waves.

Equations 2.4 and 2.5 describe the general condition of multiple ultrasonic scattering in an emulsion. Further simplification of the mathematical model can be achieved by specification of scattering conditions. In the condition that the ultrasound wavelength is much larger than the particle size, the high order reflection between the particles is negligible and the simplification is shown in Equation 2.8.

$$\left(\frac{k}{k_0}\right)^2 = 1 + \frac{4\pi N(A_{S0}+3A_{S1})}{k_0^3} + \frac{48\pi^2 N^2 A_{S0} A_{S1}}{k_0^3} \quad \textbf{(2.8)}$$

where A_{S0} and A_{S1} is the attenuation from the first two orders of reflection.

However, in the intermediate wavelength regime, which the ultrasound wavelength is similar to the particle size, high order scattering coefficients cannot be ignored.

Importantly, the scattering coefficient is frequency dependent; therefore, by spectral analysis of the received signals, it can be possible to determine the particle size. This technique can be applied in a non-invasive configuration, is relatively inexpensive and can provide real-time monitoring. More importantly, it is possible to apply to an opaque sample. Therefore, it is an ideal technique for high throughput products, e.g. cosmetics products, which require a high standard of hygiene and are normally opaque. The main limitation of this technique is that the small gas bubbles significantly disturb the scattering effect; due to gas bubbles acting as an effective scattering source, even at very low concentrations [41].

2.3 Passive ultrasonic technique

The passive ultrasonic monitoring technique consists of the measurement and analysis of the acoustic emission (AE) signals created by the process itself. AE can contain valuable information and is caused by physical and chemical events occurring within the process. Passive ultrasonic monitoring systems can be divided into 3 sections, which are illustrated in Figure 2.6.

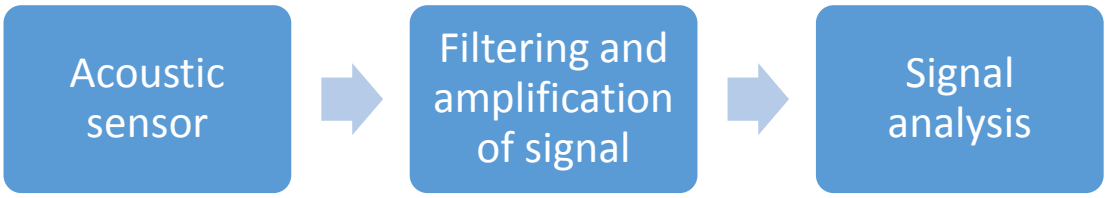

Figure 2.6 *Passive ultrasonic monitoring system*

Due to most of the measurements taking place in a multi-acoustic source environment, it can be difficult to extract the relevant information from the acoustic signals. Therefore, dedicated signal processing techniques are required to analyse the signals, such as auto-correlation, cross-correlation and Fourier analysis. These signal processing techniques are described in detail in Section 2.5. Passive ultrasonic monitoring in chemical processing control can be sorted into 3 categories by its measurement objective: monitoring of gas-liquid dispersions; monitoring of solid- liquid dispersion; and equipment monitoring.

In gas-liquid dispersion monitoring [42, 43], the existing techniques are either impractical for on-line operation or intrusive to the process under investigation. Photography/video techniques have been used in the characterisation of gas dispersions, but it is limited by the requirement of transparent equipment and liquid media. The probe technique is used in the monitoring of the interfacial area, bubble size and gas holdup[44]; however, it requires direct contact with the gas bubbles. The passive ultrasonic technique is an ideal alternative, because of its non-invasive and real time monitoring ability. By detection of AE, it is possible to analyse the interfacial area, gas bubble size, type of flow regime, and amount of power dissipated within the system.

In gas-liquid dispersion, AE is caused by the mass transfer from the gas phase into the liquid (e.g. aeration of a bio-reaction), or from the liquid into gas phase (e.g. scrubbing of exhaust gases). AE from the formation of bubbles was well studied in oceanography to identify the source of ambient sound in the sea and subsequently used to detect marine traffic [45]. The bubble oscillates when its volume is displaced from its equilibrium position, and hence produces an acoustic pressure pulse. The frequency of the emission, Equation 2.9, is related to the bubble size [46-48].

$$\boldsymbol{f = \frac{1}{2\pi r}\sqrt{\frac{3\gamma P}{\rho}}} \tag{2.9}$$

where r is the bubble radius,

P is the pressure in liquid,

γ is the ratio of specific heats of gas,

ρ is the density of gas.

More investigations about this topic have been conducted recently, e.g. the study into the bubble size distribution in gas-liquid dispersions by analysis of the sound spectrum, [49], and information extraction from a sound spectrum, which is acquired from a vessel agitated using a stirring process causing a high level background noise [50, 51].

Another AE source is from solid-fluid dispersions, mainly because of particle collisions with each other or colliding with objects or vessel walls, and the chemical reaction process itself. Great efforts have been undertaking in the research of measuring particle size and its distribution in powder [52, 53]. It was demonstrated that two rigid spheres of different sizes colliding with each other will emit acoustic signals at frequencies related to the acoustic mean of their fundamental resonant frequency. By analysis of the spectrum of AE, the average particle size and its range or distribution can be acquired. As many chemical reactions, particularly in a reaction with phase changes, are acoustically active they will emit ultrasound during the reaction process. An excellent publication on this topic can be found in [54].

AE detection is also applied to equipment monitoring and there are several common applications, e.g., structural integrity [55], corrosion monitoring [56] and leak detection [57]. Again an excellent review can be found in [58].

2.4 Nonlinear ultrasound

2.4.1 Theory of nonlinear ultrasound

The practical world is nonlinear and hence it is apparent that sound propagation can have nonlinear effects. The first description of nonlinearity of sound, which is shown in Equations 2.10 and 2.11, was by Euler more than 300 years ago [59].

$$\boldsymbol{D\rho/Dt + \rho\nabla U = 0} \tag{2.10}$$

$$\boldsymbol{\rho(DU/Dt) + \nabla P = F} \tag{2.11}$$

where ρ is the density of media,

P is the pressure in the media,

D/Dt is the material derivative,

U is the particle velocity,

F is the external body force vector per unit volume.

Next, Lagrange (1760), Poisson (1808), and Stokes (1848) built the mathematical foundation of nonlinearity theory [60]. Research in nonlinear ultrasound achieved significant progress in the 1900s. United States and Russia have independently found theoretical solutions for the propagation of plane, cylindrical and spherical waves of finite amplitudes in thermoviscous and relaxing fluids, which included experimental verification. The second order nonlinearity parameter B/A is an important parameter that describes the material nonlinearity of the ultrasound transmitting media [61].

$$B/A = 2\rho c\left\{\left(\frac{\partial c}{\partial P}\right)_T\right\}_{\rho=const} + \left(2cT\beta {C_P}^{-1}\right)\left\{\left(\frac{\partial c}{\partial P}\right)_T\right\}_{\rho=const} \tag{2.12}$$

where c is the sound velocity in the transmitting media,

P is the pressure in the field,

T is the absolute temperature,

C_P is the specific heat at constant pressure,

β is the volume coefficient of thermal expansion.

B/A is used to indicate the level of nonlinearity associated with a load medium and is related to the ability to form higher harmonics from the original, finite amplitude,

sinusoidal wave. There is also a close relationship between *B/A* and the molecular structure of the fluid involving the intermolecular or the interatomic potentials [62].

The second order acoustic nonlinearity parameter *B/A* of the medium is measured mainly by two methods: the thermodynamic method or the finite-amplitude method. The thermodynamic method is based on the use of Equation 2.12. The finite amplitude method is based on the measurement of the 2nd harmonic component of the transmitting wave. To calculate the ultrasonic wave pressure amplitude at the source, the expression is given by Equation 2.13. An excellent review about the measurement of *B/A* is provided by [59, 62].

$$\left[\frac{P(x)}{xP^2}\right]_{xP^2\to 0} = \frac{(2+B/A)}{x\rho c^3} exp[-(\alpha_1 + \alpha_2/2)x] \tag{2.13}$$

where ρ is the density of the transmitting media,

c is the velocity of sound in the media,

α_1 is the attenuation coefficient for the fundamental frequency,

α_2 is the attenuation coefficient for the second harmonic frequency.

Waveform distortion is the result of the nonlinear propagation effects, mainly caused by two reasons: frequency dependant dissipation and high order harmonic generation. Waveform distortion is an important phenomenon to indicate the presence of any nonlinear process(es) during ultrasound propagation. Importantly, there are specific parameters to describe the distortion. *l* is called the discontinuity distance and is expressed as

$$l = \{(B/2A + 1)k_W M\}^{-1}(m) \tag{2.14}$$

where k_W is the wave number,

M is the acoustic Mach number, expressing the original amplitude of the finite amplitude

From Equation 2.14, *l* is the distance that the first vertical tangent of the finite amplitude wave forms at the zero-crossing point [59], which is illustrated at Figure 2.7. Moreover, there are more parameters that can be used to describe the nonlinear propagation process, e.g. dissipation constant *b*, Gol'dberg number *Γ [63]* and acoustic Reynolds number Re_ω [64], but the discontinuity factor, *l,* is the most commonly used

currently. An excellent review about the parameter associated with nonlinear property of transmitting media is presented in [59].

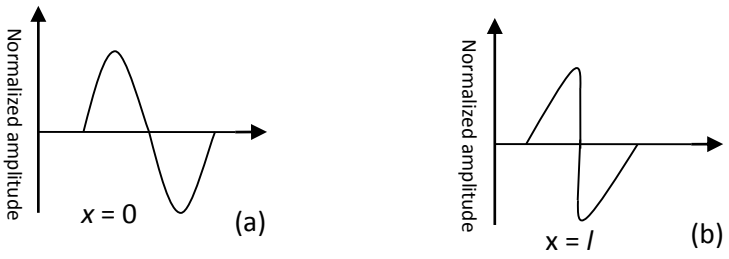

Figure 2.7 *Distortion associated with waveform propagation due to Nonlinear effects: (a) distance x = 0, (b) distance x = l*

2.4.2 Application of nonlinear ultrasound

2.4.2.1 Medical harmonic diagnosing

Harmonic imaging techniques were first proposed during the 1990s and rapidly commercialized within a few years. However, in the previous decades, engineers and clinicians were not familiar with nonlinear ultrasound and typically used low pass filters to remove harmonic components. Muir first demonstrated the existence of second harmonics in water during a sonar application in 1980[65]. Then the capability to generate harmonic signals in a propagating ultrasonic wave was confirmed through a series of images in water [65, 66] .

The tissue harmonic imaging (THI) technique [9, 10] or the so called native harmonic images technique was developed in late 1990s. It uses harmonics to improve image quality and contrast resolution in tissue. The absorption of ultrasound increases as the frequency increases. Therefore, the compromise between picture resolution and penetration has to been made in the traditional B-mode scanner operational mode. The development of THI technique has resulted in a simultaneous increase in both the image resolution and penetration depth. Moreover, this technique has been shown to reduce noise and clutter and improve signal to noise ratio.

Harmonic imaging techniques with ultrasound contrast agent (UCA) is another main application of nonlinear ultrasound in medical diagnosis. UCA is a shelled microbubble, first used to enhance the fundamental signal response. Burns et al (1994) demonstrated a gain of more than 30dB in signal to clutter ratio and superior imaging of the microvasculature by the application of contrast harmonic imaging in the study of the blood flow in abdominal aortas and kidneys of rabbits [11]. This technique is now commercialized and used to detect flow in small vessels by selectively enhancing the signal from blood and at the same time suppressing the echoes from surrounding tissue.

2.4.2.2 Other applications of nonlinear ultrasound

The parametric acoustic array technique is one of the applications based on the theoretical and experimental development of nonlinear ultrasound, which was proposed in the 1960s [67]. It uses the principle that two finite amplitude, plane, collimated primary waves with different frequencies, superimpose and interact nonlinearly with each other, then produce a different frequency beam with low side lobe levels. This idea is based on the solution from Lighthill's inhomogeneous wave equation for aerodynamic generation of sound [68, 69]. The solution indicates that the half power beam width decreases as absorption coefficient and primary frequency decrease, which can increase the directivity of the ultrasound beam and reduce the side lobe level significantly. Parametric acoustic arrays have been applied in underwater sound [68, 70], tomography [71], and active noise control [72].

2.5 Signal processing for ultrasonic processing control

Signal processing is a critical part of a chemical process control system. It is important to the control the reliability and repeatability of information used in the decision process stage. In this Section, a brief description of the principle digital signal processing (DSP) used in this Thesis is presented.

2.5.1 Root mean square (RMS) value

The RMS value is a method to indicate the received signal's energy. The expression in continuous form is:

$$\boldsymbol{z_{RMS}} = \sqrt{\frac{\mathbf{1}}{\boldsymbol{t_2 - t_1}} \int_{t_1}^{t_2} |\boldsymbol{f(t)}|^2 \boldsymbol{dt}} \tag{2.15}$$

The equation in discrete form is:

$$\boldsymbol{z_{RMS}} = \sqrt{\sum_{n=1}^{n=N} \boldsymbol{z_n}^2 / N} \tag{2.16}$$

2.5.2 Fourier transform

The Fourier transform is a basic tool to transfer time domain signals into the frequency domain. The continuous expression is:

$$\boldsymbol{\hat{y}(f)} = \int_{-\infty}^{\infty} \boldsymbol{y(t) e^{-i2\pi tf} dt} \tag{2.17}$$

Where t is time,

f is the frequency.

The discrete Fourier transform (DFT) is the discrete version of Fourier transform and is express as:

$$\boldsymbol{y_j} = \sum_{n=0}^{N-1} \boldsymbol{y_n e^{-\frac{2\pi i}{N} jn}} \tag{2.18}$$

Where $j = 0 \ldots N\text{-}1$,

i is imaginary unit,

$e^{-\frac{2\pi i}{N}}$ is a primitive Nth root of unity.

The Fast Fourier transform (FFT) is an efficient computational implementation of the discrete Fourier transform algorithm. FFT has more than one implementation, but most well-known algorithms are dependent on the factorization of *N*, which can reduce the calculation number from n^2 to $nlog(n)$. In this Thesis, Equations 2.19 and 2.20 are used.

$$\boldsymbol{y(m)} = \sum_{\boldsymbol{j=1}}^{\boldsymbol{N}} \boldsymbol{y(j)\omega_N^{(j-1)(m-1)}} \tag{2.19}$$

$$\boldsymbol{y(j)} = \boldsymbol{(1/N)} \sum_{\boldsymbol{m=1}}^{\boldsymbol{N}} \boldsymbol{y(m)\omega_N^{-(j-1)(m-1)}} \tag{2.20}$$

where $\omega_N = e^{(-2\pi i)/N}$

2.5.3 Cross – correlation

Cross – correlation is a signal processing technique, which can extract the signals of interest embedded within noise, and is dependent on knowledge of the signal of interest. It is widely used in communication applications and known as matched filtering. The standard expression is given in Equation 2.21:

$$\boldsymbol{(y * g)(t)} \stackrel{\text{def}}{=} \int_{-\infty}^{\infty} \boldsymbol{y^*(\tau)g(t+\tau)d\tau} \tag{2.21}$$

where *y* and *g* are the processed signals,

y^* is the complex conjugate of y.

The discrete version of cross-correlation is:

$$\boldsymbol{(y * g)[n]} \stackrel{\text{def}}{=} \sum_{\boldsymbol{m=-\infty}}^{\infty} \boldsymbol{y^*[m]g[n+m]} \tag{2.22}$$

This technique has been used in nonlinear ultrasound applications. By using a wideband chirp excitation signal and then cross-correlating the received signal, after interaction with the load of interest, with a pre-determined signal, the specific signals of interest can be extracted [28]. In terms of applying a matched filter to extract the 2nd harmonic components from a received signal, the pre-determined signal used in the processing will take the form of a chirp signal centred on a frequency which is twice the original excitation frequency. For example, the excitation signal is recorded and then

digitalized, which is shown in Figure 2.8. The input chirp signal has characteristics of start frequency of 1.75 MHz and end frequency of 2.75 MHz, with pulse duration of 4.5μs. Please note that a linear chirp signal without envelope shaping is used for demonstration purposes here. By down sampling this recorded signal, the processed signal is double the original frequency, which is displayed in Figure 2.9. Next, the received signals shown in Figure 2.10 are assumed to contain a second harmonic component which is -20dB down on the fundamental signal components. From this Figure, it is clear that the second harmonic is difficult to be observed. By cross-correlating the received signals (Figure 2.10) with the processed signal (Figure 2.9), the second harmonic signals can be extracted and the result from this example is presented in Figure 2.11. Importantly, the same methodology can be applied to extract sub-harmonic or higher order harmonic signals.

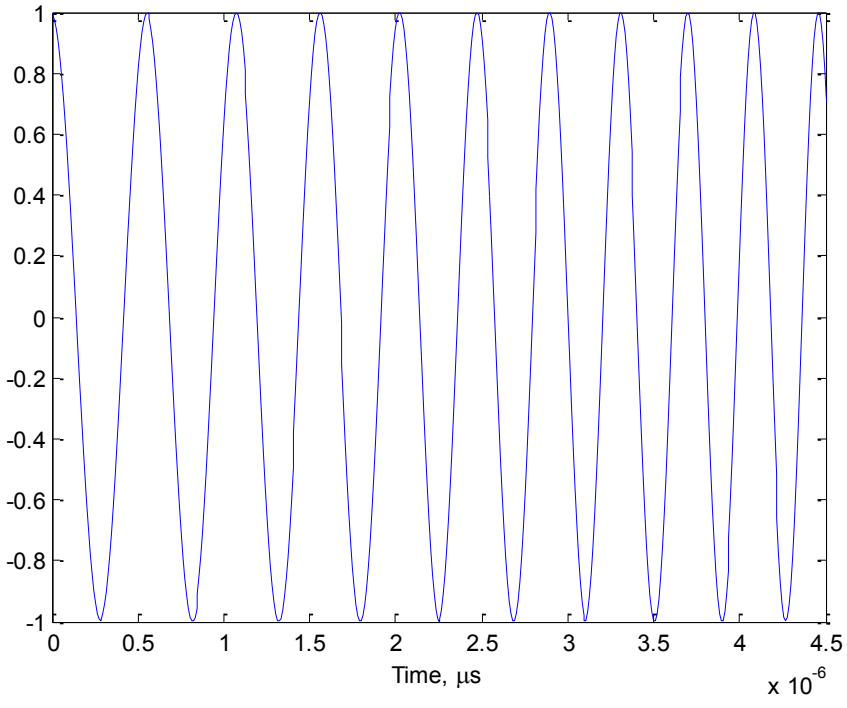

(a)

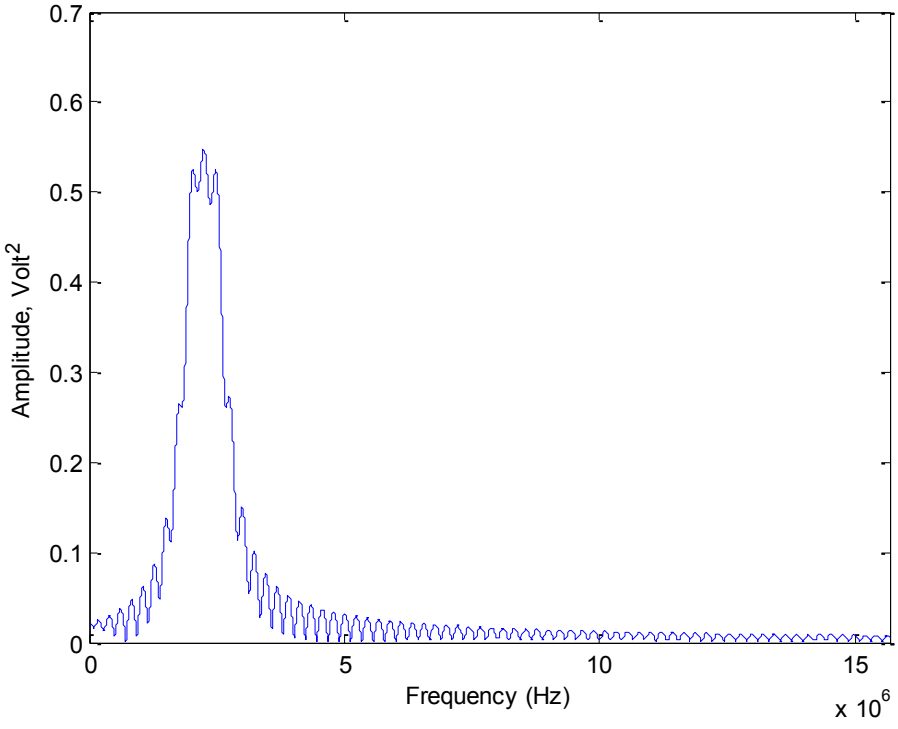

(b)

Figure 2.8 *Input linear chirp signal, (a) time domain signal, (b) frequency domain signal*

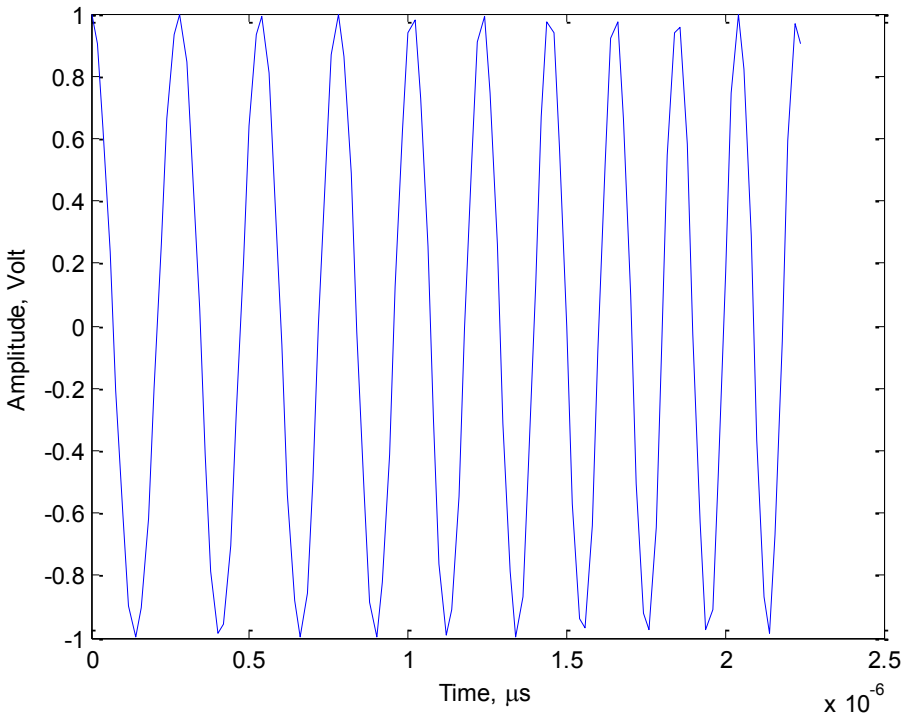

(a)

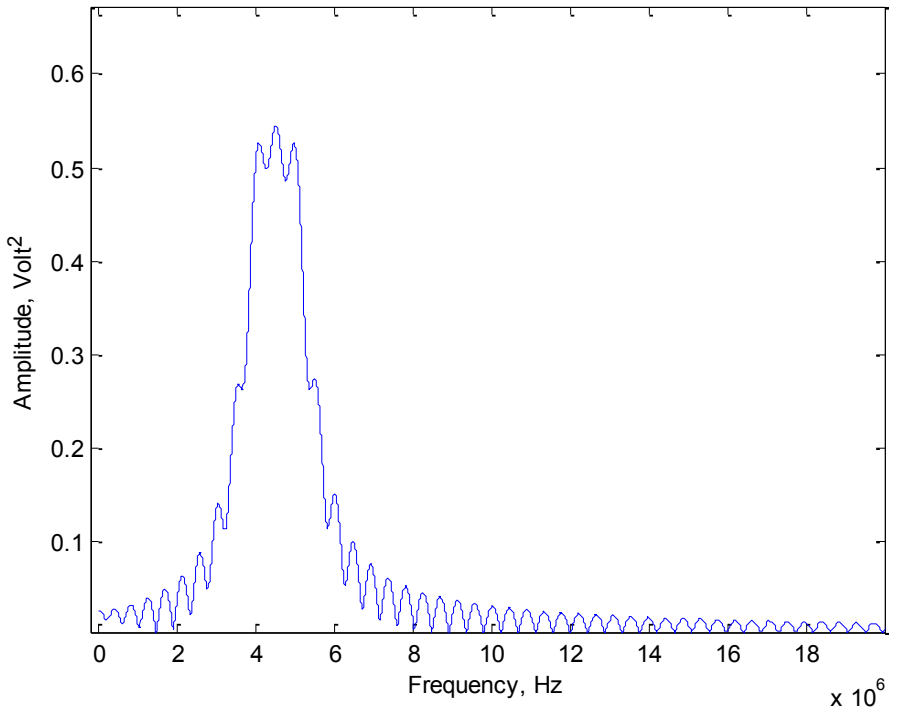

(b)

Figure 2.9 *Down sampling signal for extraction of second harmonic component, (a) time domain signal, (b) frequency domain signal*

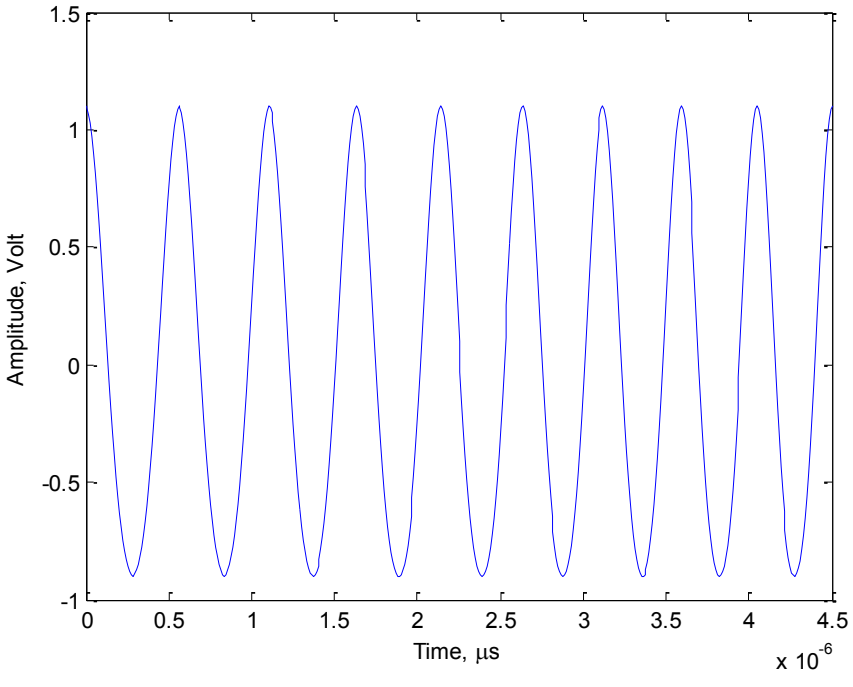

(a)

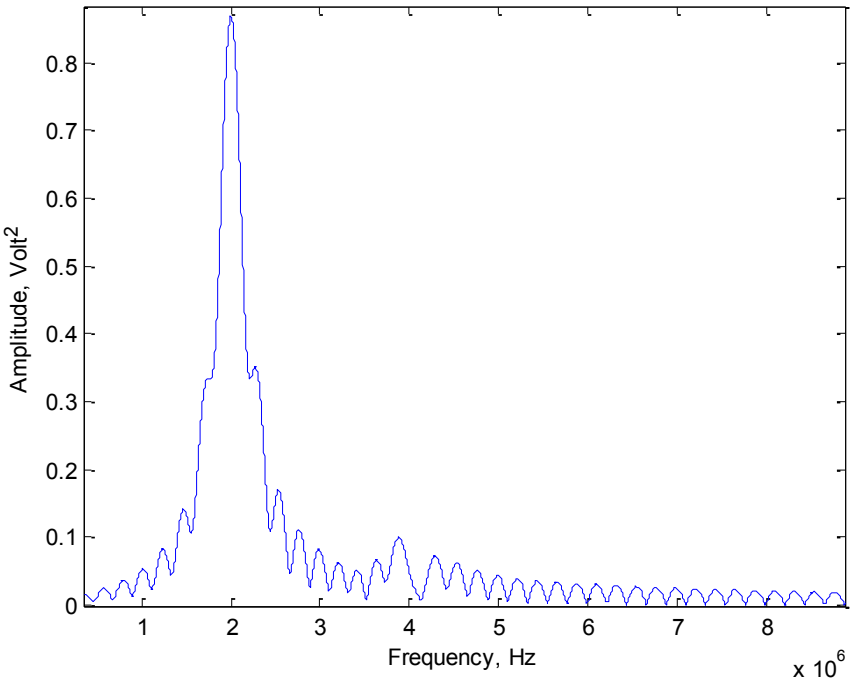

(b)

Figure 2.10 *Assumed received signals, (a) time domain signals, (b) frequency domain signals*

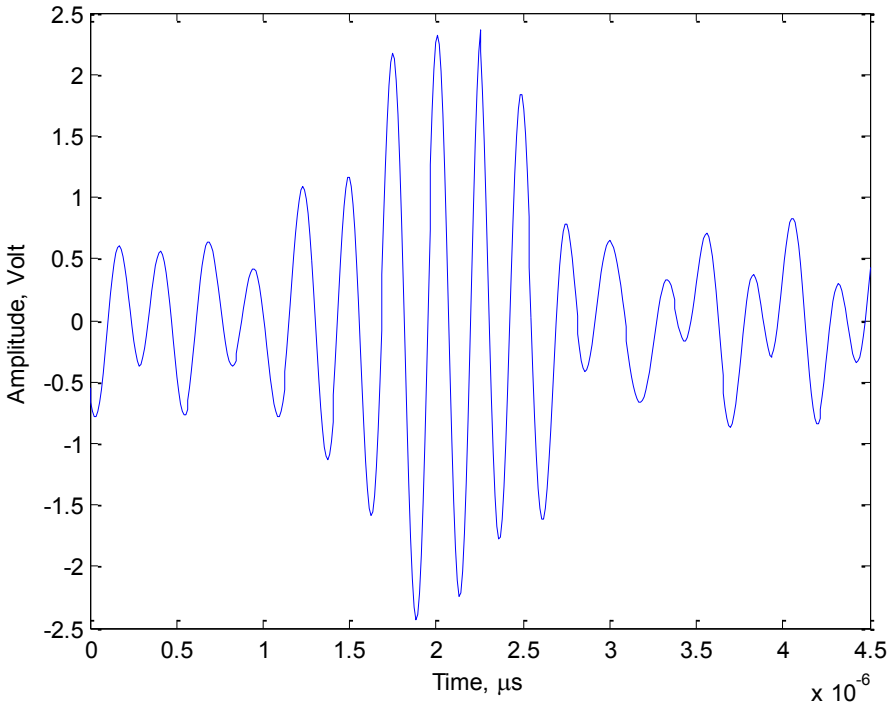

(a)

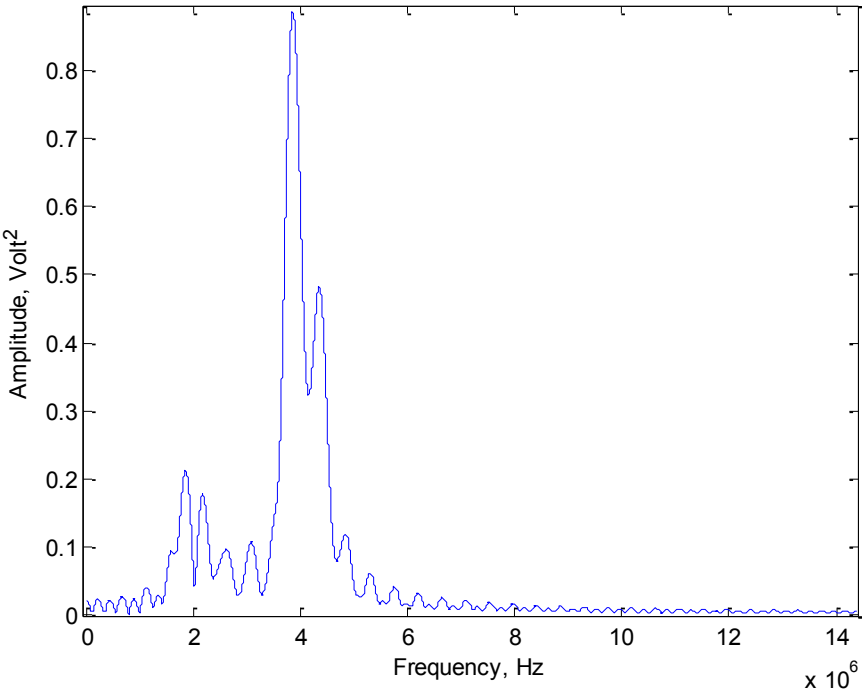

(b)

Figure 2.11 *Cross correlated signal, (a) time domain signal, (b) frequency domain signal*

2.6 Application of an ultrasonic monitoring technique

2.6.1 Chemical process control

Ultrasound has been utilised as a potential method to support chemistry processing control since the beginning of the last century, but only recently has the ultrasonic techniques started to find practical application in industrial processes. A review of appropriate technologies will now be provided including level measurement, flow rate measurement, temperature measurement, density measurement and particle size measurement.

2.6.1.1 Ultrasonic liquid level measurement

Liquid level measurement is the earliest application of an ultrasound technique in the chemistry industry [1]. This technique is based on Equation 2.1 and the pulse echo configuration with the transducer located at the base of the vessel, as illustrated in Figure 2.12. A transducer is mounted on the bottom of the container and generates ultrasound which propagates through the load, is reflected from the boundary between the air and the liquid, with the reflected signals acquired by the transducer. From the received signal, the transmission time can be acquired and hence the liquid level can be calculated.

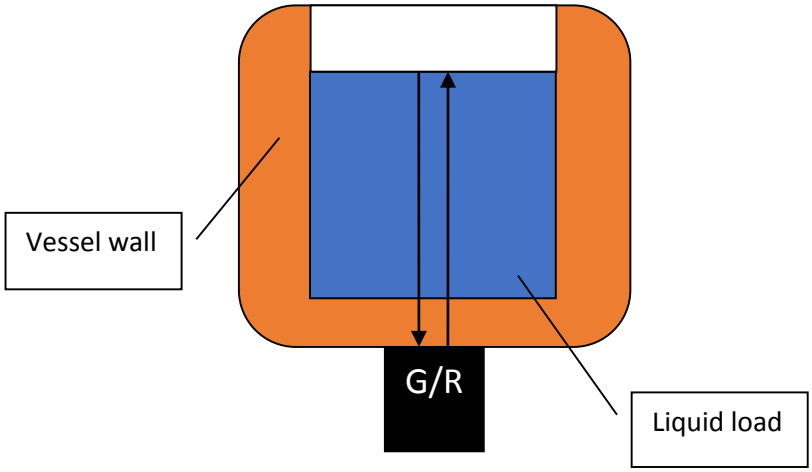

Figure 2.12 *Illustration of level measurement system*

2.6.1.2 Flow velocity measurement

The utilization of ultrasound to measure flow velocity is another mature technique applied in chemical processing control. There are mainly two types of ultrasonic techniques; transmission flow meter and Doppler shift flow meter [2, 3]. The transmission flow meter is based on the time domain velocity measurement. Two ultrasound transducers are mounted in a pipe at a specified angle, then a pulse is transmitted both with and against the flow direction and measurement of the difference between the receiving time T_{up} and T_{down} used to calculate the flow velocity and sound speed of flow liquid using Equations 2.23 and 2.24.

$$v_{flow} = \frac{L}{2\,sin(\alpha)} \times \frac{T_{up} - T_{down}}{T_{up} T_{down}} \tag{2.23}$$

$$c = \frac{L}{2} \times \frac{T_{up} + T_{down}}{T_{up} T_{down}} \tag{2.24}$$

where v_{flow} is fluid or gas velocity,

L is the distance between receiving and transmitting transducers,

α is the inclination angle,

c is the sound speed in the transmitting fluid or gas.

The Doppler Effect can also be employed in this measurement system. Ultrasound is fired with a desired frequency into a liquid flow and the reflected signal is received from the scattering objects in the liquid. These signals are then analysed in the frequency domain. From differences between the measured frequencies for the excitation and scattered signals, the velocity of the flow can be calculated.

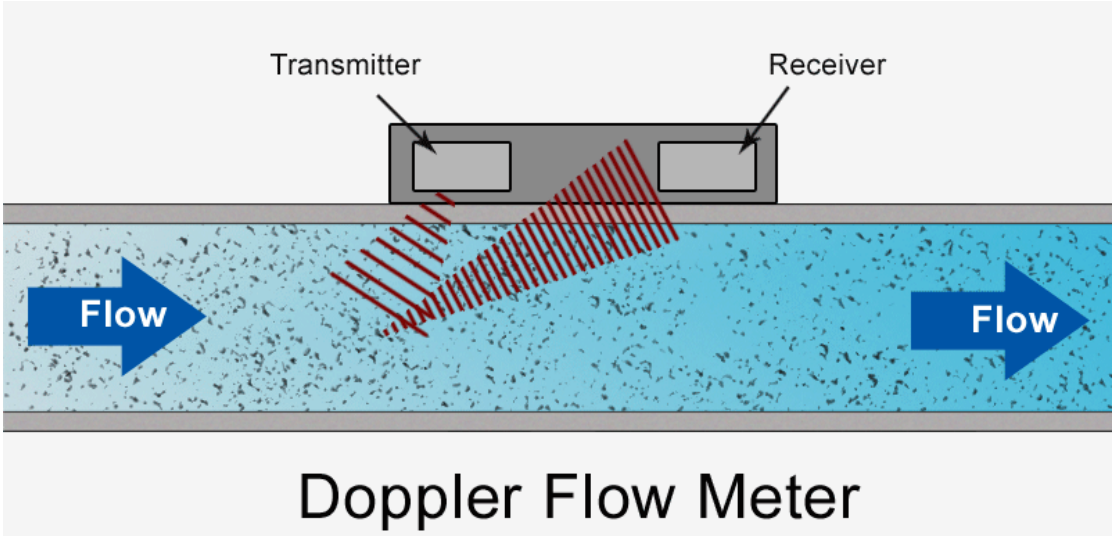

Figure 2.13 *Typical flow meter system arrangement [73]*

The transmission flow meter is mainly affected by temperature and material density fluctuations when compared with the Doppler shift flow meter. However, because of the simplicity of the method, it is more widely applied in chemical industry monitoring applications.

2.6.1.3 Density measurement

Density measurements [74] using ultrasonic techniques is based on the measurement of the acoustic impedance and the sound velocity of the material, as given in the relationship shown in Equation 2.25:

$$Z_A = \rho v \tag{2.25}$$

where Z_A is the acoustic impedance of the measured material,

ρ is the density of the measured material,

v is the acoustic velocity of the measured material .

Assuming that ultrasound propagates in a lossless and uniform media, the acoustic impedance is able to be acquired by measuring the reflected wave amplitude from the boundary between the measuring material and the calibrated material, e.g. water.

Therefore, by measuring the transmission time and the received signal intensity, the density of the material can be calculated based on Equations 2.25 and 2.26.

$$\boldsymbol{R_C = \frac{Z_{AM} - Z_{AC}}{Z_{AM} + Z_{AC}}} \quad (2.\ 26)$$

Where R_C is the reflection coefficient,

Z_{AM} is the acoustic impedance of the measuring material,

Z_{AC} is the acoustic impedance of the calibrated material.

To acquire precise measurement, a typical multi-angle reflection coefficient measurement configuration is commonly used, which is illustrated in Figure 2.14. Further reviews of these techniques can be found in [74] and [75].

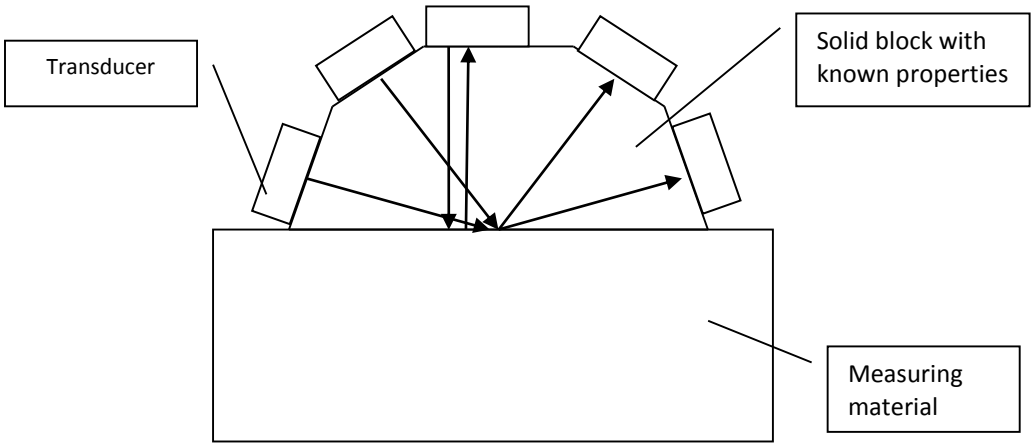

Figure 2.14 *Multi-angle density measurement configuration*

2.6.1.4 Temperature measurement

Sound velocity is dependent on the material properties, but also strongly associated with the environmental temperature. Ultrasonic temperature sensors are based on the measurement of sound speed with a calibrated sensor [4, 76]. This technique is typically deployed invasively. The measurements are mainly used in the pitch catch or pulse echo configurations. By carefully calibration of the system, this approach can be applied in the chemical industry, which may need to measure the product under high pressure or in a

toxic environment, and in the food industry, which may require high hygiene standard [77].

2.6.1.5 Particle size measurement

It is important to control the particle size in some chemical reaction processes, such as the particle size of an emulsion during a reaction. There are alternative techniques, e.g., spectroscopy analysis [78]; however, ultrasound has several advantages: (1) can be used in high concentration emulsions which can be opaque; (2) rapid measurement to monitor the particle size in real time; (3) relatively less expensive; (4) non-destructive and non-invasive. The measurement is based on the analysis of the spectrum of the ultrasound, which is reflected or produced from the particle suspension. Both passive and active ultrasound techniques can be found in this application regime and typically relate a particular particle size to a corresponding unique resonant frequency.

The passive ultrasound techniques are based on the detection of acoustic emission (AE) from the reaction process, as discussed in Section 2.3. The AE frequencies depend on the particles size, material properties and the vessel reactor. Passive ultrasound techniques are widely used in the chemical industry and food industry, and excellent reviews are presented by [58, 79].

Active ultrasonic monitoring to extract particle size information can be based on pitch catch or pulse echo configurations, as described in Section 2.2. The ultrasound velocity and attenuation in the emulsion/suspension is a function of frequency for a given particle distribution [5, 6]. The velocity and attenuation measurement structure and scattering theory can be found in Section 2.2. Ultrasonic particle size monitoring has been applied in the mineral, chemical and oil industries to analyse powder size based on attenuation measurements [80]. In addition, there are reports of particle size measurement of fat and protein droplets in milk and yogurt in the food industry [6].

2.7 Summary

Ultrasound monitoring techniques are currently becoming an important technique in chemical processing control systems, due to two aspects: advances in computation technology; and new piezoelectric transducer approaches. The former allows the utilization of more complex signal processing techniques, while the latter provides high fidelity signals for use in the processing stage. The applications of ultrasonic spectrum monitoring and nonlinear ultrasound are good examples.

This Chapter has briefly reviewed the background of ultrasonic processing control theory, techniques and its application. The basic ideas of utilization for monitoring applications and typical ultrasonic system configurations are presented. This Chapter also expresses the recent developments in nonlinear ultrasound and the signal processing techniques. Finally, the typical industrial applications of ultrasonic monitoring techniques are mentioned.

The next Chapter will present the development of an ultrasonic system for the characterization of hair conditioner and shampoo products. The setup of the experiment is based on the backscattering approach and the received signals were analysed in both linear and nonlinear regimes. These preliminary results show the potential for application of this system in the chemical processing control.

Chapter 3

Characterization of HTT hair conditioner and shampoo products using an active ultrasonic approach

3.1 Introduction

In the chemical industry, ultrasonic monitoring systems and spectroscopy techniques are both utilized in process control methodologies. Spectroscopy techniques are mainly used to analyze a samples' molecular structure. Whereas, ultrasonic systems are mainly employed in measurement of density, temperature, and liquid flow rate [36, 81]. As these two techniques provide complementary information, a chemical processing control system may consist of both. However, spectroscopy techniques are expensive, and incapable in on-line operation for opaque chemical products. Therefore, ultrasonic systems that can be employed to monitor and/or characterize the reaction, particularly for opaque materials, are of interest to industry. Importantly, it can be applied in a non-invasive configuration, is relatively inexpensive and can provide real-time monitoring information, especially if this technique is based on determining a chemical product's formulation differences rather than on the product's physical properties' differences.

This Chapter concerns the application of active ultrasonic monitoring for high throughput technologies (HTT) products, like, shampoo and conditioner products. In the manufacturing process, samples of the HTT product are tested at several stages in the production line. These provide valuable information on the quality and consistency of the product. This work investigates the potential of using active ultrasound in a backscattering configuration[82], as discussed in Section 2.2.3, for the on-line characterization of such HTT products.

Prior to the research described in this Chapter, a feasibility study was undertaken in collaboration with Analytical Chemistry, at Strathclyde. In this work, the ultrasonic velocity of the analyzed sample is one of the main measurement parameters and used to characterize the HTT product [83]. However, this approach is not suitable when samples differ in formulation, but are identical or similar in density. The velocity, c in liquid [36, 81] is mainly dependent on density, as shown in Equation 3.1.

$$\boldsymbol{c = \frac{\gamma}{\rho \beta_T}} \tag{3.1}$$

Where γ is the ratio of heat capacities; β_T is isothermal compressibility, and both can be treated as a constant for each material.

Moreover, the accuracy of acoustic velocity is limited by the temperature variation and nonlinear properties of the test samples. A nonlinear response during ultrasound transmission or propagation, distorts the signal's waveform and power spectrum. This influences the sharpness of the signal's rising edges and the position of the maximum peak to peak value, which are usually used to measure the propagation time within the signal of interest.

To address this problem associated with characterization solely based on the velocity measurement, a backscattering configuration combined with spectral analysis techniques has been adopted. Scattering of signals occurs in heterogeneous media, such as suspensions and emulsions. As the ultrasonic wave strikes a discontinuity (e.g. a particle, droplet or gas bubble) it is scattered in different directions from the transmit direction of the incident wave. Backscattering signals can consist of fundamental signals, sub-harmonic and harmonic signals, which may contain information related to particle size, particle concentration and particle material properties. Therefore, this approach has potential in the characterization of chemical products.

In chemical applications, the ultrasound monitoring system is typically applied in a complex environment, in which signals can reflect from the pipe walls, stirrers, and large gas bubbles, increasing noise in the received ultrasonic signals from the system under investigation, which results in low SNR. It is hypothesised that the nonlinear monitoring technique can improve the system SNR through insensitivity to signals from the process which occur in the linear regime, for example, reflections from pipe walls and stirrers. Moreover, the gas bubbles in the sample will have a lower resonant frequency [84] than the excitation frequency of 2.25MHz and hence, scatter the signals linearly in this case.

For this work, the initial experimental configuration uses a commercial ultrasonic immersion transducer with a frequency of 2.25MHz, which was reported as the optimal frequency for ultrasound scattering by examined HTT samples in the preceding feasibility study by Irwin [83], to introduce ultrasonic energy into the sample. The HTT product scatters the propagating ultrasonic energy, which is received by a second transducer orientated at a 90^{o} angle to the axis of the excitation transducer. The detection device is placed directly in contact with the sample. Both linear and second harmonic spectral components have been evaluated by changing the receiving transducer (i.e. conventional

transducers with different operational centre frequencies) and implementing matched filtering data processing of the backscattered signals.

At the beginning of the investigation, a series of experiments were carried out to determine the optimal excitation voltage level for the experimental system established. Next, the ultrasound contrast agent (UCA) was added to the liquid load to verify the experiment setup. UCA's were used as they are a proven ultrasound scattering source typically used in the biomedical field. By changing the UCA concentration, the relationship of the received signal intensities in the fundamental and second harmonic frequency regimes to the UCA concentration was determined.

With the experimental setup established, measurements of the ultrasonic backscattered signals produced by a HTT product were carried out and the results analysed. The concentration level of the HTT product was varied from 20 % to 100 % to investigate the relationship between viscosity, density and the received signal in both the fundamental and harmonic frequency regime. In addition, 4 control samples of HTT product from the pharmaceutical industry were examined to investigate whether the formula of product affects the scattered signal response.

In the initial stages, commercial 2.25MHz and 5 MHz Panametrics transducers were used to collect the fundamental and second harmonic signals respectively. It was considered that there were problems with repeatability between experiments when the transducer was swapped. Hence, to improve the robustness of the experiment, a dual frequency transducer was designed to simultaneously acquire at both 2.25MHz and 4.5MHz for the backscattering configuration to minimize uncertainties in the acquired backscattering results. Hence, by using a 2.25MHz transmitter, this dual frequency device was able to collect both the fundamental and second harmonic scattered components simultaneously during the same experiment. Good correspondence between the single frequency mode transducer results and the dual mode transducer results will be shown in this Chapter.

3.2 HTT hair conditioner and shampoo

Shampoo and hair conditioner [85] are typical examples of high throughput cosmetic products. The first produced shampoo contained naturally-derived surfactants, which is similar to soap. The first modern shampoo with synthetic surfactants appeared in 1930s. Shampoos now usually combine a surfactant with a co-surfactant, and other ingredients like salt (sodium chloride) vitamins and amino acids, etc. Hair conditioner has a longer history. Natural oils, like tea tree oil and jojoba oil, were used in earlier conditioner products. Modern hair conditioners are now based on silicone, fatty alcohols and quaternary ammonium compounds. Both hair conditioner and shampoo are emulsions contain small particles and droplets that can be considered as potential ultrasonic scattering sources.

In this Chapter, four industrial samples of conditioner and shampoo products produced from a high throughput process were used to evaluate the potential of ultrasonic monitoring techniques based on an ultrasonic backscattering system approach. These samples represent two formulations each of conditioner (CondA and CondB) and shampoo (ShampA and ShampB), with each subset having the same density, but differing in the molecular weight of the polymers used in the formulation. Table 3.1 provides descriptions of these 4 HTT samples. In addition, a commercial hair conditioner was diluted with distilled water to expand the backscatter experimental programme. Concentration levels from 20% to 100% in 20% increments were used.

Table 3.1 *Details of HTT samples provided by Unilever*

Sample name	Sample description	Additional details
CondA	White, opaque, viscous liquid.	Hair conditioner sample supplied by industry; has the same density as Conditioner B, but due to differences in formulation, contains different molecular weight polymers.
CondB	White, opaque, viscous liquid.	Hair conditioner sample supplied by industry; has the same density as Conditioner A, but due to differences in formulation, contains different molecular weight polymers.
ShampA	White, opaque, viscous liquid.	Shampoo sample supplied by industry; contains a higher molecular weight polymer than in Shampoo B.
ShampB	White, opaque, viscous liquid.	Shampoo sample supplied by industry; contains a lower molecular weight polymer than in Shampoo A.

3.3 Preceding Foundation Work

In this Section, the initial feasibility study carried out by a MSC student, Irwin[83], is described. She used a through transmission configuration to compare the acoustic properties of samples, e.g. velocity and attenuation, to evaluate the potential of through transmission configuration in the characterization of HTT products.

3.3.1 Experimental setup

A through transmission configuration experiment was designed based on time measurement and attenuation measurements, as illustrated in Figure 3.1. Here, two transducers have been used in a water bath, with the sample under test inserted into the water. The signal propagation time from the excitation transducer to the receiving transducer was measured and the velocity of sound in the load medium calculated using:

$$d_{total} = t_{water} \times c_{water} + t_{sample} \times c_{sample} \tag{3.2}$$

Where, d_{total} is the total distance travelled by the ultrasound wave, t_{water} is the time transmitting in the water, c_{water} is the sound velocity of water, t_{sample} is the time transmitting in the sample and c_{sample} is the sound velocity of the sample. This approach has ignored the propagation through the wall of the sample bottle. Although, this would introduce an error in the results, it is not critical for this Thesis as this work is included only to provide the reader with an appreciation of preceding research in this area.

As the transmitting time in the water path is fixed, the sound velocity in the sample can be calculated. Note, in this work, only time domain signals were analysed.

For the attenuation measurement, the receiving intensity *I* can be used as follows:

$$I = I_0 e^{-(\alpha d + \beta y)} \tag{3.3}$$

where, I_0 is the initial ultrasound intensity, α is the attenuation coefficient in water, d is the transmitting distance in water, β is the ultrasound attenuation coefficient in the sample and y is the transmitting distance in the sample.

In these experiments, α, d and y are constants; therefore, the receiving signal's intensities were directly related to the attenuation coefficient in the sample.

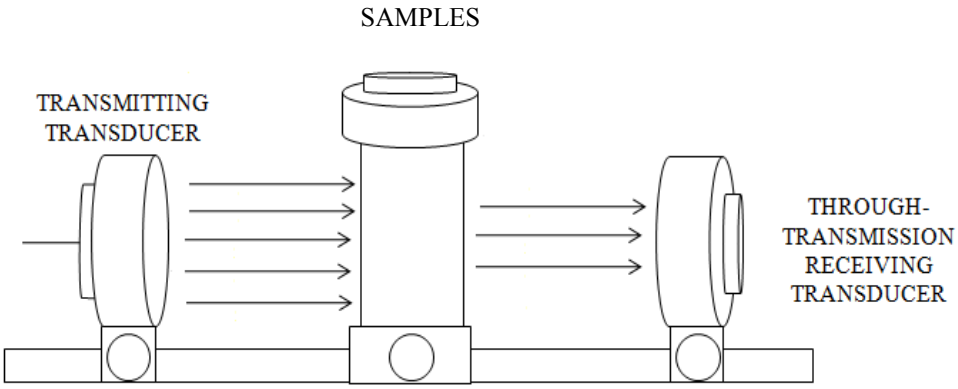

Figure 3.1 *Through transmission configuration used in the feasibility study*

For this work, the transducers and sample bottle were submerged in water. A tone burst signal of 10 cycles with the frequency of 2.25 MHz, weighted using a hamming window, was generated by an Agilent 33250A function generator to excite the transmitting transducer. Ultrasound then propagated through the water bath and sample to be collected by the receiving transducer positioned in the same axis as the transmitting device, as illustrated in Figure 3.1. The received signals were digitalized and stored in a PC. The PC also controls the system and is used to synchronize the excitation and data collection operations. By analysis of the signals, information such as the maximum peak to peak value positions and attenuation rate were acquired.

In this through transmission configuration, signals were collected with a sampling rate of 100MHz and a time widow of 200 us. An example time domain signal is shown in Figure 3.2. In this Figure, the maximum peak value I_{max} and arrival time of this peak value t_{max} are illustrated. These parameters are extracted from the time domains signals and used to determine velocity and attenuation associated with the sample under investigation.

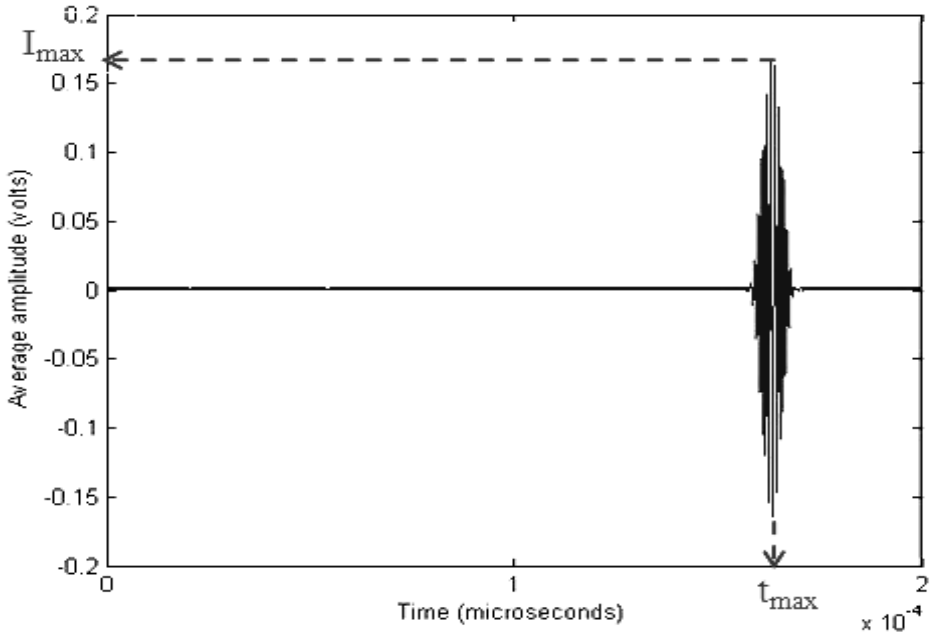

Figure 3.2 *Typical time domain received signal from through transmission ultrasonic system used in feasibility study*

3.3.2 Experimental results

As described previously, both transmitting and receiving transducer have a centre frequency of 2.25MHz and the ultrasonic intensity I_{max} and transmitting time t_{max} were investigated to provide characterization information related to HTT products. The obtained results for I_{max} and t_{max} are shown in Tables 3.2 and 3.3 respectively. Table 3.2 confirms that CondA and CondB have a similar sound velocity, and ShampA and ShampB have the same sound velocity. As known, the conditioner and shampoo have different density, and it is shown that by using the t_{max} parameter it is not possible to classify the samples using this approach. Table 3.3 displays the results in terms of attenuation and shows that the samples also have similar attenuation.

Table 3.2 *t_{max} results for testing sample bottles using 2.25 – 2.25 MHz*

Conditioner	CondA	CondB
Mean t_{max} (s)	1.611×10^{-4}	1.612×10^{-4}
Standard Deviation (s) (n = 10)	3.521×10^{-8}	3.689×10^{-8}
Shampoo	ShampA	ShampB
Mean t_{max} (s)	1.607×10^{-4}	1.607×10^{-4}
Standard Deviation (s) (n = 10)	3.950×10^{-8}	4.332×10^{-8}

Table 3.3 *I_{max} results for testing sample bottles using 2.25 – 2.25 MHz*

Conditioner	CondA	CondB
Mean I_{max} (a.u.)	0.7623	0.7504
Standard Deviation (n = 10)	2.062×10^{-2}	2.058×10^{-2}
Shampoo	ShampA	ShampB
Mean I_{max} (a.u.)	0.7129	0.6982
Standard Deviation (n = 10)	1.027×10^{-2}	1.654×10^{-2}

3.3.3 Discussion

For this through transmission configuration, it was difficult to distinguish each sample of product, due to the measurement of similar density and velocity parameters. This is because the associated velocity and attenuation parameters are mainly related to the product's density and viscosity. From the attenuation results in Table 3.3, it may be possible to classify these products, but the difference is small and would be unreliable in a practical industrial application.

3.4 Backscatter experimental set up and data processing

3.4.1 Experimental set up

An alternative approach to the MSc feasibility study was undertaken to investigate a novel ultrasonic system for the characterization of HTT products. This entailed a change in the system configuration to a backscattering approach, with the backscatter at the fundamental and second harmonic frequencies considered for their potential to inform the process control system.

In this backscatter experiment, a linear chirp signal, whose frequency was varied from 1.75MHz to 2.75MHz, was used as the excitation signal for a 2.25MHz Panametrics ultrasonic transducer. This wideband signal was selected to improve the system response from the sample and accommodate variation in particle size. This excitation signal was generated by an Agilent 33250A arbitrary function generator (AFG) and subsequently amplified by a 50dB power amplifier. In this scenario, the operating frequency of the receiving transducer was 2.25MHz or 5MHz to enable analysis at fundamental and second harmonic frequency regimes, respectively. The received signals were pre-amplified and digitalized by a PC. The test tank is filled with water, with the transmitting transducer (TX) placed into the water bath and the reception device (RX) located in contact with the sample under investigation at the top of the sample bottle. Thus the backscattered signals were collected at an angle of 90^{o} to the incident ultrasonic energy, as shown in Figure 3.4. Thus, the receiving device will not detect any of the through-propagation signals, but only the scattered signals due to the HTT product itself.

The sample bottle has been positioned at the near/far field boundary of the transmitter to maximize the energy within the sample based on the near field equation, which is given at Equation 3.2. The corresponding pressure field prediction, based on Huygens – Fresnel principle [86], is illustrated in Figure 3.3. This Figure was produced by measuring the transducer surface displacement using a scanning laser vibrometer (Polytec OFV 056), which was then used as the input to a Matlab implementation of Huygens–Fresnel principle.

$$N_F = D_r^2/4\lambda \tag{3.4}$$

where N_F is the near field length, D_r is the diameter of the transducer, and λ is the wavelength of ultrasound.

Using Equation 3.2, the near/far field boundary should occur at 84 mm. This is corroborated by the pressure field prediction shown in Figure 3.3. Using this information, the sample was located 85 mm from the transmitting transducer, at the position of maximum energy. Figure 3.4 illustrates the experimental set up in both image and block diagram formats.

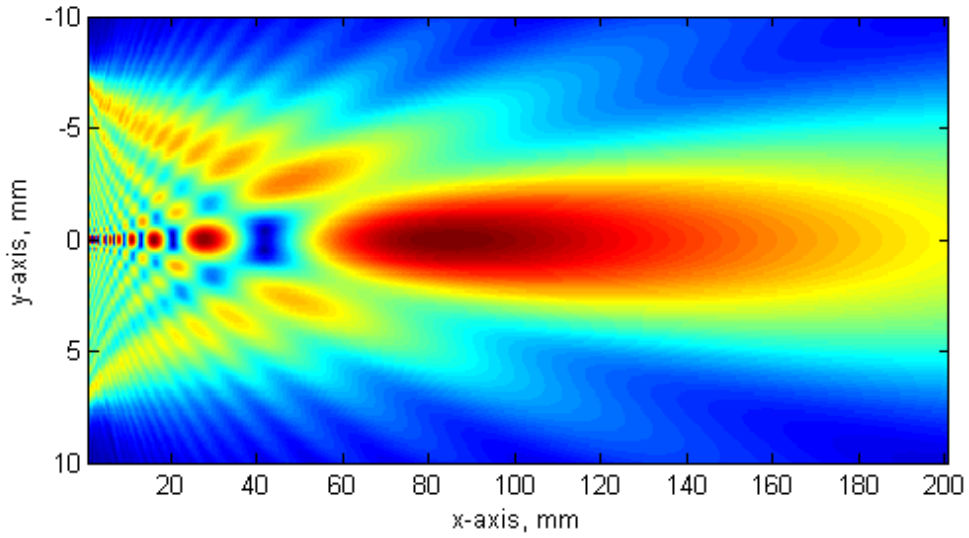

Figure 3.3 *Pressure field prediction for the Panamterics 2.25 MHz transducer*

3.4.2 Data processing

For this work, linear chirp signals were used to excite the transmitting transducer and the received backscattered signals were analyzed using Matlab functions. Fast Fourier Transform (FFT) and matched filtering signal processing techniques were applied to extract information from the received backscattered ultrasonic signals at the relevant frequency band: either fundamental frequency or second harmonic dependent on whether the linear or nonlinear response was being considered, as illustrated in Figure 3.5. Matched filtering is a cross-correlation technique and requires modification of the

‘original’ chirp waveform to match the desired frequency band, as described in Section 2.5, if the desired frequency range differs from the original excitation waveform.

In order to compare the effectiveness of these various transducer combinations and experimental conditions, the area under a user defined frequency range in the processed received signals spectrum was used to determine the backscattering power associated with each ultrasonic technique. To simply the calculation, for the fundamental signal, the area is the integration of each point value in the window from 1.75 to 2.75 MHz, which is the bandwidth of the transmitted chirp signal; and for the second harmonic signal, the signal intensity is the integration of each point value from the 3.5 to 5.5 MHz as illustrated in Figure 3.5. Also, to improve the SNR and the reliability of the acquired datasets, the measurement was collected 10 times and the corresponding frequency spectra averaged.

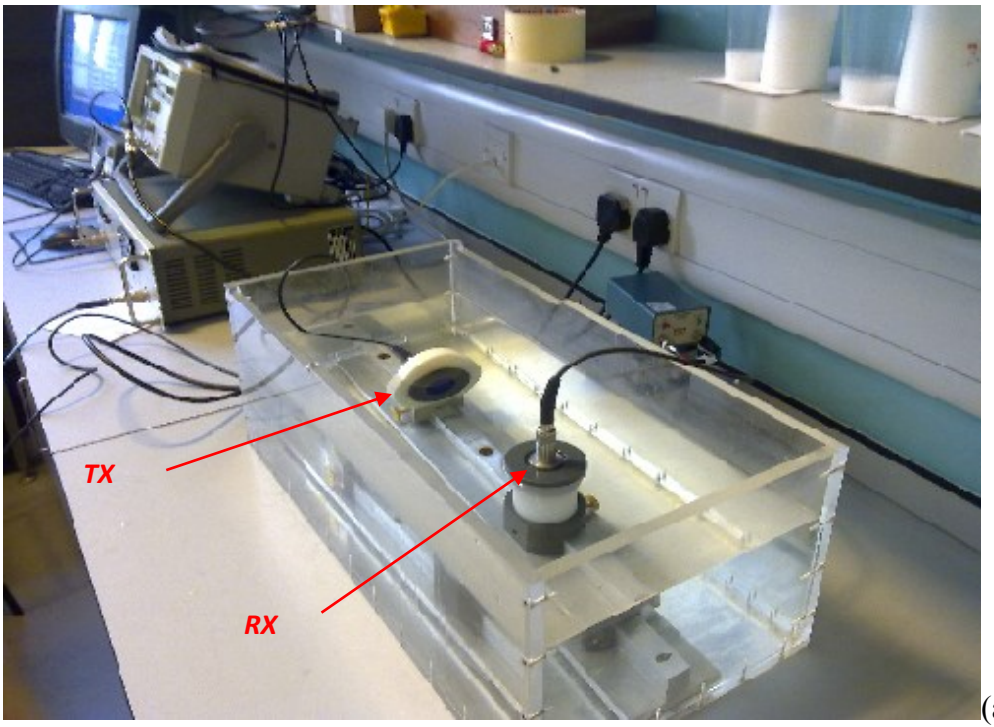

(a)

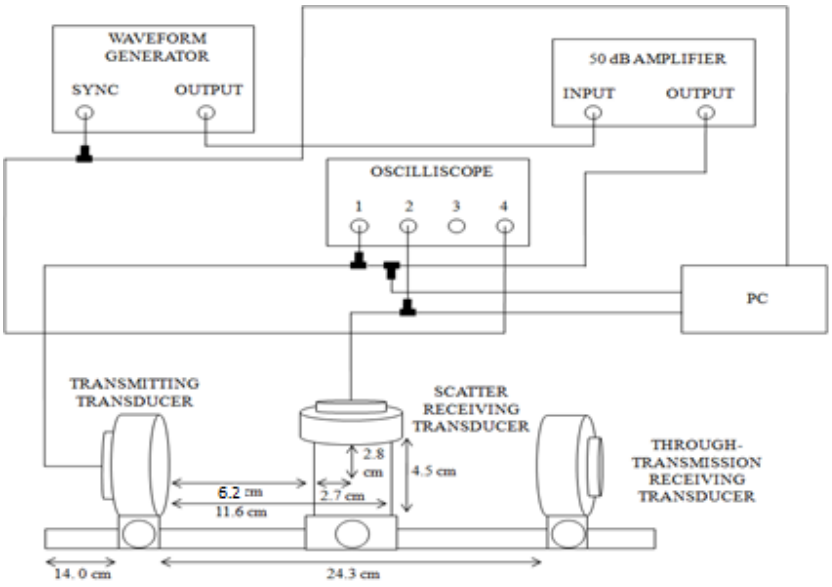

(b)

Figure 3.4 *Backscatter experimental configuration (a) actual implementation; (b) CAD representation*

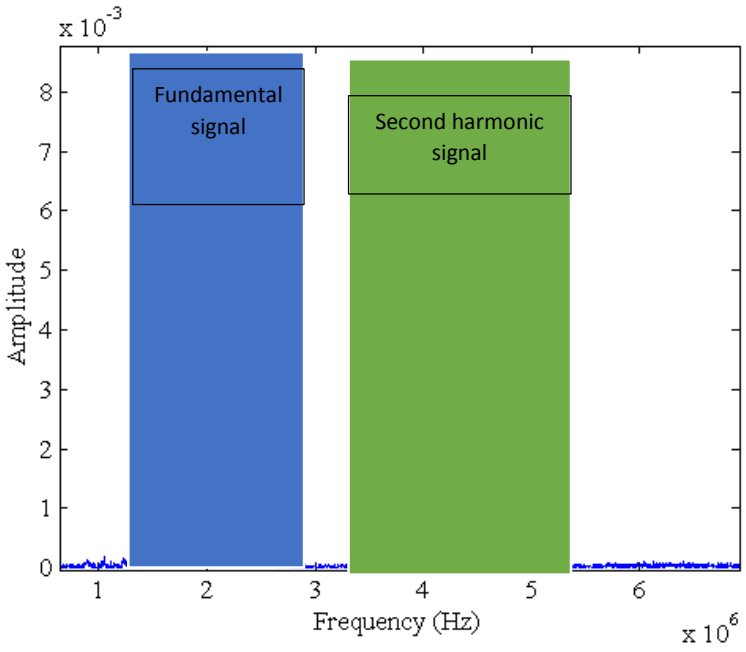

Figure 3.5 *Match filtering processed spectral characteristic showing both fundamental and second harmonic components*

3.5 Dual mode transducer design and manufacture

The analysis of the ultrasound signals was carried out in the frequency domain using the fundamental and second harmonic signals. Therefore, the bandwidth of the receiving transducer ideally needs to cover the frequency range from 1.75 MHz to 5.5MHz. Moreover, the shampoo and hair conditioners are highly attenuating media and the receiving transducer was off-axis relative to the propagating wave. Hence, the received scattering signals were low in amplitude. This means in addition to offering wideband operation, high sensitivity was also required from the receiving device. Due to the bandwidth limitation of single frequency mode transducers, the fundamental and second harmonic signals cannot be acquired simultaneously. Hence, the dual mode transducer was designed and manufactured for this purpose. Importantly, the development of this transducer meant that the removal of transducers between linear and nonlinear acquisitions, which interrupts the consistency of the experiment and reduces the experimental repeatability, was not required.

3.5.1 Design and simulation result

A dual mode transducer was designed and manufactured, to enable the monitoring system to collect the fundamental and second harmonic signals simultaneously. The transducer was comprised of separate disk and ring piezoelectric ceramic composite materials, as shown in Figure 3.5, which were fabricated separately. PZFlex (Weidlinger Associates, CA) was used to design both parts and the simulation results are presented later in this Section. The central disk was a 30% PZT5H/ CY1301-HY1300 piezocomposite [87] and was designed with a mechanical resonance frequency of 2.25MHz. The annular ring element was fabricated using the same constituent active and passive materials, but with a 50% ceramic volume fraction. This was designed with a mechanical resonance frequency of 4.5MHz. In the final device, the two composites were separated by Syntactic Acoustic Damping Material (SADM), which has high acoustic damping properties, to minimize cross-talk between the two composite elements. A thin epoxy (Vantico HY1300/CY1301) layer was deposited on the transducer front face to marinise the transducer. The manufacturing details for each device are shown in Table

3.4.

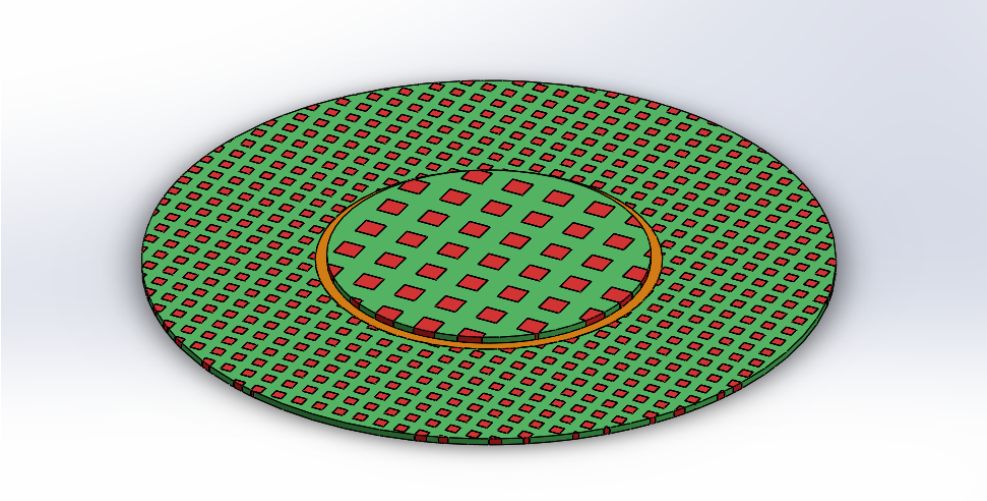

Figure 3.6 *Dual mode transducer configuration*

Table 3.4 *Fabrication details for dual mode transducer*

Mode	Frequency	Saw width	Pitch width	Diameter	thickness
Central disk	2.25 MHz	0.14 mm	0.2 mm	14 mm	0.6 mm
Outer ring	4.5 MHz	0.05 mm	0.1 mm	30 mm-15mm	0.3 mm

A full simulation programme for each design was carried out using the finite element software package, PZFlex. The design criteria were to operate with the mechanical resonant frequency at the appropriate frequency (2.25MHz for the central disk and 4.5MHz for the outer ring) and exhibit uni-modal operation at the fundamental thickness resonance mode. The results for the selected piezocomposite configurations are shown in Figure 3.7.

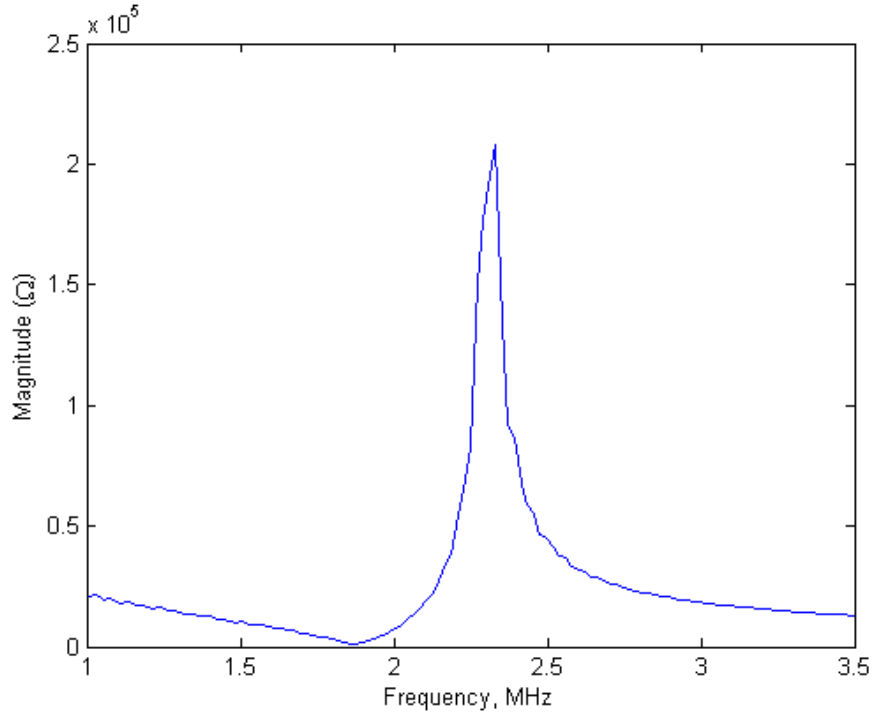

(a)

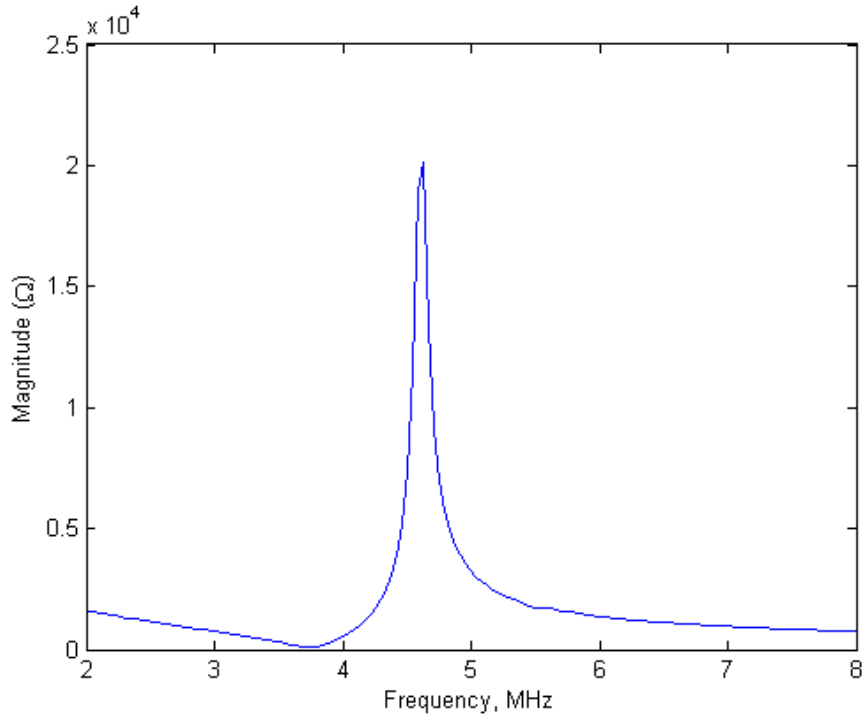

(b)

Figure 3.7 *Predicted electrical impedance for both devices utilised in the dual mode transducer, (a) 2.25MHz probe and (b) 4.5MHz probe*

3.5.2 Transducer fabrication

Figure 3.8 shows the two piezocomposite devices incorporated into a steel cylindrical housing. After this stage, a lid was bonded onto the back of the housing and the device fully sealed to ensure it was able to operate in immersion. The measured electrical impedance characteristic of the dual mode transducer is illustrated in Figure 3.9. It is evident that the mechanical resonances of both devices are separated by approximately a factor of two. There are some small parasitic modes in the lower frequency element, Figure 3.9(a), but these were considered a minimal risk to the transducer efficiency when operating as a receiver for this prototype device.

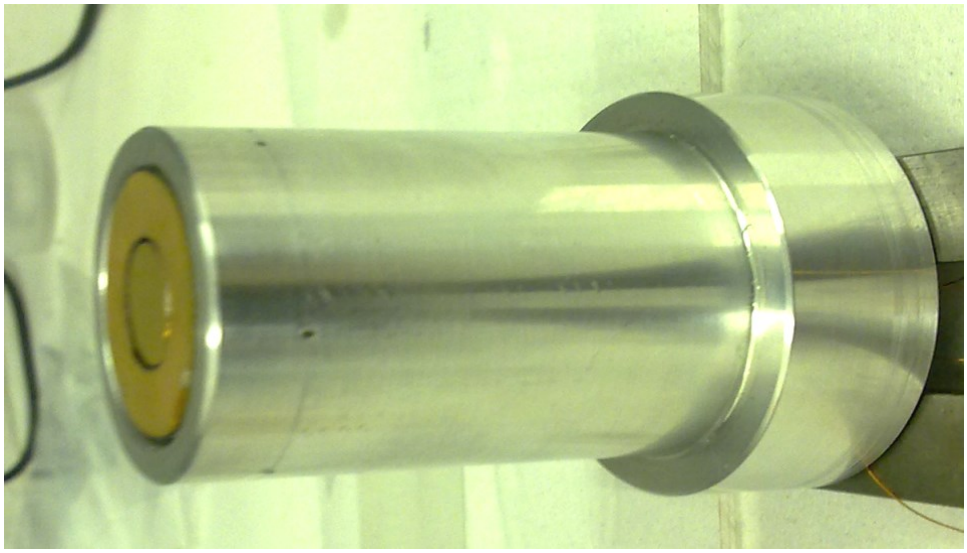

Figure 3.8 *Dual mode transducer during fabrication process*

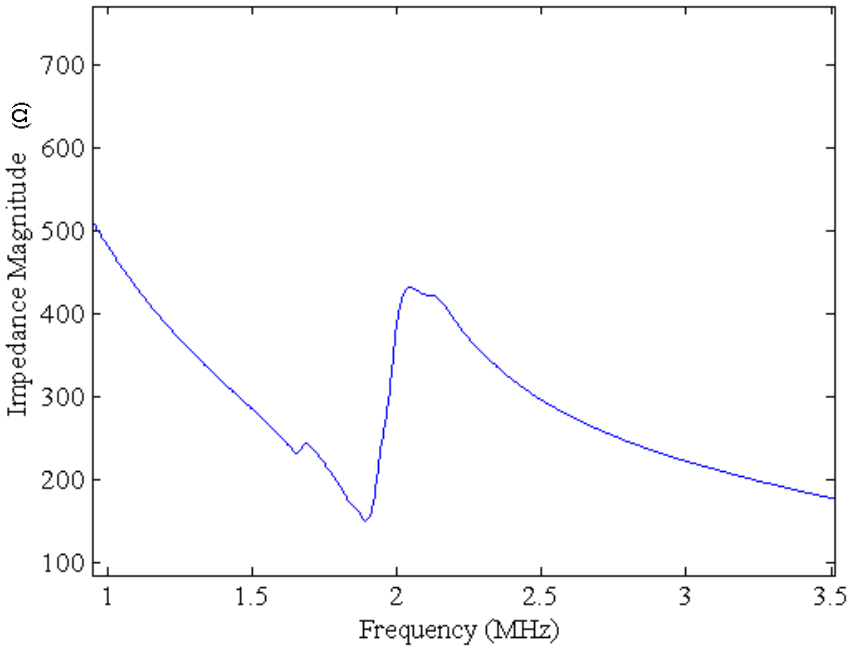

(a)

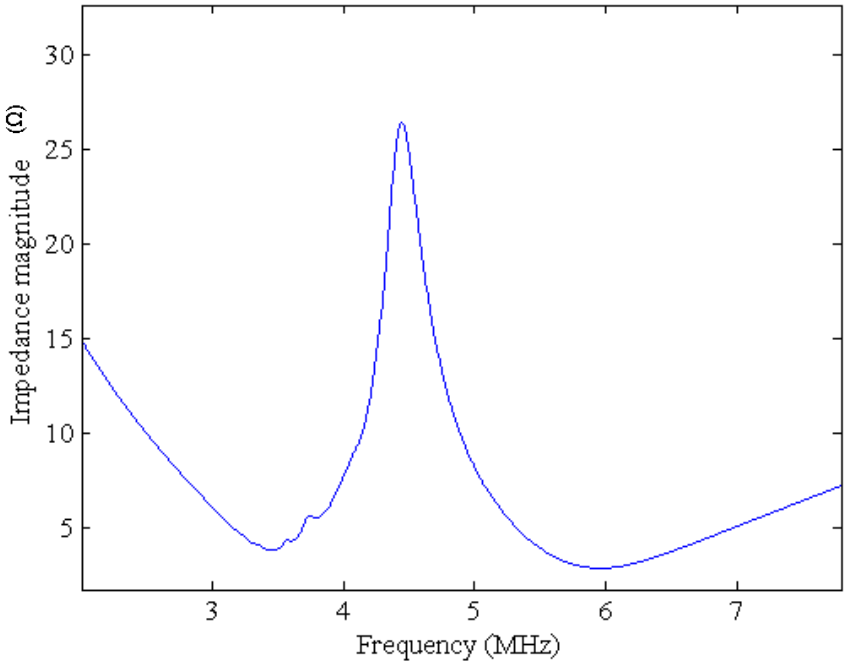

(b)

Figure 3.9 *Measured electrical impedance for both devices utilised in the dual mode transducer, (a) 2.25MHz probe and (b) 4.5MHz probe*

3.6 Experiment results from backscatter ultrasonic configuration

An initial series of experiments were conducted to evaluate the optimum operational parameters for the backscattering experiments. Here, the initial experimental setup has been used, in which commercial Panametrics transducers are used as the transmitter and receiver.

3.6.1 Experimental parameters setup

The initial experimentation was undertaken to evaluate the influence of the excitation voltage, and hence the magnitude of the propagating pressure wave, on the received backscattered energy. The excitation voltages were varied from 0.1V to 1V, on the AFG, which was subsequently amplified through a 50dB power amplifier. The relationship between the voltage generated by the AFG and the voltage delivered to the transducer is presented in Figure 3.10.

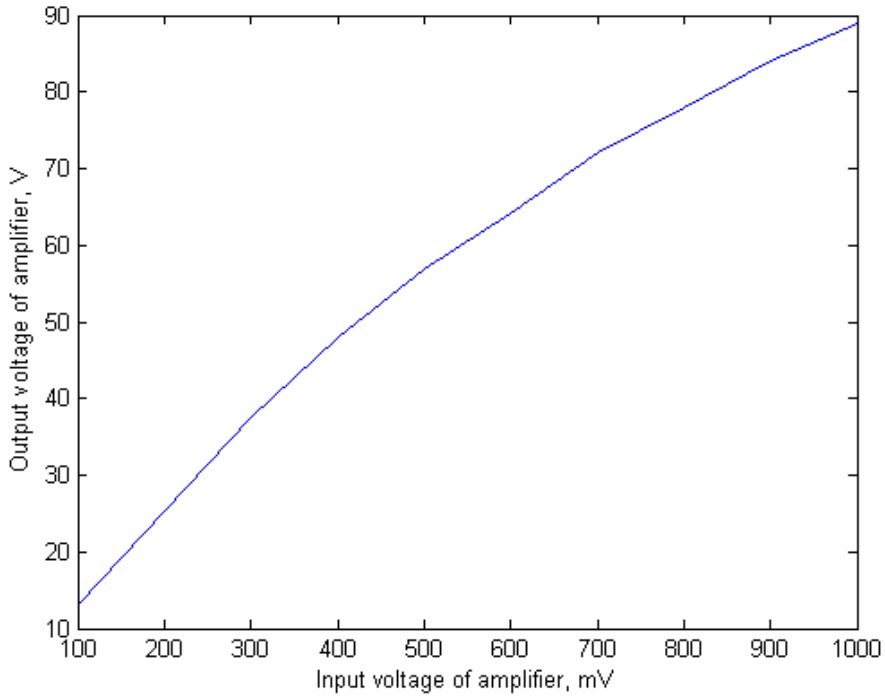

Figure 3.10 *Relationship between AFG voltage and amplified voltage delivered to transmitting transducer.*

Next, the received backscatter signals from a standard commercial hair conditioner was investigated. Each experiment was carried out 10 times and the scattering signals were collected, averaged and analyzed in the frequency domain at both fundamental signal and second harmonic regimes. The signal's intensity under the frequency regime of interest was calculated based on the description in Section 3.3.2. Figures 3.11 and 3.12 display the relationship of fundamental and second harmonic signal's intensities to the variation of excitation power. Please note that the matched filtering technique was not applied in these results. Therefore, these results can reflect the relationship between the signal's intensities and the excitation level directly. But for rest of this Chapter, the matching filtering technique will be used to extract both frequency regimes. From these Figures, the signal's intensities in the fundamental frequency regime is 2 orders larger than for signal intensities associated with the second harmonic frequency region. However, the second harmonic signals increase more dramatically in higher voltage from 500 mV to 900 mV. In the remaining experimental results, the voltage level of 800 mV was used as this was attributed to reasonable performance in both frequency regimes of interest.

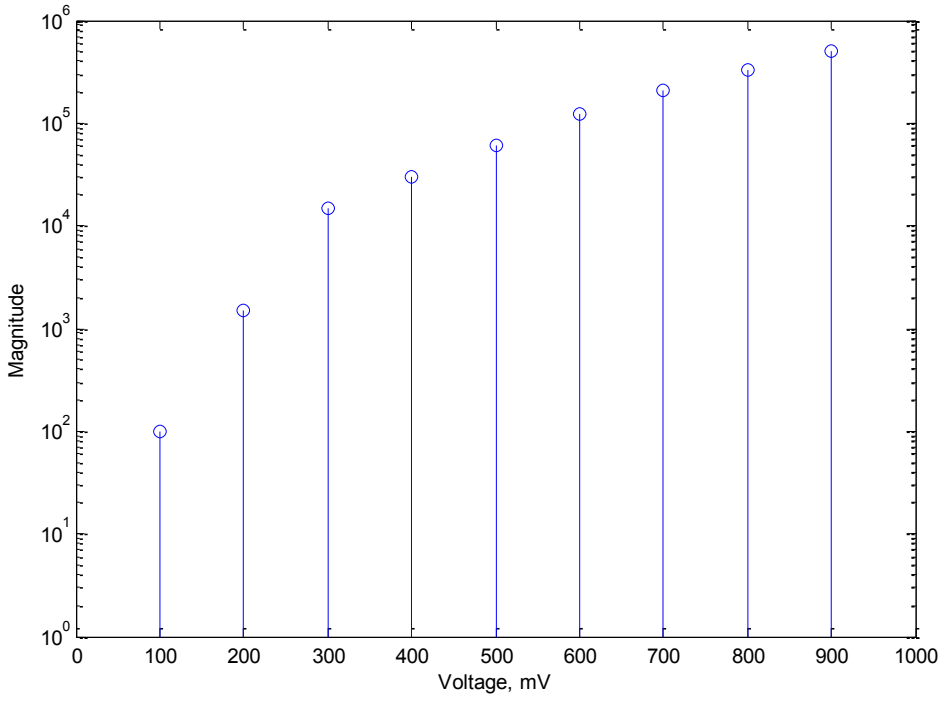

Figure 3.11 *Measured scattering energy at the fundamental frequency regime as a function of excitation voltage*

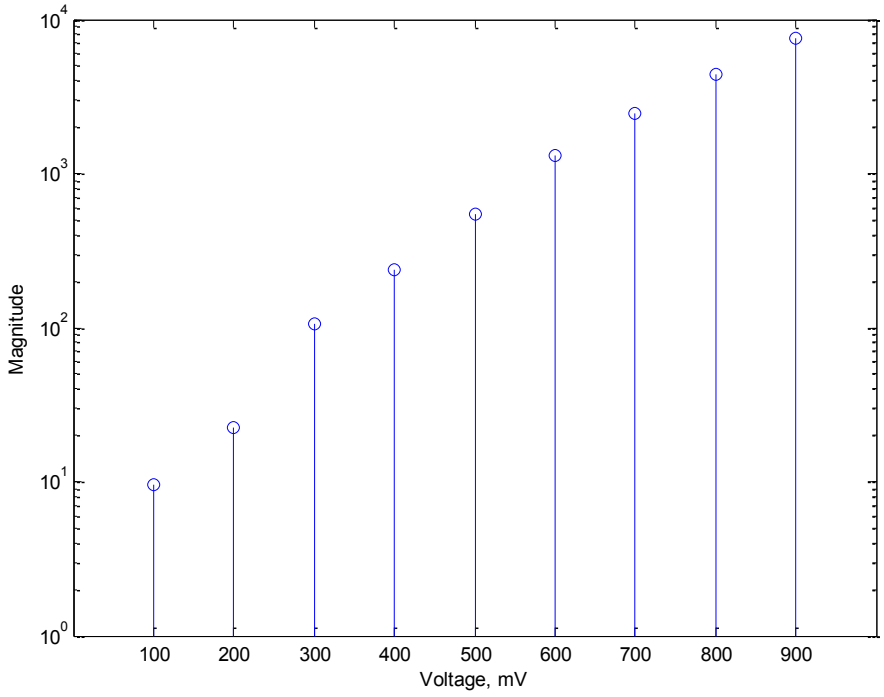

Figure 3.12 *Measured scattering energy at the second harmonic frequency regime as a function of excitation voltage*

3.6.2 Investigation into the influence of sample concentration

3.6.2.1 Ultrasonic contrast agent concentration level experiment

Ultrasonic contrast agent suspensions can be an ideal source for both fundamental and nonlinear scattering phenomena [11]. This experiment was designed to provide confidence in the ability of the backscattering system to measure concentration levels for both the linear and harmonic regimes. The ultrasound contrast agent is diluted with distilled water to the following concentration levels: 0.0045 mg/ml, 0.012mg/ml and 0.0225 mg/ml.

The experiment results presented in Figures 3.13 and 3.14 indicates that both fundamental and second harmonic scattering energy at the concentration level of 0.012mg/ml is enhanced compared to the other concentrations. Intuitively, it was expected that the scattered energy would increase further at the highest concentration level, but the increased attenuation in this sample has impeded the propagation of the backscattered sound to the receiving transducer. Also, there is scattering energy from

distilled water alone. This indicates that the system has a small background noise, due to the water containing a small amount of gas bubbles and particles. Moreover, it should be noticed that the signal's intensities from the fundamental frequency regime is significant larger than the second harmonic signals.

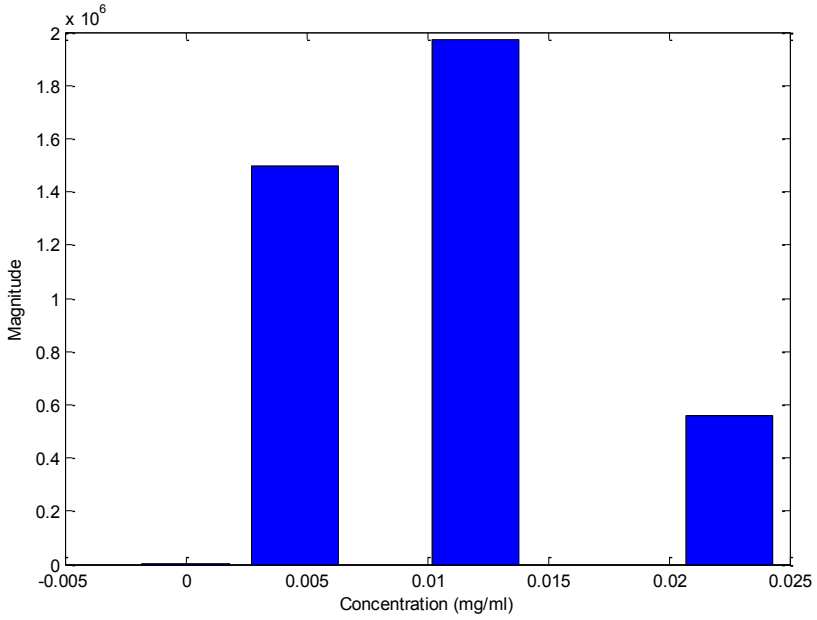

Figure 3.13 *Energy calculated at the fundamental frequency regime for backscattering from UCA concentrations*

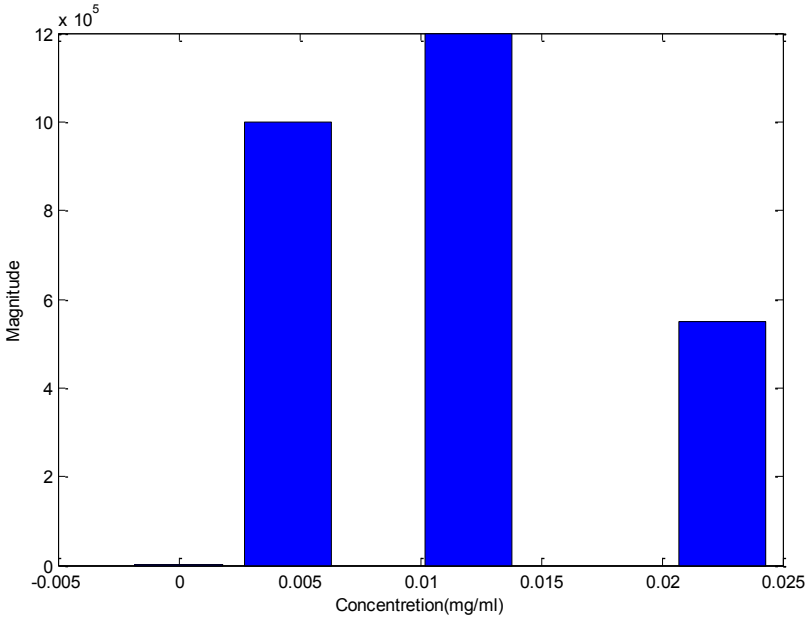

Figure 3.14 *Energy calculated at the second harmonic frequency regime for backscattering from UCA concentrations*

3.6.2.2 Single frequency mode transducer in hair conditioner concentration level experiment

The initial processed results for backscatter energy as a function of concentration of a commercial conditioner product using the Panametrics transducers as the receiver are shown in Figures 3.15 and 3.16. Here, the concentration of conditioner was modified using distilled water. Analysing the area under the frequency spectra associated with both the linear and second harmonic frequency regimes produced similar results, with the maximum power calculated for conditioner concentrations between 40% and 60%. Again, the fundamental signal intensities are much larger than those produced by the second harmonic signals.

3.6.2.3 Dual mode transducer in hair conditioner concentration level experiment

To address the issue of repeatability when the receiving transducer is changed for every linear and nonlinear measurement, a single device with two operating frequencies has been designed (Section 3.5). Replacing the commercial receivers with this device and repeating the experiment with the concentration level of a hair condition product as the experimental variable produced the results shown in Figures 3.17 and 3.18. The linear (Figure 3.17) and nonlinear (Figure 3.18) results acquired by the dual mode transducer show good consistency in the profile of the calculated power. It is clear that the fundamental signal's intensities are much larger than the second harmonic signals, but both the fundamental and second harmonic signals demonstrate a similar trend, with both techniques peaking between 60-80% concentrations.

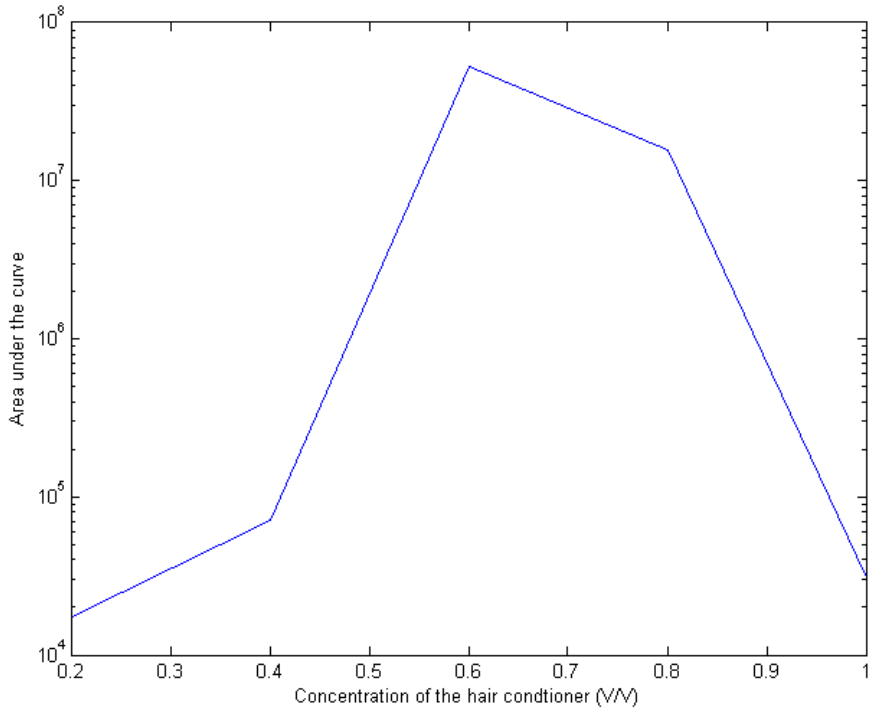

Figure 3.15 *Calculated backscattered power at the fundamental frequency as a function of hair conditioner concentration*

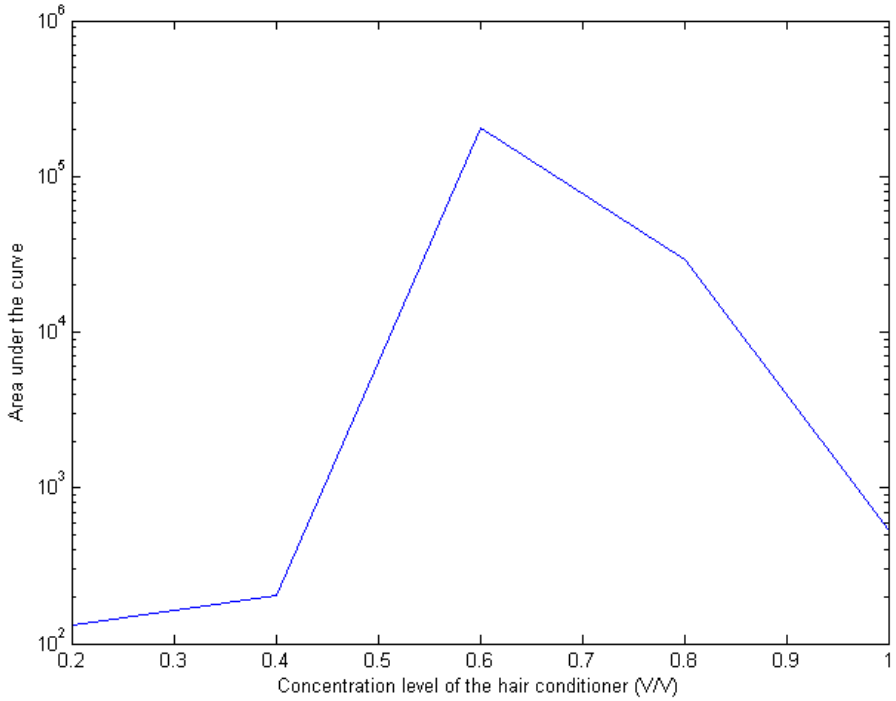

Figure 3.16 *Calculated backscattered power at the second harmonic frequency as a function of hair conditioner concentration*

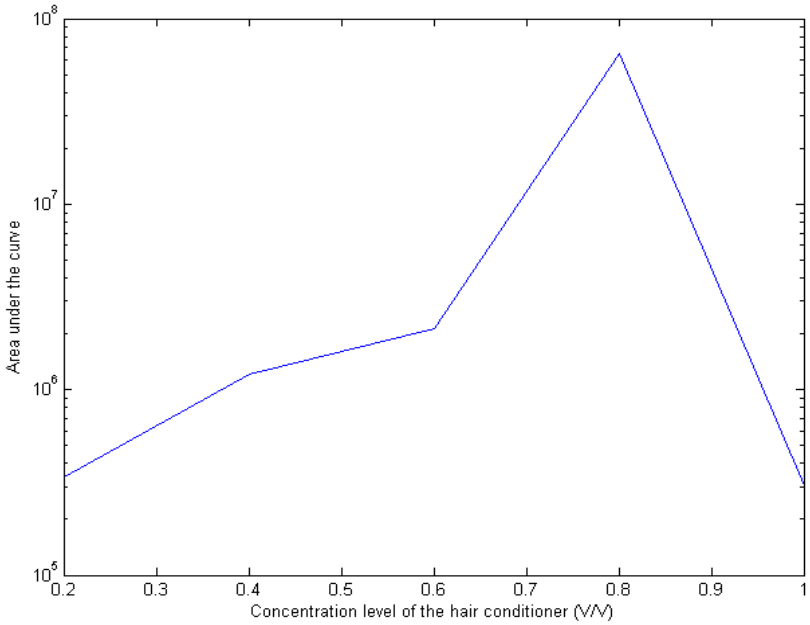

Figure 3.17 *Calculated backscattered power using 2.25MHz element from dual mode transducer as a function of hair conditioner concentration*

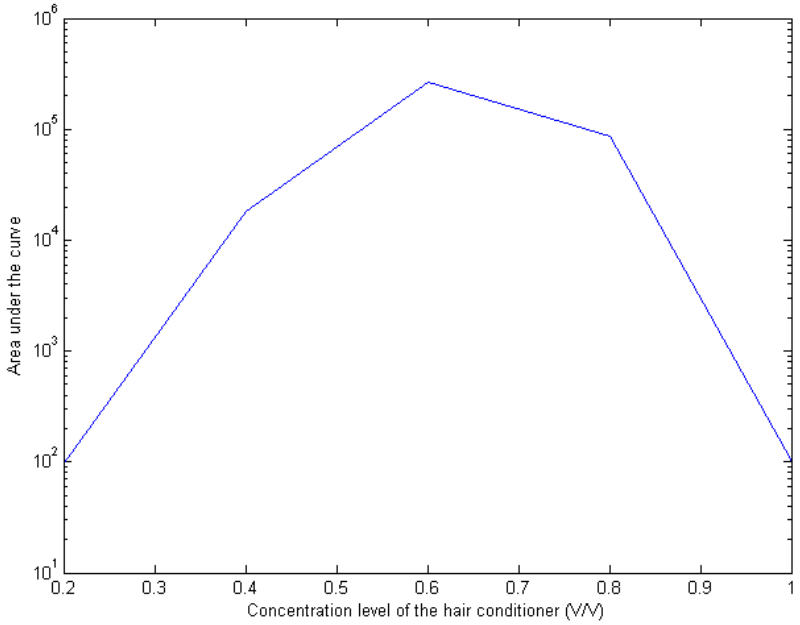

Figure 3.18 *Calculated backscattered power using 4.5MHz element from dual mode transducer as a function of hair conditioner concentration*

3.6.3 HTT product results

The final experimental test used the four industrial samples, comprising two samples each of conditioner and shampoo. As stated in Section 3.2, these sample pairs were similar in density, with different molecular weight particles used in the fabrication process. Both ultrasonic backscattering system approaches were used to evaluate these samples: commercial ultrasonic reception devices; and the dual mode device. In all cases, 10 datasets were recorded and averaged into one result and this process repeated three times.

First the single frequency mode transducers 2.25MHz and 5MHz were applied and the signals were collected in both linear and second harmonic frequency regimes. The results are presented in tabular form in Table 3.5. Interestingly, the data could be used to discriminate between CondA and CondB using data from the fundamental frequency regime, while both frequency regimes show clear differences between the shampoo samples.

Table 3.5 *HTT product results using single frequency mode transducers in the experimental configuration*

Conditioner	CondA	CondB
1st	5.3E6	1.3E6
2nd	472	428

Shampoo	ShampA	ShampB
1st	4.0E5	1.1E6
2nd	23539	15821

When the receive transducer was changed to the dual mode device, both frequency regimes were collected simultaneously. The processed results are shown in Table 3.6. Interestingly, with these results it would be possible to distinguish between the sample pairs. A number of different analytical approaches could be used to differentiate between these samples, for example a straight-forward comparison of energy in either regime or the ratio of energies in each regime.

Table 3.6 *HTT product results using the dual mode transducer in the experimental configuration*

Conditioner	CondA	CondB
1st	2.4E10	4.0E9
2nd	29727	50372

Shampoo	ShampA	ShampB
1st	4.5E9	7.7E5
2nd	96075	174305

3.7 Discussion

In this Chapter an ultrasonic backscattering configuration has been applied to characterize HTT products. Two experimental approaches have been used to investigate the potential of combining both linear and nonlinear spectral domain signals for the characterization of HTT products, with some differences in the measured results. The initial experimental programme used single frequency mode transducers and produced a reasonable set of results which demonstrated potential for classification of different HTT product samples. The dual mode transducer was produced to improve the reliability of the technique by simultaneously acquiring both the linear and nonlinear spectral components. The results from the dual mode transducer with the actual HTT product samples were consistent with the initial results in the fundamental frequency regime. Moreover, results from the dual mode transducer showed promise in classifying the product quality in the second harmonic frequency regime. This inconsistency was possibly caused by differences in the centre frequency between the single frequency mode transducer and the dual mode transducer, which are 5 MHz and 4.5 MHz respectively.

Interestingly, the concentration results, using the UCA as the scatter material, show that the backscattering power could be reduced due to increased attenuation in highly concentrated samples. This may introduce a maximum concentration for which this monitoring approach can be operated.

During the experimental work, it was found that the repeatability of the concentration experiment was limited by the sample preparation procedure. The mixing between conditioner and distilled water introduced bubbles. Especially for the high conditioner concentration sample, the bubbles could be trapped and proved difficult to remove. From Figure 3.17, the scattering power was out of the normal range in the fundamental frequency at 80% of concentration. This has a different trend to the result of the single frequency mode transducer. The different aperture size of transducer is considered as the main cause for this difference. The 2.25 MHz frequency mode element of dual mode transducer has the diameter of 14 mm, which is half of the diameter of the 2.25 MHz single frequency mode transducer. According to Equation 3.2, its near field length is 21 mm, which is quarter of single frequency mode transducer. By using Huygens – Fresnel

principle, the natural focal depth of the 2.25 MHz element of dual mode transducer is 23 mm, which is illustrated in Figure 3.19. As the sample container has a depth of 45 mm, the single frequency mode transducer operated in near field, but the dual frequency mode transducer operated at its natural focusing depth which leads it to be more sensitive to the backscattered signals in the sample. Interestingly, the second harmonic result, shown in Figure 3.18, followed a similar trend to the single frequency mode transducers. This is considered to be due to the relatively large size of the trapped air bubbles compared to the microstructure particle size, which became the dominant source of backscattered signals at the fundamental frequency, but did not significantly affect the second harmonic signal. This is highlighted in the 80% concentration results in Figures 3.17 and 3.18, in which the higher viscosity od the sample has trapped more air bubbles and introduced an increase in the signal amplitude of the linear signal.

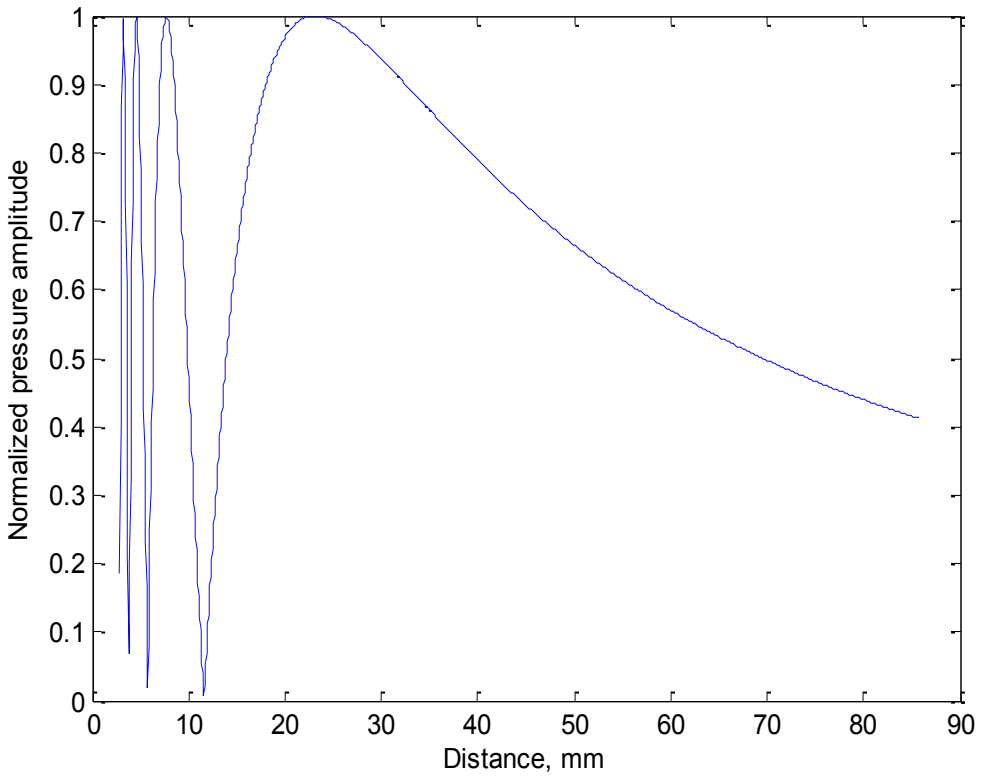

Figure 3.19 *Pressure field prediction for the 2.25 MHz element of dual mode transducer in centre axis*

Overall, this Chapter has described the first ultrasonic system designed to measure both linear and nonlinear backscattered signals from a chemical product. These initial results shown promise for the future development of such systems, but the author concedes that there will have to be significant developmental work to ensure that such a system can be used in a robust and repeatable manner.

Chapter 4

Review of high intensity ultrasound and Sonochemistry

4.1 Introduction

High intensity ultrasonic energy, which produces heat, cavitation and streaming effects, is utilized in many industrial applications, such as vessel cleaning, ultrasound welding, and Sonochemistry [13, 88-90]. Research has been carried out from early last century and has rapidly developed since the 1960s [90, 91]. The propagation of high intensity ultrasound in a liquid medium can have significant nonlinear properties, which are typically negligible for low intensity ultrasound propagation. Cavitation and streaming phenomena occurring within high intensity ultrasonic fields have been well studied in both theoretical and experimental domains [90, 92-95]. The formation, growth, and collapse of the bubble, lead to enormous heat release and emission of a high pressure shock wave to create extreme physical and chemical conditions in the liquid medium. Ultrasound streaming is due to the ultrasonic energy transfer into the form of kinetic energy in the propagation medium, which is closely related to the radiation force – another nonlinear phenomenon associated with high intensity ultrasound. Both phenomena are critical for the scale up of a Sonochemical system.

Sonochemistry was widely employed after the 1980s due to the advent of inexpensive and reliable high power ultrasound transducers, like the Tonpilz configuration [96]. The main mechanism associated with Sonochemistry is the cavitation phenomena generated by high intensity ultrasound. The extreme conditions created by cavitation can enable enhancement of a chemical reaction or provides catalysis for the reaction process. Some excellent review papers or books for Sonochemistry can be found in [29, 30, 96].

In this Chapter, the effects of high intensity ultrasound propagation in a liquid medium, such as cavitation, ultrasound streaming and heat generation are reviewed in Section 4.2. In Section 4.3, the theory of generation of high intensity ultrasound and its application are introduced. Finally, the application of Sonochemistry and the associated equipment, such as transducer, power generation circuitry and reaction vessel configuration, are presented.

4.2 Behaviour of high intensity ultrasound in a liquid medium

4.2.1 Ultrasonic cavitation

Cavitation is a nonlinear effect of the high intensity ultrasonic field. It is a phenomenon that refers to the formation, growth and collapse of cavities. A cavity within a high intensity field experiences both rarefaction and compression phases. In the rarefaction phase, the cavity expands because of the negative pressure, potentially becoming several times the original dimension. The next stage is the compression phase, during which, the dimension of the cavity dramatically reduces from its maximum size. This oscillation continues and the bubble size grows until the bubble finally collapses from the increasing internal pressure.

To rupture a liquid, it theoretically needs at least 10,000 atm of acoustic pressure, however, in experimental results, a liquid ruptures in an ultrasonic pressure field at a significantly lower level [97]. The reason is that in water there are different dissolved substances, such as gas and other particles. A vapour-gas bubble will decrease the local strength of the liquid, and become a nucleation site for cavitation. However, it is difficult to identify the supporting theory of cavitation nuclei, because the large bubble would float up and the small bubbles would dissolve into water. There are 3 hypotheses that try to explain this: the first hypothesis states that the small bubbles contain a film at the surface [98]; the second hypothesis states that the bubbles surface distributes some type of charges, which prevent the bubble dissolving [99]; the third hypothesis is based on the concept of a solid non-wettable particle with a crack filled with an insoluble gas to act as a cavitation nuclei [100], and this latter hypothesis is more in agreement with experimental observation.

The cavitation nuclei under the rarefaction phase experience an expansion process, and compress during the compression phase. By experimental observation, the cavitation can be divided into two categories: inertial cavitation and non-inertial cavitation. For inertial cavitation, and in the rarefaction phase, the bubbles expand larger than the threshold for cavity collapse, which is 2.3 R_0, where R_0 is the original size of the bubbles [101]. This leads to collapse in the compression phase. For the non-inertial cavitation, the bubbles

oscillate between the rarefaction and compression phases. This process can last for several cycles before the bubbles expand larger than the threshold and become inertial cavitation, although it is also possible for the cavitation to develop into a stable pulsation mode. For industrial applications, the inertial cavitation is typically of interest and usually simplified to cavitation. The cavitation collapse can release huge energy in a short time, such as heat, > 1000 ^{o}C, and hydraulic shock waves, with several tens of thousands of MPa. These phenomena gave rise to great interest after World War II for their potential in industrial applications.

4.2.1.1 Cavitation theory

The cavitation can be considered as a function of the amplitude of the acoustic pressure under static conditions. There is a threshold pressure that the cavitation phenomena must exceed, called the critical pressure. Its expression was derived by Blacke from the theory of an equilibrium vapour – gas – filled bubble in a static-pressure liquid [90, 91, 102].

$$\boldsymbol{P_c^v = P_l - P_v + \frac{2}{3\sqrt{3}}\sqrt{\frac{(2\sigma_L/R_0)^3}{P_l - P_v + 2\sigma_L/R_0}}} \tag{4.1}$$

where P_l is pressure in the liquid,

P_v is the vapour pressure, which is a constant parameter under constant temperature,

R_0 is the initial radius of the cavity,

σ_L is cavity surface tension.

Equation 4.1 assumes that the cavity has a spherical surface and is filled with a gas vapour mixture under a static pressure field. Moreover, the cavity dimension is much smaller than the ultrasonic wavelength. In this equation, the critical pressure is independent of frequency. However, cavitation is formed through pulsation under a dynamic ultrasonic field as demonstrated by experimental observation. Therefore, a more accurate mathematical model was needed to describe the behaviour of cavitation.

The Noltingk – Nepppiras equation was developed to describe the dynamic behaviour of the bubble during pulsation [92].

$$R\frac{d^2R}{dt^2}+\frac{3}{2}\left(\frac{dR}{dt}\right)^2+\frac{1}{\rho_L}\left[P_0-P_v-P_m sin\omega t+\frac{2\sigma_L}{R}-\left(P_0+\frac{2\sigma_L}{R_0}\right)\left(\frac{R_0}{R}\right)^{3\tau}\right]=0 \quad (4.2)$$

where P_m is pressure amplitude of ultrasonic field,

ω is the angular frequency,

τ equates to 1 and 4/3 for isothermal and adiabatic pulsations, respectively,

ρ_L is the liquid density,

t is time,

R is the cavity radius.

This equation is not able to be solved in a general form; nevertheless, it is able to be solved numerically. The Noltingk – Nepppiras equation models the pulsation of the bubbles in a dynamic acoustic field with reasonable accuracy. The problem with this equation is that it assumes the surrounding liquid is not compressible and leads to the poor prediction of the final stages of bubble collapse. In the cavity collapse stage, the velocity of the cavity boundary would be near or even larger than the sound velocity, which makes the assumption invalid. Therefore, this equation does not allow accurate determination of collapse velocities and related peak pressures in the cavity. Also, the equation does not account for energy loss, and hence the cavity is undamped in this model.

The Herring – Flinn equation is the improved version of the Noltingk – Nepppiras equation, which introduces the liquid compressibility and viscosity. This equation not only allows adequate determination of stable cavity behaviour, but also enables improved accuracy in the prediction of the collapse velocity and minimum collapse radius of the cavity [95].

$$R\left(1-2\frac{v}{c}\right)\frac{d^2R}{dt^2}+\frac{3}{2}\left(1-\frac{4}{3}\frac{v}{c}\right)\left(\frac{dR}{dt}\right)^2+\frac{1}{\rho_L}\left[P_0-P_v-P_m sin\omega t+\frac{2\sigma_L}{R_0}+\frac{4\eta v}{R}-\left(P_0+\frac{2\sigma_L}{R_0}\right)\left(\frac{R_0}{R}\right)^{3\gamma}\right]+\frac{R}{\rho_L}\frac{v}{c}\left(1-\frac{U}{c}\right)\frac{dP(R)}{dR}=0 \quad (4.3)$$

Where v is the velocity of the bubble boundary,

c is the sound velocity in liquid in the linear approximation,

η is the coefficient of viscosity.

The Herring – Flinn equation is an improvement compared with the Noltingk –

Nepppiras equation; however, when the cavity boundary velocity is larger than the sound velocity in the liquid, the Herring – Flinn equation only provides a qualitative description of the cavity collapse. More effort has been done in the theoretical development to understand the cavitation phenomenon. The Kirkwood – Bethe – Gilmore equation provides a more accurate approximation of cavitation behaviour, especially at cavity collapse [95, 103, 104].

$$\boldsymbol{R\left(1-\frac{v}{c}\right)\frac{d^2R}{dt^2}+\frac{3}{2}\left(1-\frac{v}{3c}\right)\left(\frac{dR}{dt}\right)^2-\left(1+\frac{v}{c}\right)H-\frac{v}{c}\left(1-\frac{v}{c}\right)R\frac{dH}{dR}=0} \tag{4.4}$$

where $H = \int_{P_\infty}^{P(R)} \frac{dP}{\rho_L}$,

P_∞ represents the pressure infinitely far from the cavity,

P(R) is the pressure on the cavity surface on the radius of R.

The reader should be aware that Equations 4.2 to 4.4 cannot be solved in a general form; therefore, the cavitation motion, which includes cavitation as a function of the acoustic field frequency, vibration pressure amplitude, or as a function of cavity size, viscosity and surface tension, etc., is not able to be described completely based on these equations. Nevertheless, qualitative analysis based on numerical solution is still able to be achieved.

From these equations, it has been shown that the bubble pulsation characteristic is related to the acoustic pressure field. If the pressure is smaller than a particular value, the bubble would pulsate nonlinearly without collapse, if the pressure is larger than that value, the bubble would be unstable. Also, it is noticed that the amplitude of stable bubble pulsation will rise, if the frequency of the acoustic field gets close to the resonant frequency of the bubble. From the solution of these equations, the ultrasonic energy transformed into the emitting shock wave can reach tens of MPa according to both experiment and theory, and this collapse can result in localised temperatures of 10,000K [105]. This has been termed a ‘hot spot’ in the liquid medium and this terminology will be used throughout this Thesis.

4.2.1.2 Cavitation experimental investigation

Experiments about cavitation have also been carried out to investigate the relationship between acoustic pressure, acoustic frequency and the initial radius of a cavity. However, the experimental results from different authors are not consistent due to the difficulty in measuring cavitation and the uncertainty of cavitation occurring [90]. The results shown here are included to provide a general idea how the cavitation behaviour changes under the influence of the acoustic field parameters and the effect of the initial radius of the bubbles.

Figure 4.1 shows the influence of the frequency of the acoustic field to the critical pressure of cavitation [22]. Increasing the frequency of the ultrasonic field requires an increased pressure to create cavitation, which is matched to the theoretical prediction by Equations 4.2 – 4.3. This is because the rarefaction phase is longer in the low frequency acoustic signals, which permits the bubble size to increase further over this longer time period and reach the minimum collapse radius.

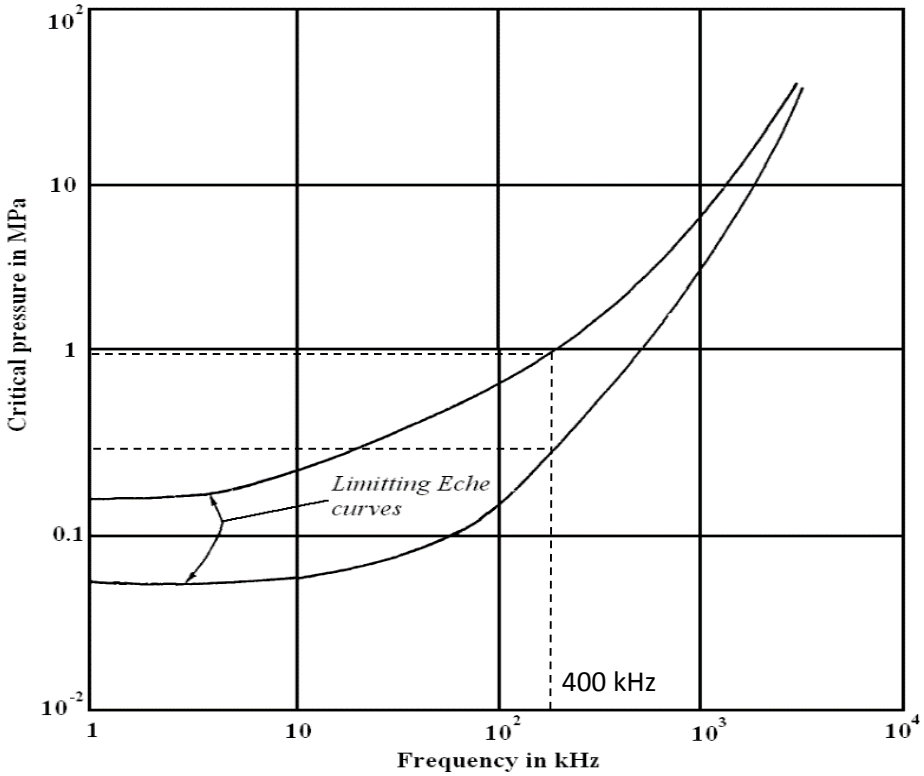

Figure 4.1 *Threshold pressure of cavitation as a function of frequency[106], where the 400kHz frequency utilised in this Thesis is highlighted.*

Experiments using a high speed camera have been carried out capture the process of the cavitation from generation, through growth and finally, to collapse [37, 93]. These experiments observe several types of cavitation. Some cavitation events would break violently and split into several small bubbles; some cavitation would reach the first maximum radius and then release small amount of gas, and then pulsate and grow into the second maximum radius. It was proved that this process can repeat several times before the bubble completely collapses. The stable cavitation with nonlinear pulsation was also observed [90, 107].

The ultrasonic properties associated with a cavitation field have also been investigated. It has been demonstrated that the cavitation field increases ultrasonic attenuation. The generated bubbles scatter the ultrasonic energy from the propagating ultrasound. This is the main cause of the ultrasonic energy decreasing during propagation. The other causes, result in a small amount of energy loss but cannot be ignored. The forming of cavitation, shock wave emission and heat releasing in cavitation collapse, consume the energy which is transformed from the principal ultrasonic energy source [93].

4.2.2 Other effects associated with high intensity ultrasound fields

Nonlinearity is significant in high intensity ultrasound fields, and cannot be ignored during industrial applications. The main phenomena include: cavitation, radiation pressure and streaming. Cavitation is the main mechanism for high intensity ultrasound industry applications. However, the radiation pressure and streaming also accompany high intensity ultrasound. They too significantly affect industry applications, and will be reviewed briefly in this Section.

4.2.2.1 Ultrasonic radiation pressure

During the ultrasonic propagation, a steady ponderomotive force is applied to obstacles in the propagation path and is called the ultrasonic radiation pressure [90, 108]. In the linear approximation, the positive and negative pressures equate to each other and the net pressure would be zero. However, in practice, there are ponderomotive forces on the obstacles, which is in the form of energy conversion associated with the ultrasonic wave kinetic energy. Because the radiation pressure is small compared with the vibration pressure, it used to be neglected. However, in a high intensity ultrasound field, the radiation pressure is detectable and cannot be ignored in a practical implementation.

Radiation pressure is determined by three aspects, the property of the propagating ultrasonic wave, the material properties and the type of obstacle encountered. To be specific, it includes the change of momentum flux of the wave incident on obstacles and the scattered wave's momentum flux, which includes the diffraction of an acoustic wave and the reflective properties of an obstacle. Therefore, radiation pressure can only be calculated in a particular environment with knowledge of the details of the ultrasound field boundary condition and obstacles. The following theories are based on the hypothesis that an ultrasonic beam with finite dimensions is propagating in an unbounded unperturbed medium, which has a constant density without ultrasound attenuation. In this free ultrasonic field, the radiation force within a specific surface is determined by the volume of momentum flux singled out through this surface, and its time-averaged expression is:

$$\boldsymbol{F} = -\oint \bar{\boldsymbol{\Pi}} \boldsymbol{n_v} \boldsymbol{ds} \tag{4.5}$$

where $\bar{\Pi}$ is the time-averaged momentum flux density tensor,

n_v is the vector components of the unit outer normal to the surfaces.

The following is an example of the momentum flux density tensor for an ultrasound wave propagating in x-axis.

$$\bar{\Pi} = \begin{vmatrix} \bar{P} + \overline{\rho v_x^2} & 0 & 0 \\ 0 & \bar{P} & 0 \\ 0 & 0 & 0 \end{vmatrix} \tag{4.6}$$

where $\bar{P}$ average acoustic pressure over a period,

ρ is the density constant of the medium,

v_x is the particle velocity in x direction.

Measurement of the radiation pressure in the ultrasonic field is difficult. The radiation force is three or four orders smaller than the acoustic pressure, and could be easily disturbed by background noise, for example, 'acoustic flows' in a viscous medium and wave reflections.

To simplify the model the following assumptions are adopted: the obstacle exhibits a perfect absorbing property, with its dimensions much larger than those of the ultrasonic beam width, where the beam width is much larger than the wavelength. These assumptions make the diffraction effects negligible. In this case, the ultrasonic wave propagates perpendicularly to a plane and for obstacles with the surface area S the radiation force can be expressed as:

$$\boldsymbol{F = S_A \overline{W}} \tag{4.7}$$

where S_A is the surface area,

$\overline{W}$ is the average power density of the ultrasonic wave.

For obstacles to have a complete reflective property, the momentum flux density must change by a factor of 2, giving:

$$\boldsymbol{F = 2 S_A \overline{W}} \tag{4.8}$$

The theory of radiation forces becomes complicated for arbitrarily shaped obstacles and in this Section the simplest situation is described. Further theory and experimental

reviews can be found in [90, 91].

4.2.2.2 Ultrasound streaming

Ultrasound streaming is another nonlinear effect of high intensity ultrasound. It is stimulated by the radiation pressure, and then develops into a non-uniform acoustic pressure field. The investigation of streaming can be traced back to Faraday's experiment in 1831 and the first theory about streaming flows was produced by Rayleigh in 1900 [109].

The kinetic energy of ultrasound streaming is when the ultrasonic wave energy is absorbed by the transmitting medium. By the law of conservation of energy, the kinetic energy density of ultrasound streaming equates to the loss of the ultrasonic energy. Therefore, for a stationary streaming flow in the x direction:

$$\boldsymbol{\rho v(x)^2 = \overline{W}(0) - \overline{W}(x)} \tag{4.9}$$

where $\overline{W}(0)$ and $\overline{W}(x)$ are the energy densities of the ultrasonic wave at the origin and at point x.

ρ is the density of the transmitting medium,

$v(x)$ is the velocity of ultrasound streaming in point x.

If heat dissipation is taken into account in the viscous medium, the velocity of ultrasound streaming is given in by.

$$\boldsymbol{v = \frac{\Delta P R^2}{4\eta x}} \tag{4.10}$$

where R is the radius of the beam,

η is the viscosity coefficient of the medium

ΔP is the difference of the static pressures between origin and point x.

Equation 4.10 is also called the Poiseuille equation. It explains the ultrasonic streaming from the energy point of view. However, this equation only applies in free field conditions with a linear approximation. Since the ultrasonic streaming is a nonlinear phenomenon, the Poiseuille equation has difficulty describing it in detail. To more accurately model ultrasonic streaming, the following equation based on the hydrodynamic equations of

viscous compressible liquid can be used.

$$\boldsymbol{\rho}\frac{\partial \boldsymbol{v}''}{\partial \boldsymbol{t}} + \boldsymbol{\eta}\Delta\boldsymbol{v}'' - \left(\frac{\mathbf{4}}{\mathbf{3}}\boldsymbol{\eta} + \boldsymbol{\eta}'\right)\mathbf{grad}(\mathbf{div}(\boldsymbol{v}'')) = -\mathbf{grad}(\boldsymbol{P}'') - \boldsymbol{F}'' \qquad (4.11)$$

$$\frac{\partial \boldsymbol{\rho}''}{\partial \boldsymbol{t}} + \mathbf{div}(\boldsymbol{\rho}'\boldsymbol{v}') + \boldsymbol{\rho}\mathbf{div}(\boldsymbol{v}'') \qquad (4.12)$$

where $F'' = \frac{\partial(P'v')}{\partial t} + \rho_0 v' \mathrm{div} v' + \rho_0 (v' \mathrm{div}) v'$,

grad a = ∇a, a = a(x, y, z) ,

div $\boldsymbol{b} = \nabla \boldsymbol{b}$, $\boldsymbol{b} = \boldsymbol{b}(ix, jy, kz)$, *i, j, k* are unit vectors,

∇ is the Hamiltonian $\nabla = i\frac{\partial}{\partial x} + j\frac{\partial}{\partial y} + k\frac{\partial}{\partial z}$,

Δ is the Laplacian $\Delta = \nabla^2 = \frac{\partial}{\partial x^2} + \frac{\partial}{\partial y^2} + \frac{\partial}{\partial z^2}$,

ρ is the density of transmitting medium, ρ' and ρ'' are the first order and second order approximations respectively,

P is the pressure, P' and P'' are the first order and second order approximations respectively,

v is the velocity of ultrasonic streaming, v' and v'' are the first order and second order approximations respectively,

Equations 4.11 and 4.12 are second order approximations from the nonlinear hydrodynamic equation. Ultrasonic streaming is determined by the ultrasonic energy distribution, the medium properties (e.g. shear viscosity coefficient), and the boundary conditions for the hydrodynamic velocity field.

Ultrasonic streaming is also widely applied in industry, for example, cleaning and waste water treatment. Recently, it has also been the applied in the biomedical field, as a biosensor and for drug delivery. Some excellent reviews can be found in [110, 111].

4.3 Sonochemistry

4.3.1 Introduction

The chemical and biological effects of ultrasound were first found early last century [112]. However, the mechanism of chemical effects by high intensity ultrasound was not understood at that time. It was hypothesised not to be from the vibration of the medium during propagation of the ultrasonic energy, because the frequency of ultrasound is normally less than 20MHz, which cannot bring influence at the molecular level. The mechanism of Sonochemistry via cavitation was described in Section 4.2. The collapse of cavities results in a hot spot with elevated temperatures of 5000 ℃ and pressures of 500 atm, which is comparable to the sun's surface temperature and pressure at the deepest ocean areas. The heat released from this process can be the energy source for chemical reactions. It is similar to flame chemistry, which provides thermal excitation to the reaction.

Cavitation occurs in a liquid medium, which involves most chemical reactions, and can be widely applied to enhance chemical reactions. The cavitation activity related to chemical reactions are mainly divided into two categories, homogeneous Sonochemistry and heterogeneous Sonochemistry [15, 113]. Homogeneous Sonochemistry is based on the single liquid phase and heterogeneous reactions are based on liquid – solid or liquid – powder systems. Both mechanisms of ultrasound-assisted chemical reaction are presented in the following sections.

A Sonochemistry system includes an ultrasound source and a reaction vessel. The ultrasound source normally comprises of a transducer and an associated power supply. Traditional ultrasound transducers are mostly based on the magnetostrictive or piezoceramic effects. The mechanoacoutic transducer is rarely applied in Sonochemistry due to its low efficiency and its limitation in achieving high intensity ultrasound. A brief review of ultrasound transducers for Sonochemistry is given in Section 4.3.3. Also, a brief description of the power supply for such ultrasonic devices will also be provided

The reaction vessel is where the chemical reaction happens. For laboratory applications, an ultrasound cleaning bath, which is illustrated in Figure 4.6, and a probe

based system, which is illustrated in Figure 4.7, are the main kinds of reactor systems applied in experimental work. An ultrasound horn can be a critical part of the ultrasound probe system to deliver the vibration from transducer into load. For the Sonochemistry industry, a proper scale up vessel design should be able to maximize the utilization of the ultrasonic power and achieve effective control of temperature and pressure during the reaction process.

4.3.2 Sonochemistry mechanism and application to reactions

Some chemical reaction processes consume huge amounts of energy. Traditional energy sources include heat, light and ionizing radiation. High intensity ultrasound can be used as an energy source for chemical reactions and is known as the field of Sonochemistry. As discussed previously, cavitation is accompanied with enormous heat release and a high pressure shock wave in a local region. Hence, ultrasonic cavitation as an interacting energy in a chemical reaction is characterised by its short lifetime, but high pressure and high intensity energy. These properties enable reactions that require high temperature and high pressure to be carried out in room temperature and low pressure environments [16, 113].

In homogeneous liquids, heat is generated during the cavitation formation and growth process, and in the last stage of cavitation, heat release is much slower than the cavity collapse. Hence, this process produces a short lifetime, localized hot spot and the reaction is enhanced by this hot spot effect of cavitation. To verify the hot spot theory through direct measurement of its transient temperature and shock wave pressure is difficult because of the short lifetime of the energy hot spot, which only lasts several microseconds. Fortunately, it can be indirectly measured. Some chemical reactions only occur with a temperature above a certain level, and their reaction rates are strongly dependent on temperature. Competing unimolecular reactions, which are well studied and used to determine the effective temperature, are one template for cavitation investigation [14, 114]. The experiments were done by Tsang[114], and the experimental results were consistent with theory. As another hypothesis of homogeneous Sonochemistry mechanism, micro-discharge was proposed. This theory states that the internal charge of

bubbles would be rapidly discharged when in a compressing phase, which results in the chemical reaction happening [94, 115]. However, experiment results are not consistent with this theory; therefore, it is treated as a reserved opinion.

The chemical effect of high intensity ultrasound propagating in water has been well studied. Primary products from this process include H_2 and H_2O_2. It also generates other products, such as H_2O^-, H^-, HO^- and e^-, which are strong reductants or oxidants. These act as high energy intermediates, and then result in secondary oxidation and ultimately a reduction in the reaction [18, 113, 115, 116]. Other sonolysis of organic liquids still needs to be investigated. It was believed that high intensity ultrasound treatment in an organic liquid would generate free radicals [17, 117]. For example, the sonolysis of simple hydrocarbons will generate H_2, CH_4 and alkenes, which can be found in the high temperature pyrolysis process.

Heterogeneous reactions have more requirements on the reaction environment. Some of them require extreme conditions, such as several hundred atm pressure and a temperature of several hundred ^oC. However, with high intensity ultrasound catalysis, some of these reactions can be carried out at room temperature and low pressure. In liquid – solid systems, the environment near the surface of the solid is asymmetric, which results a deformation of the cavity during its collapse. A microjet with a velocity of more than 100 m/s can be generated from the cavity [118, 119]. Both shock wave and microjets can cause erosion of the solid surface, but the impact in terms of the enhancement of chemical reaction still needs to be further investigated. In the liquid-solid powder system, the inter-particle collisions produced by the shock wave can dissolve the powder and enhance the reaction efficiency, for example, Cr, Mo and W powders, which have melting points of 1857 ^oC, 2617 ^oC and 3410 ^oC, respectively, have been reported to be affected in this way [116, 120, 121].

The chemical effects of high intensity ultrasound makes some difficult reactions achievable of room temperature and low pressure. The formation of the early transition metals carbonyls can be carried out with moderate rate, under the conditions of 100 to 300 atm of CO and a temperature of 100 ^oC to 300 ^oC [122-124]. In the condition of low temperature and low pressure of CO with high intensity ultrasound treatment, a good yield of carbonyl anions is given across a wide range of metals. High intensity ultrasound also

can be the catalysis for the process of molecular intercalation, which is slow, normally requiring high operational temperatures and long reaction times. Interestingly, high intensity ultrasound can increase the reaction rate by 200 fold [125-127]. Some excellent reviews about Sonochemistry reactions and catalyses can be found in [16, 18, 113, 116, 128].

4.3.3 Ultrasonic source for Sonochemistry

The transducer device, power generation and control system need appropriate design to deliver the energy efficiently from the electrical source into the reaction medium. Each component in the Sonochemistry system will now be described.

4.3.3.1 Transducer device

Magnetostrictive and piezoelectric transducers are the two main categories of transducer used in Sonochemistry applications [15, 113]. The magnetostrictive transducer is based on the magnetostrictive effect. When a magnetic field is applied in a ferromagnetic material, it induces elastic strain with corresponding changes in shape and dimensions. The expression for this effect is as follows:

$$\boldsymbol{S = s^H T_S + d^t_{PM} H} \tag{4.13.1}$$

$$\boldsymbol{B = d_{PM} T_S + \mu^T H} \tag{4.13.2}$$

where S^H is elastic compliance coefficients in constant magnetic field strength,

d_{PM} is piezomagnetic coefficient,

μ^T is permeability coefficient under constant stress,

B is magnetic induction,

H is magnetic field strength and T_S is stress.

The magnetostrictive transducer was widely used as the high intensity ultrasound device before World War II. It is typically composed of a closed core and a mass in the front, as illustrated in Figure 4.2. Magnetostrictive transducers are high in tensile strength and low in input electrical impedance. However, eddy current effects cause high electrical losses and low coupling efficiency between electrical and mechanical phases. Therefore,

the core is not made in a single piece; instead, a stack core design is adopted to reduce the influence of eddy currents and hence improve the electro-mechanical efficiency.

Non-metallic materials, such as metglas, are high in impedance and can further reduce eddy current generation, but exhibit poor piezomagnetic coefficient values. Rare earth-iron compounds have been a revolutionary material since 1970s for their combination of both high impedance property and magnetostrictive performance. Terfenol-D is one widely applied compound, and its ingredients include Terbium, Tb, Dysprosim, Dy, Iron, Fe [129, 130]. The new appearance of compound materials makes the magnetostrictive material competitive with piezoceramic transducers. Also, there are novel designs such as: the hybrid transducer configuration of magnetostrictive and piezoceramic materials [131, 132].

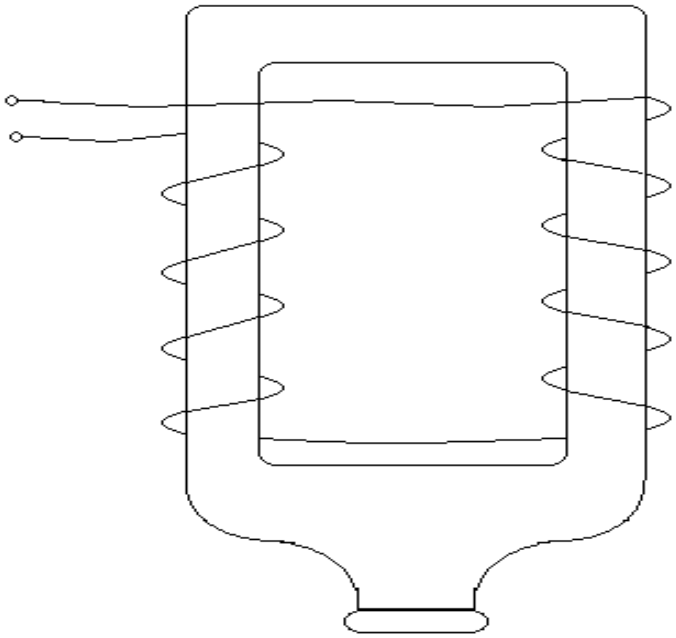

Figure 4.2 *Structural overview of a magnetostrictive transducer*

Piezoelectric transducers are based on the piezoelectric effect. The piezoelectric effect is concerned with the interaction between the applied electrical field and the physical mechanical change to the piezoelectric material. The poling process applies a strong electric field across the material and Weiss domains in the piezoelectric material are

aligned rather than having a random distribution. When an electrical field is applied, the dipoles tend to remain aligned, which results in the change of dimension of the material being linear. This effect can be described by the set of equations:

$$\boldsymbol{S = s^E T_S + d_{PE}^t E} \tag{4.14.1}$$

$$\boldsymbol{D_E = d_{PE} T_S + \varepsilon^T E} \tag{4.14.2}$$

where S is the strain of the material,

s^E is the compliance under constant electrical field,

d_{PE}^t is the converse piezoelectric coefficient,

E is the electric field strength applied,

D is the electric charge density displacement,

d_{PE} is the direct piezoelectric coefficient,

T_S is the stress,

ε^T is the permittivity under constant stress.

Piezoelectric materials can be found in nature, like Berlinite, Sucrose (sugar) and Quartz, but these materials are poor in performance, and rarely applied in transducer designs. Man-made material includes crystal like, Gallium orthophosphate, Polyvinylidene fluoride (PVDF), and ceramic, for example, Barium titanate, Lead titanate, Lead zirconate titanate (PZT).

Piezoceramic materials have a wide range of applications from low to high power, for example, medical diagnosing, non-destructive evaluation, cleaning and Sonochemistry. In low power application, soft PZT tends to be used. This material is high in piezoelectric modulus and permittivity but with higher mechanical loss due to internal friction. The hard PZT materials, for example, PZT4, PZT4D and PZT8, have low piezoelectric constants and typically less loss.

The basic structure of the piezoceramic transducer includes a matching layer, ceramic disk, and backing block, as illustrated in Figure 4.3. The matching layer increases the coupling efficiency between the ceramic and the load medium. The backing block increases the sensors' bandwidth, but lowers the sensitivity of the transducer.

For high power applications, a special design is necessary for several reasons. The high power transducer operating with low frequency is usually required for industrial applications. It is difficult to achieve this using a single piece of ceramic with the structure shown in Figure 4.3, due to the requirement of a large thickness ceramic. The displacement of the ceramic during the high power process is large; therefore, the ceramic is under the risk of fracture. The Tonpilz transducer design, or so called sandwich transducer, is a popular industrial design and is shown in Figure 4.4. In this structure, the matching layer is normally comprised of a light metal, like aluminium, and the backing material should be heavier than the front layer, normally incorporating steel; therefore, most mechanical energy is delivered in the forward direction. The two piezoceramic layers are stacked with the poling direction opposite to each other, and compressed by a bolt. The Tonpilz transducer is widely applied in industry for its simplicity, inexpensive manufacture, and efficiency.

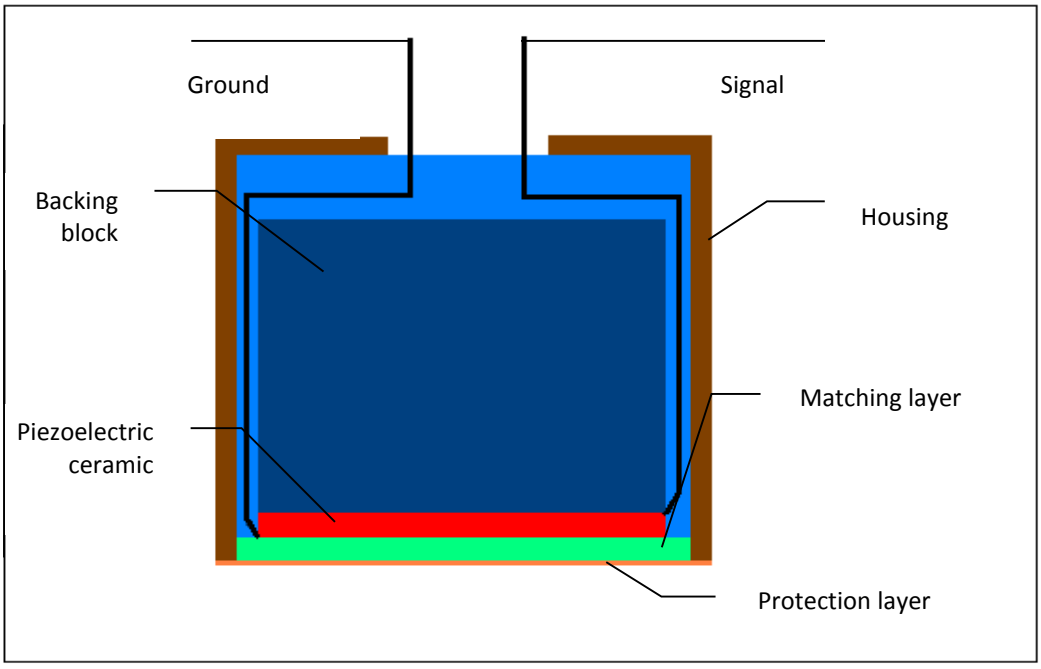

Figure 4.3 *Basic structure for a conventional piezoelectric transducer*

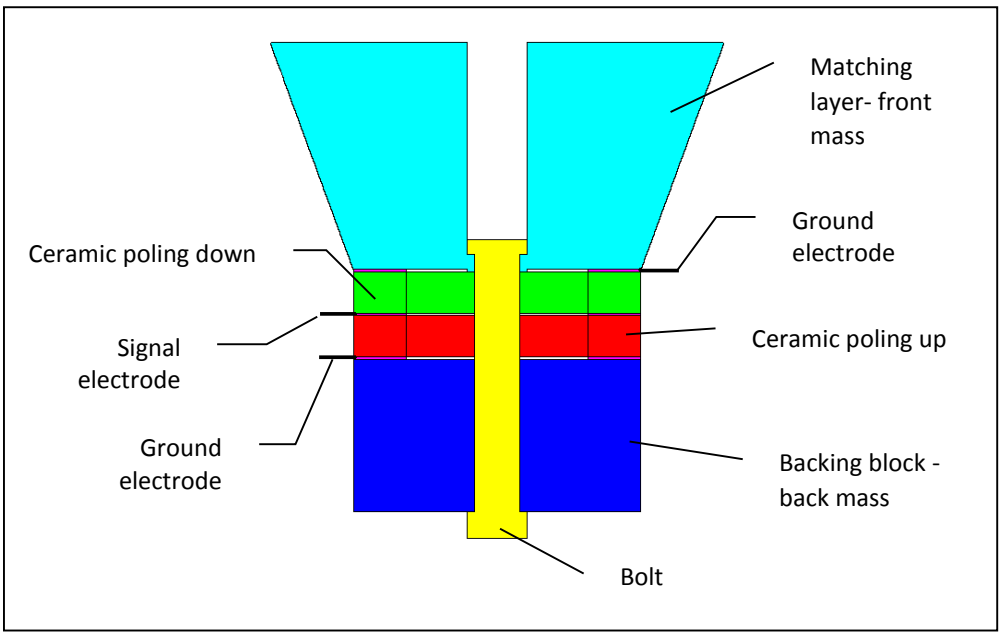

Figure 4.4 *Structure associated with a Tonpilz (sandwich) transducer configuration*

A piezoelectric ceramic composite [133-136] is a combination between a piezoceramic and another material, typically a polymer. In the end of 1980s and early 1990s, piezocomposite designs demonstrated great improvement and dominated designs in many fields, such as medical diagnosing and non-destructive evaluation. It has an advantage in phased array applications, for its low cross talk, wide bandwidth and low acoustic impedance [135, 137, 138]. More details will be presented in Chapter 5.

4.3.3.2 Power generation

Ultrasound transducers for industrial applications typically have a frequency range from 20 kHz to 100 kHz and low input electrical impedance from several tens of ohms to several hundred ohms. The power required for industrial applications can vary from ten Watts to thousands of Watts. A complete power supply system includes signal generation, power amplification, impedance matching and feedback block and is presented in Figure 4.5.

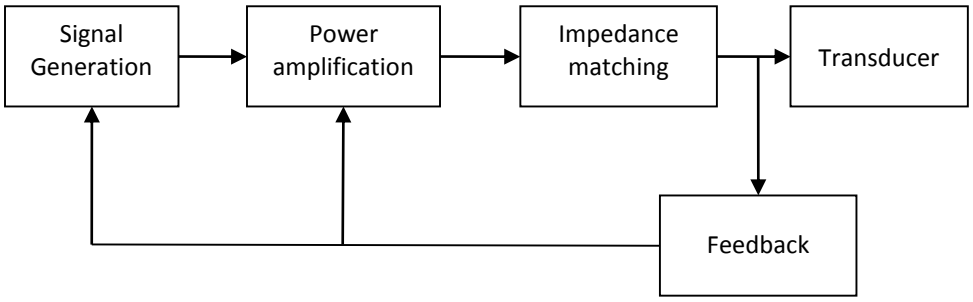

Figure 4.5 *Generic structure for a high power ultrasonic generation system*

In power generation, vacuum-tube oscillators were widely applied before the development of power electronic components, such as the transistor and thyristor. Power electronic devices are more efficient, reliable and more compact with the additional benefit of being light in weight. The electronic amplification circuit is usually based on the push-pull circuit [139, 140] or power switching circuit [141]. For the application of high intensity focused ultrasound (HIFU) in a medical clinic, power generation requires high frequency ranging from several hundred kHz to several MHz. Moreover, a new set of challenges are associated with the multi-channel phase control system necessary for HIFU generation by phased array transducer. Further details and explanation can be found in Chapter 5.

4.3.4 Sonochemistry reaction system

Sonochemistry reactions at a laboratory scale traditionally use either an ultrasonic cleaning bath or ultrasonic probe design. The cleaning bath application normally has several single element transducers, and an ultrasonic probe system usually has a single element transducer directly coupling into the reaction medium.

Ultrasonic clean baths are originally for cleaning purposes, operate in the frequency range 20 kHz and 40 kHz and have been adapted to Sonochemistry for their ability to generate cavitation [113, 142]. The basic structure is shown in Figure 4.6. A steel bath, with multiple ultrasound transducers bonded onto the bottom external surface, is filled with water containing 1 to 2 percentage of surfactant to reduce the water surface tension.

Pressure field calibrations can be carried out before using the ultrasound cleaning bath to ensure that reaction can be located in a position of maximum pressure to achieve best performance. To carry out such a chemical reaction, there is no requirement for a specific reactor vessel and it is typically sufficient to use traditional chemical glass vessel with flat bottom, which allows ultrasound to pass through to the reaction. A stirring facility may be required for the reaction, especially for liquid-solid powder reaction types, which require full exposure of the powder reagent to the reaction medium. At the same time, it is important that the stirrer does not attenuate the ultrasound wave energy. An ultrasonic cleaning bath is inexpensive and easy to use; however, there are several drawbacks. The main disadvantage is that it has small power to contribute to the reaction, typically less than 5 Wcm^{-2}. To increase cavitation intensity, and hence enhance chemical reaction efficiency, reaction with non-corrosive and non-volatile reagents can be directly used in a cleaning bath, as shown in Figure 4.10, as opposed to the standard arrangement in which the load medium is within a container/beaker, as illustrated in Figure 4.6. In addition, only a few frequencies between 20 kHz and 40 kHz are available in commercial products. Another drawback for commercial ultrasound cleaning baths is the lack of power and temperature control, but this can be managed in custom made systems.

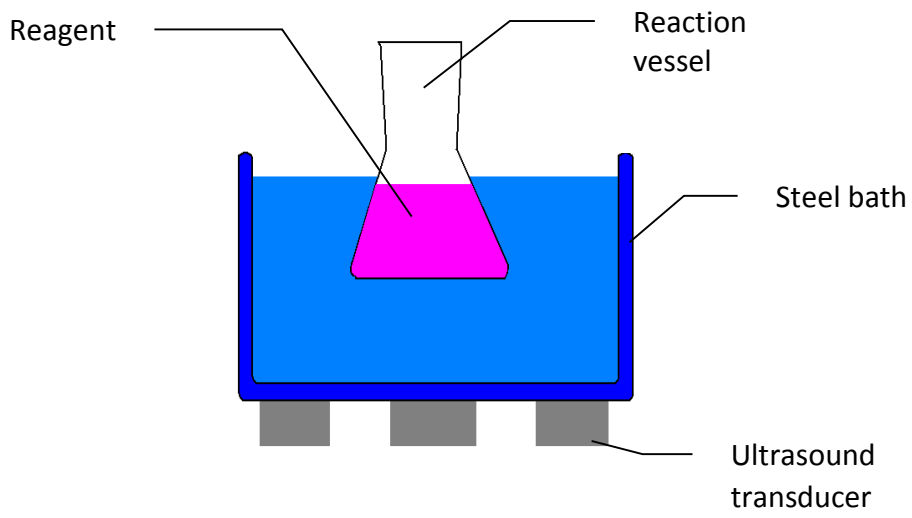

Figure 4.6 *Typical ultrasound cleaning bath arrangement for Sonochemical reactions*

The ultrasonic probe system is another typical Sonochemistry laboratory system [15, 113]. It is typically composed of four parts: power generator, transducer, horn and reaction vessel, as shown in Figure 4.7. The power generator should be able to tune its frequency within a small range to match the resonant frequency of the transducer, because cavitation erosion on horns' tip changes its resonant frequency slightly. Devices for probe systems usually incorporate piezoelectric or magnetostrictive transducers. To avoid overheating caused by high power excitation, piezoelectric and magnetostrictive transducers can employ cooling fans or water cooling systems.

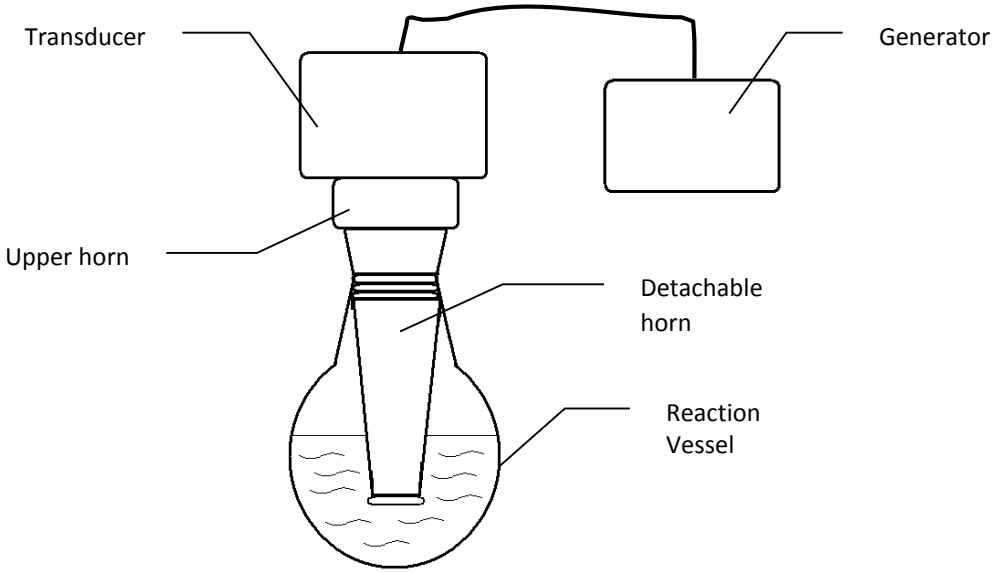

Figure 4.7 *Ultrasound probe system, incorporating an ultrasonic horn arrangement*

The horn component is used to deliver and amplify the vibration from the transducer into the reaction medium [90, 113, 143]. The upper horn is a solid metal block, typically made using titanium alloy. It requires properties of high dynamic fatigue strength, low acoustic loss, resistance to cavitation erosion and chemical inertness. It mainly has four types: uniform cylinder, linear taper, exponential taper and stepped geometries. Figure 4.8 illustrates the four horn configurations. The uniform cylinder type does not amplify the vibration; the linear taper and exponential taper amplify the vibration with a gain of Dim/dim; and the stepped type horn amplifies the vibration with a gain of Dim^2/dim^2. The ultrasound energy is directly delivered into the reaction medium by a horn attached

to the transducer, therefore, it can be more efficient and powerful (up to 150 Wcm^{-2}). However, these systems are more expensive, and a special glass vessel is needed to withstand the severe cavitation conditions produced by such a high power ultrasound system.

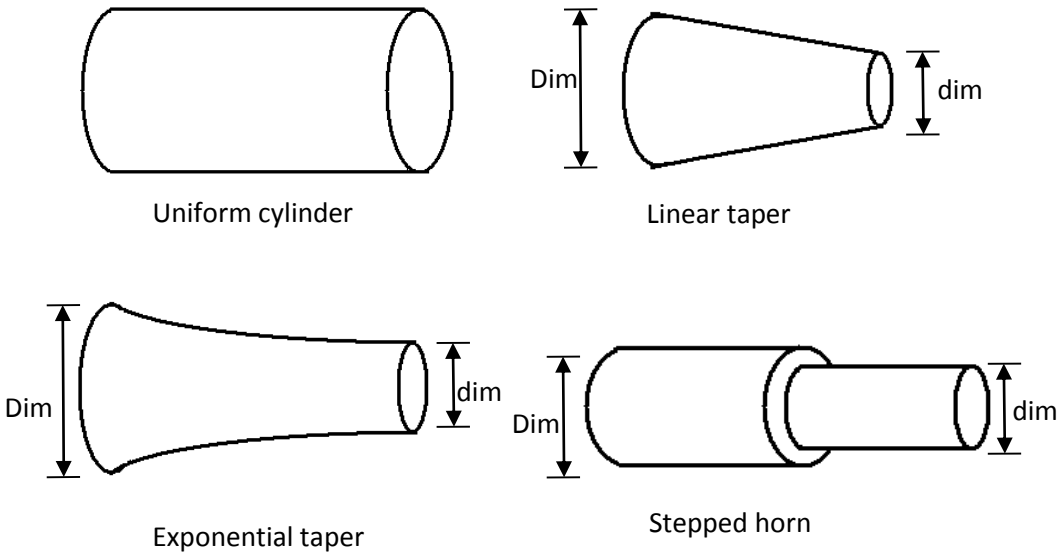

Figure 4.8 *Representations of the four different types of horn*

It should be noted that cavitation erodes the tip of horn in these configurations, which not only changes the resonant frequency of the transducer but also pollutes the reaction medium.

The reactor vessel for an ultrasound probe requires a temperature control system, because enormous heat is generated during the sonochemical process. Stirring is not always necessary due to strong ultrasound streaming accompanied with the high intensity ultrasound field. Moreover, because of the degassing nature associated with high power ultrasound, an additional gas port can be required, as illustrated in Figure 4.9.

The vessel design is based on the requirement of the reaction. For example, a special seal is required for reactions involving reflux, inert atmospheres, and pressure being different from ambient. In these cases, Polytetrafluoroethylene (PFTE) is mostly used for sealing the vessel. The sealing methods depend on the required reaction condition. For a

pressure cell, which requires a high pressure condition, a completely sealed design is needed as illustrated in Figure 4.9. In this design, the PFTE sleeve would lock the cell from outside to provide extra sealing performance in high pressure operating conditions. More details of such systems can be found in [15, 113].

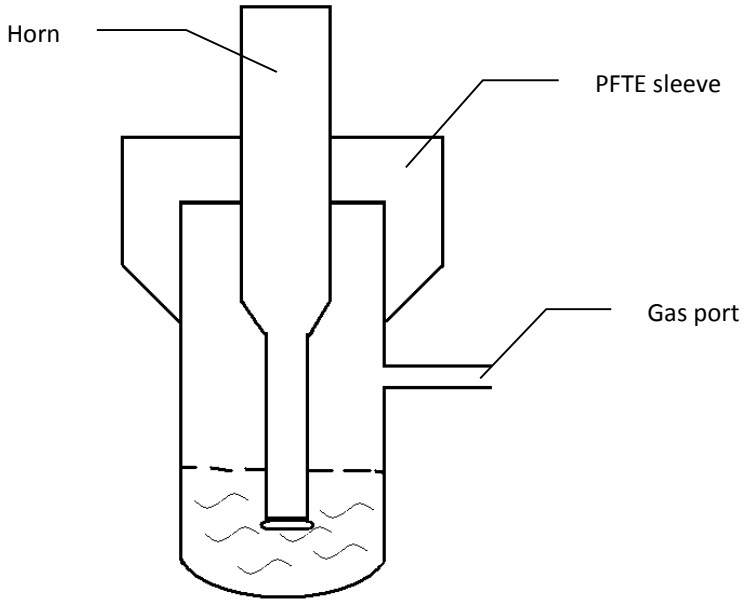

Figure 4.9 *Representation of a pressure reaction cell structure*

Scale up of Sonochemistry reaction equipment for the chemistry industry is a challenge [144]. Several design aspects have to be considered rather than focussing solely on cavitation generation. At first, the reacting medium's properties, such as viscosity, vapour pressure and solid particle size, would significantly affect cavitation generation. Also, the temperature and pressures conditions are critical for some chemical reactions. Therefore, heating and temperature control systems and sealing should be included in reactor design considerations to match the reaction specification. Power and frequency control with feedback measurement would be desired in most conditions. As mentioned in Section 4.3.2, ultrasound cavitation in organic media would produce ions, such as H^- or HO^- in the case of water, which can be desired or undesired based on the particular reaction. Therefore, the level of cavitation needs to be controlled by adjustment of the excitation power and frequency.

The scale up of a reactor is mainly divided into batch and flow systems, or in some cases the combination of both. Ultrasound cleaning baths and ultrasound probe systems are related to the batch system approach. The ultrasound cleaning bath is more suitable to lower intensity ultrasound cavitation production, because it is difficult to cool and there is a low energy transfer efficiency from the ultrasound transducer to the reaction medium. In industrial applications, the reaction tends to take place directly in the bath for its enhanced efficiency benefit, rather than incorporating a glass vessel in the bath. An ultrasound bath has advantages in its simplicity for adding in a stirring facility and sealing it to elevate the pressure inside the reactor. Figure 4.10 illustrates a typical structure of an ultrasound bath for Sonochemistry.

The high attenuation property associated with a cavitation field limits the size of the bath [145], with focusing providing a solution for the near field cavitation attenuation effects. By using several transducers with the natural focusing method, transducers are excited with relatively small amounts of power and ultrasound energy is focused on the geometric centre of the bath as illustrated in Figure 4.11. The transfer efficiency of ultrasound from the transducer to the reaction medium can be improved by using an oil interface between the transducer and glass wall. However, the problem is that the focusing has a limited spatial area to interact with the chemical system and cannot be manipulated. It means that there would be large areas of the bath that would not be insonified by ultrasound cavitation.

Bath designs with multi-frequency and phase control are reported in the paper by Mutasa [148], which achieves a more evenly spread energy distribution. It can also achieve temperature control by circulating cool water surrounding the bath wall. More details can be found in [146-148].

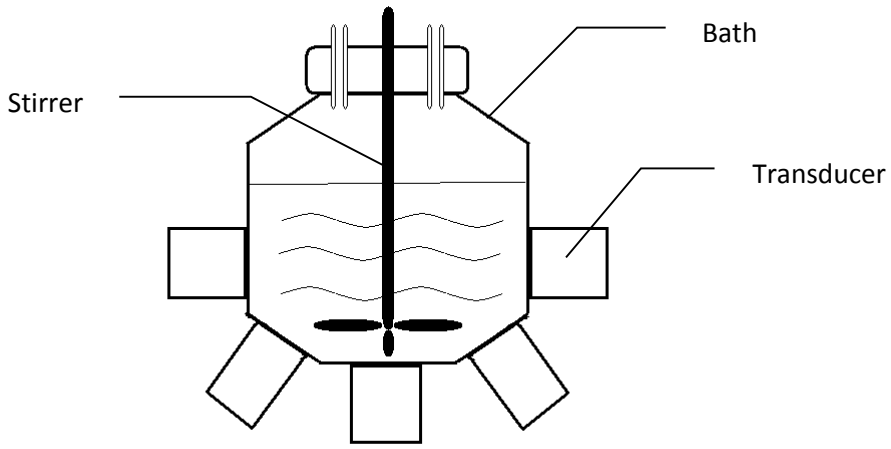

Figure 4.10 *Scale up of ultrasound bath approach for Sonochemistry applications*

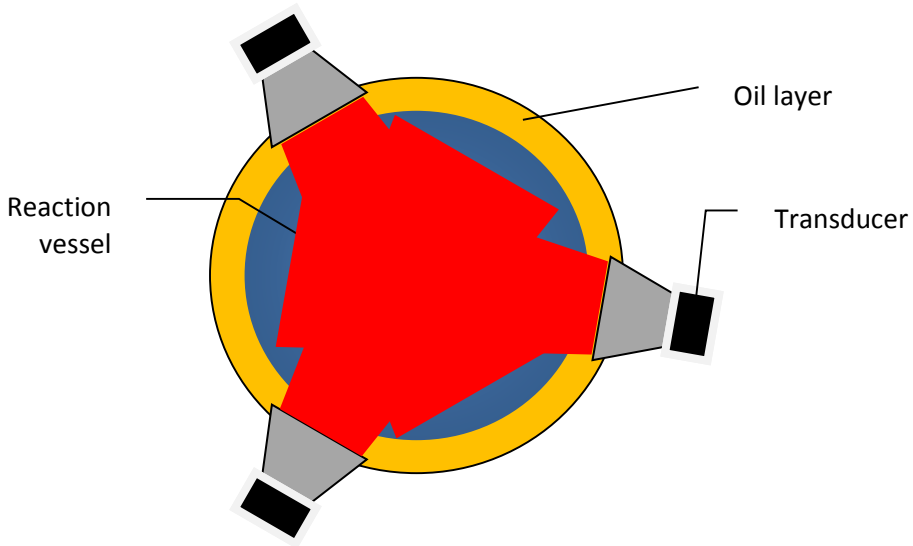

Figure 4.11 *Representative cylindrical ultrasound bath configuration for Sonochemistry applications*

An ultrasound probe system for scale up Sonochemistry applications [19, 143] can be based on the ultrasound streaming effect, which creates circulation paths and spreads out the cavitation field as shown in

Figure 4.12. By a combination of the prediction of streaming paths and cell design, the cavitation field can effectively cover most of the volume of the reactor. In addition, scale up can be achieved by increasing the number of probes.

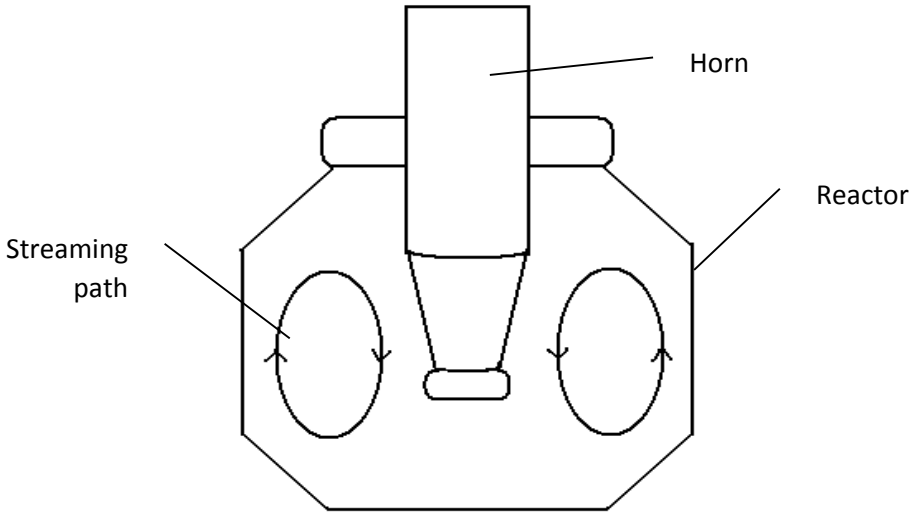

Figure 4.12 *Ultrasound probe scale up reactor using streaming to expand extent of cavitation*

In other Sonochemistry applications, flow systems are widely applied compared to batch systems. Through control of flow rate and transducer input power the desired cavitation level can be achieved and the use of a heat exchanger will provide temperature control. Such a system is illustrated in Figure 4.13.

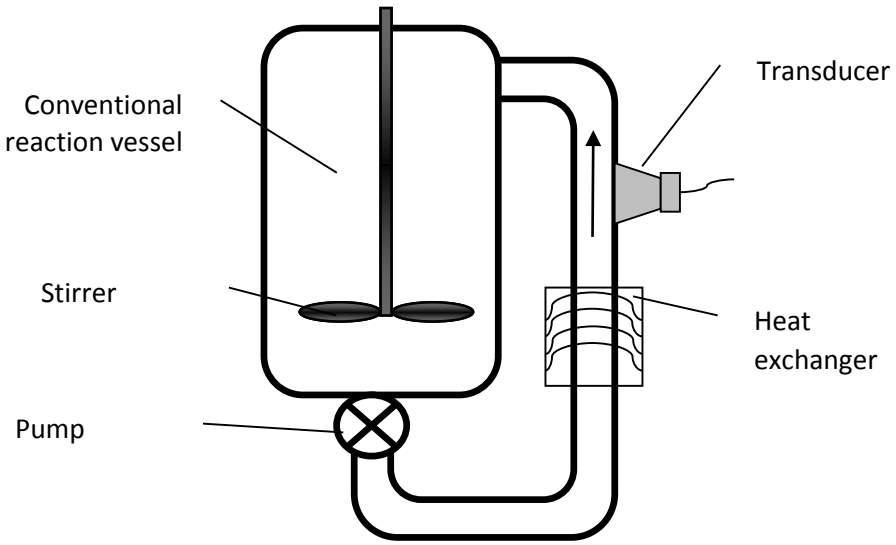

Figure 4.13 *Sonochemistry flow system arrangement*

In most flow system designs, the ultrasound transducer is mounted on the pipe wall and ultrasound energy transmits through the pipe wall into the reaction medium. The pressure field distribution inside the tube is mainly affected by the pipe's cross-sectional geometry [113]. A typical selection of geometries is shown in Figure 4.14.

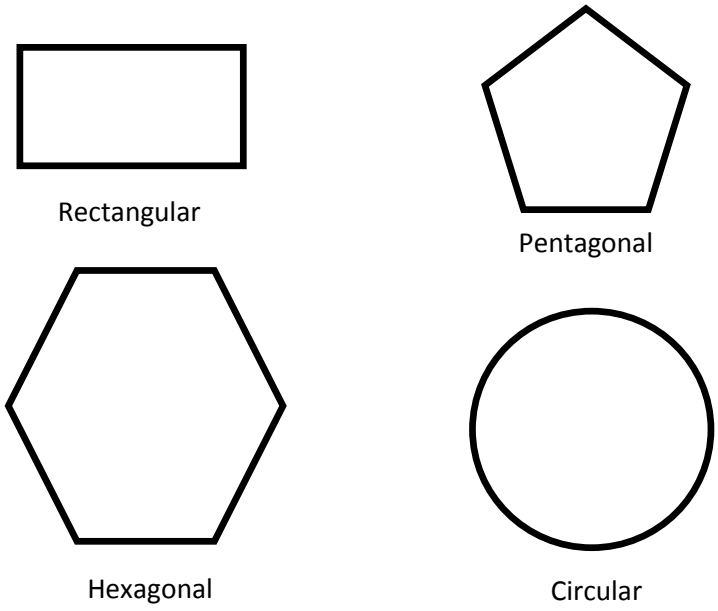

Figure 4.14 *Cross-sectional geometries appropriate for flow system applications [113]*

For the rectangular shape, the transducer is directly facing the opposite wall, and there is a possibility of erosion of the opposite wall. The pentagonal shape has a more uniform

ultrasound energy distribution, because the ultrasound is reflected at an angle [30]. Hexagonal and circular shapes generate focusing at the geometric centre. Therefore, cavitation is not likely to occur near the pipe wall, and this reduces the extent of wall erosion by cavitation.

Some excellent reviews for Sonochemistry can be found in [15, 16, 30, 128].

4.4 Summary

High intensity ultrasound produces nonlinear phenomena such as cavitation and acoustic streaming, which are the main mechanisms for most of its industrial applications. Cavitation has been well studied both theoretically and experimentally and this Chapter has provided an overview into this subject area.

Sonochemistry has been widely applied in industry from the 1980s. Its primary mechanism is cavitation generated from a high intensity ultrasonic field, which generates hot spots with temperature above 5000 ^{o}C and shock waves emitted with pressures of 1000 atm. Therefore, high intensity ultrasonics can interact with the chemical reaction as a catalyst and enable certain reactions to be carried out in low temperature and low pressure conditions with a reasonable efficiency.

It is clear that Sonochemistry applications have a wide range of applicability for industrial applications. Reactor designs are available to facilitate improved efficiency of such reactions through the use of high intensity ultrasound. One main issue is in the flexibility in operation of these systems, with the transducers fixed onto (or incorporated into) the reactor vessel. A more flexible approach may increase the uptake of this technology into industrial applications and importantly, aid the scale-up of laboratory scale systems into full industrial scale configurations.

Chapter 5

Review and applications of high intensity focused ultrasound systems

5.1 Introduction

High intensity focussed ultrasound (HIFU) is a technique which focusses ultrasonic energy into a small focal zone to generate a high intensity ultrasonic field via geometrical or electronic methods. Single element HIFU transducers with curved shaped surfaces, or incorporating a focusing lens, and phased array transducers are mainly employed to generate HIFU [27]. Piezoceramic and piezoceramic composites (piezocomposite) are the typical material used in the manufacture of HIFU transducers. Piezocomposite configurations offer lower acoustic impedance and high electro-mechanical coupling efficiency, which can lead to high energy transfer efficiency between the transducer and low acoustic impedance load media, for example, human tissue or liquid media. In general, the transducer design is application specific. For medical applications, it is important to minimize side lobe generation and ensure a precise focusing area. For industrial application, power efficiency should be emphasised.

For a single element HIFU transducer, the excitation system is similar to the conventional high power ultrasound transducer. Phased array transducer configurations are more flexible in terms of electronic steering and focusing abilities, which requires a specialised excitation system based on multi-channel power amplification, phase control techniques and beam forming strategy. These techniques are critical to prevent damage to normal tissue of patients in clinical applications, which require a fast drop of power outside the focusing area, which can be challenging through nonlinear multilayer structures, such as human tissue, chest wall and human skull. A similar approach is also important in industrial applications to maximise pressure at the focal point and suppress near field cavitation activity.

HIFU has been successfully applied in clinical surgery for prostate cancer treatment [149]. Further investigation to utilize HIFU as a non-invasive technique for surgery and radiotherapy has been carried out [150, 151]. Whereas, HIFU for industrial applications is a relatively new approach.

5.2 Single element HIFU transducer

Single element HIFU transducers can produce a high intensity field of greater than 2000 W/cm^{-2} with an input electrical power less than 100 W [151, 152]. The single element HIFU transducer is divided into two categories by the focusing mechanism: one is natural focusing by use of a concave piezoelectric ceramic or piezoelectric ceramic composite; and the other is focused using an acoustic lens. Both mechanisms are illustrated in Figure 5.1.

The curved shape HIFU transducers' focusing ability is from the natural geometric focus. Therefore, for the spherically curved surface, the focusing point will be in the spherical centre. Pre-formed piezoceramic is typically used in these designs, but the use of a flexible piezocomposite can also be an option [23, 153]. To improve the beam shape of the transducer, an electrode pattern of spherical caps can be introduced, for example, by cutting out holes or eching novel conductive patterns onto the surface, which was decribed in [154].

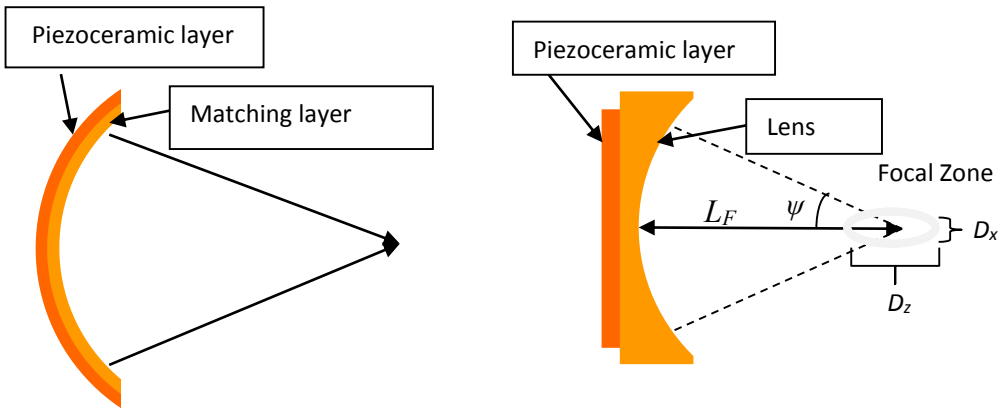

Figure 5.1 *Single element HIFU transducer; (a) Curved shape HIFU transducer, (b) Flat surface HIFU transducer with acoustic lens*

The single element HIFU transducer with a flat surface, focuses the ultrasonic energy by using an acoustic lens. The mechanism of focusing is simillar to the optical lens. The

refraction rule of ultrasound (Snell's law) is shown as:

$$\frac{\boldsymbol{sin\theta_1}}{\boldsymbol{sin\theta_2}} = \frac{\boldsymbol{c_2}}{\boldsymbol{c_1}} \tag{5.15}$$

Where θ_1 is the incident angle in medium 1,

θ_2 is the incident angle in medium 2,

c_1 is the velocity of sound in medium 1,

c_2 is the velocity of sound in medium 2.

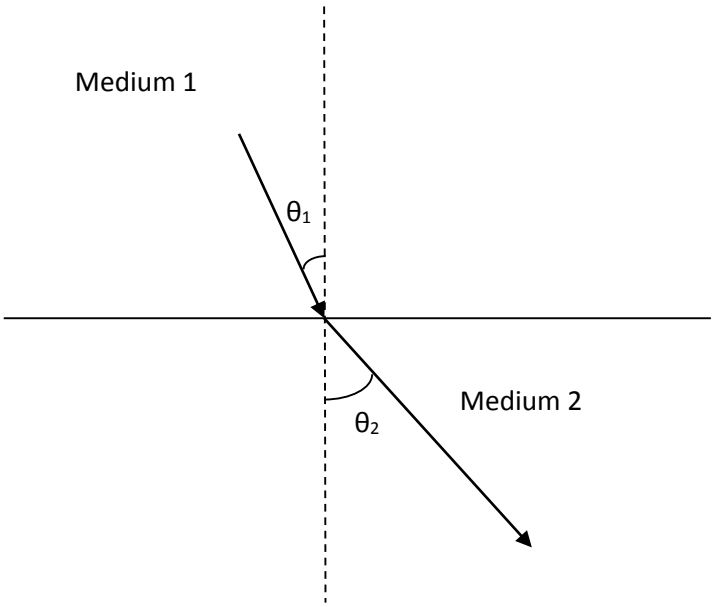

Figure 5.2 *Refraction of ultrasound at the interface between two materials*

Acoustic lenses can be made from perspex or silicon rubber [155, 156], which have larger sound velocity than water. Therefore, according Equation 5.1, to focus ultrasound, the acoustic lens should have a concave curvature, as shown in Figure 5.1(b).

For clinical surgery applications, a small -6dB focusing area is critical to match the medical regulations. It can be calculated by following equation [157].

$$\boldsymbol{D_x = D_y \approx \delta_t \lambda \cdot \left(\frac{L_F}{D_L}\right)} \tag{5.2.1}$$

$$\boldsymbol{D_z \approx \delta_a \cdot D_x} \tag{5.2.2}$$

where λ is the wave length of ultrasound in medium,

δ_t is the dimensionless factor, which equates to 1 if $\psi < 50^o$,

$\delta_a \approx 15(1\text{-}0.01\psi)$,

L_F is the focusing length,

D_L is the lens diameter,

ψ is the aperture angle.

Also, the gain factor G, which is the ratio between the transmitted intensity I_0 and the intensity at the focal point I_F, by assuming ultrasound transmitting in a lossless medium and aperture angle $\psi < 15^o$, is given by [157]:

$$\boldsymbol{G = \frac{I_F}{I_0} = \frac{\pi}{4}\left(\frac{L}{D_y}\right)^2} \tag{5.3}$$

When the aperture angle $\psi < 50^o$, the approximations of Equations 5.2 and 5.3 have an error of less than 20%.

In high power applications, an acoustic lens is typically made of material, which exhibits low acoustic loss and has an appropriate acoustic impedance, chosen to enhance the coupling efficiency between the transducer and the load [156].

A single element HIFU transducer has the advantage of high efficiency and simpilifies both the manufacture and the electrical excitation schemes. However, the main problems of single element HIFU transducer are that focusing can only be steered mechanically, which results in poor versatility. Moreover, the focusing ability would degrate when ultrasound propagates through a nonlinear layer.

5.3 Piezocomposite material as the active phase in a HIFU device

The technical advances associated with the piezocomposite material configuration were important in the development of array transducers during the last three decades. Piezocomposite materials, also known as piezoelectric ceramic composites, is a combination of a piezoelectric material with a passive polymer. 1-3 piezocomposite [138, 158, 159], and 2-2 piezocomposite [160-162] are the most common piezocomposite structures, which are now described.

1-3 and 2-2 connectivity piezoelectric composite configuration are mostly employed in high power applications. The 1-3 piezoceramic composite configuration comprises piezoceramic rods embedded in a polymer matrix with the poling direction perpendicular to the composite surface, as illustrated in Figure 5.3 (a). The pillars can be distributed periodically or randomly, depending on the design and manufacturing process [138, 158, 159].

The 2-2 piezoelectric composite configuration is when piezoceramic plates are distributed periodically in the polymer, which is shown in Figure 5.3(b). 2-2 piezoelectric composite and 1-3 piezoelectric composite structures have similar properties and performance under the same pillar width and saw width conditions [159, 163]. However, the 1-3 configuration is suitable for both 1-D and 2-D array transducer schemes, whereas the 2-2 configuration is only suitable for 1-D array transducer structures. However, under the same pillar width and pitch width, a 2-2 piezoelectric composite has the higher ceramic volume fraction.

It has been reported that piezocomposite materials are not suitable for high power applications as a single element transducer for several reasons. Piezocomposite configurations exhibit lower efficiency than piezoceramic materials for high power application due to high mechanical loss, which is the result of interaction between the active and passive phase [164, 165]. This mechanical loss property is determined by piezoceramic material properties, if the polymer filler is not highly attenuating. Therefore, PZT4, PZT4D and PZT8 which are high in efficiency, should be adopted as active phase

materials of piezocomposites in HIFU applications to reduce the mechanical loss of the piezoelectric ceramic composite.

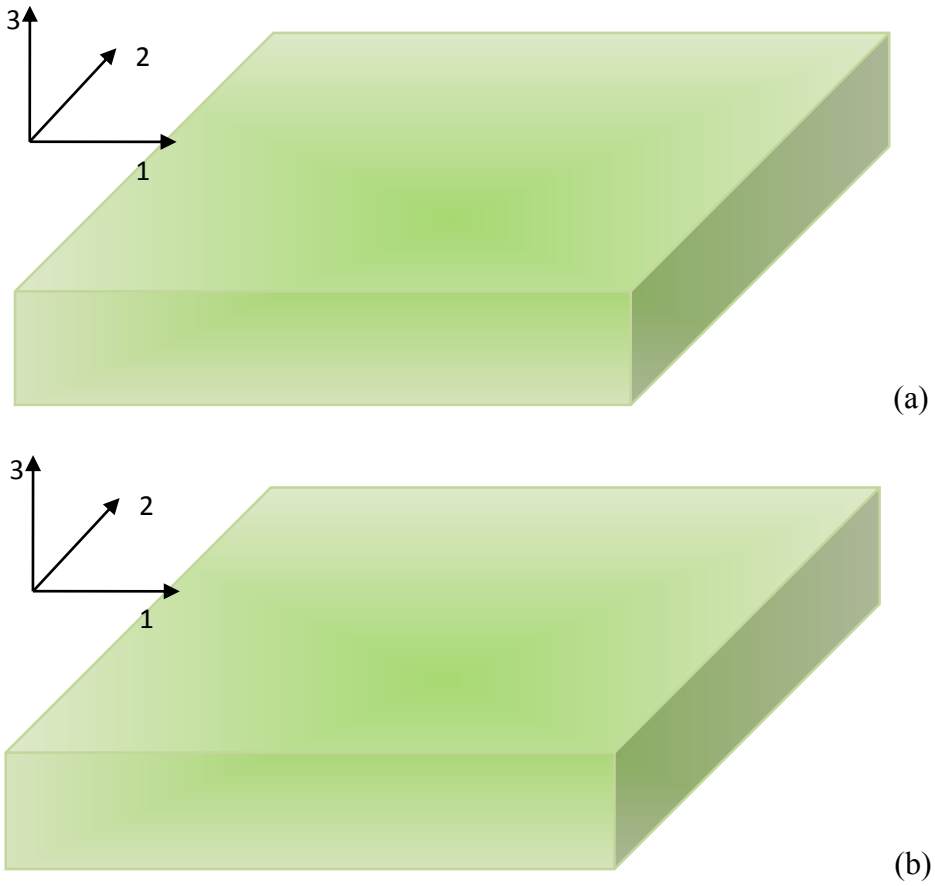

Figure 5.3 *Standard piezocomposite arrangements; (a) 1-3 connectivity configuration, (b) 2-2 connectivity configuration*

It is also difficult to manufacture a piezocomposite for low frequency high intensity application. As discussed in Chapter 4, the operating frequency for industrial Sonochemistry applications is normally under 100 kHz. This would require a large thickness of active piezoelectric material and for a piezocomposite, the dicing depth would be challenging and the solution of using a multi-layer composite design results in further manufacture difficulty.

Also in terms of the passive filler material, low heat conductivity and low glass transition temperature will limit the maximum piezocomposite driving power level. In

high power applications, any raised temperature will reduce the efficiency of the whole system. To deal with this heating problem, high Tg polymers, for example, polymer filled with alumina powder, would be one choice to enhance the piezoceramic composite's heat conductivity [166, 167], and reduce the temperature of the active transducer during high power operation.

The electrical impedance of piezocomposite material is approximated as the sum of parallel contributions of the piezoceramic and the polymer. Because the dielectric constant of ceramic, which is in the range from 100s to 1000s, is much larger than that of the polymer, which is from 2s to 10s, the contribution from the polymer is normally ignored. Therefore, the electrical impedance is determined by the active phase of the piezocomposite. High ceramic volume fraction configurations are used to reduce the electrical impedance of piezocomposites and to further enhance the transmission efficiency of the transducer by allowing higher current under the same voltage excitation condition.

However, some properties of the piezocomposite, such as low acoustic impedance, high electromechanical coupling constant and low cross talk, offer advantages over conventional piezoceramic designs for phased array transducer designs for use in high power applications. The ultrasonic energy transfer efficiency [168] at the interface between the transducer and the load is decided by an acoustic impedance match. The smaller the difference between the two acoustic impedances the less reflected energy there is from the interface**.** The density and elastic stiffness of the piezocomposite are both smaller than the ceramic but larger than the polymer. Hence, it has a lower acoustic impedance than the ceramic (20-30 MRayl) and higher than the polymer (1-5 MRayl). This relationship is linear and at large ceramic volume fractions, the acoustic impedance is relatively high, which will reduce the transfer efficiency of ultrasonic energy from transducer into a low acoustic impedance load. A careful design of a matching layer can improve the transfer efficiency. It allows the practical implementation of high ceramic volume fraction transducers and ensures reasonable transfer efficiency, at the same time [169].

The electromechanical coupling coefficient is another important property. A higher electromechanical coupling constant means an increase in the transfer efficiency between

electrical and mechanical energy within the piezoelectric material itself. Importantly, a piezocomposite material can have a higher electromechanical coupling coefficient when compared to a standard piezoceramic. In a piezocomposite structure, the stiff ceramic rods are surrounded by a soft, light polymer, therefore, the rod has more freedom to move in the lateral direction. According to Poisson's ratio, it produces a larger displacement than a fully mechanically stiff piezoceramic material. Figure 5.4 illustrates the influence of the ceramic volume fraction on the electromechanical coupling efficient, k_t. It can be seen that the piezocomposite has a peak in the mid-range of the ceramic volume fraction and is low in both the low volume fraction and high volume fraction regions.

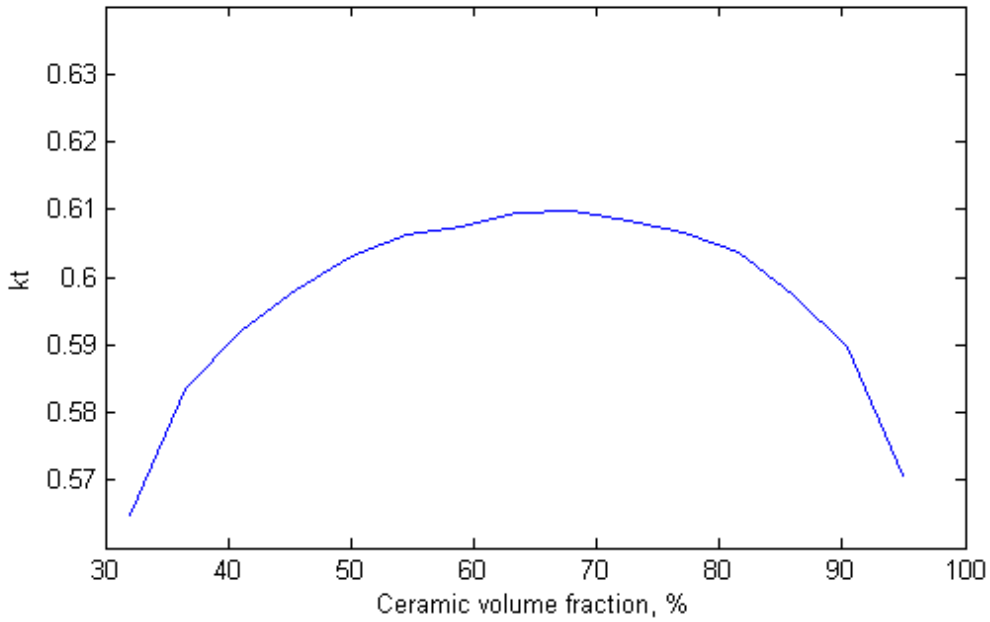

Figure 5.4 *Predicted electromechanical coupling coefficient as a function of ceramic volume fraction for piezocomposite of PZT4D and medium set epoxy (MSE) (Vantico HY956EN/CY221) in 1-3 connectivity configurations [168, 170]*

Piezocomposite configurations can also be designed to exhibit inherently low electrical cross-talk. This is a function of the lateral attenuation property of the passive filler material.

5.4 Matching layer design for HIFU devices

A matching layer is designed to increase the energy transfer efficiency from the transducer to the load medium. The transmitting efficiency is decided by the ratio between the acoustic impedance of the transducer and the load medium. This can be calculated using Equation 5.4 [108].

$$\frac{P_T}{P_I} = \frac{2Z_{AT}}{Z_{AT}+Z_{AI}} \tag{5.4}$$

where P_T is the stress of the transmitted wave,

P_I is the stress of the incident wave,

Z_{AT} is the acoustic impedance of transmitted medium,

Z_{AI} is the acoustic impedance of incident medium.

For operation into a low acoustic impedance load, a matching layer is required for both piezoceramic and piezocomposite transducer designs. Albeit, different designs would be required due to the different acoustic impedance between these materials.

As high ceramic volume fraction configurations are widely used in HIFU transducer design, the two-layer design approach is adopted in this Thesis to promote high transducer transmitting efficiency and increase the operational bandwidth of the device. Optimal acoustic impedance of matching layers are described by [171], and are illustrated in Figure 5.5 and Equation 5.5. This design law is used in the matching layer design described in Chapters 6 and 7.

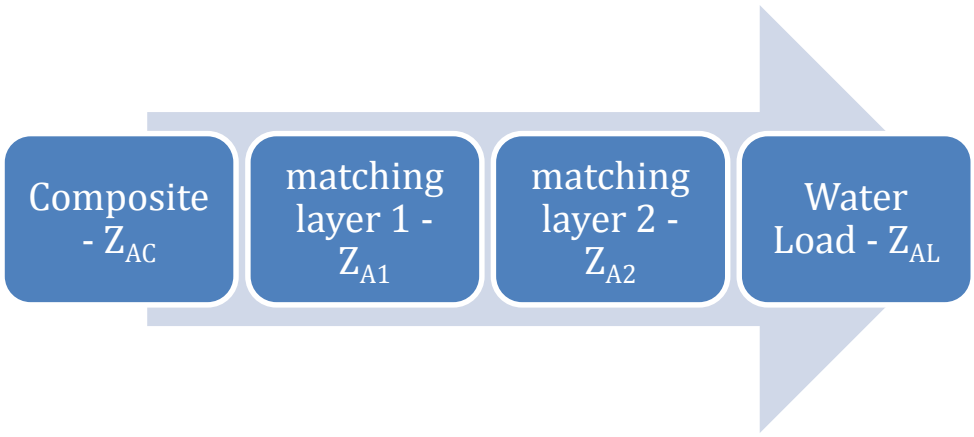

Figure 5.5 *Illustration of the dual-matching layer scheme*

$$\boldsymbol{Z_{A1} = \left(Z_{Ac}^{4} \times Z_{AL}^{3}\right)^{\frac{1}{7}}} \tag{5.5.1}$$

$$\boldsymbol{Z_{A2} = \left(Z_{Ac} \times Z_{AL}^{6}\right)^{\frac{1}{7}}} \tag{5.5.2}$$

where Z_{A1}, Z_{A2}, Z_{AC}, and Z_{CL} are the acoustic impedance of first matching layer, second matching layer, piezocomposite and load medium, respectively.

5.5 Phased array transducer configurations

For phased array transducer operation, each element is independently excited with control over the phase and amplitude of the individual electrical signal used to drive each array element. These discrete projected ultrasonic waves interfere with each other to generate a desired ultrasonic field, for example achieving a focal point or to steer the ultrasonic beam at the chosen angle.

The array transducers are normally made using piezocomposite structures, using either 1-3 or 2-2 configurations, as discussed in Section 5.3. However, there are examples of HIFU array transducers incorporating standard piezoceramic. As this work concentrated on both 1-3 and 2-2 connectivity piezocomposites, HIFU array transducers using piezoceramic are only briefly mentioned.

Phased array transducers are divided into several types, such as 1-D linear planar, 2-D matrix, annular, 2-D segmented annular and 1.5-D matrix, which are illustrated in Figure 5.6. Importantly, all of these configurations have previously been applied in HIFU applications and will be discussed individually.

1-D phased array transducers have element widths that are much smaller than its length, as shown in Figure 5.6. It generates a beam with elliptical shape, which can be steered in the vertical (z-axis) and horizontal (x-axis) direction. The advantages of the 1-D array probes are their simple structure and relative simplicity of phased array control and power amplification [172].

The annular phased array transducer is similar in design and operation to the linear phased array transducer configuration and is displayed in Figure 5.7. The annular elements project a beam with a spherical geometry and electronic control can steer the beam along the central axis, i.e. in the direction that is perpendicular to the probe surface. It has a better focusing energy than the 1-D phased array transducers, but cannot steer the beam to other angles away from the central axis [21, 173].

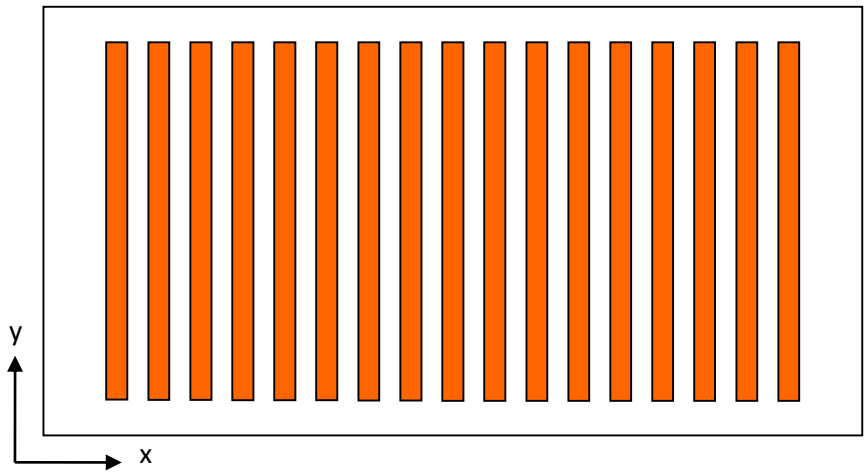

Figure 5.6 *1-D phased array transducer layout*

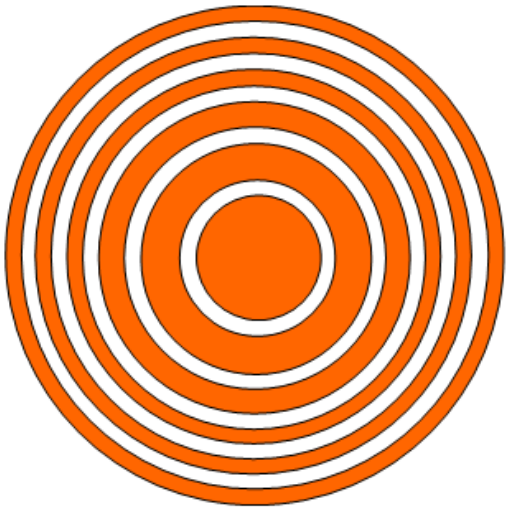

Figure 5.7 *Annular phased array transducer layout*

The 2-D matrix probe, which is shown in Figure 5.8, projects an elliptical shape of ultrasonic beam from each element. It has a significant advantage in control of the ultrasonic beam in 3 dimensions within the load. Thus, energy focusing can be manipulated within a volume in the medium. However, the development of the 2-D phased array transducers is limited by the complexity associated with the manufacturing processes and the small array element size, which is not conducive for application in a high power transduction scheme [174, 175].

The 2-D segmented annular phased array transducer is the combination of the concepts

between the annular and 2-D matrix array configurations. It is similar to the 1-D annular transducer, but now the ring element is segmented into a number of smaller elements as shown in Figure 5.9. The probe can produce spherical or elliptical ultrasonic field projections and can vary the focal depth and angle. This kind of probe also has high performance, albeit with drawbacks such as, complexity in manufacture and limited angular steering capability [176].

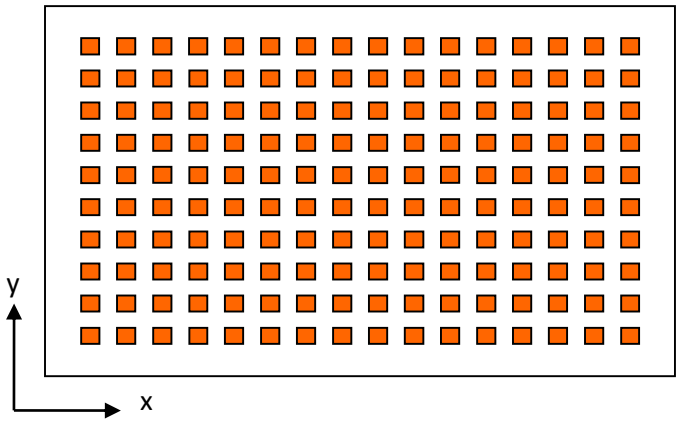

Figure 5.8 *2-D phased array matrix transducer*

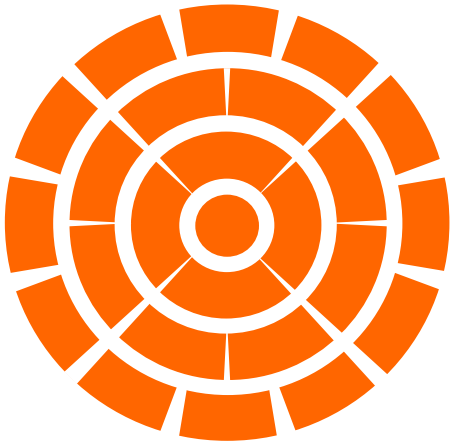

Figure 5.9 *2-D phased array annular transducer configuration*

The 1.5-D phased array transducer configuration is a compromise between beam steering performance and manufacturing complexity. In this layout, the array element length associated with a 1-D configuration has been split into a small number of discrete elements. Moreover these elements can have different lengths, as illustrated in Figure

5.10. This design enables limited 3-D steering ability by introducing a relatively small number of elements in the second dimension (relative to a standard 1-D configuration as depicted in Figure 5.6) [20, 23].

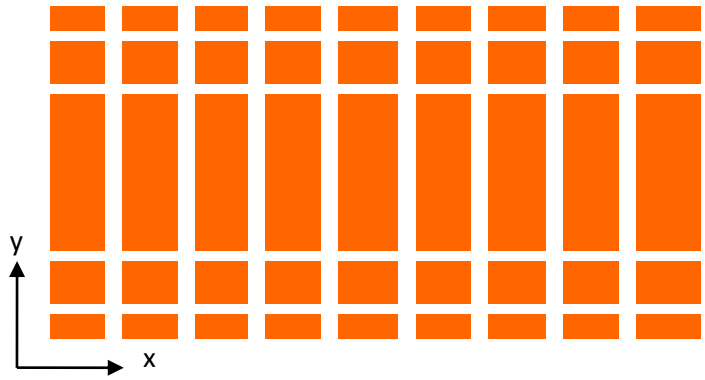

Figure 5.10 *1.5-D phased array transducer configuration*

In recent years, the combination of using a concave transducer surface profile with the phased array technology has been reported, which provides high performance in energy focusing and wide angle beam steering. For example, cylindrical curvature shape is combined with 1-D and 1.5-D array, to add or enhance the focusing ability in the y direction [20, 23, 172]. Also, there are reports that concave spherical transducer surfaces have been combined with annular and 2-D array design [173, 175].

The array transducer designs commonly incorporating an active piezocomposite layer can have low mechanical cross-talk between elements. This is usually an important aspect in the design of imaging arrays.

There are some alternative array configurations that have been reported. A ceramic lateral mode coupling array transducer was investigated by Song and Hynynen [177]. Each element is built by using a single cylindrical PZT-4 ceramic tube and is operated in its width mode. Some special array arrangements other than periodic element distribution described above have also been investigated. For example, a sparse random array configuration was adopted by Goss and Frizzell, to eliminate side lobes [175].

To design a phased array transducer, the relationship between element size, focusing ability and directivity is important to understand. In this Thesis, the 1-D phased array configuration was adopted, and here, a model based on the Huygens–Fresnel principle was employed to predict the pressure distribution as a function of these key array parameters to aid understanding of array operation. In this model, a phased array transducer with an aperture of 60 × 20 mm and 32 elements operating into a water load is simulated. The element pitch width is 1.8 mm and the element saw width is 0.6 mm. The beam was axially focused at a depth of 50 mm. Variation in the excitation frequency and hence, the ratio between element pitch width and ultrasound wavelength, is used to investigate array performance. The pressure distribution was simulated, as illustrated in Figure 5.12, and the -3dB beam width was calculated as shown in Figure 5.11. It is clear that an increase in operational frequency will increase the focusing resolution. However, from Figure 5.12 (c), significant sidelobes have been generated when the element size is in the order of one wavelength. An engineering compromise is achieved when the element size is half wavelength, with high resolution of focusing and no significant sidelobe activity, as illustrated in Figure 5.12 (b).

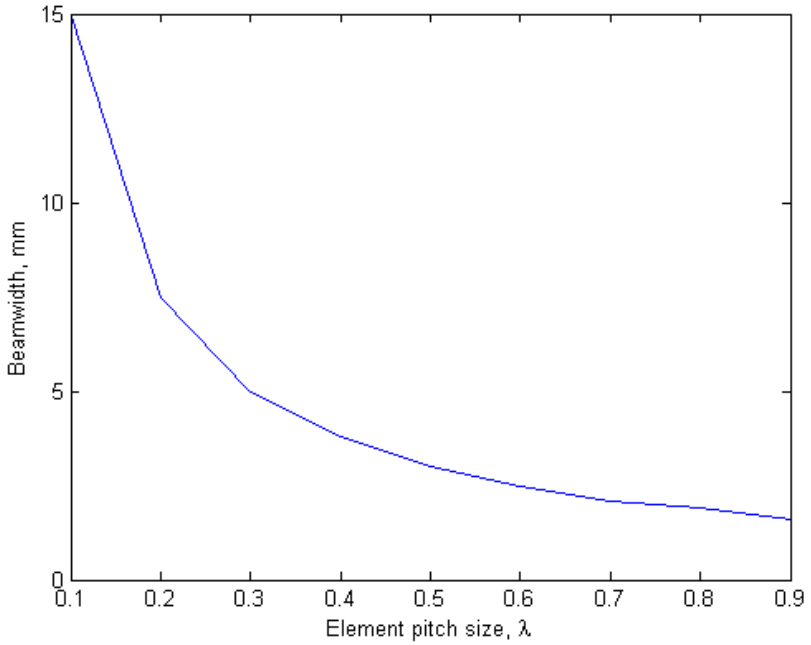

Figure 5.11 *Relationship between the array element pitch (as a function of wavelength) to the beam width in the focal region*

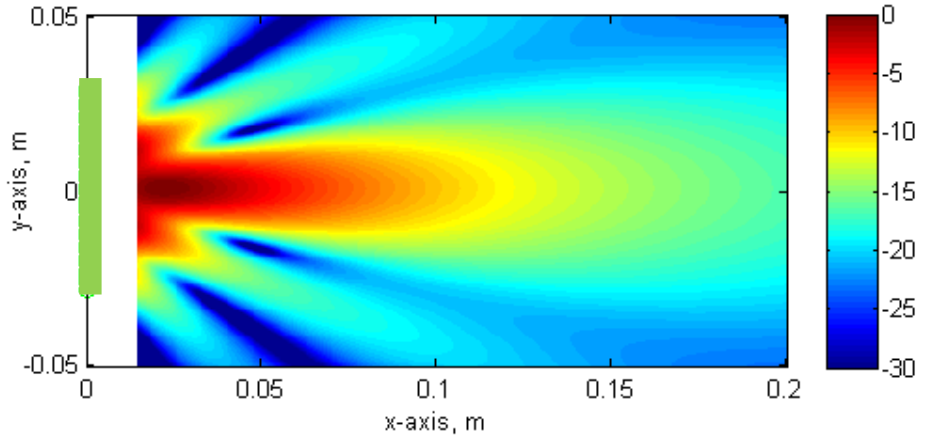

(a)

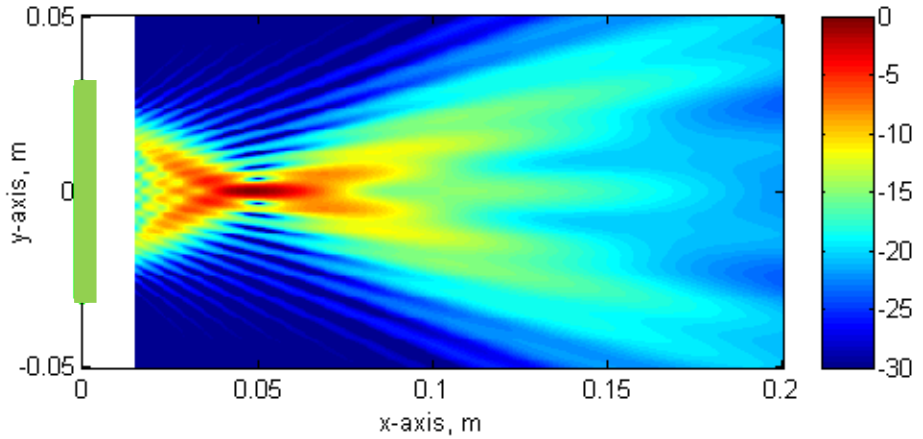

(b)

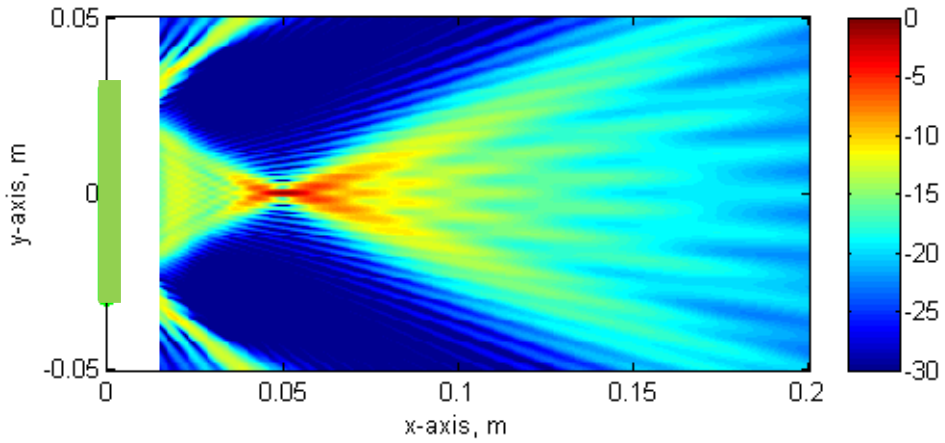

(c)

Figure 5.12 *Normalized pressure distribution of a phased array transducer with different element pitch size in terms of wavelength, (a) element pitch size of 0.1 λ, (b) element pitch size of 0.5 λ, (c) element pitch size of λ*

5.6 Excitation requirements for HIFU generation

The generation of HIFU can be organised into two main parts: the hardware—power generation and phased array controller; and its excitation strategy—focusing law and beam forming technique.

5.6.1 Hardware for HIFU generation

For the single element HIFU transducer case, the hardware is the same as for the conventional high intensity ultrasound applicator systems, which was mentioned previously in Section 4.3.4. The excitation of the phased array transducers for high intensity focused ultrasound pressure field generation requires multi-channel phase control and power amplification systems. Development of phased array transducers with complex element arrangements, the increasing number of channels, the high precision of phase control and the high voltage signal excitation schemes are the main challenges for a HIFU excitation system. A 500 element phased array system, which enabled high accuracy focusing in human skulls, was reported by Hynyen et al. [178]. Moreover, it was demonstrated that 8 bit phase shift resolution is essential for HIFU applications in the medical field [179-181].

A complete phased array controller incorporates a control system, phase regulation block, power generation and matching circuit block, which is illustrated in Figure 5.13. The control system is mainly used in system performance monitoring, system output control and safety interlock setting. These three tasks are related to each other and cannot be separated. Feedback from the output is essential to reduce power level and phase shift errors. It is reported by Daum et al. [179] that the feedback will reduce the differences of output power among array elements from 20% to 1%. To ensure accurate phase shift performance, a phase locked loop (PLL) approach is normally adopted. The feedback system also provides a safety interlock feature. For HIFU applied in clinical surgery, it is important to monitor the output level. Channels with error output should be reported and shut down automatically to prevent risk to patients.

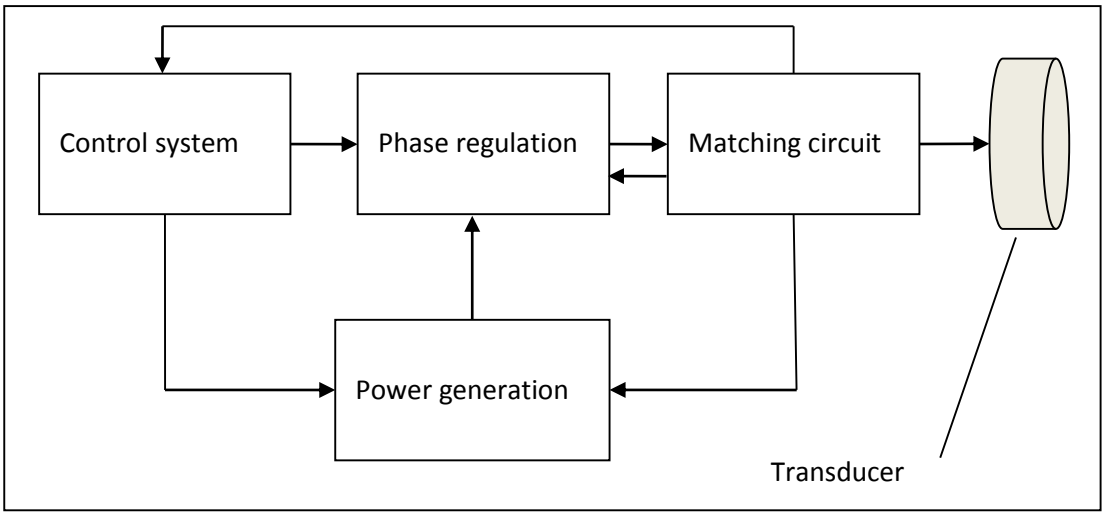

Figure 5.13 *Block diagram illustrating the driving system associated with control of a phased array transducer*

Phase regulation is a mature technique and routinely used for antenna array operation in the radio frequency (RF) domain. However, as the aerial array is operated at a much higher frequency than ultrasound, its phase regulation circuit is complex, with a large number of electronic components, compared to the typical ultrasound system. Therefore, phased regulation techniques for aerial arrays are not suitable for ultrasound phase array systems. For HIFU applications, other techniques, such as preloadable counters and discrete delay based systems, have been investigated and implemented [179-181]. Preloadable counters have the simplest structure, but the requirement for an ultra-high frequency clock, makes it difficult to implement in practise. For an 8-bit phase shift system, it requires 256 times the sample rate of the output signals operating frequency. Discrete delay based systems combine both counters and delay circuit techniques. The delay chips can provide 4-bit resolution of phase shift, and therefore, only 16 times the sampling rate of the ultrasound signal is necessary.

The power amplification circuit of the phased array controller is similar to power amplification circuits used for high intensity ultrasound. Switching power amplifiers, such as class D or class E amplifier types, are commonly used. These kinds of amplifier have theoretical 100% efficiency, and can reach 90% efficiency in practice. Daum et al. reported the design of a system that can provide 60W power with a 70% efficiency for

each channel of array controller [179]. The main loss is from the filtering of output to eliminate high order harmonic components.

Electrical matching circuitry is typically necessary to maximise the energy transfer between the phased array controller and the HIFU transducer. A standard phased array controller will have a 50Ω output impedance, whereas the piezoelectric elements may present an electrical impedance magnitude an order of magnitude higher. Moreover, this electrical circuitry enables direct measurement of the output power [179-181].

5.6.2 Excitation strategy for HIFU

The focusing, or delay, law for HIFU transducers is important for effective phased array transducer operation. This directly relates to focusing accuracy and focusing efficiency. The direct synthesis of beam patterns is the simplest method of focusing. The delay of signals is decided by the sound velocity of the load medium and distance from the element to the focusing point. The amplitude of excitation is assumed identical in each element. However, the limitation is that the nonlinearity of the ultrasound transmitting medium results in a poor realisation of the focusing area and focusing efficiency. These are caused by mainly two reasons: the refraction from the multi-layer interface structure, such as skull, human tissue, chest wall or reaction vessel; the other is the nonlinear propagation associated with high intensity ultrasound. To avoid focusing error and enhance focusing efficiency, a delay law with phase compensation and adjustment of excitation of individual phased array elements was investigated and several possible solutions proposed [174, 182-189].

Pseudo-inverse focus patterns synthesis is based on the pseudo-inverse approach solution of the discretization of the Rayleigh-Summerfield function with a given matrix propagation operator containing complex pressures at a set of control points. Hence, the solution of an unknown vector of the driving signal to an array element can be obtained. In this method, the refraction of ultrasound can be taken into account during computation of the focal law scheme [174, 182-184].

The back-projection method is a magnetic resonance image (MRI) guided method. Assuming HIFU is working in a n-layer structured media, a signal is sent into the medium

and reflected by the n^{th} layer interface. Then by combining MRI data, the normal velocity of the inhomogeneous transmitting media can be obtained and the correct phase distribution of the array calculated [185, 186].

Time-reversal is a method that utilises an ultrasonic point source at the desired focus point. The phase distribution of the array is determined by receiving signals on each element from this point source. In a practical implementation, for example, human brain or high temperature and high pressure reaction vessel, it is difficult to embed an ultrasound point source. Hence, some alternative methods have been proposed. The computed phase distribution from a virtual source is determined from CT image data, or from FEM simulation. However, this method is time consuming and suffers errors due to modelling inconsistencies. This results in low focusing efficiency – about 83% of efficiency compared to an actual source. There is an idea to induce cavitation as the reference source for the time-reversal method, which can reach about 97% of the theoretical maximum intensity [187, 188]. Moreover, micro-bubbles, such as ultrasound contrast agent can be used as a bio-marker. The reflected signals from such contrast agents are received by each array element and used to decide the appropriate phase distribution [189].

In addition to the delay law, the form of the excitation signal is also important. In a standard imaging array system, pulse or chirp excitation is the normal method to drive the array elements. For HIFU application the excitation is usually sorted into 2 main categories: continuous wave (CW) and burst. Normally, for industrial high power application, CW is more commonly used, since more power can be delivered. For clinical implementation, tone bursts with low percentage duty cycle are normally employed. Medical devices are usually more compact and burst signals allow the device to cool down during the off-cycle associated with the tone burst scheme. Typically, sine waves are used, however, wideband excitation signals have also been investigated for HIFU applications. It was reported by Dupenloup and Chapelon, that wideband signals, such as chirp or pseudo random code signals, reduce grating lobe effects in HIFU tissue ablation [190]. And the ratio associated with the relative intensities of sidelobe and mainlobe is inversely proportional to the bandwidth of the signal and aperture of the array. However, this theory is difficult to implement due to high power transducers being typically

narrowband devices to maximise high power delivery efficiency.

5.7 Applications of HIFU

HIFU, for its ability to focus ultrasonic energy in a specific area without inducing high levels of ultrasound intensity in the surrounding area, has been widely employed in the medical clinical field. The first research for HIFU can be traced back to the 1940s, where Lynn et al. used a high power focused ultrasound transducer to identify localized damage without side effects to neighbouring tissue [191]. HIFU for medical clinical applications have been widely investigated in the past two decades to match the significant advancements in medical image technology. However, to date, only a few applications have been investigated for enhancement of industrial processes.

5.7.1 Clinical HIFU applications

HIFU in clinical applications have 3 main areas of application: HIFU therapy, ultrasound enhanced drugs delivery and shock wave lithotripsy. HIFU therapy is normally operated with frequencies between 1MHz to 10 MHz and power levels in the focusing region of 1500 W/cm^2 to 3000 W/cm^2. Tissue temperature increase is the main mechanism associated with HIFU therapy, which can reach above 70^oC during treatment.

The absorption of ultrasonic energy by the tissue region in the focal zone raises the temperature, which then destroys tissue proteins. By this mechanism, HIFU can be used in tumour necrosis, hemostasis and immunotherapy. Tumour necrosis has a wide application range and is used to treat issues in the brain, soft tissue cancer, benign prostatic hypertrophy (BPH) and prostate cancer. Over 1400 patents with cancerous tumours in bone and soft tissue in China have received HIFU treatment. Also, liver and kidney cancer treatments by using HIFU were carried out in Oxford, England [192]. It was also reported by Blana et al. that HIFU treatment improves the survival rate for localized prostate cancer patients [149]. Importantly, the generation of cavitation is normally suppressed during the therapy treatments. However, there has been an intention to utilize cavitation to enhance tissue ablation [24-26]. A set of short width pulses with low percentage of duty cycle was used to excite the transducer. Using this technique, a small tractable cavitation region is produced and used to improve the surgical ablation using a relative low intensity ultrasound, at a high frequency condition [24-26]. Moreover, there is beneficial side effect to HIFU therapy, where an enhanced immune

response after necrosis tumour treatment has been reported and this prevents new tumour growth [149].

Haemostasis is another interesting application for HIFU. Bleeding occurs in trauma situations and during surgical procedures. It is found that HIFU is able to occlude blood vessels and hence stop bleeding. Applications of HIFU haemostasis in emergency medical care, fatal blood sharing and tumour blood supply have been reported [193-195].

HIFU was also investigated as a tool for drug delivery enhancement [196, 197]. It improves the transport of chemicals and genes across biological barriers, for example, cells, tissues and blood clots. The main operating principal is that microjets produced from a cavitation bubble collapse can puncture a drug carrying capsule and assist drugs to permeate through biological barriers. Another approach has been proposed, in which flow around an oscillating bubble generates compressive tensile and stress on the cell wall. Thus, cavitation is considered a useful mechanism for drug delivery applications. In these therapy systems, HIFU normally operates at a low operational frequency to generate cavitation, with low intensity ultrasound excitation utilised to avoid damage to the normal tissue in the propagation path.

Lithotripsy is a non-invasive method to remove kidney stones and gall stones. The lithotripter generates high energy, short duration focused microsecond pulses with a repeat frequency of 1-2 Hz, which results in 20-140 MPa of positive pressure and 8-15 MPa of negative pressure. Its destructive mechanisms include erosion, spallation, dynamic fatigue and shear and circumferential compression. An excellent review of lithotripsy is presented by Biley, et al. [192].

5.7.2 Industrial HIFU applications

Compared to medical clinical applications, investigations of HIFU in industry are limited to Sonochemistry and the food industry. HIFU can generate cavitation with relatively low driving amplitudes due to its focusing ability. It becomes an advantage for high frequency applications, which require a higher acoustic pressure amplitude to generate cavitation An investigation into the cavitation field distribution generated by a 1.2MHz focused transducer was reported by Cao et al. [198]. Other reports about HIFU in Sonochemistry can be found in [189, 198, 199]. At this stage, HIFU applied in

Sonochemistry still remains in the experimental stage with small scale systems, and mainly single element HIFU transducers investigated.

HIFU was also investigated as a tool for application in the food industry. It was reported by Lopez-Ferrer et al., that high intensity focused ultrasound assisted trypsin digestion of proteins [200]. High-throughput identification of proteins is important to proteomics; however, it is time consuming to use traditional procedures to prepare samples. HIFU assisted methods reduced this process from 12 hours to less than 1 minute. The physical mechanism delivering this improvement is not fully understood yet, but it has been hypothesised that the diffusion rates are increasing as the result of cavitation and heating. There was also a report from Catarino et al., describing a combination of HIFU and inductively coupled plasma mass spectrometry (ICP-MS) to evaluate the contaminant elements in Portuguese musts and wines [201]. Hence, it is apparent that HIFU can find application in industrial applications and further reading in this field can be found in [22, 202].

5.8 Summary

High intensity focused ultrasound has quickly developed in recent years and has generated great interest in its application in medical clinical treatments and therapies, such as ablation for surgery and enhancement of drug delivery. Devices to generate HIFU can be either a single element transducer or a phased array transducer. Single element HIFU transducers are simple in manufacture and excitation, but require mechanical manipulation to move the location of its focusing zone. Moreover, these devices have degraded performance in a nonlinear transmitting medium. The phased array technique comes with higher performance in terms of beam steering and adaptive focusing ability. However, these are complex in both manufacture and excitation methodology. In this Chapter, both single element HIFU transducers and phased array transducers were presented and their fundamental operation described.

HIFU applications are still mainly focused on clinical use. HIFU based cancer therapies and drug delivery enhancement are widely researched. Compared to clinical applications of HIFU, applications in industry are limited and it is considered as a developing technology.

The concept of using HIFU for an industrial application is explored in Chapters 6 and 7. The design of HIFU array transducers using both 1-3 connectivity and 2-2 connectivity piezocomposites forms the focus for each Chapter.

Chapter 6

Design, simulation and manufacture of 1-3 connectivity piezocomposite transducers for HIFU application in Sonochemistry

6.1 Introduction

Sonochemistry is a field in which the application of ultrasound is used to interact with a chemical reaction. Typically this is based on cavitation generation through high intensity, low frequency ultrasound. Traditionally, such ultrasound generation systems use single element ultrasonic transducers, such as Tonpilz and magnetostrictive transducers. These transducers were discussed in Chapter 4 and are simple in structure, inexpensive and exhibit high power efficiency. Such an ultrasound generation system can contain several transducers, operating at different frequencies and phase [146, 148]. However, multi-transducer systems require complex design of the reactor to make sure ultrasonic energy is evenly spread within the vessel. Moreover, constructing and deconstructing interference of ultrasound waves can lead to high intensity ultrasonic pressure in near field and hence, produce cavitation close to the transducer surface. This cavitation field greatly attenuates the ultrasonic energy, and prohibits the scale up of a Sonochemical reactor. High power composite array transducer systems offer a potential solution. These devices use relatively low power excitation to produce a high intensity focused ultrasound region in the load medium. Importantly, this prevents the introduction of cavitation in the near field and has the added advantage of beam steering ability, which can manipulate the focal region within the load.

In this Chapter, the design process for 1-3 connectivity piezocomposite array transducers for operation in a high power, low frequency application is presented. Three low frequency, high power 16-element array transducers have been designed and fabricated, with operating frequencies of 210 kHz, 290 kHz and 420 kHz. Preliminary characterization of these devices, including electrical impedance and surface displacement measurements, correlates well with the expected performance predicted via PZFlex. A comparison of the ability of each device to generate a cavitating field, at a number of focal positions, was conducted using a hydrophone and conventional aluminium foil experiments were used to evaluate the performance of the 420 kHz array. Analysis of the design and manufacturing process, alongside the experimental results, is used to provide suggestions for further improvements for the high power array design.

Finite element modelling (FEM) is a simulation tool which is used to aid transducer

design [87, 136]. In this Chapter, the FEM analysis software package PZFlex was used to simulate the design of the piezocomposite configurations for application in a HIFU array device. A review of piezocomposite technology and arrays was presented in Chapter 5.

6.2 Design specification for 1-3 composite transducers for HIFU application

The traditional frequency range applied in Sonochemistry applications is under 600kHz [30, 203, 204], with the majority of systems operating under 100kHz, as the cavitation threshold increases as a function of frequency. Interestingly, medical HIFU operates in the megahertz range in order to avoid cavitational effects and produce a tighter focused region [25, 150, 205]. The transducers presented in this Chapter are designed to operate between these two regimes, within the nominal frequency range 200-400 kHz. When compared to standard Sonochemistry applications in the sub-100kHz range, the proposed frequency range will reduce the complexity in manufacturing thick piezocomposite plates and also provide an enhancement in the focusing and steering ability of the array due to the smaller wavelengths within the 200-400 kHz range.

PZT4D piezoelectric ceramic, which is appropriate for high power applications, was used as the active phase in each of the piezocomposite designs. This material was available in dimensions 80 x 40 x 10mm and hence, appropriate for use in the frequency range 200-400 kHz. In all three arrays, the passive filler material is Vantico HY966EN/CY221 (Huntsman, UK) which is a medium setting epoxy (MSE) with sufficient shear wave attenuation at the frequency of interest to limit inter element cross-talk [87]. Typical design rules for saw width and ceramic pillar width were applied [137, 206]. The dimensional details of these 3 transducers are presented in Table 6.1. These parameters were selected after a thorough FEM programme to determine appropriate piezocomposite designs within the desired frequency band. Details of the simulation results will be presented in Section 6.3.

In this work, the piezocomposite transducer was designed to generate high power; therefore, a high mechanical-Q value is of greater importance rather than the bandwidth of the device. Moreover, for this particular application, the introduction of a backing block will influence dissipation of thermal energy from the active phase during high power operation, due to low heat conductivity of the backing material. Consequently, no backing material has been introduced in any of these three transducers.

Table 6.1 *Manufacture specifications for the 1-3 connectivity piezocomposite designs*

Piezocomposite Identifier	**A**	**B**	**C**
Operating frequency, kHz	200	300	400
Saw Pitch, mm	1.5	1	1
Saw Width, mm	0.6	0.3	0.3
Ceramic Volume Fraction (%)	36	49	49
Pillar Aspect Ratio	0.1125	0.1667	0.175
Finish Dimensions, mm	80x40x8	60x30x6	60x30x4

In matching layer design considerations, normally a single matching layer design is sufficient for water loaded applications, especially for low ceramic volume fraction (CVF) piezocomposite designs. For this work, to further improve coupling between the piezocomposite and the water load, a two layer matching design has been implemented. The first layer is a particle loaded hard setting epoxy (HSE) using Vantico HY1300/CY1301 (Huntsman, UK) filled with 73% w/w calcined alumina (Logitech, UK) to give an acoustic impedance of 6.3 MRayl. The second, outer, matching layer is MSE with an acoustic impedance of 2.3 MRayl. The dual layer matching design approach described by [171] has been used to determine the layer thicknesses as detailed in Table 6.2.

Table 6.2 *Matching layer configuration*

Piezocomposite Identifier	**A**	**B**	**C**
Loaded HSE, mm	3.4	2.4	1.6
MSE, mm	3.0	2.1	1.4

In clinical HIFU applications, in order to adhere to clinical safety considerations, there is a requirement to precisely control the focusing region and ensure rapid power drop off outside the focus area. However, these are not primary considerations for Sonochemistry applications, where a large focus spot size and high sidelobe level may be tolerable. Therefore, the linear array configurations used for these devices are relatively crude. For high resolution imaging applications it is considered that each array element will contain

at least 3 ceramic pillars to promote homogeneous behaviour of the composite microstructure [136]. In this work, there are only two ceramic pillars comprising the width of each array element. This is to simplify the fabrication process by ensuring the ceramic pillars are wider and therefore, more robust. Consequently, it will be important to consider the surface vibrational characteristics to ensure any inhomogeneity has negligible impact on the operation of the array transducers. Moreover, the element arrangement does not follow the conventional λ/2 element spacing guidelines, which can reduce sidelobe levels and improve focusing capability [207]. For information, the array element pitch to wavelength ratio for each configuration is also provided as a function of λ.

Table ***6.3*** details the array element configuration for each of the three array designs. For information, the array element pitch to wavelength ratio for each configuration is also provided as a function of λ.

Table 6.3 *Linear array element layout for each piezocomposite configuration*

1-3 Piezocomposite	**A**	**B**	**C**
Element Pitch, mm	4.6	3	3
Active Element Width, mm	2.4	1.7	1.7
No. of Elements	16	16	16
Pitch/Wavelength Ratio	0.6λ	0.6λ	0.8λ

6.3 FEM simulation of 1-3 connectivity piezocomposite configurations

6.3.1 Simulation methodology

The simulation of the HIFU transducer configuration will assist in the design process. It is important to evaluate the design by simulation to prevent unwanted artifacts in the transducer performance. In this Chapter, the FEM software package PZFlex, which predicts the electrical impedance analysis, impulse response, and beam form prediction of the transducer by simulation, is employed. Figure 6.1 provides an illustration of the basic 2D finite element model used in this Chapter, where the piezoceramic and epoxy widths will differ for each piezocomposite configuration as detailed in Table 6.1. Moreover, the array element electrode width will also vary as described in Table 6.3, although this equates to each array element covering exactly 2 piezoceramic pillars. This can be observed in the Figure, with the thick gold lines representing a thin film electrode (note – electrode width is not to scale).

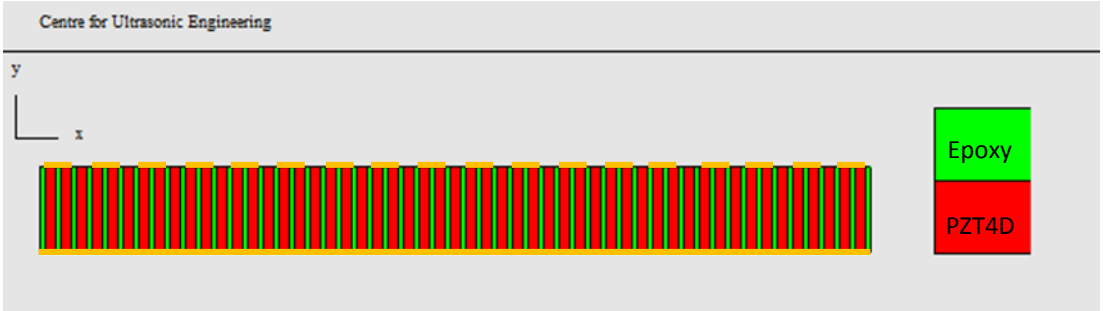

Figure 6.1 *Illustration of the 2D finite element model used to simulate the piezocomposite structure*

In the initial simulation of electrical impedance of the HIFU transducer configurations, no matching and backing layers were applied and the piezocomposites were coupled using free boundary conditions. The impedance of the single array element in the centre of the piezocomposite was analysed without an external electric circuit connected to the device. In this process, wideband short pulse signals were generated to excite the piezocomposite. Then the voltage and current on the excited electrodes are recorded and analysed in frequency domain to calculate the electrical impedance as a function of

frequency.

It was decided to simulate the pulse-echo response for each array, as this is a typical experimental array characterisation technique. Thus, it will be possible to compare the experimental and simulated results. Moreover, in the simulation of the pulse echo response, the extrapolation technique was employed. The piezocomposite was modelled as directly coupled to the water load through the two layer matching design, as described in Section 6.2. A wideband short pulse signal excitation drove the element electrode through a 50 Ω resistor. The generated ultrasonic wave propagated through the water and interacted with an ideal reflector on 50mm. The reflected signals were received by the same element, which is connected to a 1MΩ resistor. The receiving signals were analysed in both time domain and frequency domain, and the mechanical-Q value and bandwidth of the simulated transducers analysed.

Beam forming prediction is important to this specific application, due to the requirement for focusing and steering ability. It is of interest to fully understand the capabilities of these piezocomposite arrays before manufacture. In this case, the designed piezocomposite array, incorporating the 2 matching layer system, was directly coupled to the water load. Focus law delays were calculated and included into the FEM model to focus at a depth of 100 mm and at angles of 0^o and 10^o to the central axis of the array.

6.3.2 Simulation results

The predicted electrical impedance spectra for the uniformly electroded piezocomposite configurations A, B, and C are shown in Figure 6.2. These clearly show a unimodal piezoelectric behaviour for the whole piezocomposite each configuration. Next, the predicted electrical impedance spectra for the single element of piezocomposite array configurations are shown in Figure 6.3. It should be noted that these were predicted for single element excitation and hence, the parasitic modes within these predictions are as a result of array element periodicity [134, 136]. The electrical impedance minimum relates to the operational frequency for these HIFU devices and has been predicted at 210kHz, 290kHz and 420kHz for arrays A, B and C respectively.

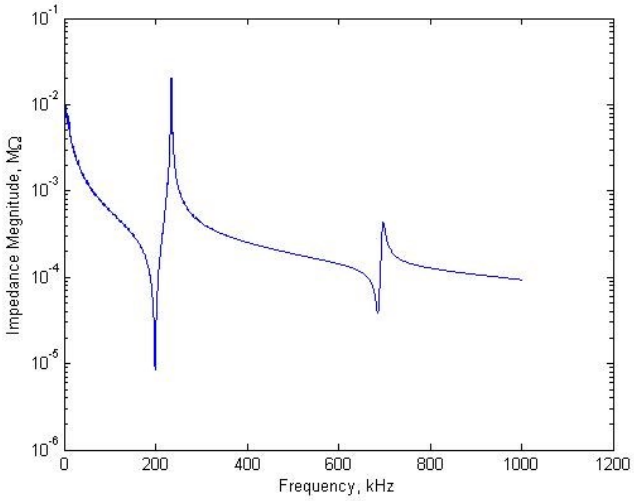

(a)

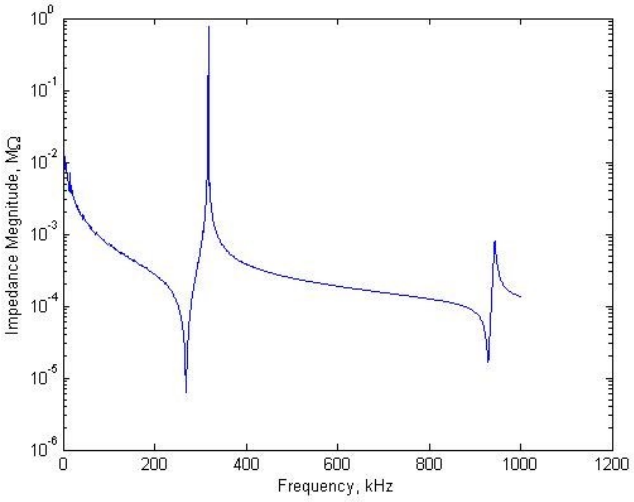

(b)

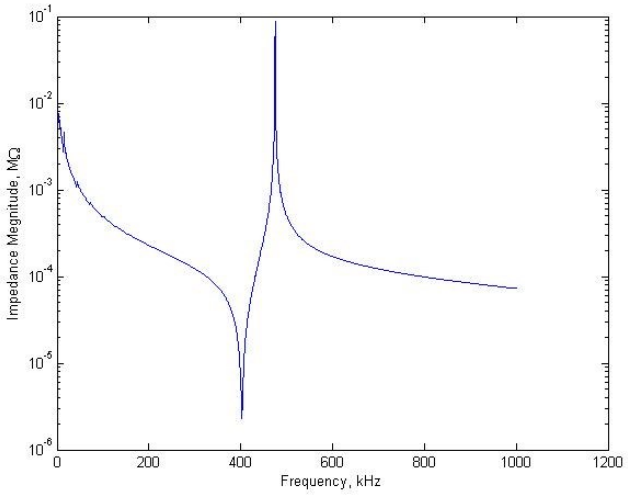

(c)

Figure 6.2 *Predicted electrical impedance spectrum for each piezocomposite configuration uniformly electroded*
(a) 1-3 Piezocomposite A, (b) 1-3 Piezocomposite B, (c) 1-3 Piezocomposite C

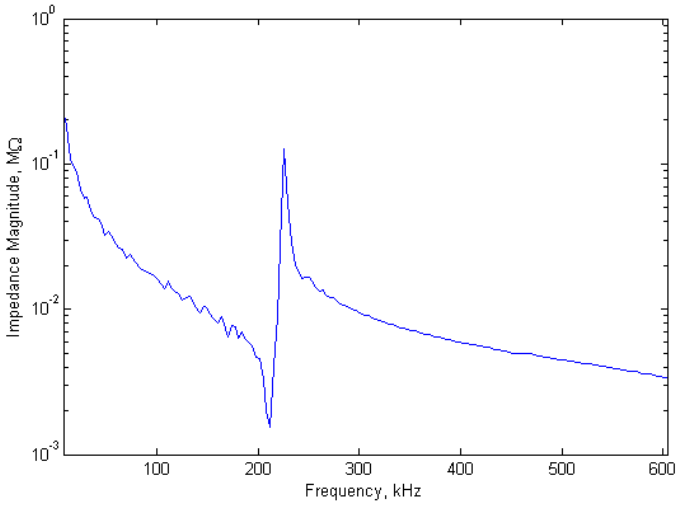

(a)

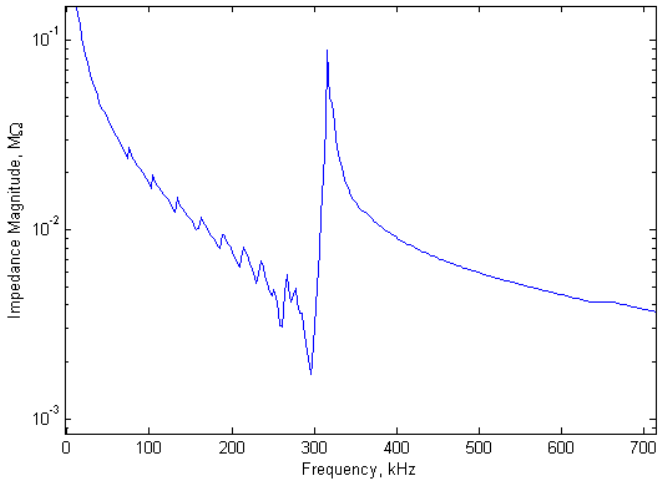

(b)

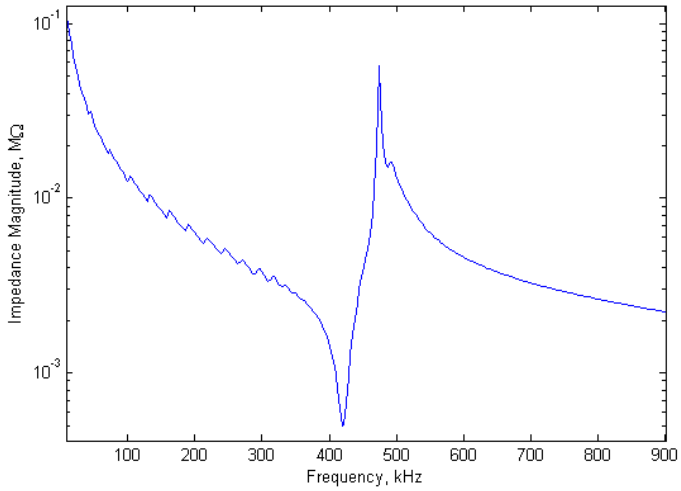

(c)

Figure 6.3 *Predicted electrical impedance spectrum for each piezocomposite configuration, with only a single array element excitation*
(a) 1-3 Piezocomposite A, (b) 1-3 Piezocomposite B, (c) 1-3 Piezocomposite C

The pulse echo simulation results are shown in Figure 6.4 - Figure 6.6 and the results collated into Table 6.4. Both 6dB bandwidth and quality factor (Q) were calculated, where the Q factor is defined as:

$$Q = \frac{f_c}{f_1 - f_2} \tag{6.1}$$

where f_c is the centre frequency,

f_1 is the upper 3dB cut off frequency,

f_2 is the lower 3dB cut off frequency.

The designed piezocomposites have Q factor, ~20, and exhibit a reasonable 6dB bandwidth of ~ 10%. These results can be explained through the fact that no backing material is used in the design and a 2-layer matching configuration is employed. The non-backing nature of this structure will increase the Q factor significantly. Moreover, the 2 matching layer structure will reduce the loss at the interface between the water load and the piezocomposite and hence, improve the sensitivity and bandwidth of transducer. It should be noted that the predicted pulse-echo spectral response for Devices A and C, Figures 6.4(b) and 6.6(b), have several peaks as a result of the additional resonance mechanisms introduced by the attachment of the matching layer.

Table 6.4 *Results extracted from pulse echo FEM results*

1-3 Piezocomposite	**A**	**B**	**C**
6dB Bandwidth, kHz	20	30.6	41
Mechanical-Q value	20	19	21

The beam forming prediction is based on pressure field simulations in PZFlex and results are displayed in Figure 6.7 - Figure 6.9. In each Figure, the top image relates to axial focus at a distance of 100mm and the bottom image illustrates the focus located at a 10^o angle to the centre axis of the array. From these results, it is clear that the 1-3 Piezocomposite C has best focusing and steering ability. This is a result of its higher operating frequency and higher array element width to wavelength ratio (see Table 6.3). The other configurations would be useable, but suffer from larger focal region, which results in a lower peak pressure, and/or significant sidelobe activity. To quantify these results, Table 6.5 presents the calculated -3dB focal region for each of the plots in Figures

6.7 - 6.9. These results indicate that Device C delivers the smallest 3dB focal region on/off axis and highest peak pressure. Consequently, Device C is considered as the best device among these three and used in the experimental assessment of cavitation generation.

Table 6.5 *Predicted focused region for each HIFU array configuration calculated using the -3dB pressure magnitude area*

	1-3 Piezocomposite A	**1-3 Piezocomposite B**	**1-3 Piezocomposite C**
0 degree	708 mm^2	963 mm^2	673 mm^2
10 degree	801 mm^2	1276 mm^2	686 mm^2

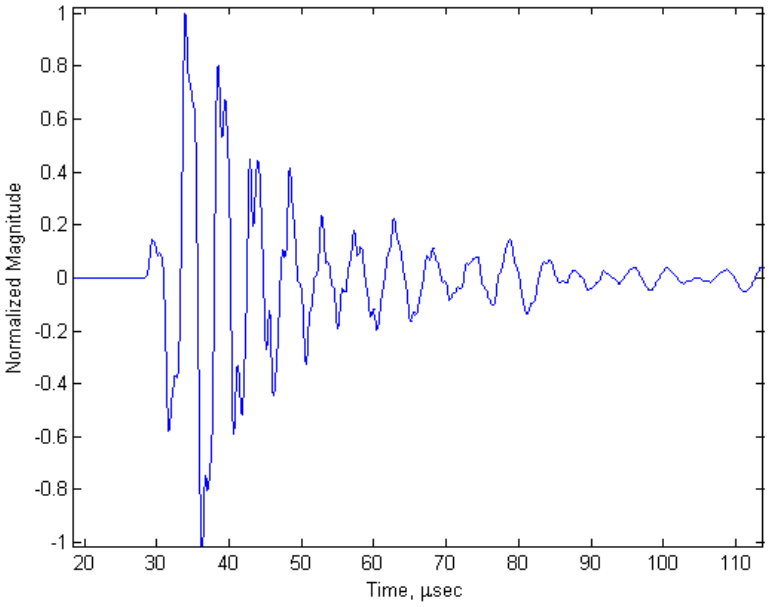

(a)

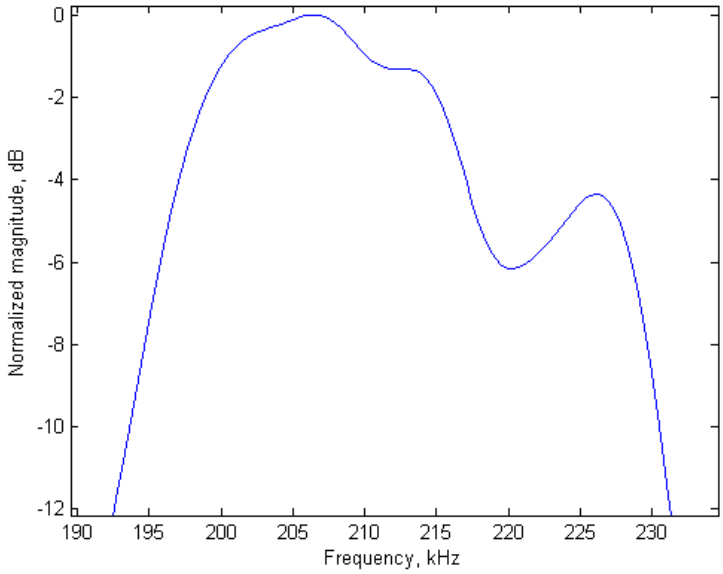

(b)

Figure 6.4 *Predicted pulse echo response of 1-3 Piezocomposite A, (a) time domain, (b) frequency domain*

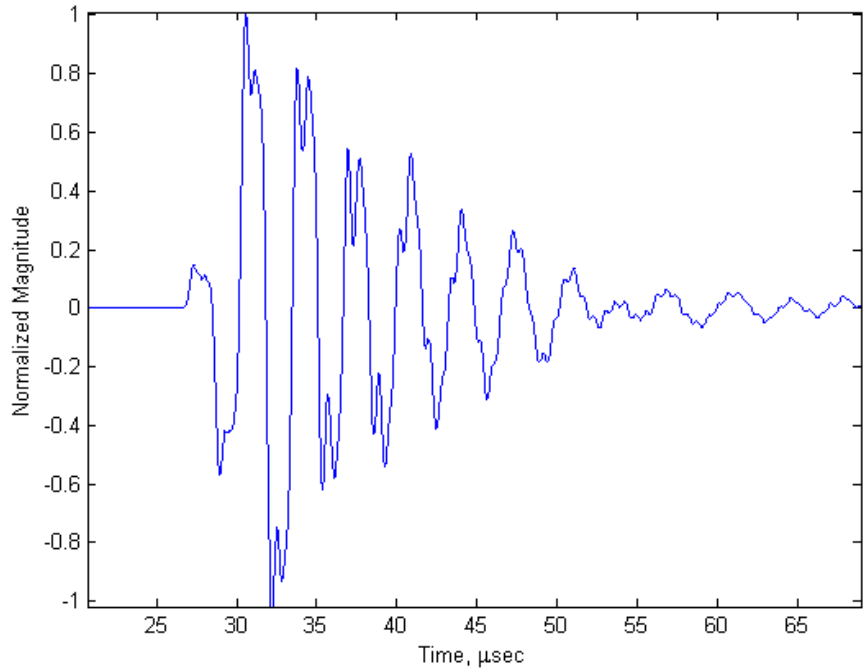

(a)

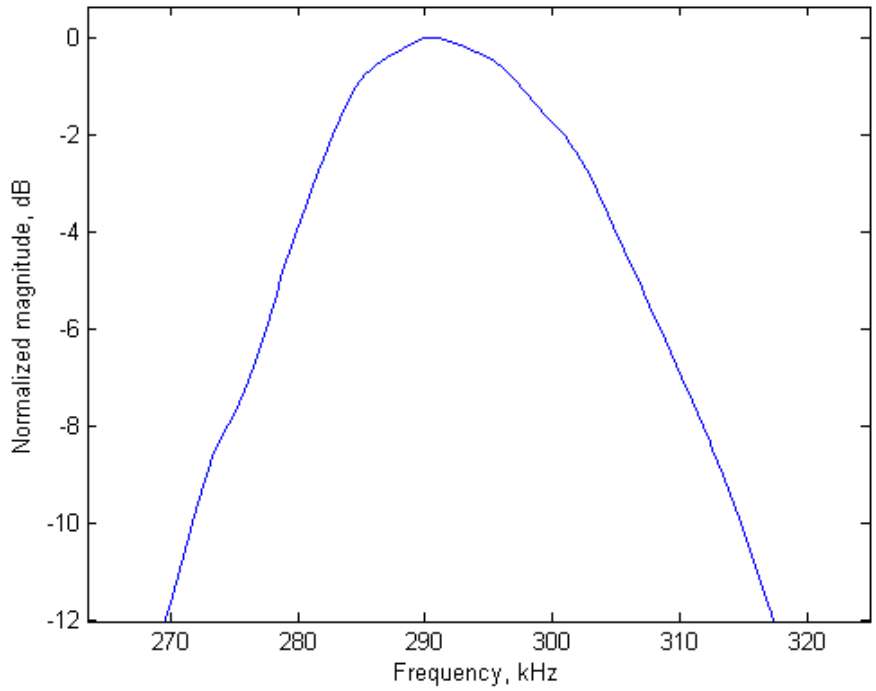

(b)

Figure 6.5 *Predicted pulse echo response of 1-3 Piezocomposite B, (a) time domain, (b) frequency domain*

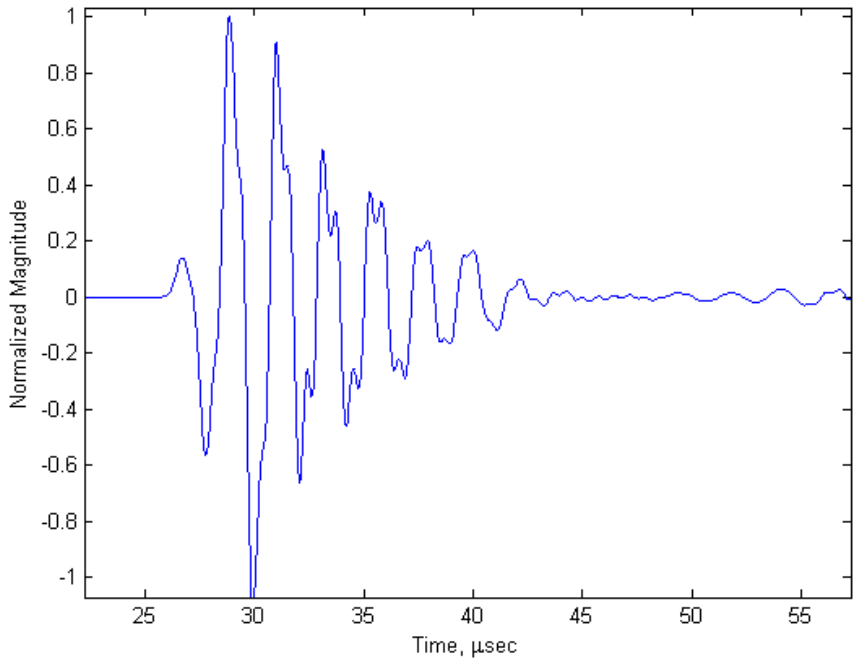

(a)

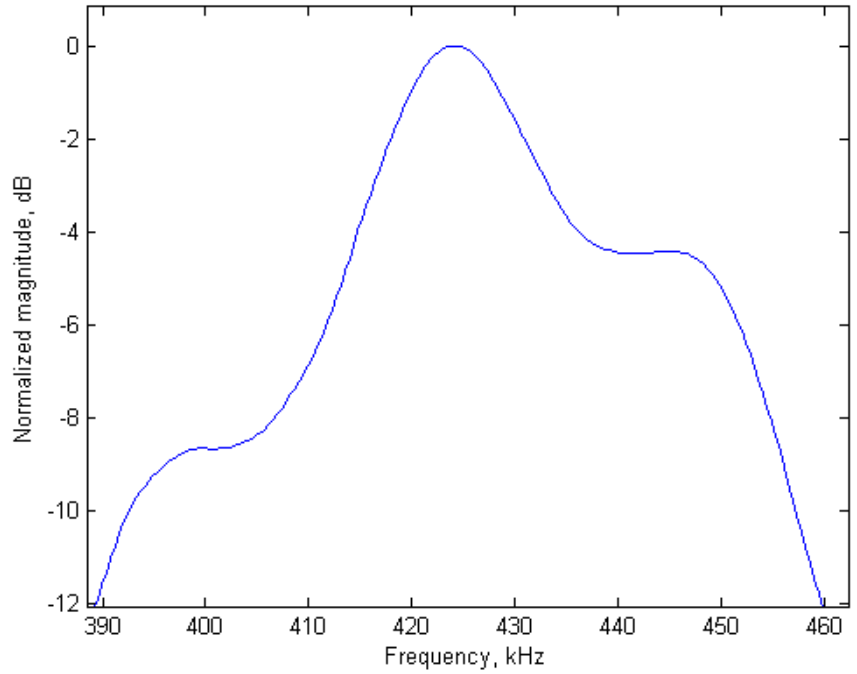

(b)

Figure 6.6 *Predicted pulse echo response of 1-3 Piezocomposite C, (a) time domain, (b) frequency domain*

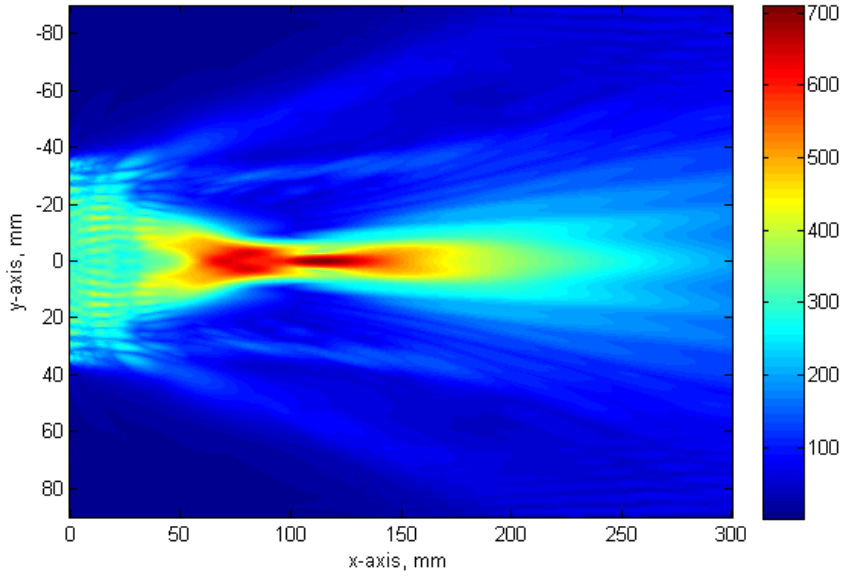

(a)

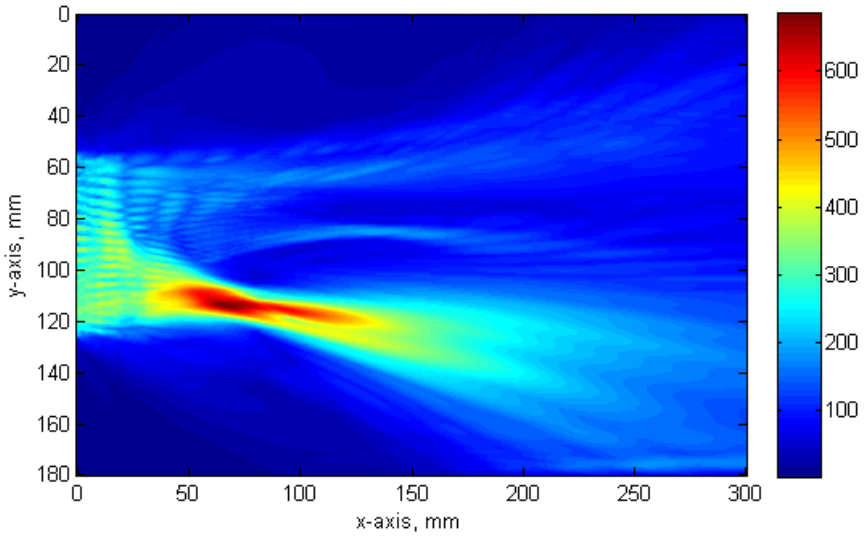

(b)

Figure 6.7 *Pressure prediction for 1-3 piezocomposite A, (a) focusing at 100 mm depth, 0 degree, (b) focusing at 100 mm depth, 15 degree*

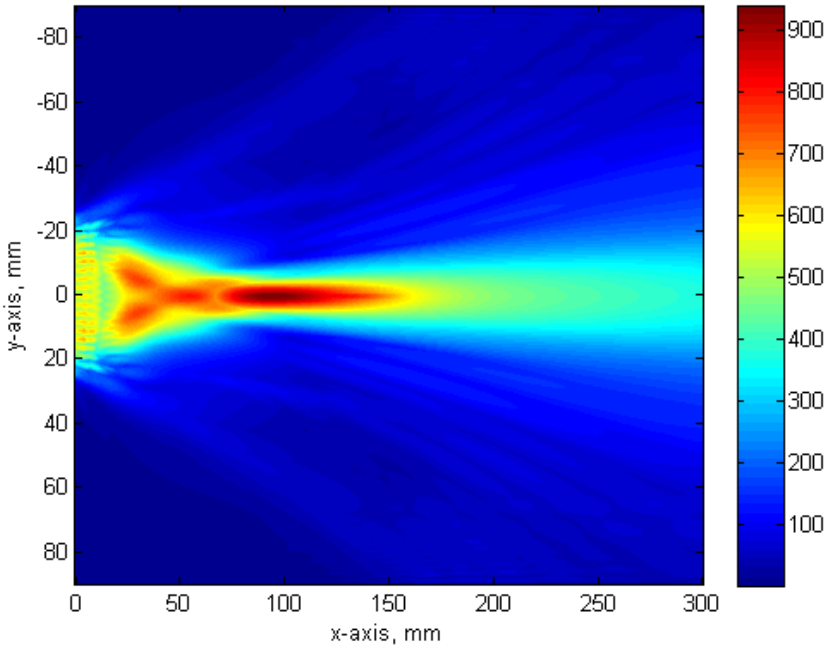

(a)

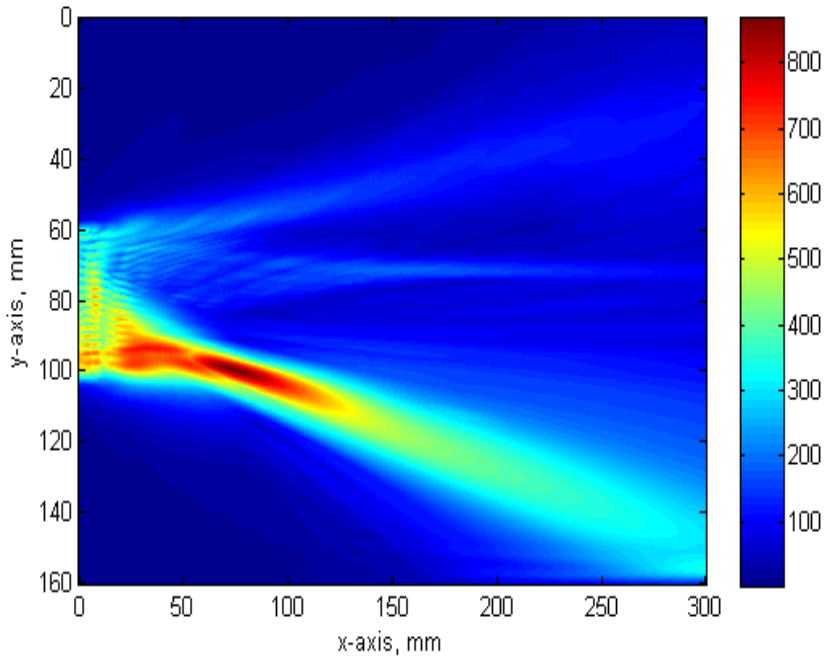

(b)

Figure 6.8 *Pressure prediction for 1-3 piezocomposite B, (a) focusing at 100 mm depth, 0 degree, (b) focusing at 100 mm depth, 15 degree*

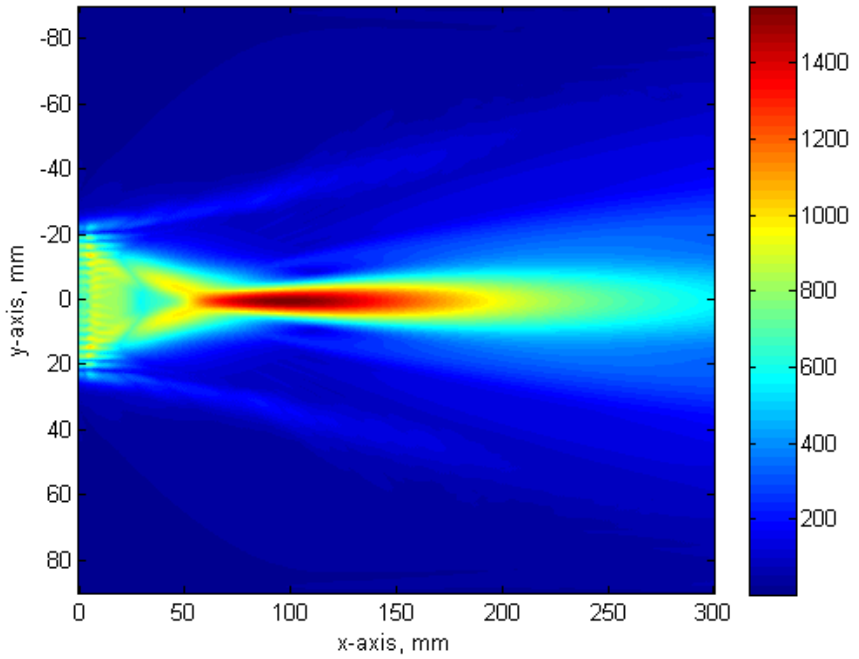

(a)

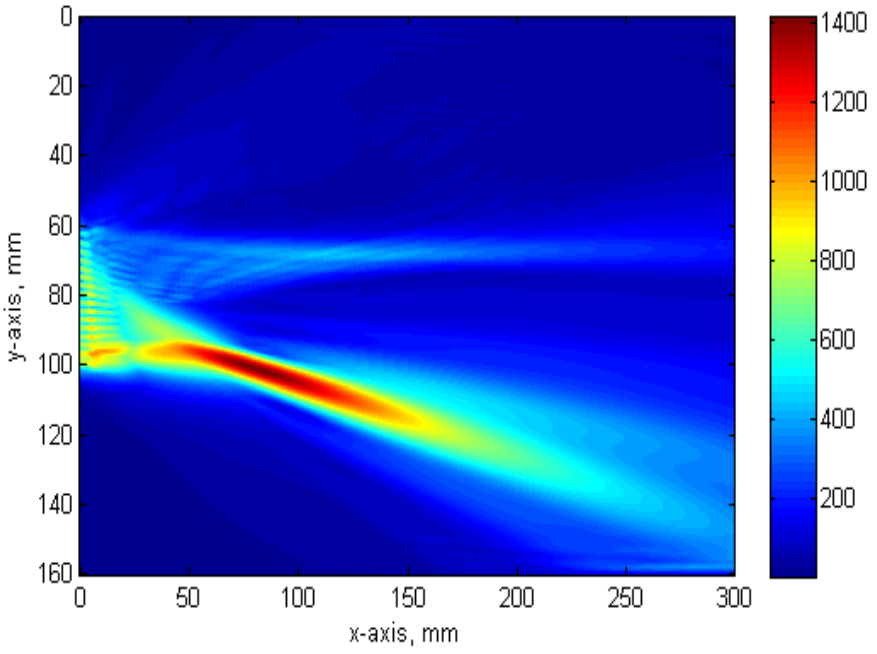

(b)

Figure 6.9 *Pressure prediction for 1-3 piezocomposite C, (a) focusing at 100 mm depth, 0 degree, (b) focusing at 100 mm depth, 15 degree*

6.4 Array transducer manufacture and calibration

6.4.1 Manufacture of piezocomposite array transducers

The piezocomposite manufacture is based on the dice and fill method [158]. The piezoceramic was diced in both directions and epoxy was used as a filler material, as detailed in Tables 6.1 – 6.3. Twisted pair wire, with electrical shielding, was used to provide interconnects to each array element. Each cable contains 4 wire pairs and hence, 4 cables were used for each array transducer. Piezocomposite C with cables connected is illustrated in Figure 6.10.

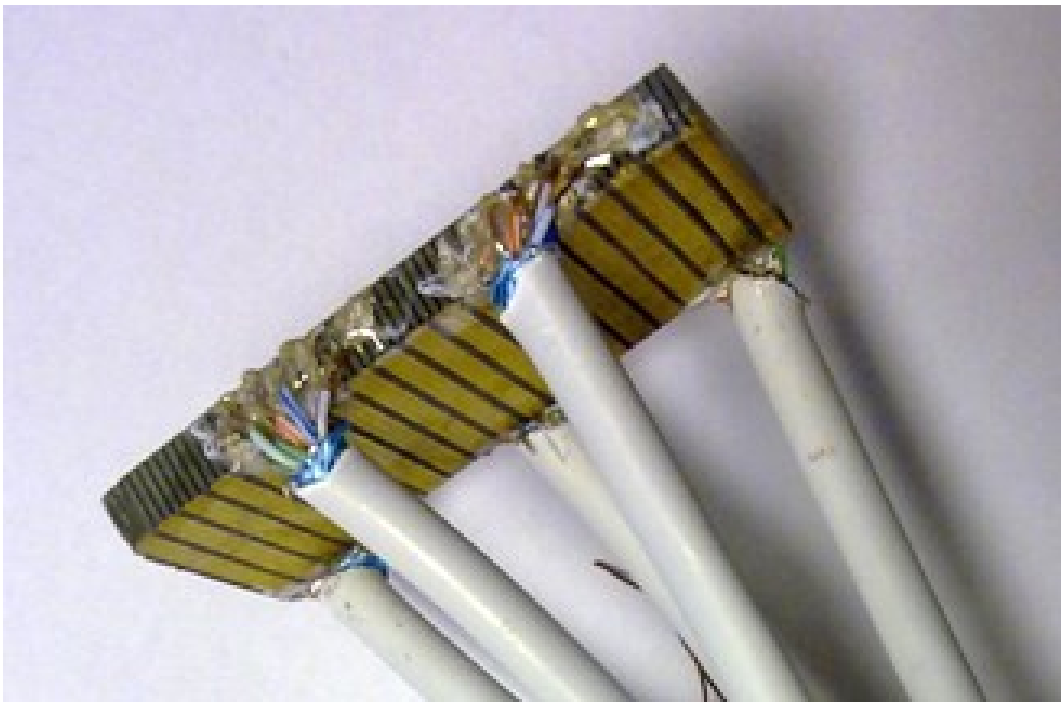

Figure 6.10 *Fabricated piezocomposite C with wires connections attached*

The transducer housing was fabricated from a stainless steel cylinder and is shown in Figure 6.11. To ensure waterproof operation of the transducer, it was sealed with a rubber seal at the rear face and each cable was fed through a water-proof gland, as shown in the left hand image of Figure 6.11. The transducer was connected to the phased array controller using an ITT connector as illustrated in Figure 6.12.

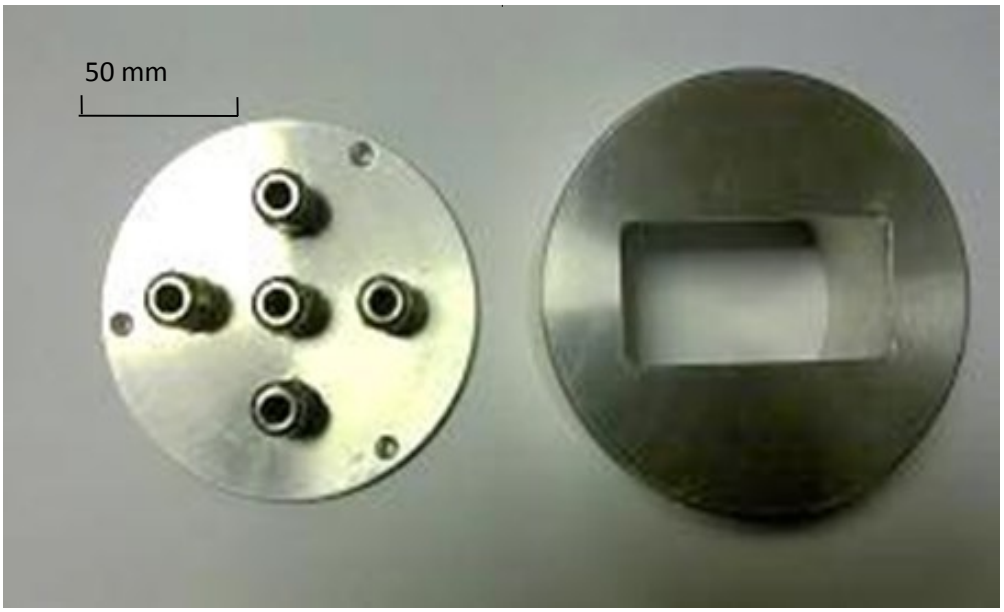

Figure 6.11 *Manufactured transducer housing: left hand side is the lid containing 5 waterproof glands; right hand side is the main body of the casing, with an aperture cut out for the array to be located*

Figure 6.12 *ITT connector used to interface the array transducer to the phased array controller*

6.4.2 Characterisation of the manufactured array transducers

A number of characterization procedures were carried out on the fabricated arrays prior to evaluation in a high power configuration. First, electrical impedance measurements were acquired using a HP 4194A Impedance Analyzer, (Agilent, UK). This provided evidence that the fabricated arrays have good correspondence to the PZFlex simulated results generated during the design phase. A comparison of the magnitude of the electrical impedance for both simulated and experimental data is presented in Figure 6.13. The impedance minimum, electrical resonant frequency, shows good correspondence, which is excellent as this is the excitation frequency for the HIFU arrays. However, at the mechanical resonant frequency the predicted impedance is significantly higher for all three devices. It is considered that this is due to the damping co-efficient for the polymer filler material being incorrectly represented in the model [208]. Importantly, as this is a transmission only device, the electrical impedance frequency is the critical feature and has been correctly predicted.

Pulse-echo experiments were then conducted to measure the transducer's bandwidth and Q factor. Here, a single element of the array was excited and the reflected echo from a flat steel reflector received by the same element and subsequently, analysed in both the time and frequency domains. Figure 6.14 presents a comparison between the experimentally measured and theoretically determined pulse-echo response for a single element of each array transducer. Table 6.6 presents the measured bandwidth and Q factor properties for each array. Interestingly, the fabricated arrays all exhibit wider bandwidth and lower Q characteristic, when compared to the FEM simulation results. This is not particularly surprising as a 2D model has been used in the simulation process. Importantly, the fabricated array performance provides confidence that these arrays can be used in a HIFU operational mode.

Table 6.6 *Measured bandwidth and Q factor for a single element in each array transducer configuration*

	1-3 Piezocomposite		
	A	B	C
6 dB Bandwidth, kHz	92	73.3	146.6
Q Factor	2.3	4.1	3.1

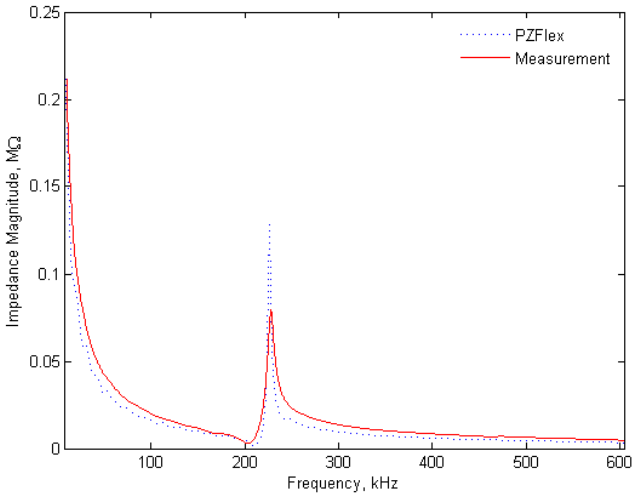

(a)

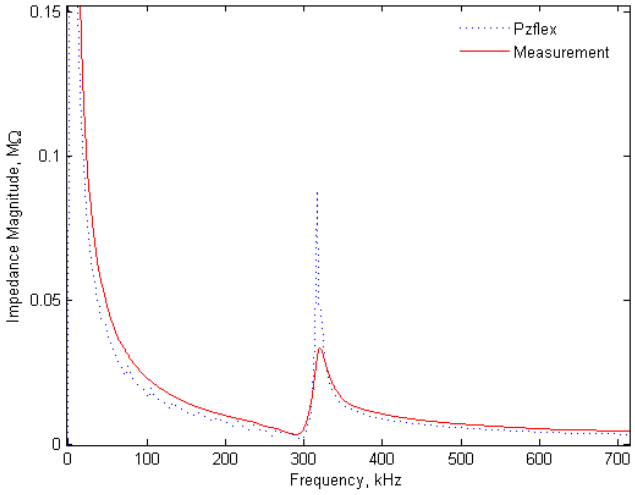

(b)

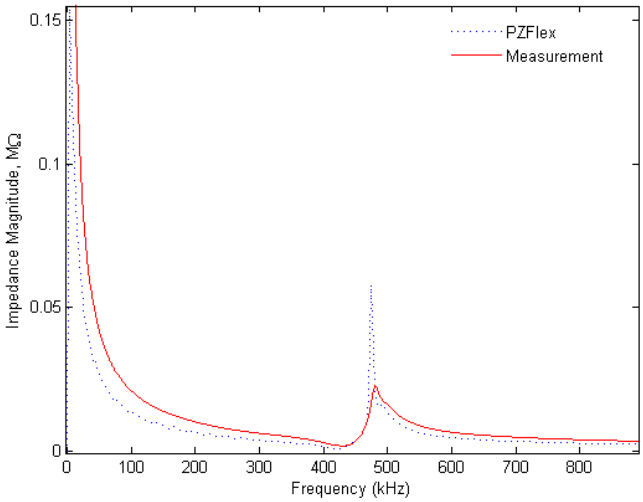

(c)

Figure 6.13 *Comparison of experimentally measured and PZFlex derived electrical impedance characteristic for (a) 1-3 Device A, (b) 1-3 Device B, (c) 1-3 Device (c)*

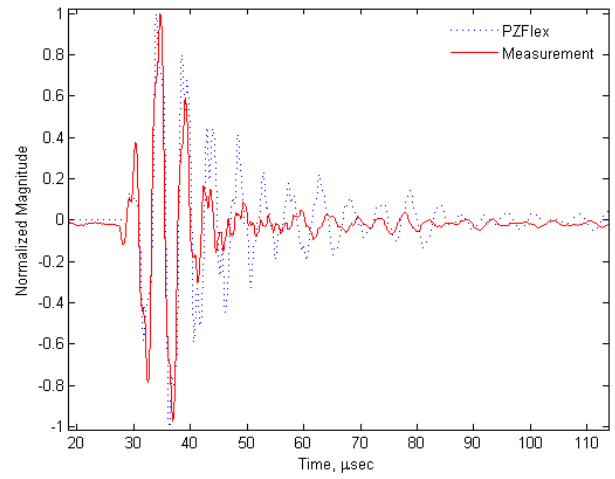

(a)

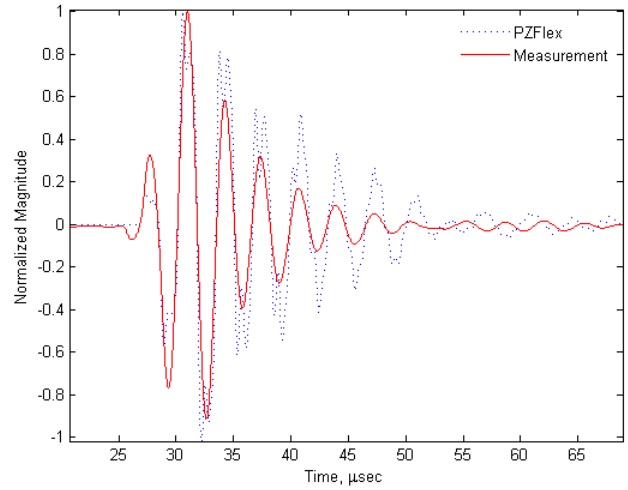

(b)

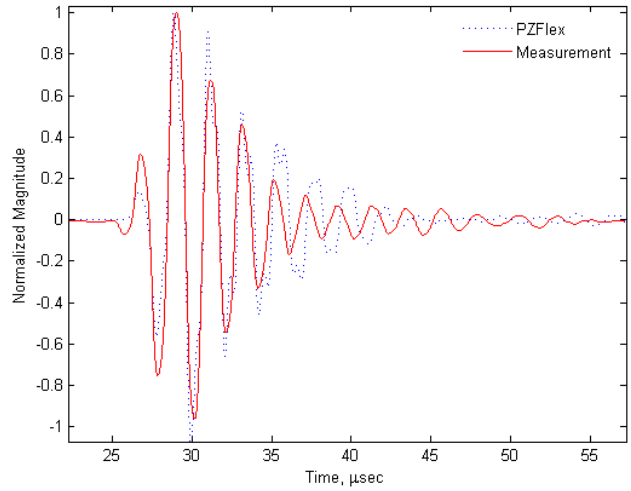

(c)

Figure 6.14 *Comparison of experimentally measured and PZFlex derived pulse-echo response from a steel reflector immersed in water for a single element of (a) 1-3 Device A, (b) 1-3 Device B, (c) 1-3 Device C.*

Next, the surface displacement of the array was characterized by using a PSV-300 scanning laser vibrometer (Polytec, Germany). A single element was excited using a tone burst at the device centre frequency and the magnitude and phase of the surface dilation measured across the array aperture. The surface vibration through the centre line of the array has then been extracted and presented in Figure 6.15. In each Figure, the peak displacement corresponds to the array element being electrically excited and it is then possible to determine the extent of mechanical cross-talk within the array by analysing the displacement levels across the entire array aperture. Calculated mechanical cross-talk for devices A, B and C are 5 dB, 6dB and 10 dB, respectively.

Finally, pressure field measurements were recorded to demonstrate the focusing and steering abilities of each fabricated array. The ultrasound pressure was measured using a HPM1/1 needle hydrophone (Precision Acoustics, UK), which minimized the disturbance of the pressure field and provided a direct measure of the acoustic pressure in the load medium. A Zetec Dynaray phased array controller was used for this procedure. The system was configured to drive the array elements with a 100V, 100ns width pulse. Focal law calculations were performed for each array configuration to generate a focal region at two distinct angles: on-axis (0^o) and $\pm 15^o$ off-axis, in each case the focus was at 100mm distance from the array. The pressure field mapping results are shown in Figure 6.16 – Figure 6.18. In these measured results, each plot has been effectively normalised by the commercial Ultravision package used to control the Dynaray phased array controller. Hence, the value of gain used in each acquisition is indicated in the figure caption.

These pressure field results show good correlation with the predictions produced through FEM analysis, as shown in Figure 6.7 to Figure 6.9. Again, Piezocomposite C demonstrates the best focusing and steering ability and it is this device that will be used in the high power evaluation phase of the work.

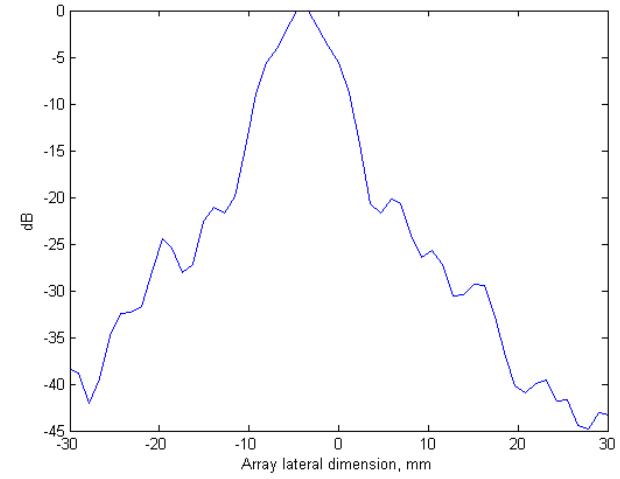

(a)

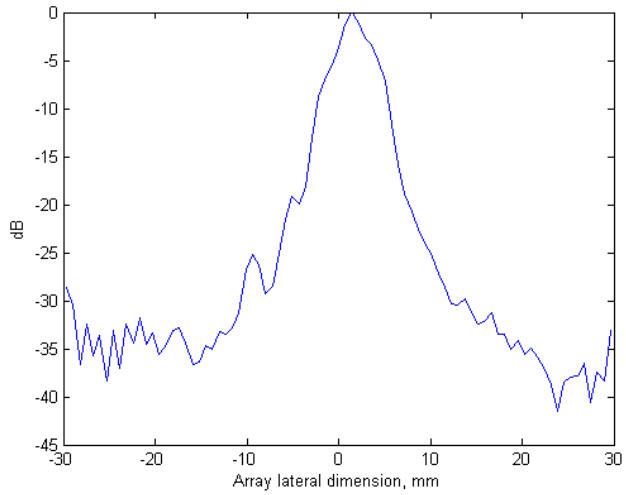

(b)

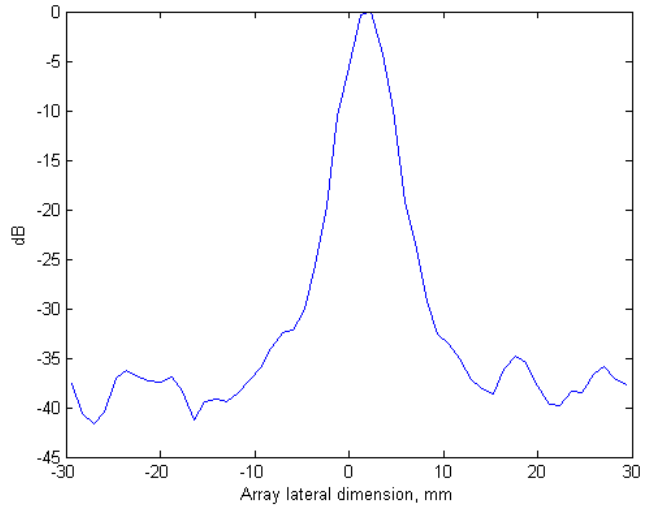

(c)

Figure 6.15 *Cross-section through the measured surface displacement for each transducer when the centre right element is excited, (a) 1-3 Device A, (b) 1-3 Device B, (c) 1-3 Device C.*

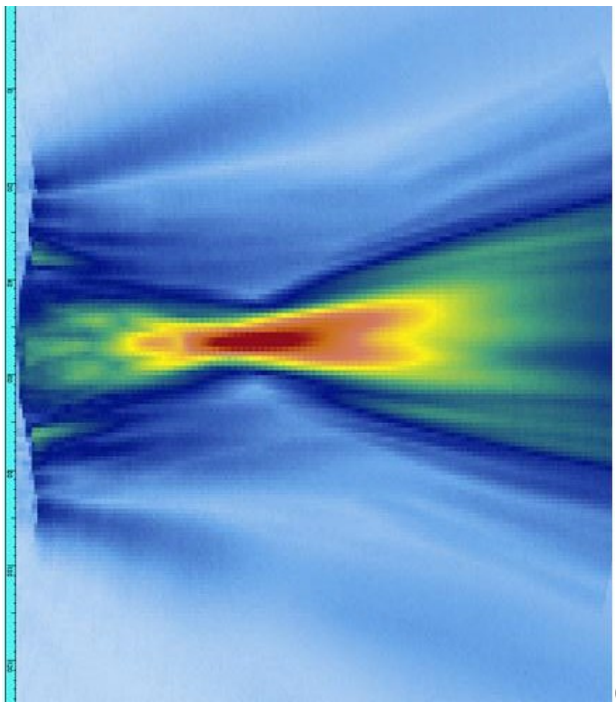

(a)

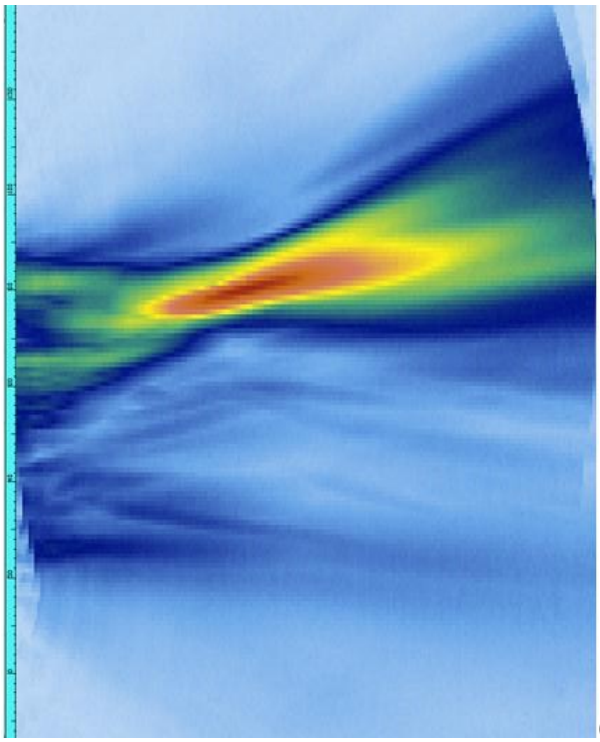

(b)

Figure 6.16 *Measured pressure field measurement for 1-3 Device A, (a) on-axis focus with 58.5dB gain, (b) off-axis focus with 58.5dB gain*

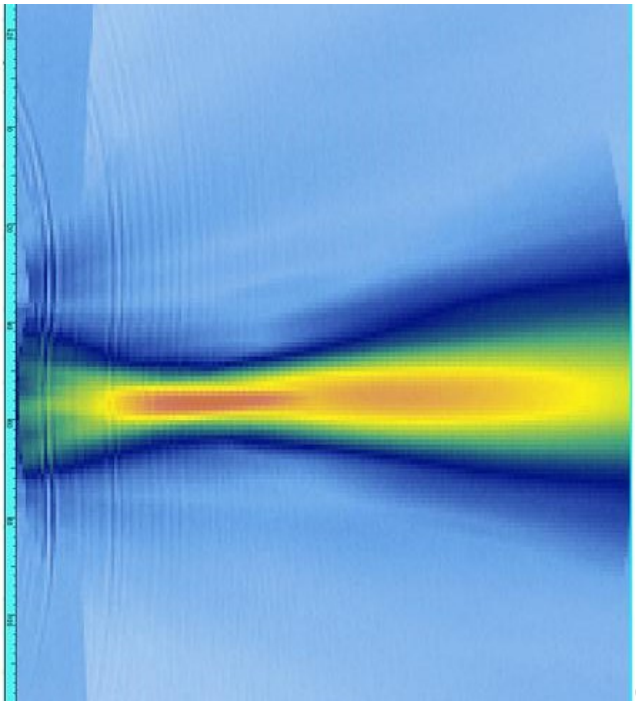

(a)

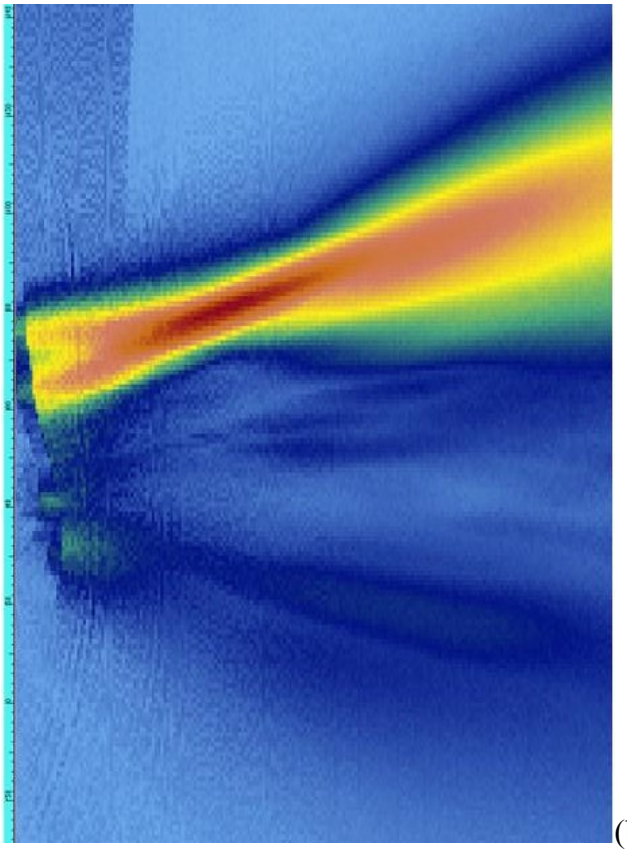

(b)

Figure 6.17 *Measured pressure field measurement for 1-3 Device B, (a) on-axis focus with 59dB gain, (b) off-axis focus with 63.5dB gain*

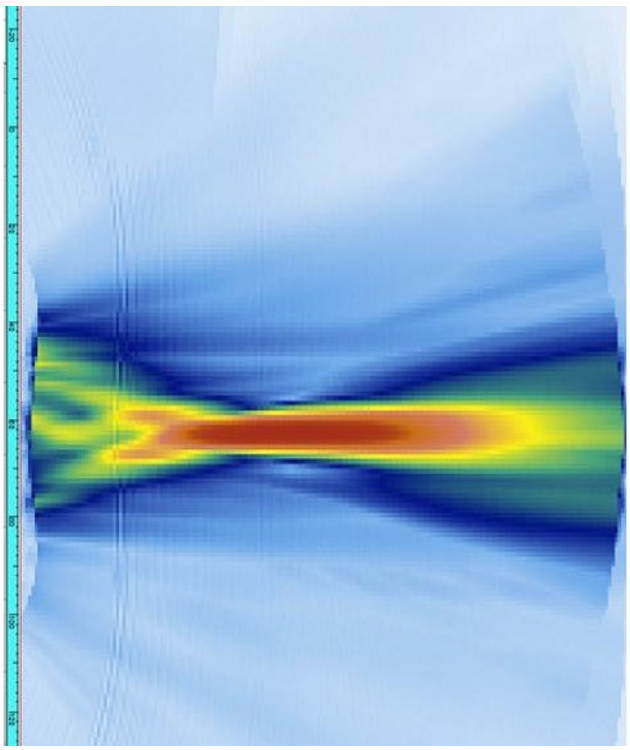

(a)

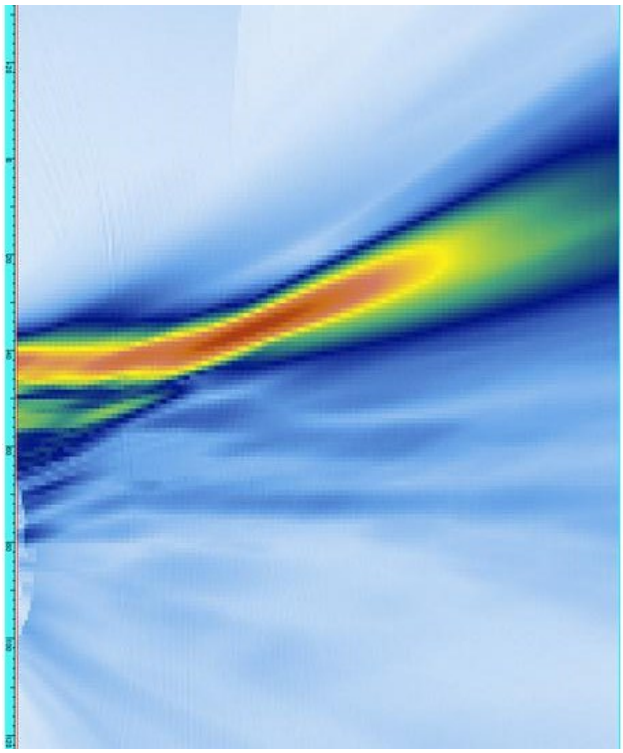

(b)

Figure 6.18 *Measured pressure field measurement for 1-3 Device C, (a) on-axis focus with 52.5dB gain, (b) off-axis focus with 52.5dB gain*

6.5 Cavitation ability evaluation

The ability to generate cavitation is important for transducers in Sonochemistry applications. The cavitation capability evaluation work is based on two methods: pressure measurement and aluminium foil experiments. The preliminary evaluation of acoustic cavitation produced by the fabricated piezocomposite arrays used the 420 kHz device. This was selected as the cavitation threshold is frequency dependent and therefore, this was the most challenging case. The test utilized a piece of aluminium foil placed in the focal region of the array. The OPEN phased array controller (LeCoeur Electronique, France) was used in order to deliver a sine wave tone burst to the array elements. The excitation signal was a 16-cycle, 420kHz sine wave with a peak-to-peak voltage of 100V. An appropriate delay law was defined for an on-axis focus at 100mm range and the aluminium foil was exposed for a period of one hour. In addition, the acoustic pressure at the focal point was measured as a function of drive voltage. Low voltage excitation (10, 20, 30, 40V) was used in these experiments to ensure subcavitation operation to protect the PVDF hydrophone device. It has been reported that the experimental cavitation threshold for a 400 kHz ultrasonic field in water is 1MPa [6] and hence by measuring the acoustic pressure generated by the focused array configuration, it is possible to determine the suitability of these arrays for Sonochemistry applications

The first experimental result measured the relationship between excitation voltage and the pressure amplitude at the focal region. This is detailed in Table 6.8 and can be used to determine the excitation voltage required to match the 1MPa cavitation threshold. Therefore, extending these results would indicate that a 95V excitation would be required to match the 1MPa threshold.

Table 6.7 *Relationship between excitation voltage level and measured pressure at focal point for device C*

Excitation Voltage, V	Pressure, MPa
10	0.116
20	0.210
30	0.290
40	0.398

The final experimental result illustrates that cavitation has been generated by device C

operating at 420 kHz. Figure 6.19 clearly shows perforations produced in a sheet of aluminium foil situated in the focal region of the array when insonified for a period of one hour. It is recognised that this timescale is too long for a conventional Sonochemistry process, but as discussed earlier in the Chapter this result has been generated using the most challenging frequency from the 3 fabricated transducers.

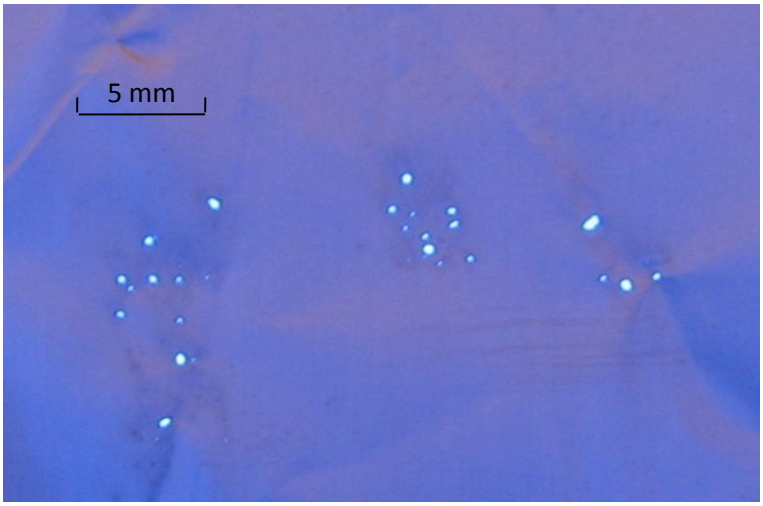

Figure 6.19 *Photomicrograph of perforated aluminium foil produced by the cavitating field in the focal region of device C*

6.6 Conclusions

This Chapter presented the design and manufacture of three prototype phased array transducers for high intensity focused ultrasound in the range 210-420 kHz. It demonstrated good correlation between the FEM simulation and experimental measurement results, which verified the use of PZFlex as a computer aided design tool.

Preliminary experimental results have been presented to evaluate the ability to generate cavitation using one of the fabricated arrays. The 420kHz HIFU array was selected for this purpose and was able to demonstrate the delivery of a high power field in a standard water tank. Importantly, this result provided confidence in the project objective and offered potential to build on this initial success.

The design, fabrication and evaluation work covered in this Chapter clearly demonstrates that HIFU arrays can be developed in the frequency range 200-400kHz. Nevertheless, there were some issues during the development phases of this work. In particular, the manufacture of thick section piezocomposite layers for operation in this frequency range was limited by the manufacturing capability of the research group at Strathclyde. Thus, only 2 piezoceramic pillars are active under each array element in the HIFU devices. Although, this limitation was not detrimental to the work objective – to develop and evaluate a prototype HIFU transducer using 1-3 connectivity piezocomposite active materials – it was considered that an alternative piezoelectric active material should be investigated. With a view to improving the reliability of the manufacturing process, a 2-2 connectivity piezocomposite structure was proposed as an appropriate option. The design, fabrication and evaluation of this type of piezocomposite structure will be addressed in Chapter 7.

Chapter 7

Design, simulation and manufacture of a 2-2 piezocomposite transducer for HIFU applications

7.1 Introduction

In this Chapter, a second design for a high efficiency power delivery and low frequency piezocomposite array transducer is presented. As discussed in Chapters 5 and 6, a piezocomposite transducer with an appropriate ceramic volume fraction has a higher electromechanical coupling efficiency, k_t, than pure piezoceramic. However, its high mechanical loss property, due to the interaction between constituent passive and active materials, limits its application in high power designs for chemical process control. To improve the piezocomposite mechanical loss property, the ceramic fraction needs to be high for the coupling efficiency to remain at a high level. As an alternative, the 2-2 connectivity piezocomposite structure offers higher ceramic volume fraction configurations compared to the standard 1-3 structure piezocomposite, for similar design criteria. For example, if both piezocomposites have a saw width of 0.3 mm and a saw pitch of 1mm, this will result in a 0.7 mm pillar width for the 1-3 piezocomposite and 0.7mm plate width for the 2-2 piezocomposite. Thus, the volume fraction of the 1-3 connectivity structure is 49%, whereas it is 70% for the 2-2 connectivity piezocomposite. In addition, as the 2-2 piezocomposite configuration is only diced in one direction, it is less susceptible to damage during manufacture, and can accommodate the use of viscous polymer filler materials compared to the standard 1-3 structure composite.

Another technique used for low frequency piezoelectric transducer designs is the application of a multi-layer stack configuration [167, 209, 210]. In this technique, alternately poled piezoceramic (or piezocomposite) layers are bonded together, as shown in Figure 7.1. Here, the overall thickness of the stack defines the fundamental operating frequency, although the device is comprised of individual layers which resonate at a significantly higher frequency. This can be an effective way to fabricate a low frequency piezoelectric transducer using basic manufacturing techniques. If using a 1-3 connectivity piezocomposite as the individual layers, this can be problematic as alignment of the pillars within each piezocomposite layer is critical and difficult to achieve [210]. Importantly, there are additional benefits to fabricating a transducer in a stacked formation:

- Lower electrical impedance magnitude, which is a function of the number of layers squared [210].

- Higher displacement magnitude from the transducer front face, which is a function of the number of layers [209, 211].

For this work, a two layer stacked design is combined with the 2-2 connectivity piezocomposite configuration to match the low frequency operational requirement and reduce manufacturing difficulty. Importantly, the stacked design and its parallel connection improve the efficiency of the device by reducing the electric impedance magnitude to a quarter of the single layer design value.

For these HIFU transducers, a 1-D periodic array element arrangement is again chosen for its simplicity and importantly, is a geometric match to a 2-2 connectivity piezocomposite structure. For this application, high intensity in the focusing region and beam steering capacity are the primary considerations, and the suppression of sidelobes is a secondary consideration, albeit an important one for the focusing efficiency. Therefore, the array design consulted conventional design laws for imaging array transducers.

Two models of 2-2 piezocomposite configurations using finite element model (FEM) analysis were established to aid the design of an array transducer for high power applications in Sonochemistry. Figure 7.1 illustrates the structure the two devices named: 2-2 Piezocomposite A and 2-2 Piezocomposite B. In the first design, 2-2 Piezocomposite A, an array element of the transducer contains 4 piezoceramic plates and each element is separated by a single plate, as illustrated in Figure 7.1(a). This design enables the transducer to have the advantages of piezocomposite behaviour, such as high electrical mechanical efficiency and low acoustic impedance. In the second design 2-2 Piezocomposite B, each array element is one ceramic plate wide. It has the drawback of high acoustic impedance; however, it has advantages on its simplicity in element arrangement design and simplicity in the manufacturing process. Simulation results for both piezocomposite designs are presented and discussed in this Chapter.

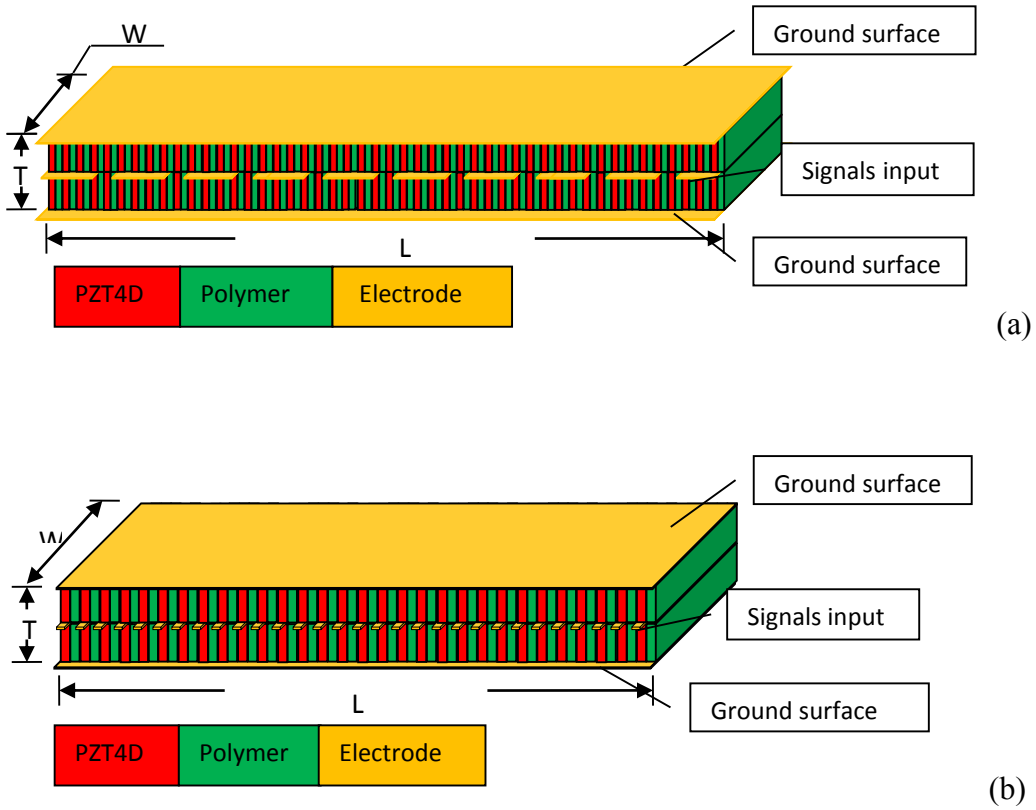

Figure 7.1 *Illustration of the microstructure for the two 2-2 connectivity piezocomposite configuration investigated for application in a HIFU transducer, (a) 2-2 Piezocomposite A, (b) 2-2 Piezocomposite B*

After analysis of the simulation result, a prototype of the 2-2 Piezocomposite B was selected to be manufactured. This prototype was characterized using electrical impedance and surface displacement measurements. In addition, its bandwidth and beam profiles were calibrated. Both 16 and 32 element array configurations are described in this Chapter and a discussion of the key fabrication and operational issues is provided at the end of the Chapter.

7.2 Finite element model development

In this Chapter, PZFlex is used as a finite element analysis tool to simulate the 2-2 piezocomposite array models shown in Figure 7.1. This Section will explain the creation of the models used in the simulation programme, with the results described in Section 7.3.

7.2.1 Piezoceramic composite design

As discussed in Chapter 6, a range of active and passive materials can be used in a piezocomposite design. For the 1-3 designs in Chapter 6, PZT4D and a medium set polymeric filler material, Vantico HY956EN/CY221, were considered suitable options and these materials are adopted again for use in the 2-2 devices discussed in this Chapter. As illustrated in Figure 7.1, 2 layered stack configurations have been selected, in which the two layers are identical and stacked with opposite polarity. Material properties for the ceramic and polymers materials are presented in Appendix A, noting that the polymer material properties have been measured experimentally in the Centre for Ultrasound Engineering laboratories.

Similarly with Chapter 6, a series of simulations were analysed to determine suitable geometries for the two 2-2 piezocomposite designs. From this the following configurations will be described in Section 7.3: for 2-2 Piezocomposite A, the plate and saw widths are 0.4 mm and 0.2 mm respectively; and for 2-2 Piezocomposite B, the plate and saw width dimensions are 1.2 mm and 0.6 mm, respectively. More details of selected the designs used for simulation are provided in Table 7.1. These high ceramic volume fraction designs (66%) can lead to a reduction in bandwidth, an increase in mechanical cross-talk and high acoustic impedance; but make the piezocomposite high in power efficiency and with a high electromechanical coupling efficiency.

The thickness of the piezocomposite mainly affects its centre frequency. For most designs, the aspect ratio between the plate width and thickness needs to be small to keep the parasitic inter-plate mode in the high frequency region, For the 2-2 piezocomposite especially, the thickness T should remain reasonably small compared with the width W of the piezocomposite, as illustrated in Figure 7.1, because the width mode frequency,

should be located at a much lower frequency, to prevent interference with the main thickness resonant mode. Therefore, for both 2-2 Piezocomposite devices, the thickness the of piezocomposite is selected as 4 mm to give an operating frequency around 400 kHz and provide a reasonable aspect ratio to separate the width mode and thickness mode resonances.

Table 7.1 *2-2 Piezocomposite transducer parameters*

	Dimensions	**Plate Width**	**Saw Width**	**CVF**
2-2 Piezocomposite A	60 x 20x4 mm	0.4 mm	0.2 mm	66%
2-2 Piezocomposite B	60 x 20x4 mm	1.2 mm	0.6 mm	66%

7.2.2 Element arrangement

Array element parameters such as element width and saw width are related to beam shape and side lobe generation of an array transducer. In the design of 2-2 Piezocomposite A, the element width is 2.2 mm, and the element saw width is 0.8 mm such that each element was composed of 4 piezoceramic plates. Each element was separated by a single ceramic plate, and two interlaced polymer strips, for reasons of standard manufacturing practice and in an effort to reduce mechanical cross-talk between array elements. The element pitch is 3 mm, which is 0.8λ for the resonant frequency of 400 kHz operating in a water load. The array aperture is 60 mm and hence, this 1-D array will contain 20 elements.

In the design of 2-2 Piezocomposite B, array element width exactly covers a single plate. In this case, the element pitch will be the same as the plate pitch, which is 1.8 mm and equivalent to half the wavelength at the operational frequency. This half wavelength design should be a great advantage in side lobe suppression and to maximise the focusing efficiency. With the same aperture as the 2-2 Piezocomposite A, this 1-D array will contain 32 elements.

FEM analysis was used to examine these designs of element arrangement. In the simulation, the top and bottom surfaces were fully electroded and grounded. The centre common electrode was the signal connection. Models were surrounded by a free boundary and central elements were excited by a wideband pulse to investigate the design's operational impedance spectrum and extent of mechanical cross-talk between array

elements. The model was then extended to include a water load and used to predict each design's beam profile and simulate the array focusing and steering capability.

7.3 FEM Simulation results and discussion

7.3.1 Electrical impedance spectrum

The electric impedance spectrum simulation result for a single array element in the centre of the aperture in the 2-2 Piezocomposite A is shown in Figure 7.2. A reasonably clean resonant mode is observed, with an impedance minimum at the electrical resonant frequency of 414 kHz. There is a small parasitic mode at 500 kHz, which is near the mechanical resonant frequency. However, because this transducer is used as a transmitter rather than the receiver, the effect of this parasitic mode on the device performance may be insignificant. In Figure 7.3, the electric impedance spectrum simulation result for a single array element in the 2-2 Piezocomposite B is shown. This result demonstrates that this design has a single resonant mode, which has an electrical resonance frequency of 400 kHz. In this Figure, the lateral resonant mode occurs at a frequency of 85 kHz, which is far away from the main resonant mode. Moreover, the periodicity of the array element structure has produced a number of smaller modes, in both devices, as expected due to Lamb waves within the structure [135, 212].

7.3.2 Surface displacement

The piezocomposite surface displacement simulation using a single element excitation is used to investigate the extent of mechanical cross-talk between array elements. The cross-talk depends not only on the properties of the active material and the passive material, but also depends on the array element arrangement [134, 213, 214]. The medium set polymer was employed in this work as the passive phase of the piezocomposite and exhibits a high lateral damping property which reduces mechanical cross-talk.

The surface displacement simulation of the 2-2 Piezocomposite A is illustrated in Figure 7.4. In this FEM model, the centre element of the array was excited by a wideband pulse, and the magnitude of the surface displacement was recorded. Figure 7.4 illustrates the displacement profile through the centre axis of the array. The predicted cross-talk between the excited element and adjacent element is less than 6 dB. Figure 7.5 shows that the cross-talk for the 2-2 Piezocomposite B in simulation is insignificant, which is less than 12 dB, which is a better performance than the 2-2 Piezocomposite A.

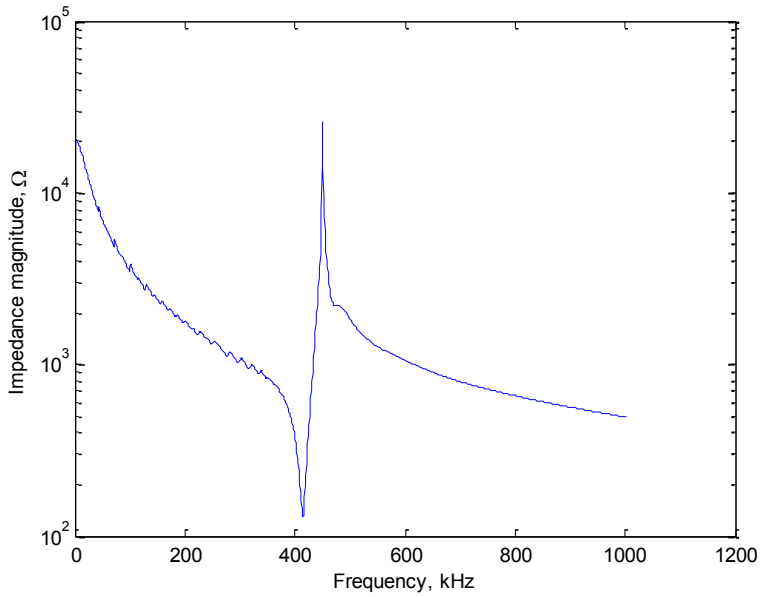

Figure 7.2 *Electrical impedance spectrum predicted for a single array element of 2-2 Piezocomposite A*

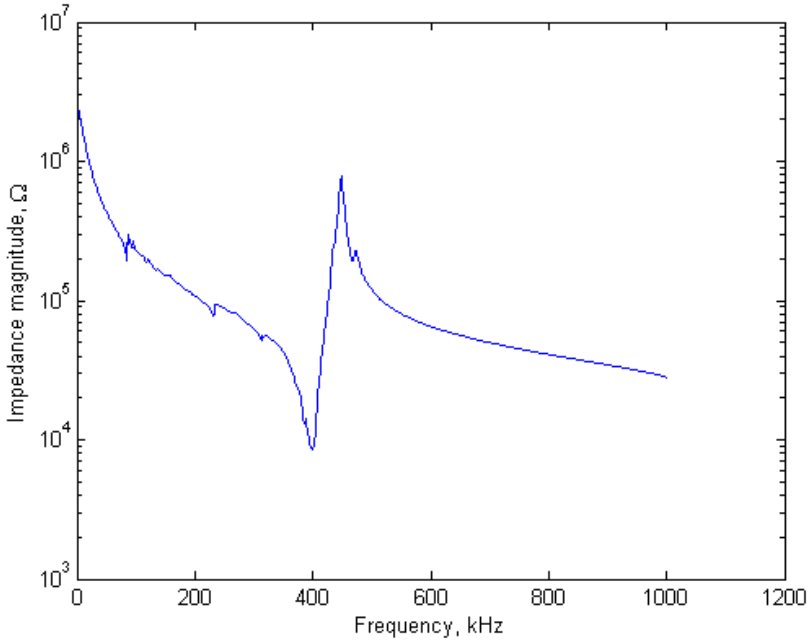

Figure 7.3 *Electrical impedance spectrum predicted for a single array element of 2-2 Piezocomposite B*

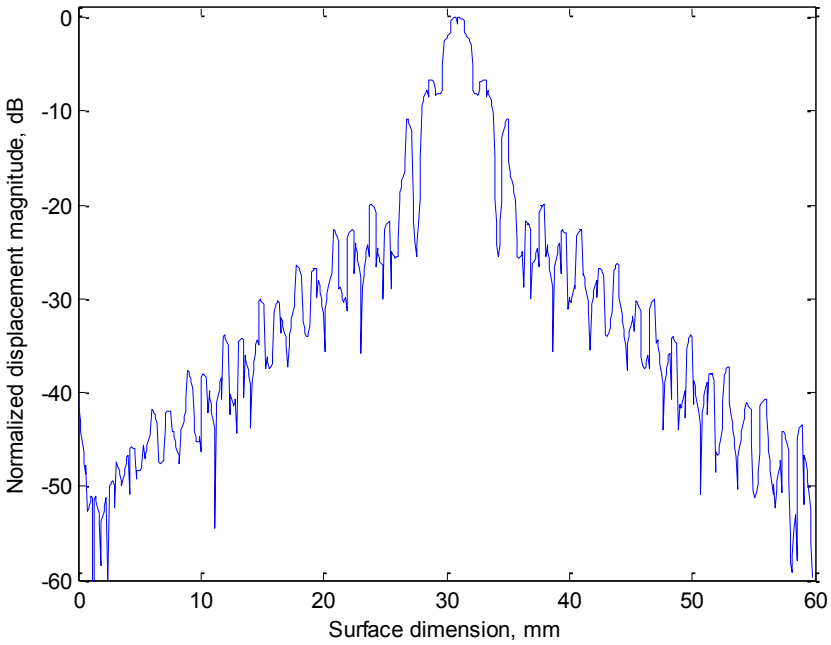

Figure 7.4 *Predicted surface displacement by single element in the centre of the aperture of 2-2 Piezocomposite A*

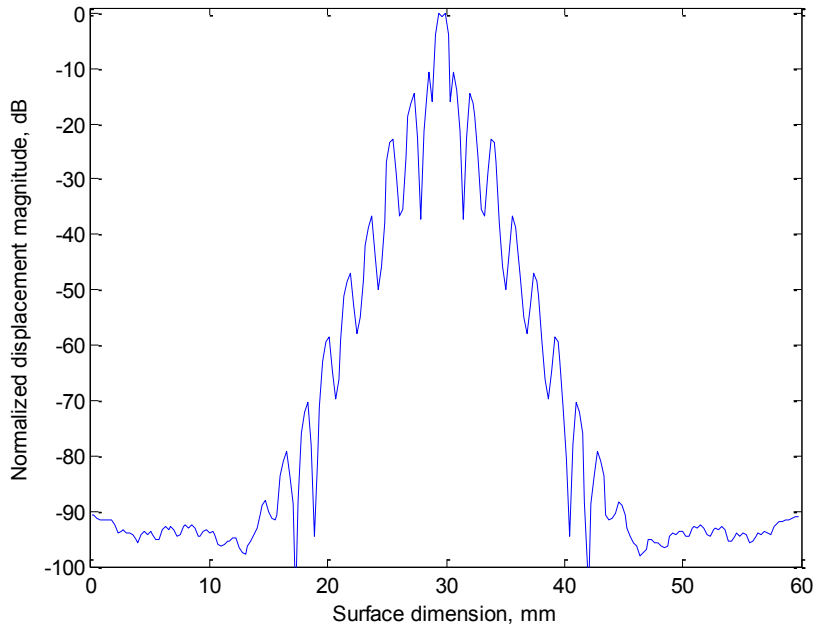

Figure 7.5 *Predicted surface displacement by single element in the centre of the aperture of 2-2 Piezocomposite B*

7.3.3 Matching layer design

To improve the transmitting efficiency between the piezocomposite and the water load, a matching layer is employed. Because of the high volume fraction of the piezoceramic in both 2-2 piezocomposite designs, the two-layer design approach [215] is adopted, as used for the 1-3 piezocomposite designs presented in Chapter 6.

7.3.3.1 Piezocomposite A matching layer design

The acoustic impedance of 2-2 Piezocomposite A is 22 MRayl and the acoustic impedance of water is 1.5 MRayl, and the optimal acoustic impedances of the matching layers [215] are 6.6 MRayl and 2.2 MRayl for the first layer and second layer, respectively. The CUE materials database (see Appendix A) was used to select appropriate materials. The materials in the database that have acoustic impedance close to the optimal design specification are a particle loaded hard setting epoxy (HSE) using Vantico HY1300/CY1301 (Huntsman, UK) filled with 73% w/w calcined alumina (Logitech, UK) and soft setting epoxy (SSE) using (Vantico HY956/CY208). The thickness of both layers are determined based on the quarter wavelength design rule. Details of the matching layer materials are presented in Table 7.2. These layers were added to the finite element model and further simulations of pulse echo response conducted, as described in Section 6.3.1. Pressure field mapping simulations were also conducted to analyse the design performance. The simulated phased array transducers focused axially at a depth of 50 mm. Moreover, the predicted pressure magnitudes have been normalized for comparison purposes.

Figure 7.6 presents the pulse-echo response simulation results and it is clear that the piezocomposite with matching layer has an extended bandwidth when compared to the unmatched case. In fact that bandwidth has increased to ~50% (200 kHz) compared to 7.5% for the condition without matching layer. Moreover, Figure 7.7 illustrates the axial pressure response for each array configuration when a focal law to focus at a depth of 50mm is applied. This simulation indicates that the inclusion of the dual matching layer has resulted in a 2 dB advantage in terms of pressure magnitude over the piezocomposite without matching layer.

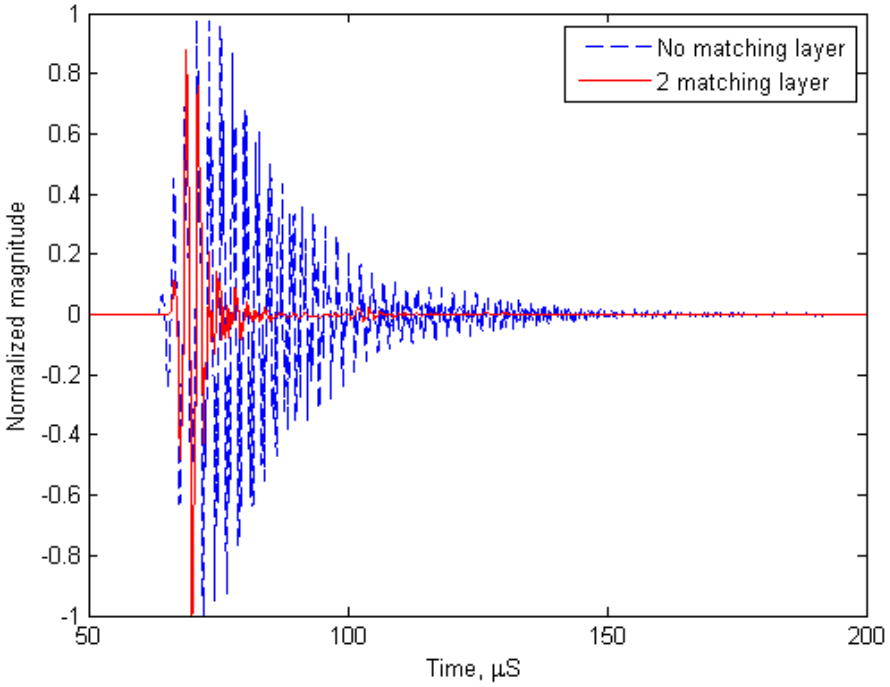

(a)

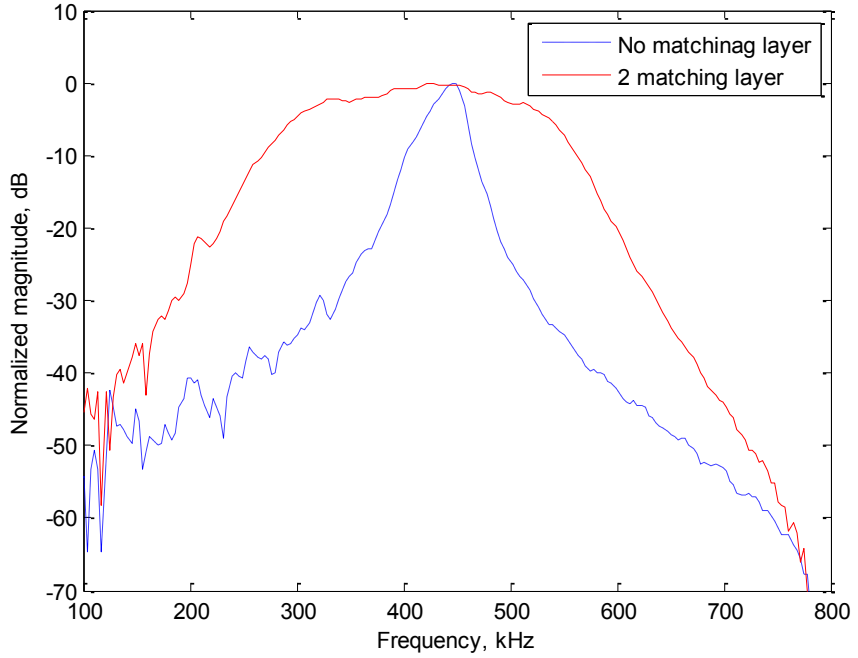

(b)

Figure 7.6 *Pulse echo simulation results for 2-2 Piezocomposite A, (a) time domain response, (b) frequency domain response*

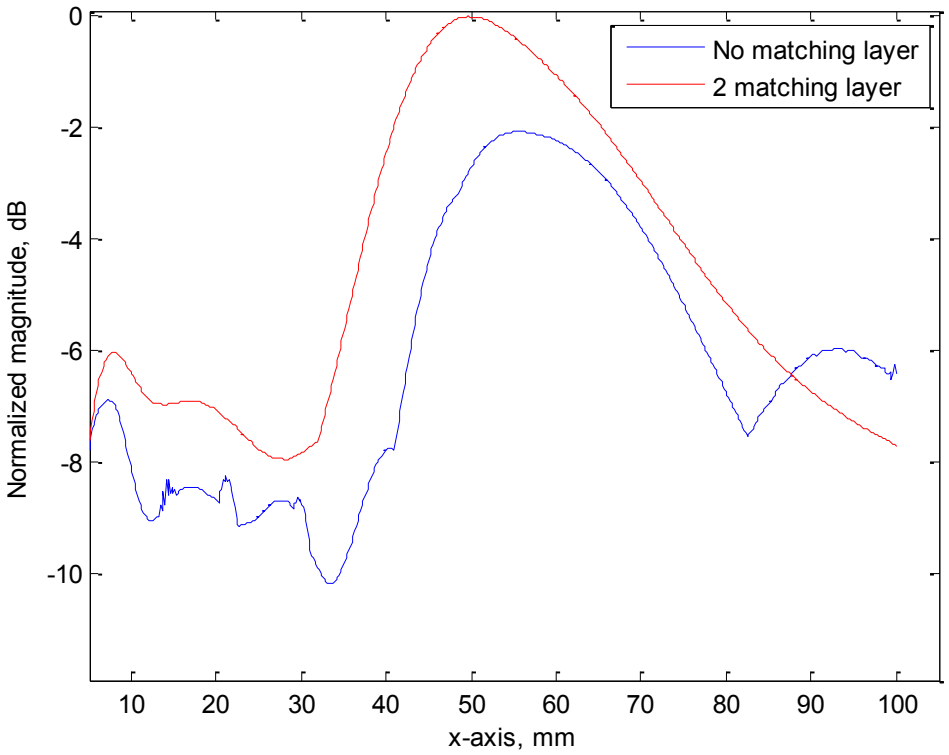

Figure 7.7 *Axial pressure field distribution for 2-2 Piezocomposite A, under pulse excitation, with matching and non-matching condition, focusing at a 50 mm depth*

Table 7.2 *Matching layer scheme for both 2-2 piezocomposite designs*

Layer number	Applied material	Applied acoustic impedance	Matching layer Thickness
Layer 1:	Alumina 73% w/w VanticoHY1300/CY1301	6.3 MRayl	1.7 mm
Layer 2:	Vantico HY956EN/CY221	2.3 MRayl	1.2 mm

7.3.3.2 Piezocomposite B matching layer design

For 2-2 Piezocomposite B, because each element only covers a single ceramic pillar, it can be not be treated as an integrated material between the ceramic and polymer. Therefore, although both 2-2 Piezocomposites, A and B, have similar ceramic volume fractions, piezocomposite B has much higher effective acoustic impedance of approximately 30 MRayl. The optimal impedance for the first matching and second matching layer is 8.3 MRayl and 2.3 MRayl, respectively. The first matching layer

material had to be given close consideration as materials within the CUE materials database around this impedance, e.g. tungsten loaded epoxy, were considered too lossy to be used as a matching layer in this application. This resulted in a compromise being required and the same material as chosen for Piezocomposite A was selected. Moreover, the layer thicknesses were identical as the operating frequency for both piezocomposites are close. Table 7.2 details appropriate materials and dimensions for use with 2-2 Piezocomposite B.

Figure 7.8 presents the predicted pulse-echo response showing that this two layer matching layer design has greatly improved the device bandwidth. From the pulse-echo spectral response for the no matching layer condition, it is clear that there is another parasitic signal causing a double peak around the operating frequency. This is likely to be associated with the compromise taken in the design of the dual layer matching system. Thus, the spectral results don't look particularly impressive, but the time domain responses clearly demonstrate the reduction in pulse length when using the matching layer arrangement. Moreover, Figure 7.9 illustrates the axial pressure response for each array configuration when a focal law to focus at a depth of 50mm is applied. This simulation indicates that the inclusion of the dual matching layer has resulted in a 3 dB of advantage in terms of pressure magnitude over the piezocomposite without matching layer.

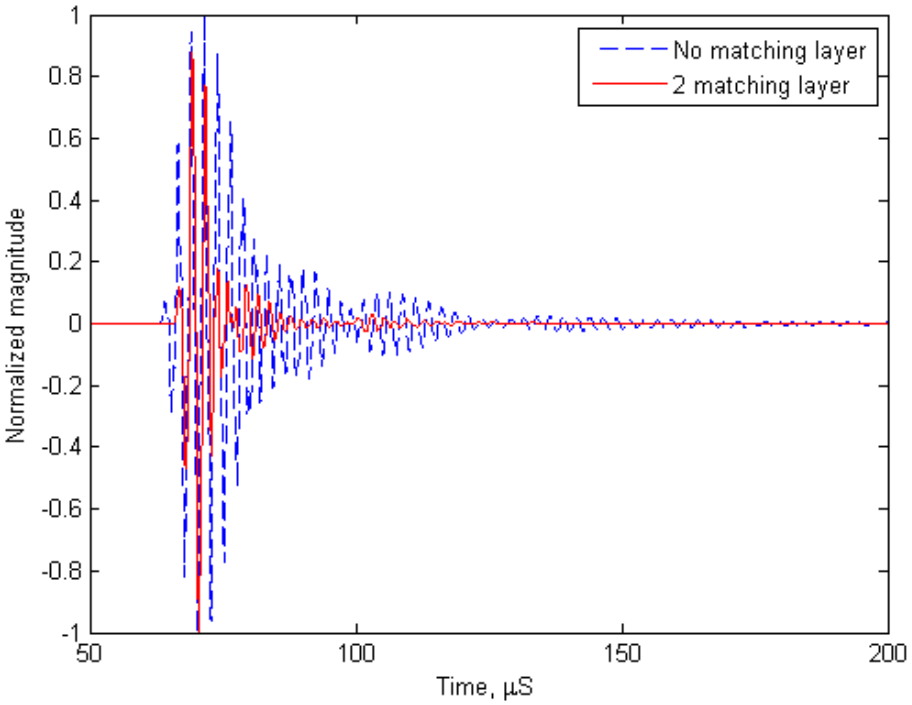

(a)

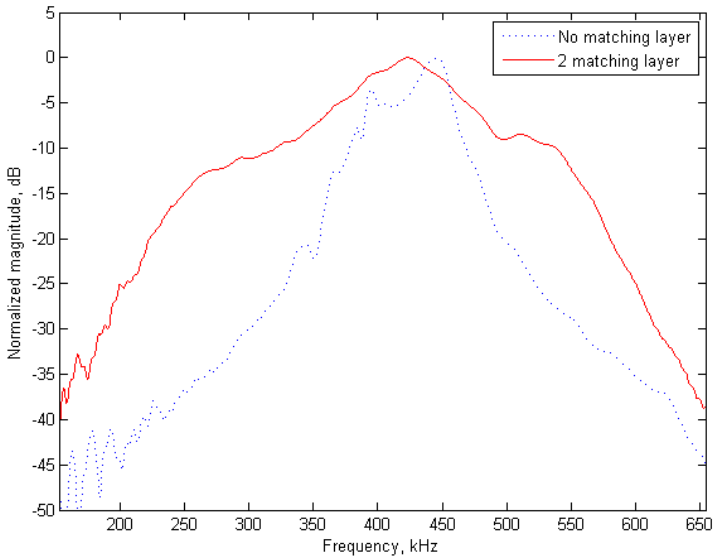

(b)

Figure 7.8 *Pulse echo simulation results for 2-2 Piezocomposite B, (a) time domain response, (b) frequency domain response*

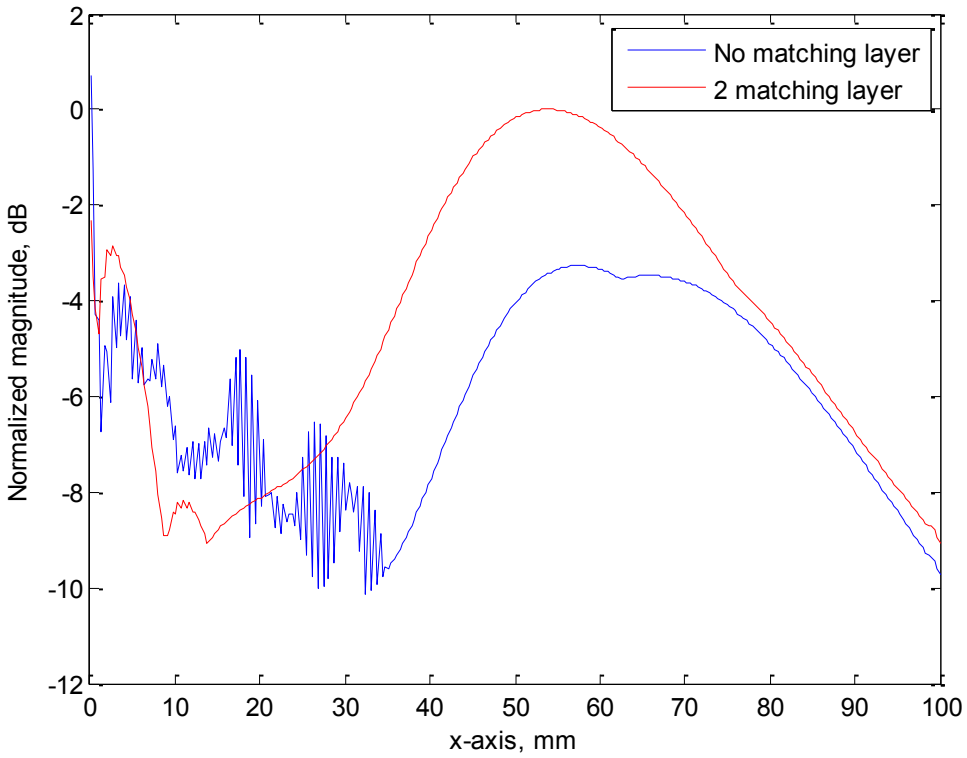

Figure 7.9 *Axial pressure field distribution for 2-2 Piezocomposite B, under pulse excitation, with matching and non-matching condition, focusing at a 50 mm depth*

7.3.4 Pressure field simulation

The final modelled simulation concerns the pressure beam profile generated by the array and investigates the focusing and steering ability of the transducer. The maximum pressure from within the focusing region was extracted and analysed qualitatively to evaluate the piezocomposite performance in terms of acoustic power delivery. In addition, the 3dB drop area in each focused region was calculated and used to evaluate the 2-2 Piezocomposite's steering and focusing ability.

Figure 7.10 and Figure 7.11 present the results of the 2-D model simulations for each 2-2 Piezocomposite coupled directly into a water load. The Figures illustrate both arrays operating with a focus at 50mm, both on-axial (0^o) and off-axis (10^o). From these Figures it can be clearly observed that both 2-2 Piezocomposites, A and B, are capable of producing a tight focusing region and able to steer the focal region off-axis. 2-2

Piezocomposite A has a 3dB power drop area of 90 mm^2 and 101 mm^2, at 0^o and 10^o orientations, respectively. For 2-2 Piezocomposite B, the 3 dB power drop areas are 49 mm^2 and 50 mm^2, at 0^o and 10^o orientations, respectively.

These results indicate that 2-2 Piezocomposite B has a tighter focus, which results from its half wavelength element pitch width arrangement and significantly larger number of elements compared to 2-2 Piezocomposite A under the same operating aperture size.

The simulation results shown in this Section have demonstrated the potential performance for both designs of 2-2 Piezocomposite. Piezocomposite A has lower acoustic amplitude and wider bandwidth, but is more difficult to manufacture due to the smaller saw cut width. Piezocomposite B has better performance in suppression of cross-talk, focusing and beam steering. Although the larger number of elements in 2-2 Piezocomposite B leads to more difficulty in cabling and excitation, it also enables more power input under the same aperture size. Accordingly, 2-2 Piezocomposite B was chosen for manufacture and calibration.

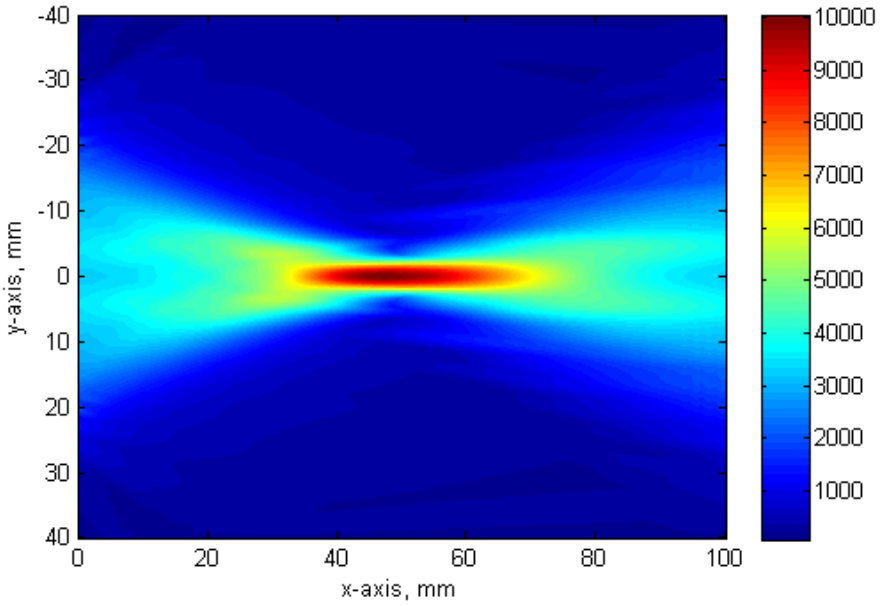

(a)

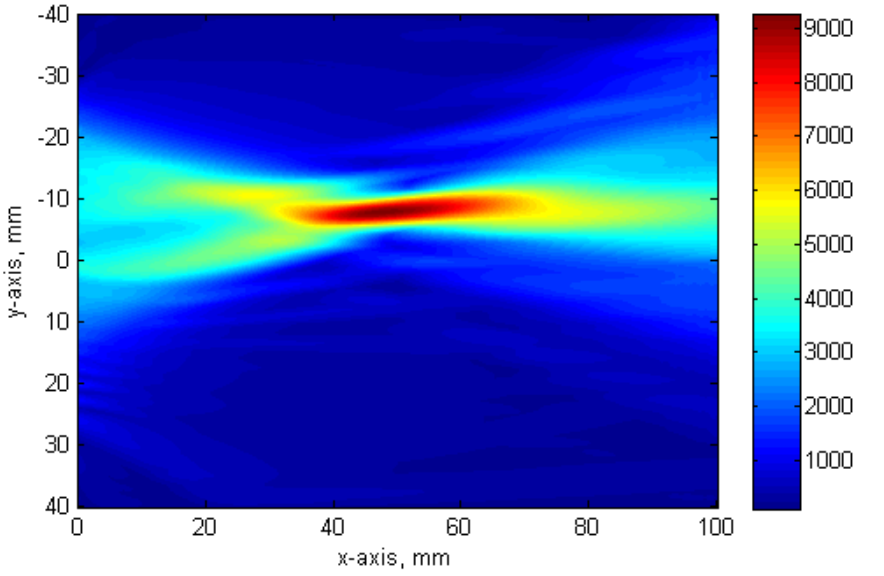

(b)

Figure 7.10 *Predicted pressure field map for 2-2 Piezocomposite A; (a) 0 degree, 50 mm depth, (b) 10 degree, 50 mm depth*

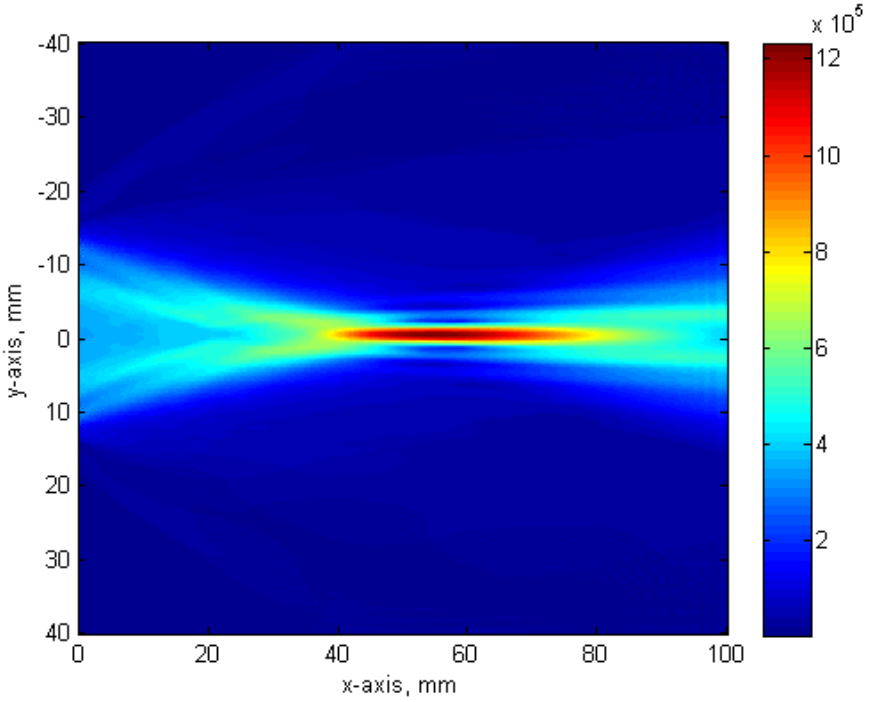

(a)

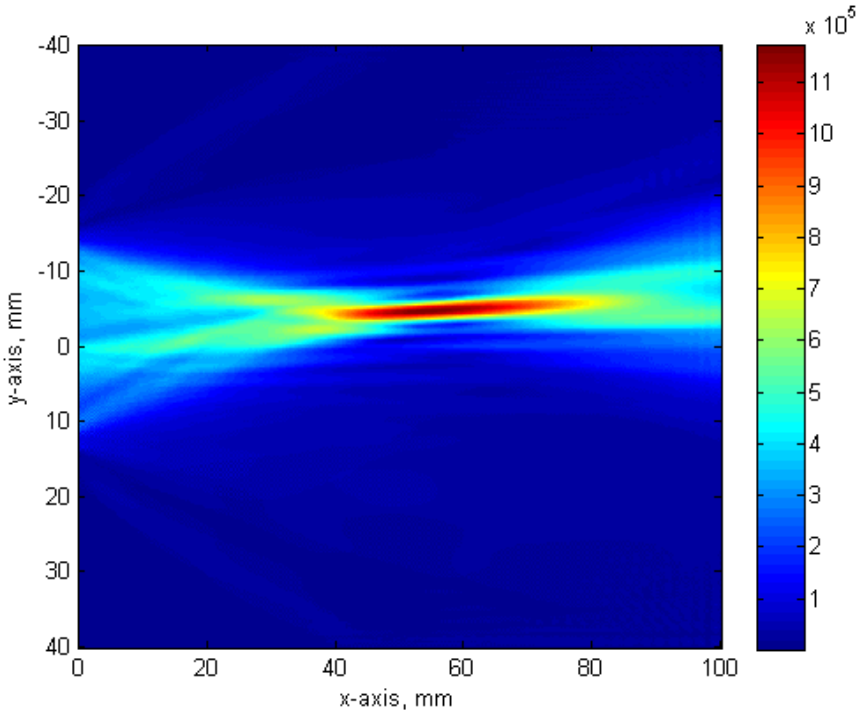

(b)

Figure 7.11 *Predicted pressure field map for 2-2 Piezocomposite B; (a) 0 degree, 50 mm depth, (b) 10 degree, 50 mm depth*

7.4 Prototype transducer manufacture and calibration

After a simulation programme, presented in Sections 7.2 – 7.3, the 2-2 Piezocomposite B was selected to be manufactured. The actual prototype has dimensions of 30x20x4 mm and contains 16 elements. This is slightly different from the lateral dimensions (and number of elements) from the simulation programme due to availability of material within the CUE fabrication laboratory. The objective in producing this prototype is to investigate the manufacturing method and experimentally characterize the performance, comparing this to the FEM results which have been re-run to take the actual array dimensions into account.

7.4.1 Array fabrication

The array structure is a 2-layer piezocomposite stack and hence, to ensure good conductivity of the central electrodes, the bonding surfaces of the two piezoceramic layers were coated with a gold electrode. Next, a thin copper sheet of 0.03 mm thickness was bonded between these two PZT4D layers with the gold electrodes in contact with the copper sheet. Importantly, an external pressure was applied using a manual press arrangement to ensure that the bondline was minimised and to maximise conductivity. Once the 2-layer PZT4D structure was fully bonded, the block was machined using a dicing saw to create a 2-2 structure, with each piezoceramic plate the equivalent width of an array element. Importantly, the thickness of the original PZT4D layers was greater than the finished thickness of the device, at 2.4mm. This provided a small stock of solid ceramic material to support the diced plates during the manufacturing process. At this stage, the saw cuts were infilled with the medium set epoxy filler material and the entire structure lapped to the finished dimension of 4mm thick. Now the ground gold electrodes, top and bottom faces were applied. The copper sheet in the centre of the structure was then used to electrically connect each array element to an external cable. This was achieved by initially connecting small length wires from the copper ends to a connector PCB. The manufactured 2-2 Piezocomposite B connected to the PCB is illustrated in Figure 7.12.

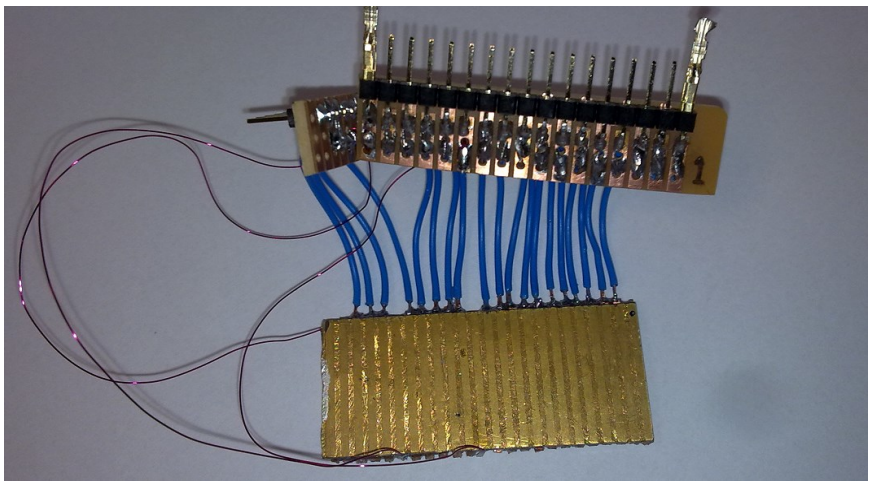

Figure 7.12 *Photograph of the fabricated Piezocomposite B connected to a PC, note the signal connections in blue and the ground connections are in copper*

7.4.2 Electrical impedance analysis

The measured electrical impedance of the 2-2 Piezocomposite B is shown in Figure 7.13. There is excellent correlation between experiment and simulation, with only a small deviation in the electrical resonance frequency, f_e. The actual electrical impedance at f_e is 350Ω, which is higher than predicted and will have an impact on the efficiency of the transducer when connected to a typical 50Ω output impedance amplifier stage. This is because of the error in the thickness of the device due to the bonding of the electrode layer in the centre of the stack.

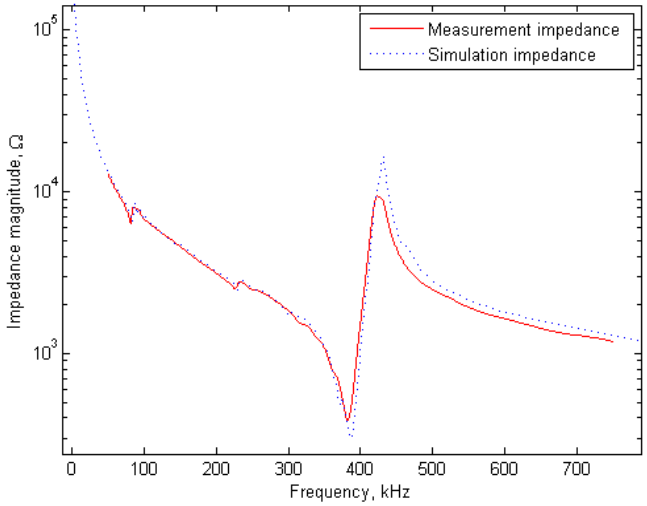

Figure 7.13 *Comparison of electrical impedance spectra for 2-2 Piezocomposite B*

7.4.3 Surface displacement measurement

A scanning laser vibrometer was used to acquire experimental measurements of the surface displacement when individual array elements were excited. An excitation voltage of 10V under continuous wave conditions, at the electrical resonance of 400 kHz, was applied. Figure 7.14(a) presents the measured surface displacement map for a single element excitation from the fabricated 2-2 Piezocomposite B. Minimal cross-talk across the array aperture is evident, but a width mode within the piezoceramic plate is evident and it should be noticed that there is an inactive area on the edge, which is because of damage of the electrode through the soldering process. Figure 7.14(b) illustrates the displacement across the array aperture (through x-axis) and passing through the peak displacement associated with the array element. It shows that the cross talk is less than 6dB.

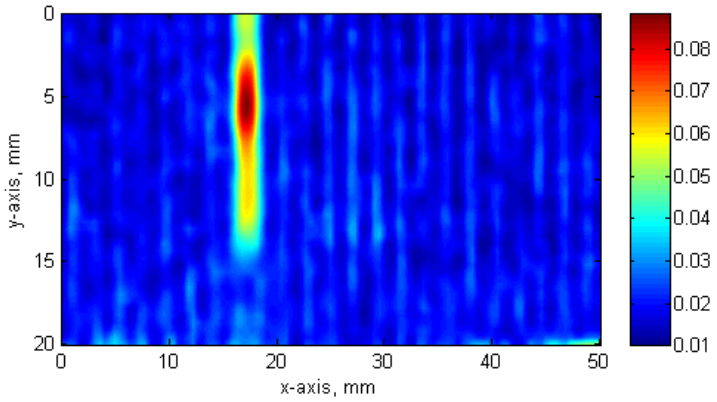

(a)

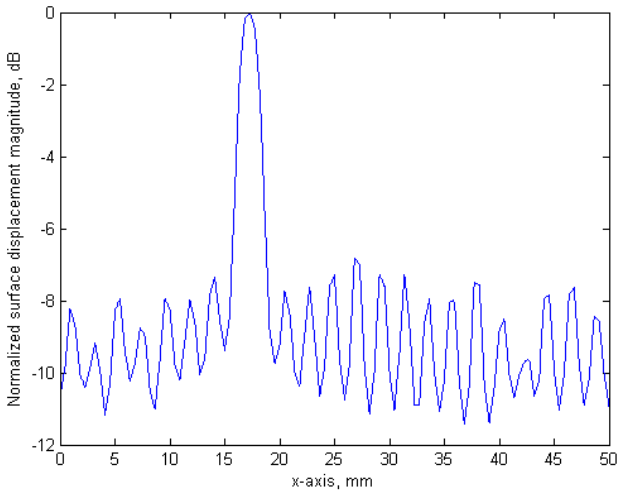

(b)

Figure 7.14 *Measured results of surface displacement for 2-2 Piezocomposite B, (a) top view, (b) cross-sectional view*

7.4.4 Housing and cabling

With the initial transducer characterisation complete, the array was incorporated into a waterproof housing and an electrical cable connection included. This was necessary to enable the further testing on transducer bandwidth and acoustic beam profile for the 2-2 Piezocomposite B to be measured. The assembly of matching layer and 2-2 Piezocomposite B is illustrated in Figure 7.15. First, the loaded hard set epoxy layer was fabricated and machined to the correct dimensions. This layer had a larger face area compared to the array. The loaded epoxy layer was then bonded onto the rear face of the array and this entire structure bonded into an aperture cut out of a steel housing. The depth associated with this aperture was previously machined to match the thickness of the second matching layer, 1.2mm, and soft set epoxy poured into this aperture to complete the transducer fixture arrangement. The finished device is shown in Figure 7.16, where the front face matching layer is visible in Figure 7.16(a). More details of the housing can be found in Appendix B. A twisted pair cable was wired into the PCB containing the array connections for the 2-2 Piezocomposite B, as shown in Figure 7.16(b). Finally, Lemo 00 series connectors were used to complete the cable and provide a connection to the Dynaray phase array controller (Zetec, Canada). The Dynaray instrument is able to control the excitation to each element of the transducer and facilitate pulse echo and beam profile experiments.

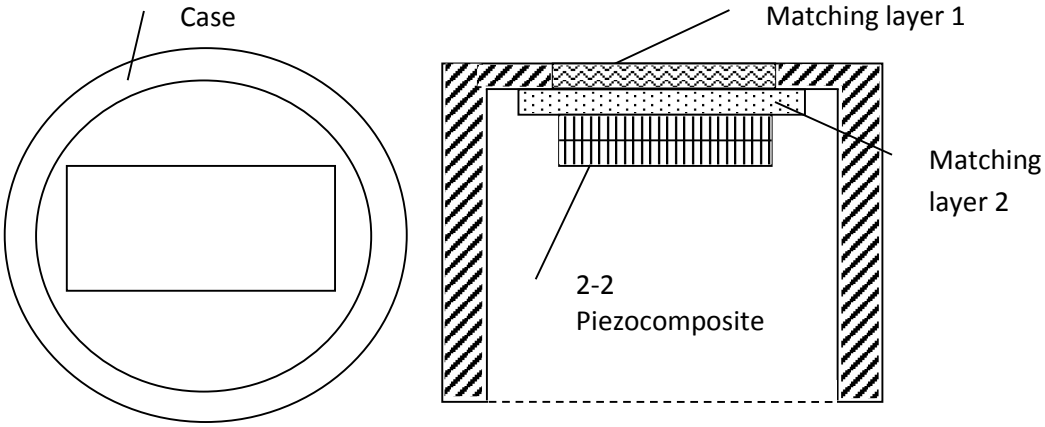

Figure 7.15 *Illustration of the assembly of the dual matching layer onto Piezocomposite B and how the array is assembled into the casing*

(a)

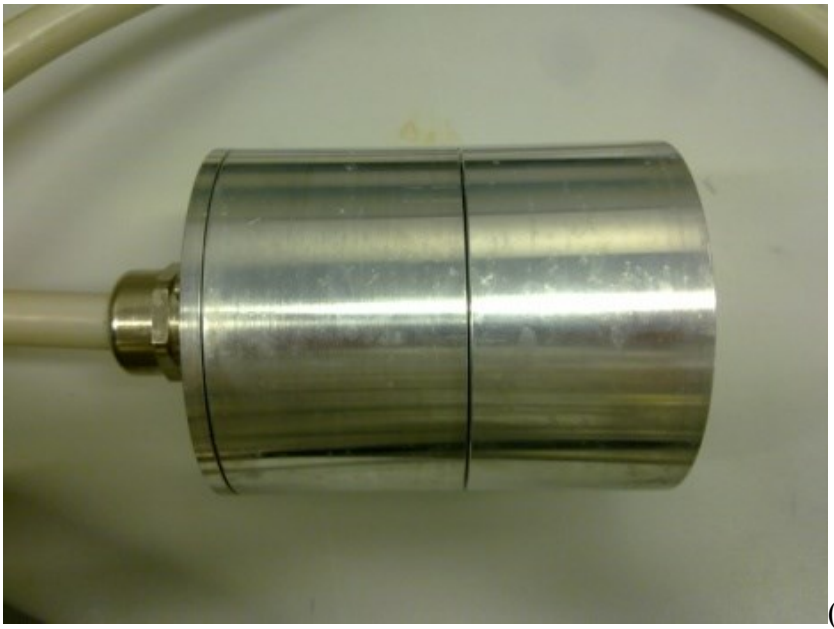

(b)

Figure 7.16 *2-2 Photographs of finished Piezocomposite B, (a) Top view, (b) side view*

7.4.5 Bandwidth characterization

Pulse-echo experiments were conducted to calibrate the transducer bandwidth and Q factor. Here, a single element of the array was excited with a 200V, 200ns width pulse using the Dynaray phased array controller. The reflected echo from a flat glass reflector, 50 mm away, and received by the same element was acquired and subsequently, analysed in both the time and frequency domains. Figure 7.17 presents a comparison between the experimentally measured echo and the predicted response using PZFlex. Again, excellent correlation is demonstrated. Moreover, from Figure 7.17 (b), the 6dB bandwidth of transducer is 30% (125kHz) and its Q factor is calculated to be 8.5. The results show that transducer has a low Q value and maintains a reasonable bandwidth.

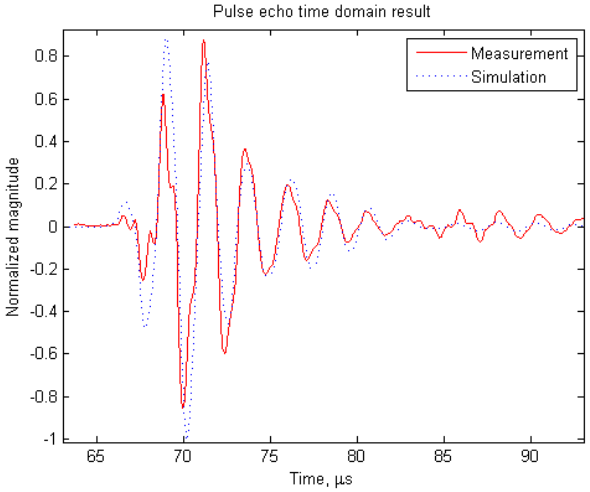

Figure 7.17 *Measured pulse echo response of 2-2 Piezocomposite B, with simulated PZFlex results included for comparison,*
(a) time domain; (b) frequency domain

7.4.6 Beam profile characterization

Pressure field measurements were recorded to characterize the beam profile generated by the 2-2 Piezocomposite B, to demonstrate the simulation reliability and to evaluate the focusing and steering capability of the manufactured device. The pressure was measured by a standard needle hydrophone with 0.5 mm probe from Precision Acoustics Ltd., which minimized the disturbance of the pressure field. Again, a Zetec Dynaray phased array controller was used to control the excitation to the transducer array. The system was configured to drive the array elements with a 40V, 1000ns width pulse. The phased array controller was used in conjunction with a high precision x - y scanner to measure the pressure field under different focal law conditions.

Focal law calculations were performed to generate a focal region at a distance 50mm away from the centre of the array at two distinct angles: axial (0^o) and off-axis at 10^o. The pressure distributions clearly show that the arrays have good beam steering ability, and good focusing ability. The performance is not comparable with the simulated beam profile predictions shown in Figure 7.11, because the fabricated array has a smaller aperture and consequently less array elements. And unfortunately, there is a sidelobe clearly present in the off-axis focus shown in Figure 7.18(b). To verify the exist model and simulation, a pressure distribution produced by a 16 elements phased array transducer was simulated and the results were displayed in Figure 7. 19.

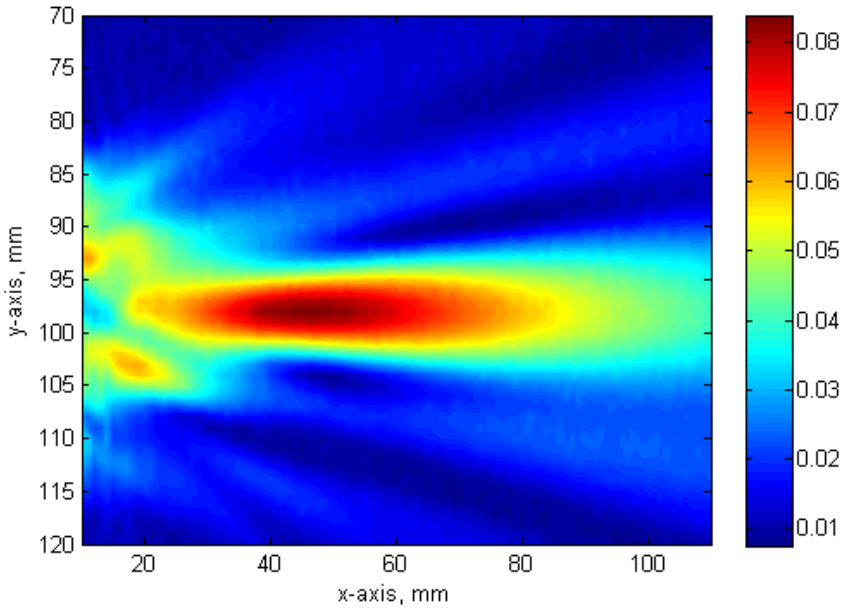

(a)

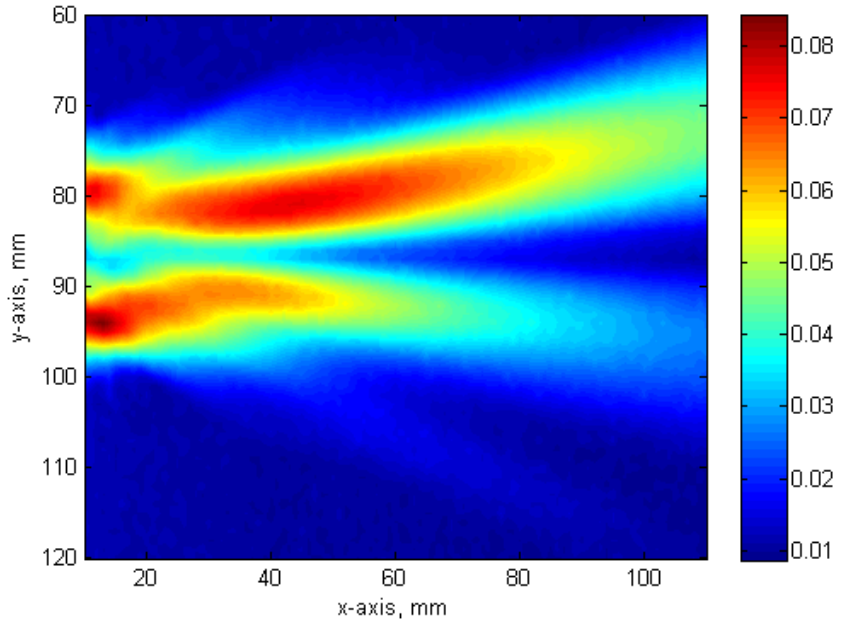

(b)

Figure 7.18 *Measured pressure field map for 2-2 Piezocomposite B operating into a water load; (a) 0 degree, 50 mm depth, (b) 10 degree, 50 mm depth*

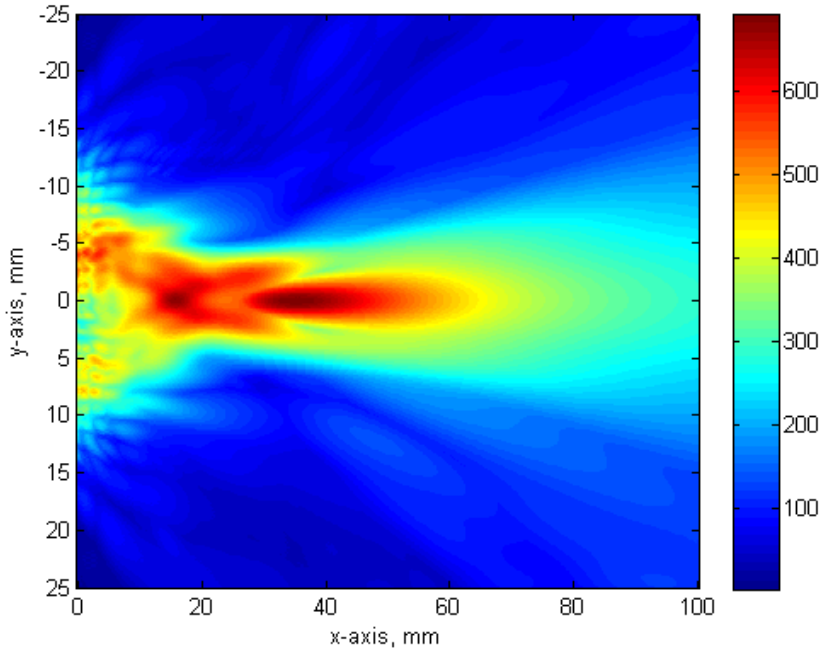

(a)

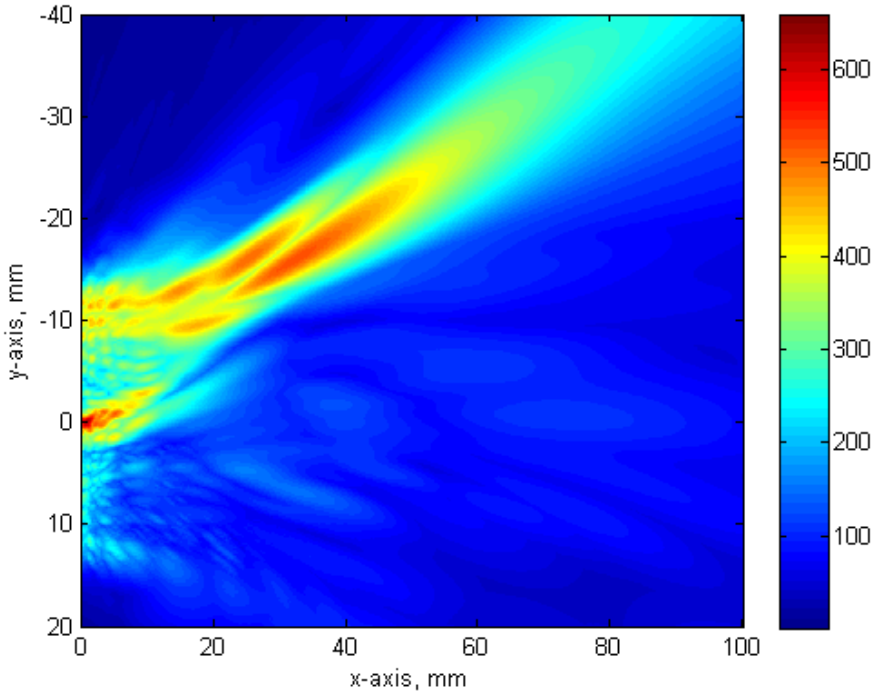

(b)

Figure 7. 19 *Simulated pressure field map for 2-2 Piezocomposite B operating into a water load; (a) 0 degree, 50 mm depth, (b) 10 degree, 50 mm depth*

7.4.7 Discussion

The experiment results have demonstrated some successes of this design approach, which is the main objective of this prototype. In particular, there is good agreement between the simulation results and experimental results for the electrical impedance spectrum, pulse echo response and beam profile. Unfortunately, as this prototype contains only 16 elements and there is not the expectation that this device would generate cavitation. However, an experiment was carried out to measure the peak pressure generated by the device. By using a 25V peak to peak excitation pulse, the transducer produced a measured pressure of 75kPa in the focal area, and as expected this proved insufficient to be used to generate a cavitation field.

At this stage, it was considered that by increasing the number of elements, a HIFU device can be manufactured to provide a higher concentration of energy in a smaller focal region. Moreover, this larger aperture array should be able to operate over a larger focusing range. The next Section will describe the process and results for a scale up of the 2-2 Piezocomposite B design.

7.5 Large aperture 2-2 Piezocomposite device

7.5.1 Transducer design considerations

The aim for the fabrication of a second 2-2 Piezocomposite device was to expand the array element count from 16 to 32 and implement changes to the manufacturing process to increase the performance of the device. In addition, this device would be excited using sine wave tone burst waveforms to effectively narrowband the excitation energy around the operational frequency of the transducer and hence, produce higher pressure field conditions when compared to the Dynaray wideband pulse scheme used previously. Here the OPEN system phased array controller (Lecoeur-electronique Ltd, France) was be used as this is equipped with an arbitrary waveform generator for each transmit channel. This necessitated the use of an ITT connector, as discussed previously in Figure 6.12.

The fabricated transducer will be referred to as a 2-2 Piezocomposite BII to differentiate the design from the original 2-2 Piezocomposite B, but link the dual layer 2-2 structure to that presented previously in Figure 7.1(b).

7.5.2 Manufacture of 2-2 Piezocomposite BII

The manufacturing approach was modified slightly to reduce the fabrication process steps. In particular, the larger aperture would be problematic to lap using the equipment in the CUE fabrication laboratory. Hence, a 60mm × 20mm × 4mm PZT4D material was machined into two 1.9 mm thick layers. As previously, these two ceramic layers were bonded together under pressure, with positive poling direction facing each other, and a 30μm thick copper sheet located in the middle of the layers, which is illustrated in Figure 7.20. This time the stack was mounted into a substrate to provide a mechanical support for the plates during manufacture, as the plates had already been machined to the final thickness. The structure was then diced, filled with polymer and the supporting substrate removed. Finally, both external large surfaces were coated with gold electrodes.

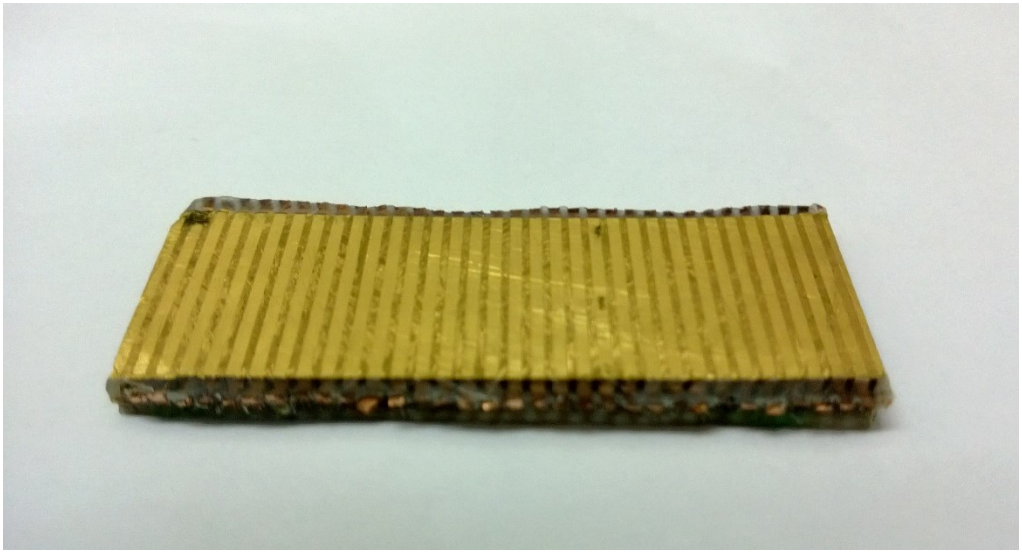

Figure 7.20 *Photograph of the fabricated Piezocomposite BII*

Figure 7.21 presents two photographs of the 2-2 Piezocomposite BII during the manufacture process. Figure 7.21 (a) illustrates the side view of the array with the first matching layer 1 bonded onto the transducer. Unfortunately, during the polymer filler curing process, the piezocomposite substrate has deformed and is slightly curved at one end of the array. This is clearly visible in the close up photograph shown in Figure 7.21 (b). This has resulted in the right edge of Piezocomposite BII not being in contact with the matching layer and will affect the performance of at least 4 elements. The second, outer, matching layer was applied in the same way as for Piezocomposite B.

The housing and cabling is the same with 2-2 Piezocomposite B, except the connector was changed to an ITT connector for connection to the OPEN system. Calibration of 2-2 Piezocomposite BII was also carried out during and after the manufacture process. In addition, an evaluation of the high power performance of the array was undertaken. In both of these stages, the same experimental measurements as discussed in Section 7.4, for Piezocomposite B were conducted.

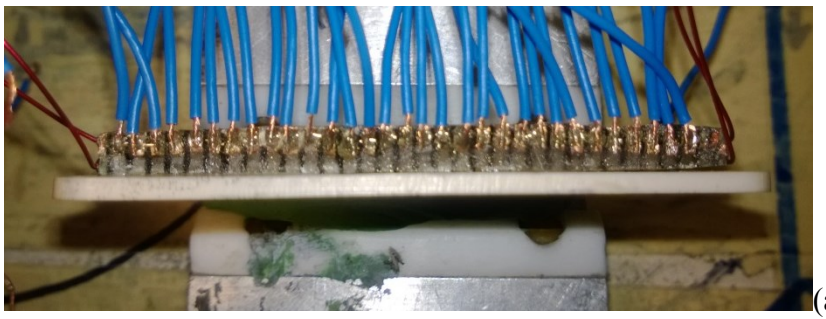
(a)

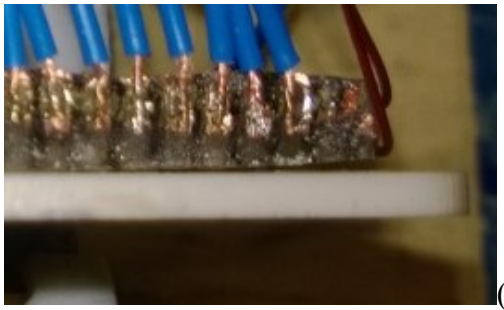
(b)

Figure 7.21 *Photographs of the 2-2 Piezocomposite BII array transducer during the fabrication process (a) side view with matching layer; (b) a close up image of a debond at the right hand edge of the array*

7.5.3 Calibration of 2-2 Piezocomposite BII

7.5.3.1 Electrical impedance analysis

These results were measured prior to the dual matching layer system being bonded onto the array and the array incorporated into the steel housing. This enabled the fabricated 2-2 piezocomposite to be analysed and assessed independently of any other aspects of the transducer construction.

Figure 7.22 is the measurement result of the electrical impedance spectrum for the central element. It shows that this result is close to the last prototype, 2-2 Piezocomposite B, but with slight differences in the mechanical resonant frequency and the magnitude of the electrical impedance at f_e. In this device, the minimum electrical impedance is 625 Ω, which is larger than that measured for Piezocomposite B (350 Ω). Hence, this will adversely influence the array performance when driven from a standard 50Ω output impedance.

Unfortunately, the impedance measurement results were not consistent over all 32

elements. The degraded characteristics occurred in elements that were located close to the edge. Figure 7.23 and Figure 7.24 show the electrical impedance spectrum of the 3rd and 30th elements. These results clearly show that the electrical resonant frequency has been shifted to a lower frequency and, as stated for the centre element, the 2-2 Piezocomposite BII elements exhibit a higher electrical impedance magnitude at the resonant frequency. Further analysis was then undertaken and the distribution of electrical resonant frequency, f_e, and the corresponding electrical impedance at this frequency are shown in Figure 7.26 and Figure 7.25, respectively. From these results it is clear that the centre elements, between approximately 11 and 26, show a reasonably consistent nature, but the elements closer to the edges have a completely different characteristic. This is due to the bowing of the piezocomposite during the polymer curing phase and is pronounced at the extremities of the device.

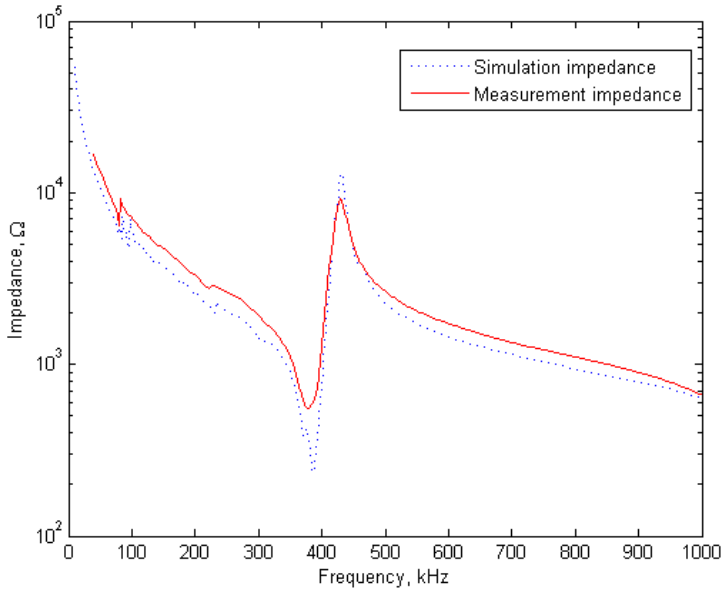

Figure 7.22 *Comparison between measured and simulated electrical impedance spectrum for a single element in the centre of 2-2 Piezocomposite BII*

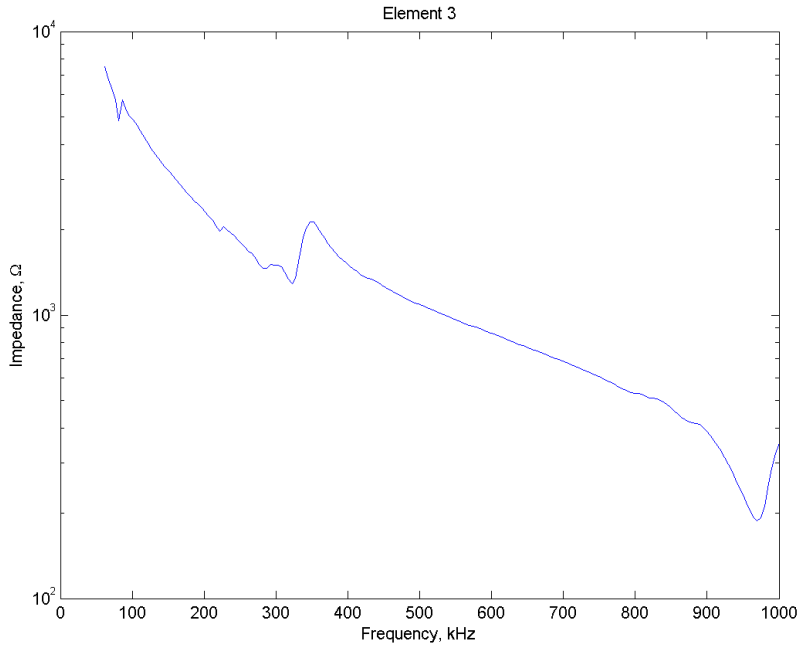

Figure 7.23 *Measured electrical impedance spectrum for 3rd element*

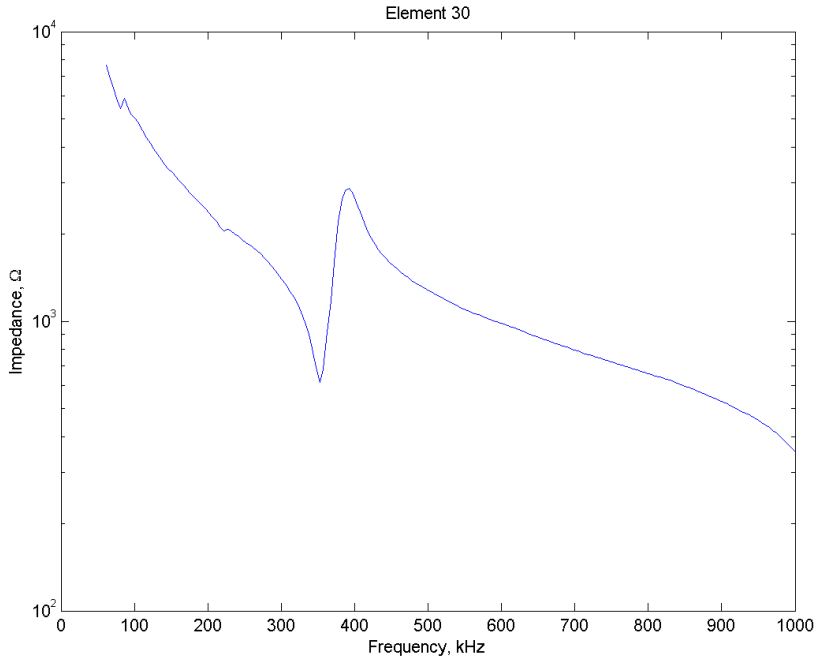

Figure 7.24 *Measured electrical impedance spectrum for 30th element*

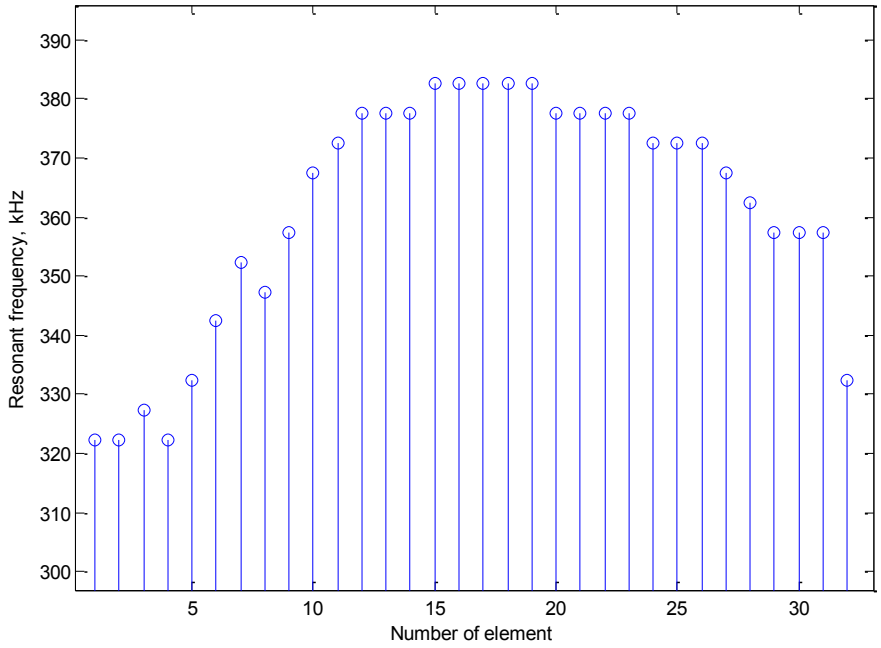

Figure 7.25 *Distribution of electrical resonant frequency for each element in the array*

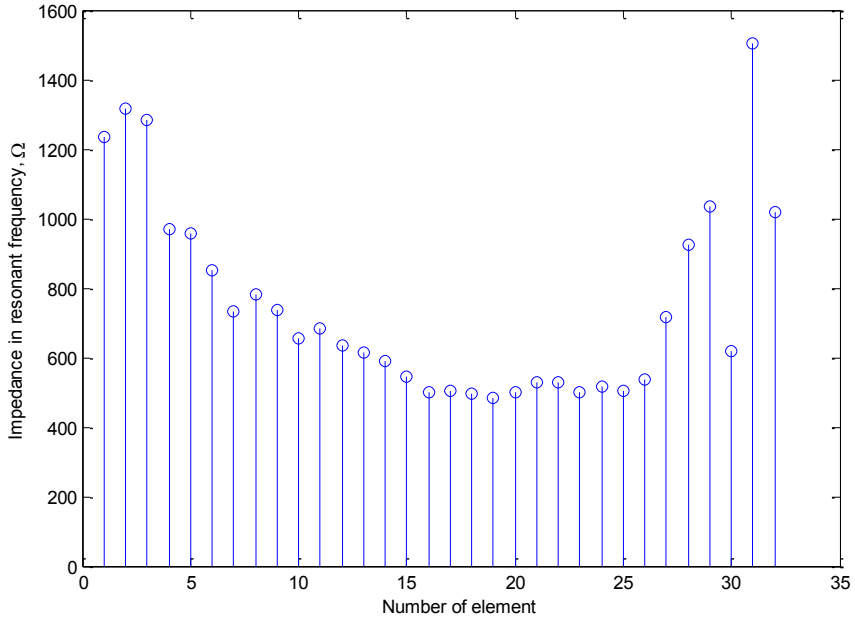

Figure 7.26 *Distribution of electrical impedance magnitude for each element in the array*

7.5.3.2 Surface displacement measurement

The following 6 pages presents the laser scan across the full aperture, in the top figure, and a cross-section through the array aperture, in the bottom slide. These are presented consistently to aid interpretation and comparison between measurements on different elements and with different conditions.

First, laser vibrometry was used to ascertain the vibrational characteristics of the array before the matching layer was attached. Figure 7.27 presents the surface displacement measurement for element #17, excited with 10V, 383kHz continuous wave. The cross-talk is low in this measurement, with the displacement across the majority of the aperture between 15-20dB down on the magnitude of the centre element.

Although, the performance of array element #17 was encouraging, other elements were shown to be underperforming. In Figure 7.26 and Figure 7.25, the 3rd element has an electrical resonance frequency of 330 kHz, with an impedance magnitude of 1300Ω, and the 30th element has an electrical resonance frequency of 360 kHz, with an impedance magnitude of 600Ω. From the surface displacement measurements, shown in Figure 7.28 and Figure 7.29, it is clear that the 30th element is operating reasonably effectively, albeit at a lower frequency when compared to the centre elements. Whereas, the 3rd element performance is extremely poor and there is no clear indication that only a single element has been excited, with high levels of mechanical cross-talk observed.

The surface displacement characteristics for these 3 elements were then repeated with the dual matching layer system bonded onto the array. These are presented in Figure 7.30 to Figure 7.32 for elements #17, #3, #30 respectively. In all these results, the array element displacement is well defined, but the mechanical cross-talk is quite low due to coupling through the matching layer system itself.

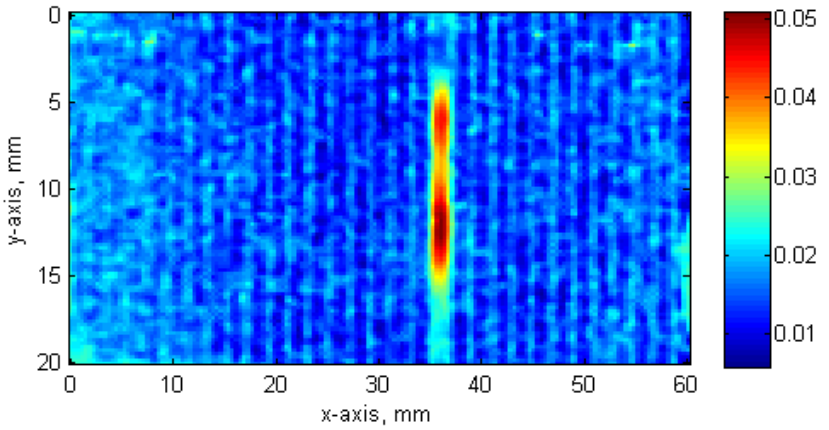

(a)

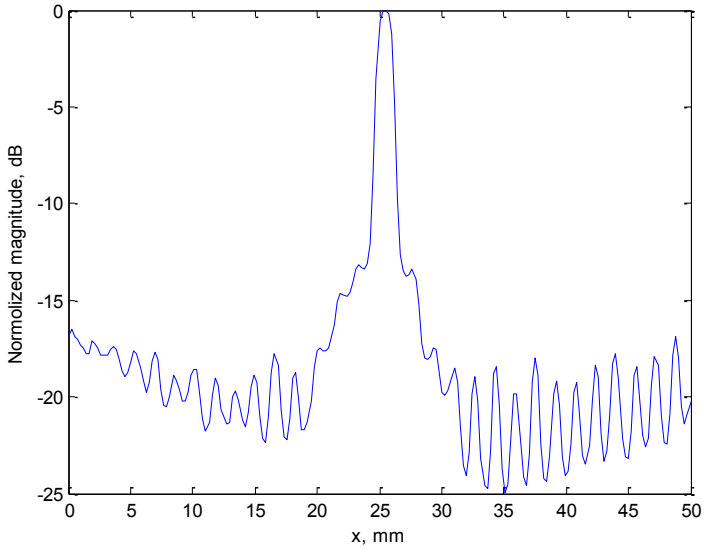

(b)

Figure 7.27 *Measurement results showing the surface displacement of 17th element of unmatched 2-2 Piezocomposite BII, (a) full aperture view, (b) cross-sectional view*

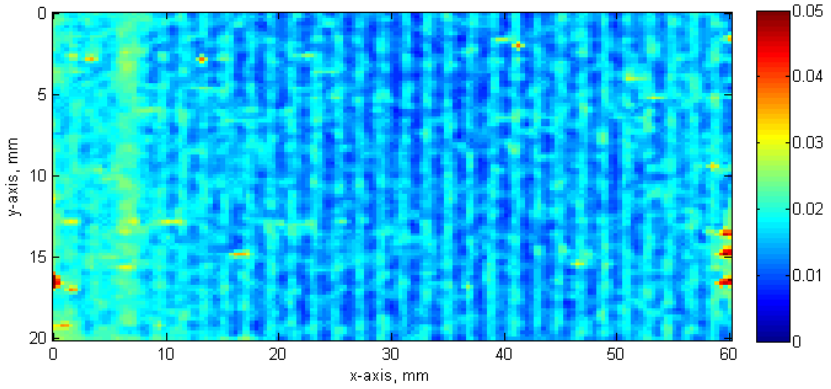

(a)

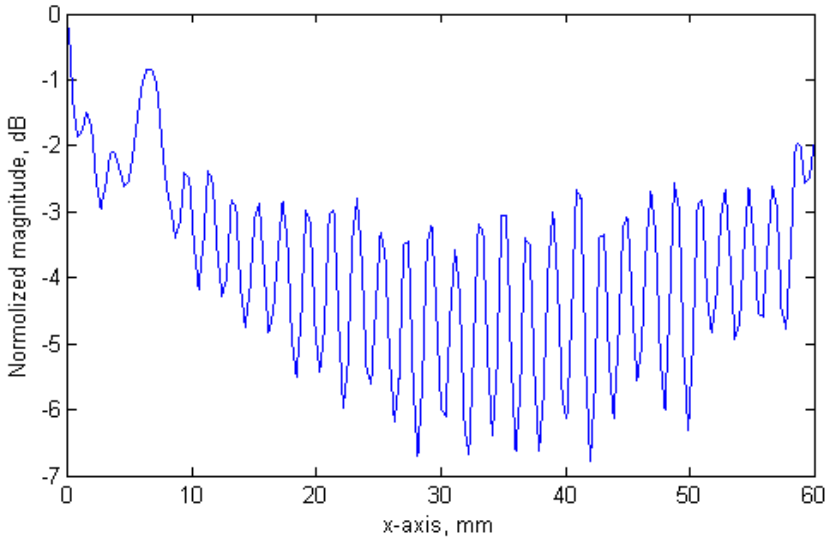

(b)

Figure 7.28 *Measurement results showing the surface displacement of 3rd element of unmatched 2-2 Piezocomposite BII; (a) full aperture view, (b) cross-sectional view*

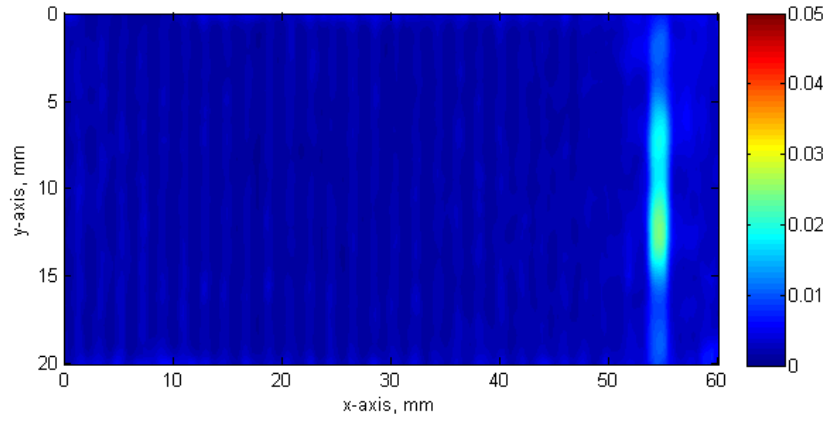

(a)

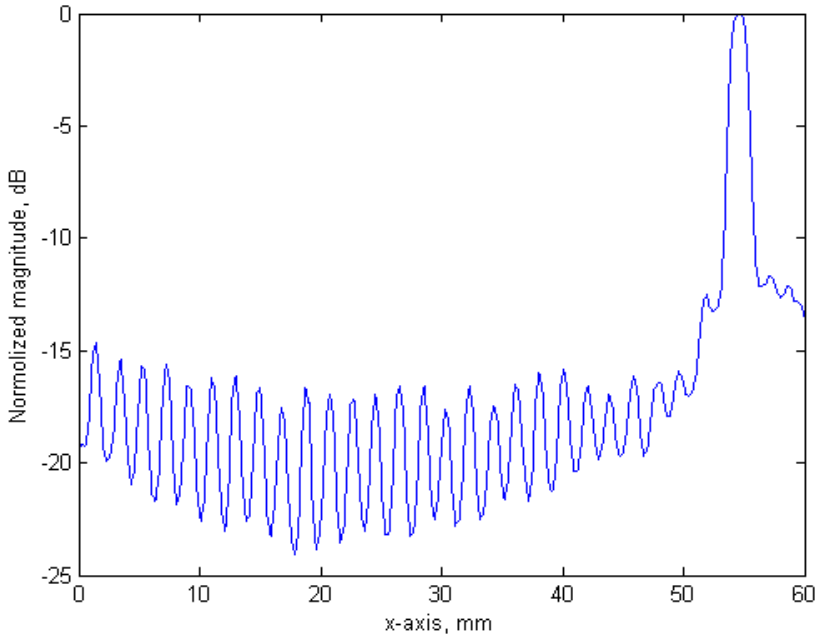

(b)

Figure 7.29 *Measurement results showing the surface displacement of 29th element of unmatched 2-2 Piezocomposite BII; (a) full aperture view, (b) cross-sectional view*

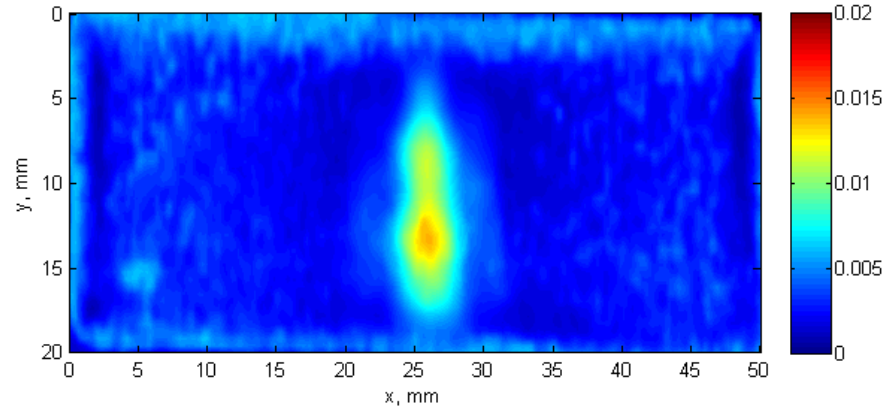

(a)

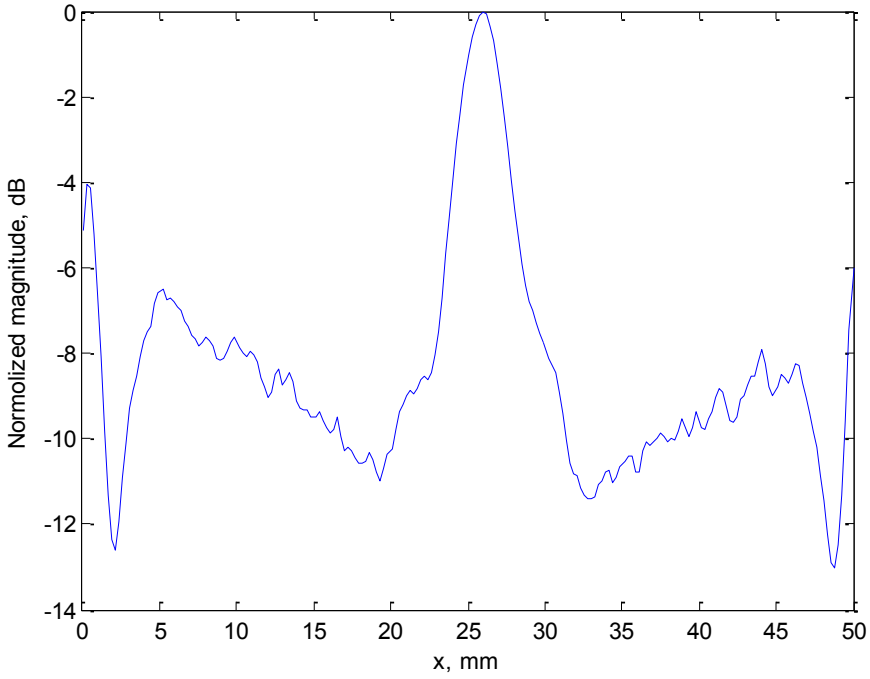

(b)

Figure 7.30 *Measurement results showing the surface displacement of 17th element of 2-2 Piezocomposite BII including matching layer; (a) full aperture view, (b) cross-sectional view*

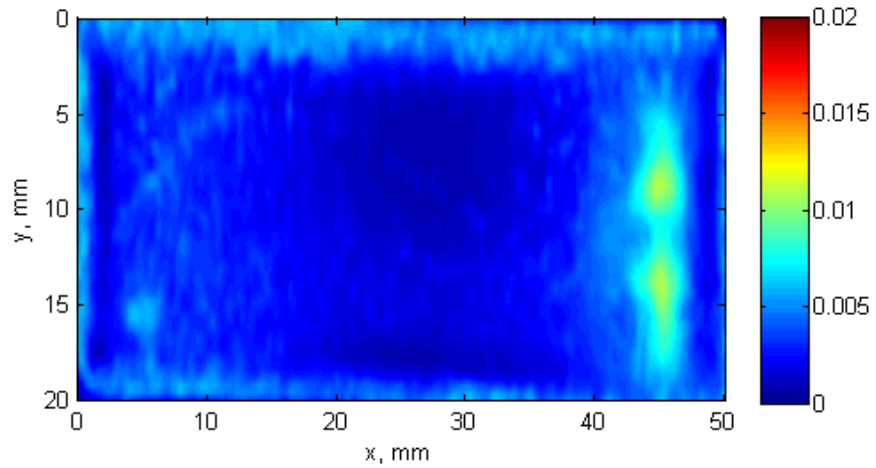

(a)

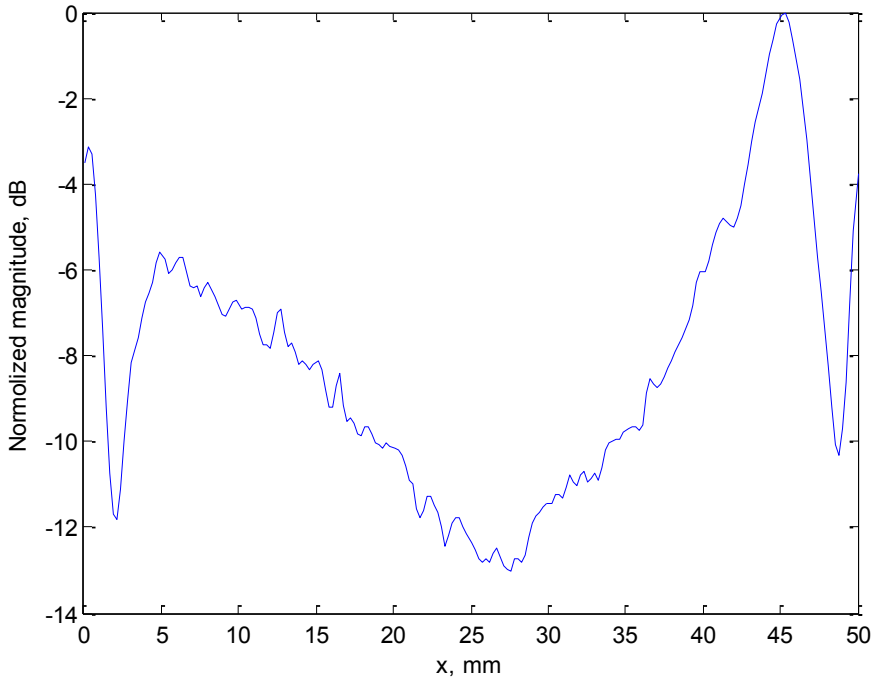

(b)

Figure 7.31 *Measurement results showing the surface displacement of 3rd element of 2-2 Piezocomposite BII including matching layer, (a) full aperture view, (b) cross-sectional view*

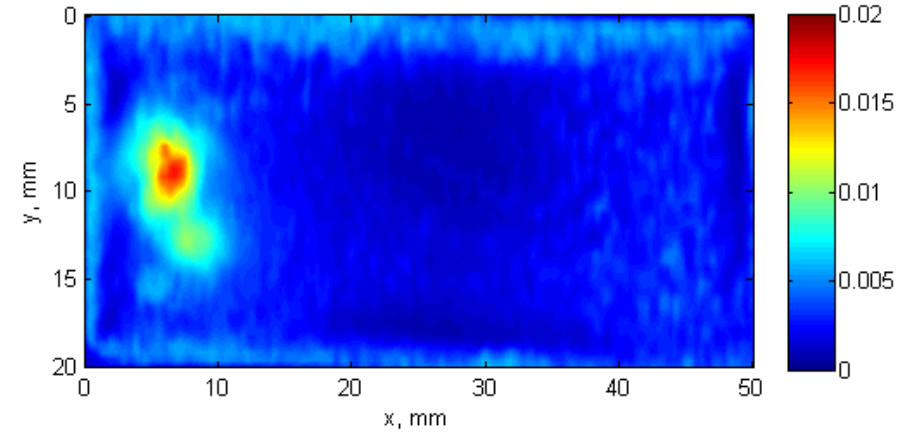

(a)

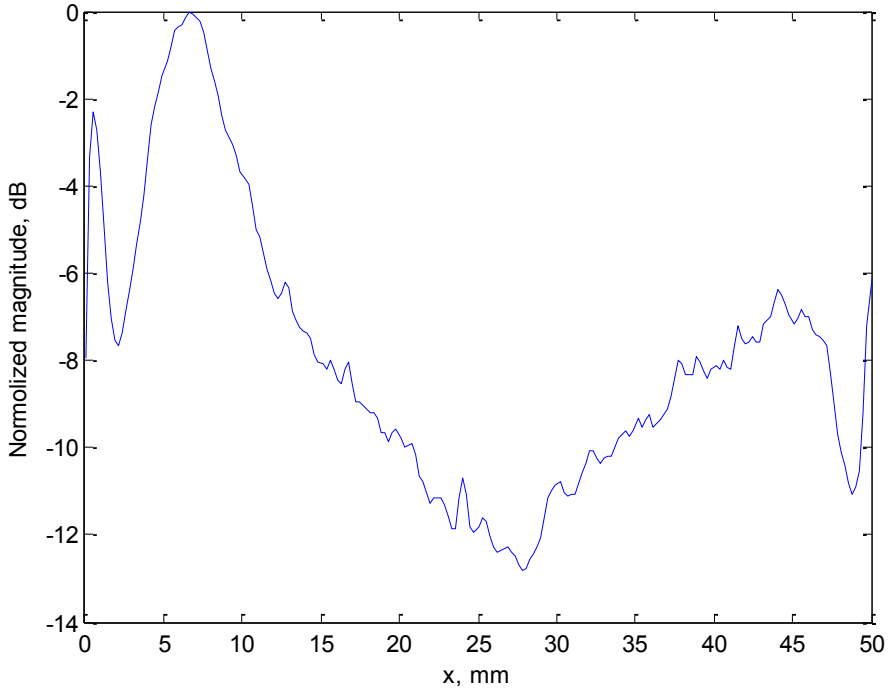

(b)

Figure 7.32 *Measurement results showing the surface displacement of 29th element of 2-2 Piezocomposite BII including matching layer, (a) full aperture view, (b) cross-sectional view*

7.5.4 Calibration of transducer

7.5.4.1 Bandwidth characterization

Again, the pulse echo response was acquired from a reflector positioned 50 mm away from the transducer. The Lecoeur OPEN system was used to excite the transducer and collect the echo signals. Due to the limitation of the system, the experimental setup is different to the experiment described in Section 7.4.2.5. A pulse that is 40 Volt and width of 200 ns was used to excite each element.

First, the pulse-echo temporal and spectral characteristics for element #17 are shown in Figure 7.33. It is clear that the performance of the fabricated device is of lower quality when compared to the simulated response. In particular, the bandwidth is lower. The measured mechanical-Q value is 10 and the element bandwidth is ~10%, or 43kHz.

While the operational bandwidth for element #17 was lower than expected, this is insignificant when the pulse-echo performance of the other elements is considered. Figure 7.34 presents the measured pulse-echo response for elements #3, #17 and #30. It is clear that the edge elements have a very low response and it is obvious that this will have a detrimental effect on the array performance under high power operating conditions.

To overcome this problem, it may be possible to use compensation on each channel to optimise the drive excitation frequency and drive voltage level to balance the array performance across all elements. This is generally impractical and would have a significant effect on the focussing ability of the array which depends on ensuring constructive interference between arriving ultrasonic wavepackets at the desired focal region.

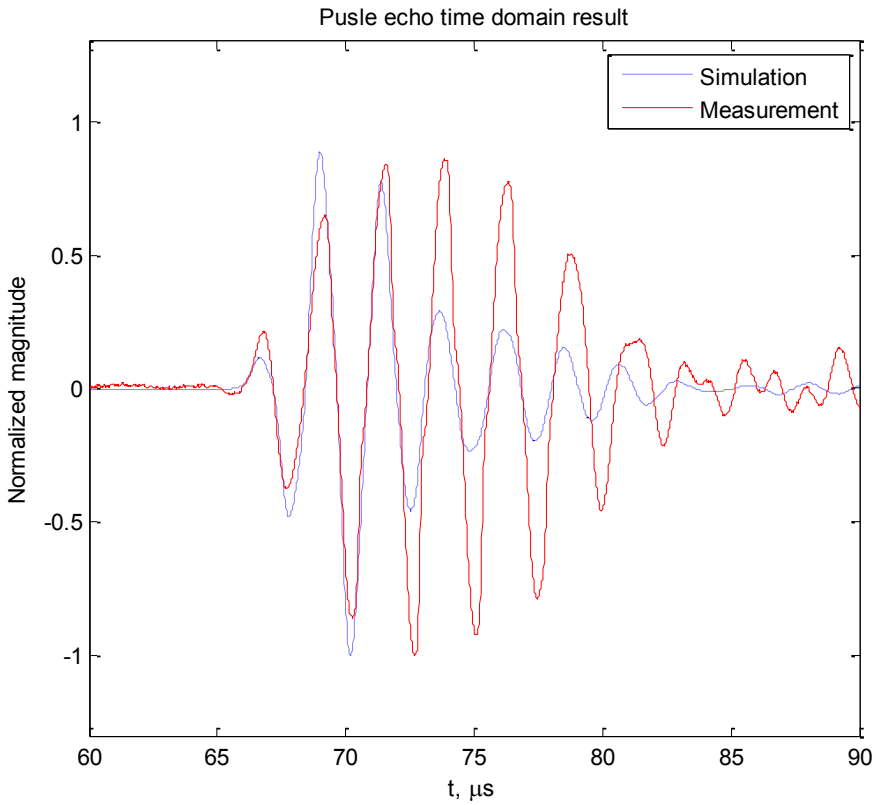

(a)

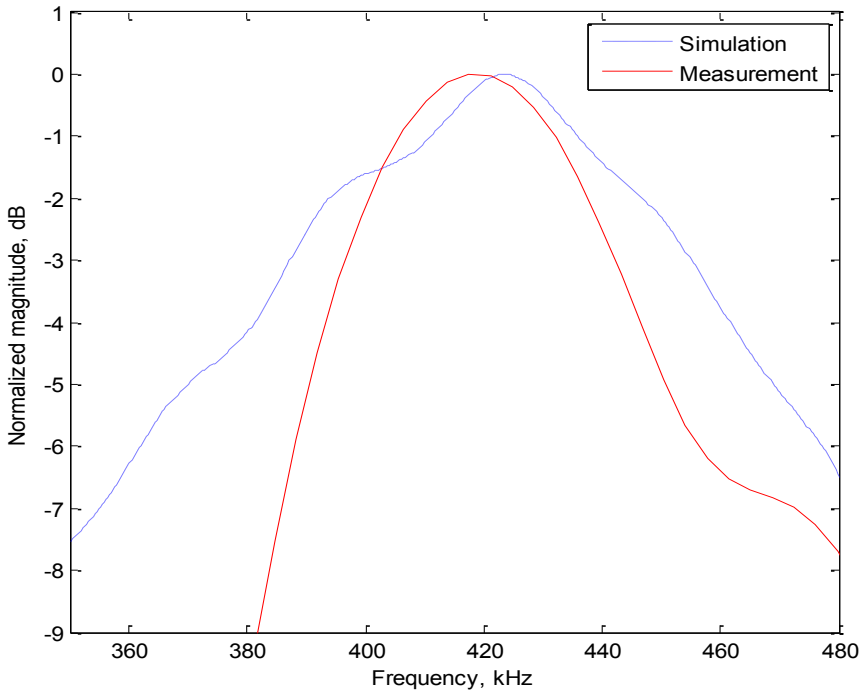

(b)

Figure 7.33 *Measured pulse echo response of the centre element in 2-2 Piezocomposite BII, (a) time domain; (b) frequency domain*

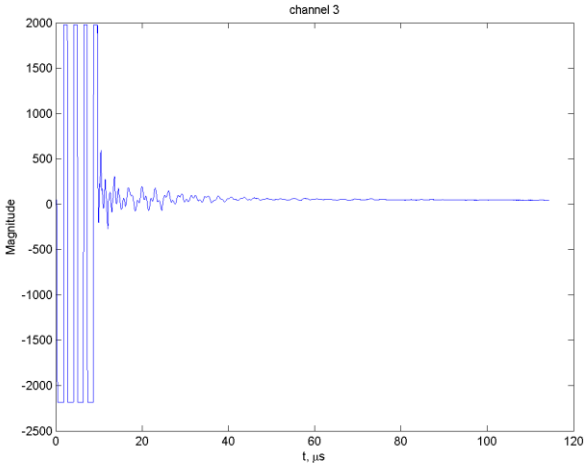

(a)

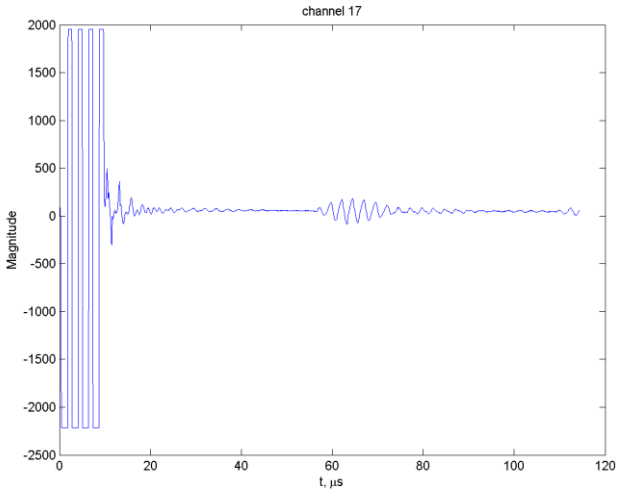

(b)

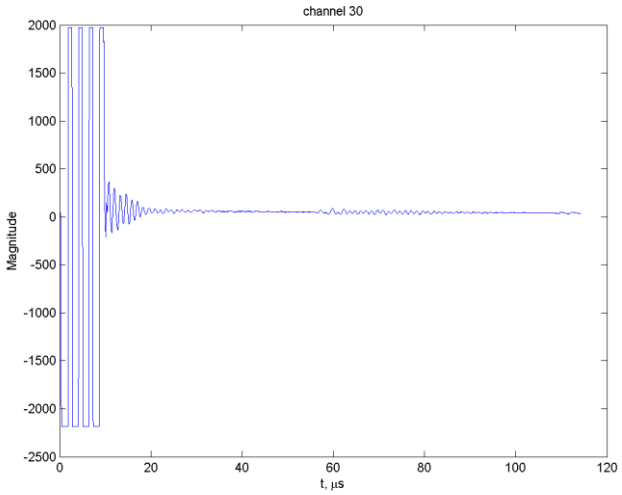

(c)

Figure 7.34 *Measured pulse echo time domain response for three elements in 2-2 Piezocomposite BII, (a) element 3, (b) element 17, (c) element 29*

7.5.4.2 Beam profile characterization

The ability of the fabricated array to generate a desired focal region was next investigated. During these experiments, a 40 V and 500 ns width pulse was used as excitation signal and the needle hydrophone used to measure pressure in the field.

Figure 7.35 illustrates the measured pressure field map for the fabricated 2-2 Piezocomposite BII at focus points located 50 mm and 100mm from the transducer. Moreover, the focal point was varied from on-axis (0^o) to off-axis (10^o) to explore the steering ability. These results were somewhat surprisingly good and illustrate that the array has a reasonable focussing ability and importantly, no sidelobes were present in these field maps.

The success of the focussing experiments at 50mm and 100mm, Figure 7.36, led to a more detailed investigation of the focussing ability of the fabricated piezocomposite array over a wider focal point range. The focal distance was varied between 20 to 120mm, in steps of 10mm. The pressure field was measured and mapped at each focal position and 3 performance metrics extracted from the processed image:

- 3dB area; is the calculated area, around the peak pressure in the focal region, in which the pressure is less than 3dB down from the peak pressure
- 3dB power factor; is the accumulative energy (pressure) within the 3dB area around the peak pressure. This is provided in terms of the voltage measured from the hydrophone and is directly proportional to pressure.
- Maximum hydrophone receive signal magnitude; is the voltage measured from the hydrophone at the peak pressure position.

These results are presented in Table 7.3. This data illustrates that the focal region size spreads out as a function of distance from the array; there is a peak in the pressure profile around 40-50mm; and that the energy in the focal region increases with distance, primarily as a function of increased focal region size.

A further evaluation of the transducer steering ability was carried out to measure the steering ability over the angular range -80 to 80 degrees, at the focal position of 50mm. Figure 7.36 presents the steering angle relationship and shows that the -3dB steering angle range is from -20^o to 20^o.

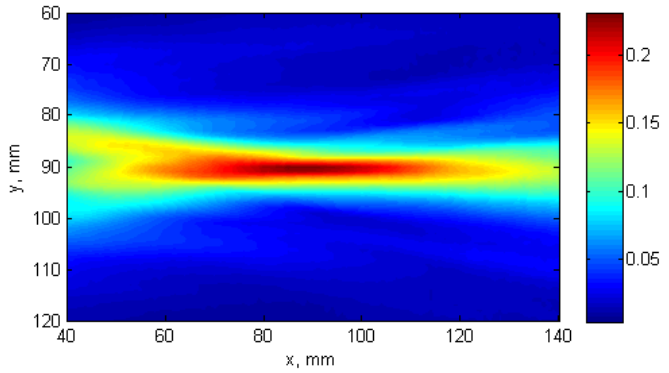

(a)

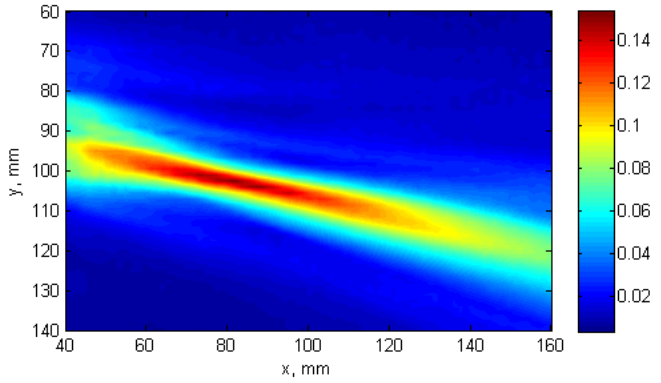

(b)

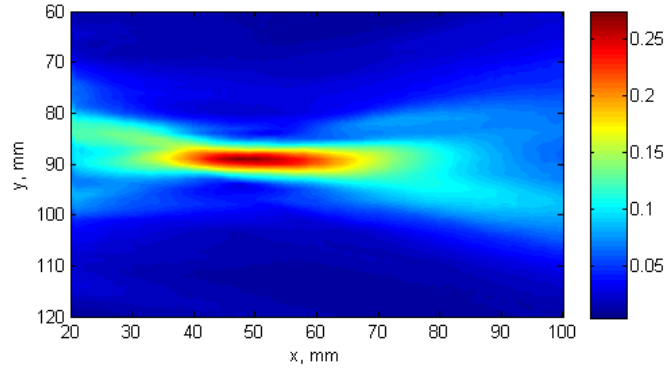

(c)

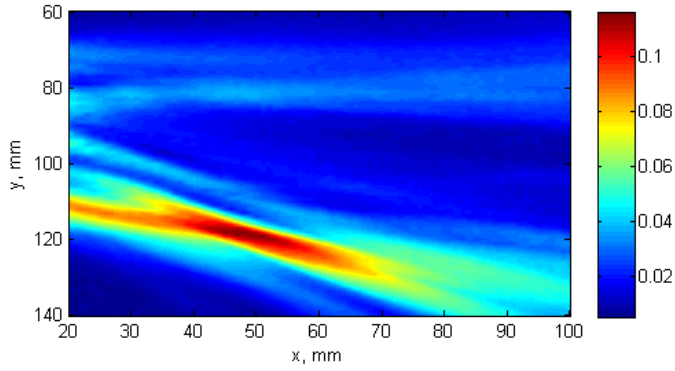

(d)

Figure 7.35 *Measured beam profile for 2-2 Piezocomposite BII operating into a water load,*
(a) focus at x= 100, y = 0, (b) focus at x= 100, y = 20,
(c) focus atn x= 50, y = 0, (d) focus at x= 50, y = 30

Table 7.3 *Calculated metrics associated with focusing ability of 2-2 Piezocomposite B1I, focussing on-axis between 20-120mm*

Focus Distance, mm	-3dB area, mm^2	3dB Hydrophone receive signal magnitude (peak-to-peak), V	Max hydrophone receive signal magnitude (peak-to-peak), V
20	30	1.53	0.178
30	36	2.29	0.22
40	57	3.86	0.24
50	78	5.31	0.24
60	102	6.78	0.23
70	126	8.14	0.22
80	153	9.58	0.21
90	177	10.60	0.21
100	354	16.42	0.17
110	306	16.02	0.19
120	342	17.29	0.18

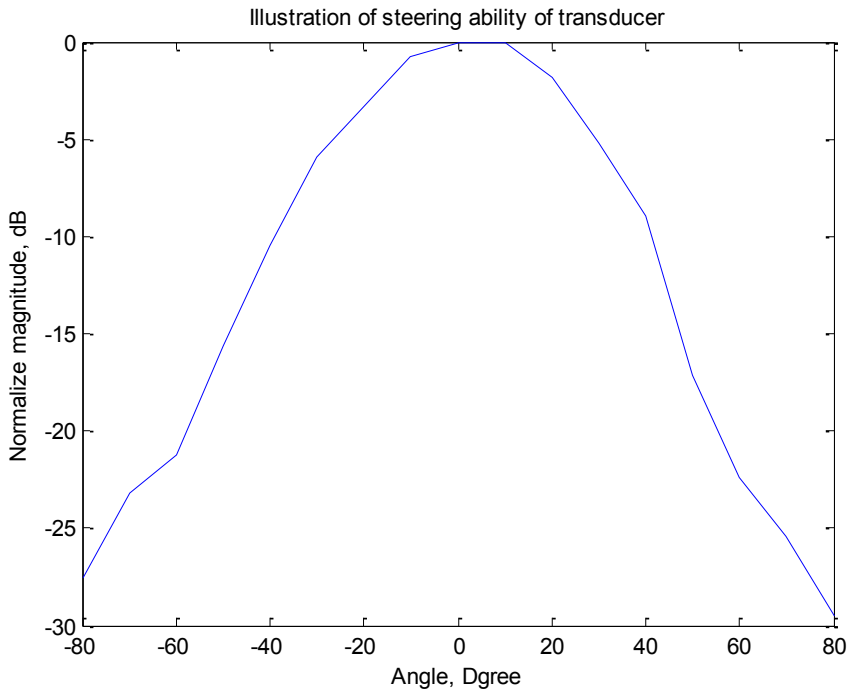

Figure 7.36 *Investigation into the steering range of the fabricated 2-2 Piezocomposite BII*

7.6 Evaluation of high power performance

The final stage in the evaluation of the fabricated 2-2 Piezocomposite BII was to drive the array elements with a tone burst, centred at the desired operating frequency, and measure the pressure, or cavitation, at the focal region. Section 7.5 provided details on the best focussing options for the array and hence, this experimental work will be carried out an on-axial focal point located 50mm from the front face of the transducer.

In this experiment, a 380 kHz, 20 cycle tone burst with a 5.3% duty cycle was used and created within the OPEN system. The peak-to-peak excitation level was varied between 20 Volts and 80 Volts, in steps of 10 Volt. At each voltage level the peak pressure at the focal region was measured using a bilaminar PVDF hydrophone (GEC Marconi research Ltd.). The recorded voltage was converted into a pressure using the calibration figure of 58 PA/V at 380kHz. The measured results are presented in Figure 7.37.

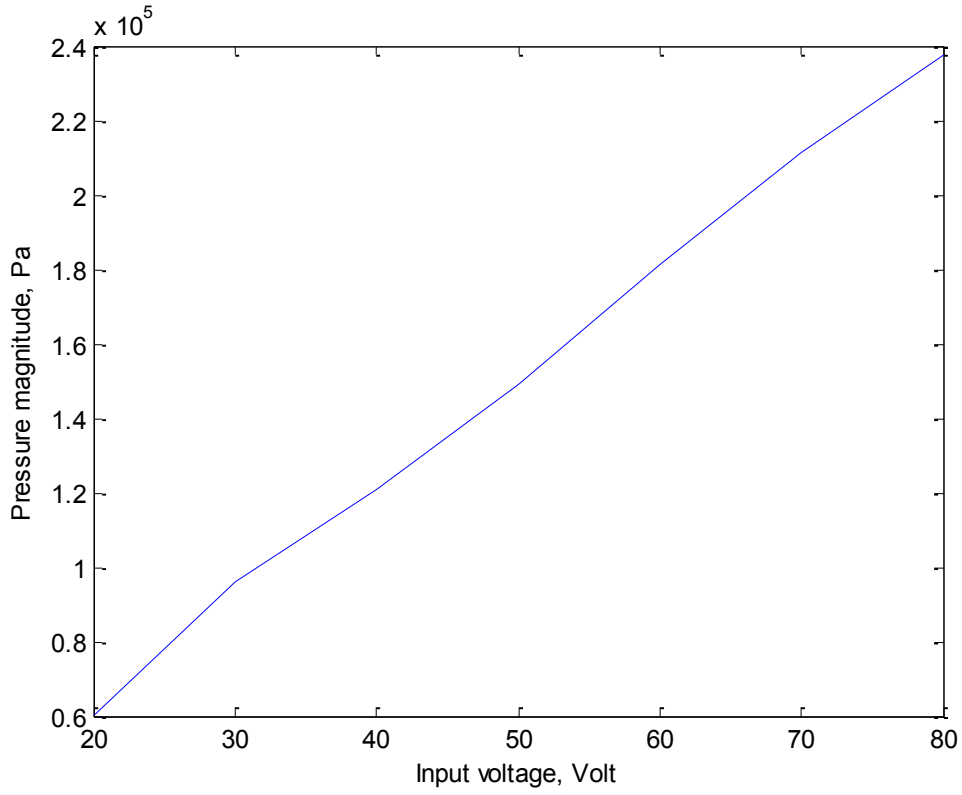

Figure 7.37 *Measured peak pressure from the 2-2 Piezocomposite BII array at a focal distance of 50mm*

From the pressure measurement results in Figure 7.35, the pressure increase with the excitation voltage is linear. Hence, it is reasonable to expect the pressure would further increase under higher excitation levels. At the frequency of 400 kHz, the cavitation generation threshold is 1 MPa [106], and extrapolating from the linear curve in Figure 7.35 gives an estimate that an excitation voltage greater than 400V (peak-to-peak) would be required to initiate cavitation. Unfortunately, the maximum voltage output of OPEN system is 100 Volts (peak-to-peak) and hence, it is clear that under the current experimental setup, the fabricated array (2-2 Piezocomposite BII) will not be able to generate cavitation as intended.

To satisfy this hypothesis, the tin foil test was also carried out. The same experiment setup was used, and the tin foil was placed at the maximum pressure point, which is 50 mm away from the device. The experiment lasted 10 minutes and there were no signs of cavitation erosion in the tested tin foil.

7.7 Discussion and conclusion

An alternative, and novel, HIFU transducer design has been presented in this Chapter. The active piezocomposite configuration was re-designed from the 1-3 connectivity concept used in Chapter 6 to a 2-2 connectivity arrangement. Moreover, a two layer stacked approach was adopted to improve the efficiency of the array elements. Overall, the concept was considered to facilitate ease of manufacture, whilst maintaining high efficiency performance.

Two design configurations were modelled and analysed to determine appropriate HIFU array designs for manufacture. The simulation results demonstrated the potential of utilising the 2-2 connectivity piezocomposite as the active material in a HIFU array transducer. The two 2-2 connectivity design options considered were: 4 plates under one array element; and with a single plate for each array element. The latter design was selected to be manufactured as it was predicted to produce a smaller focal region and was considered simpler to manufacture.

Two HIFU arrays were manufactured and reported in this Chapter, with a third device failing during the fabrication stages. Both arrays were fully characterised and demonstrated reasonable agreement with specific simulated fundamental results. Hence, the concept of utilising this approach in an array was demonstrated. However, there were problems during the manufacturing process which reduced the efficiency of the piezoelectric materials and resulted in poor performance when evaluated as a HIFU device.

The experimental performance of the fabricated arrays was disappointing and a number of modifications to the design process introduced to improve the manufacturability of the selected stacked 2-2 connectivity piezocomposite designs. Unfortunately, disbonds between the constituent layers and bowing of the active piezocomposite layers were not prevented and this resulted in a significant degradation in performance across the array aperture. Two aspects are important to discuss:

1. The inability to manufacture these devices to a high standard is considered to be a local workshop issue and that these issues could be overcome in the future. This

would require an extensive programme to fabricate a large number of piezoceramic and piezocomposite coupons to evaluate the most appropriate bonding and curing processes. Unfortunately, this was considered outwith the scope of this research project.

2. A reasonable number of array elements were functional, albeit not performing at the desired acoustic output levels, and this enabled the design concept to be validated. It is clear from the correlation between simulation and experimental results that the stacked 2-2 piezocomposite array configuration is a viable transducer option for HIFU applications. Hence, the work presented in this Chapter has been successful from the perspective of demonstrating the potential of a new transduction technique for use in Sonochemistry applications.

Chapter 8

Conclusion and Suggestions for Future work

8.1 Thesis conclusions and discussion

8.1.1 Discussion on key outputs from Thesis

This Thesis has presented two new techniques using ultrasonic technology for application in the chemical processing systems. It is important to understand that ultrasound can be used in two modes of operation in this field: low power, high frequency ultrasound for chemical processing monitoring; and high power, low frequency ultrasonic fields for chemical process enhancement. Inspiration for the novel techniques presented in this Thesis has come from the medical domain: harmonic ultrasonic image; and high intensity focused ultrasound. These medical ultrasound approaches are relatively well established and the challenge was to translate these concepts into ultrasonic systems that were compatible with chemical processing applications. There are a plethora of chemical reactions and chemical-related systems to which ultrasound could prove to be a solution to either the monitoring/characterisation or intensification problems in this industry. In fact, there are a significant number of commercial ultrasonic systems that service this particular domain. Hence, this Thesis concentrated on the characterisation of high-throughput technologies (HTT), in which maintaining high product quality is the key objective, and the development of a flexible system intensification approach, with potential for system scale-up.

Traditionally, an active ultrasonic monitoring system for chemical processing control applications typically uses linear signal processing techniques. That means, in such a system, it excites and receives signals with the same (or similar) frequency range. It was considered interesting that biomedical systems had been developed which uses non-linearity in the received signals to improve imaging resolution through analysis of the harmonic frequency components. Thus, it was decided to consider if such an approach could be used to extract additional information from a chemical reaction. In this work, HTT products (shampoo and conditioner) were investigated and a dual frequency transducer was designed to acquire the linear and harmonic backscattered signals simultaneously. Importantly, by using both the linear and second harmonic backscattered signals it was shown to be possible to differentiate between HTT samples with the same density, but different molecular structures. This would not be possible using current commercial instrumentation.

Sonochemistry is the field in which high power ultrasound is used to catalyse the chemical reaction process usually through the generation of a cavitating field. [14, 216]. Most high power ultrasonic systems that are used in Sonochemistry are composed of a number of single element transducers, which operate at a single frequency without phase control, and in many cases insufficient energy management. Moreover, in current commercial systems, the addition of multi-frequency operation and phase control features will increase the complexity of the reactor design and hence, may not be considered commercially viable. Nevertheless, as the operational parameters of the current systems are fixed, they can be inefficient to apply to dynamic chemical reactions and if a flexible ultrasonic delivery system was available it could provide a number of benefits to industrial applications.

In this Thesis, the high intensity focussed ultrasound (HIFU) phased array transducer techniques used in the medical clinical field were used as the inspiration for a flexible high power ultrasound delivery system for Sonochemistry applications. Moreover, it was considered that the such a Sonochemistry system would benefit from two important aspects: the scale up of the reactor vessel could be achieved by using the beam steering capability of the HIFU array to manipulate the location of the cavitating field within the load medium; and a reduction in the number of transducers used in the reactor, albeit the discrete transducers, used currently, would be replaced by a single, more complex device.

Two piezoelectric options for the active phase in a HIFU array have been described and a comprehensive simulation programme undertaken to design the array configurations. Array transducers have been fabricated and although a number of manufacturing issues resulted in a degraded performance for some of the device, cavitation was demonstrated from one of the arrays. Thus, it is considered that this Thesis has proposed a new high power ultrasound technique for use in Sonochemistry, but that further work using high quality manufactured arrays is required to fully validate this technique.

The two ultrasonic systems will now be discussed individually and in detail. Importantly, the key contributions to knowledge associated with each approach will be highlighted.

8.1.2 Ultrasonic monitoring/characterization system for chemical processing control

The Thesis has presented an initial evaluation of a novel technique for ultrasonic characterization of HTT products. A feasibility study was conducted prior to the start of this PhD Thesis and illustrated that conventional monitoring techniques, using velocity and attenuation measurements, were not sufficient to distinguish between different HTT product samples and be applicable in the quality control of such chemical products. Hence, Chapter 3 evaluated the use of nonlinear techniques to determine whether additional, or complementary, information on the chemical formulation could be collected from the system.

This approach was motivated by the success of harmonic imaging in the biomedical field and it was interesting to develop this novel approach from concept through to implementation. The initial stages considered potential approaches to the design, development and implementation of such a system and it was decided that this work programme would focus on the acquisition of empirical data. Next, the experimental configuration was contemplated and the reception transducer positioned at 90^{o} to the transmission device to ensure that the direct linear propagating ultrasonic energy would not dominate the received signal waveforms. This is important and ensured that the acquired signals from the transducer, which was placed in contact with the load medium through the top opening of the sample bottle, originated from the interaction between the propagating ultrasonic energy and the chemical composition of the HTT product. This type of arrangement is typically referred to as an ultrasonic backscattering system configuration. This is a non-standard ultrasonic transducer system setup for process control applications in which the transducers are typically aligned axially to maximise system SNR.

Commercial ultrasonic transducers, at operating frequencies of 2.25MHz and 5MHz, were used to evaluate the backscattered signals in both the linear, at the fundamental operating frequency, and nonlinear, at the second harmonic frequency, regimes. Here, a 2.25MHz transmitter was used throughout and the reception device changed depending on which ultrasonic regime was on interest. The transmission arrangement was calibrated to determine the excitation voltage levels to drive a linear chirp scheme and generate a

nonlinear response in the HTT samples of hair shampoo and conditioner. Whereas, the reception arrangement was dominated by the development of matched filtering techniques to enable extraction of the linear or nonlinear signals, as appropriate. Although, these results demonstrated some promise, there was an issue with repeatability of the measurements due to swapping of the standard narrowband ultrasonic devices used. Hence, a dual frequency transducer was designed using PZFlex, and then fabricated, characterised and used in the next evaluation stage for the work programme. The transducer consisted of two separate ultrasonic devices integrated into a single package. This was achieved by designing a 2MHz disc element to operate in the centre of the transducer and a 4MHz ring element operating around the circumference of the device. An acoustically absorbing material was used to provide isolation between the two piezoelectric phases in the transducer and both elements were constructed using 1-3 connectivity piezocomposite materials.

Using the dual frequency transducer, simultaneous data acquisition of both the fundamental and second harmonic signals could be achieved. This technique was applied to two sample pairs of HTT products, supplied by Unilever. Each sample pair is from the same product, either conditioner or shampoo, and they exhibit similar density and viscosity parameters but have been produced using different formulations. Hence, it would be important to distinguish between such samples in terms of product quality control. The experimental results acquired by the dual-frequency transducer were analysed in both the linear and nonlinear regimes and by comparison of the energy acquired in each spectral regime, it was possible to distinguish between the samples in each sample pair. Hence, the application of nonlinear ultrasonics for the characterisation of chemical products has been demonstrated and a new avenue of research established in this research thematic area.

Overall, this work is considered successful in demonstrating a novel approach to ultrasonic systems applied to characterisation, or monitoring, of chemical processes. It can be argued that this technique has only been applied to limited samples number and this will introduce an element of uncertainty in its applicability. Nevertheless, it is clear that a novel approach has been developed through this Thesis and applied for the first time for the quality control of HTT products in the field of chemical process control.

8.1.3 The application of HIFU array transducer technology for intensification of chemical reactions

High power ultrasound is a growing technique in the field of Sonochemistry, in which an ultrasonic transducer system is used to induce a cavitating field in a liquid load medium to influence/agitate the chemical reaction. Importantly, although there are many commercial instruments available for use in this field, they are typically fixed in their mode of operation which may be a limitation when related to the dynamic evolution of a chemical reaction. Hence, the ability to generate a high power, cavitating field with control over its location within the load medium would be of interest to the Sonochemical industry.

Again, the stimulus for this aspect of the PhD work programme came from biomedicine where a technique called high intensity focussed ultrasound (HIFU) has been used as a surgical tool. In this approach, an ultrasonic array configuration is used to deliver a high ultrasonic intensity region within a small, controlled focal region to target specific ailments, e.g cancerous cells, whilst causing no damage to healthy tissue both close to the focal region and in the propagation path. The extension of this approach for Sonochemistry applications would offer control over the location of the focal region within the load medium, and hence the location of the cavitating field which initiates the enhancement of the chemical reaction itself.

This Thesis has described the design, implementation and evaluation of two piezoelectric configurations for use as the active phase in a HIFU array designed for Sonochemistry applications. In the biomedical field, the HIFU arrays are designed to operate in the MHz frequency range. Whereas, for Sonochemistry applications, this work considered the frequency range between 200-400kHz as a compromise between the ability to generate cavitation and manufacturability of this type of array design. That is, it was recognised that a lower operating frequency, less than 100kHz, is advantageous for the generation of cavitation, but the capability within Strathclyde to manufacture ultrasonic transducers for use in a HIFU array configuration would prefer a higher operating frequency.

A simulation programme was conducted to design HIFU arrays appropriate for use in

the frequency range 200-400kHz. Moreover, the two piezoelectric configurations selected for evaluation in this Thesis were:

- 1-3 connectivity piezocomposite structure fabricated from a single (thick) plate of piezoceramic. This is a standard manufacturing approach and used routinely in both Sonar and biomedical transducer designs. The main issue in terms of this work, was to ensure the stability of the piezocomposite structure as the piezoceramic pillar size resulted in fewer ceramic pillars under each array element than typically used in array configurations.
- A stacked 2-2 connectivity piezocomposite configuration was also evaluated and this was specifically selected to match the HIFU array element layout. In this arrangement, two identical layers of piezoceramic were bonded together and diced in only one direction to create the linear array elements as required for the HIFU design. Again, the number of piezoceramic plates under each array element was a design criteria and the simplest approach to have the piezoceramic width equal to the array element width was selected for ease of manufacture. Importantly, with this approach the stacked arrangement will provide benefits in terms of transducer performance and electrical matching to the drive electronics.

The 1-3 piezocomposite design configuration demonstrated good potential from all three manufactured devices covering the specified frequency range. High correlation with the simulated results have been described in Chapter 6 and the focussing ability of each transducer demonstrated through a series of experimental results. Moreover, the highest frequency array, 420kHz, was used to assess the ability of the array to generate a cavitating field in the focal region. Here, an aluminium foil test was used to illustrate the cavitating field through its destructive nature on the foil itself.

The 2-2 stacked piezocomposite transducer design proved more difficult to manufacture. This was a surprising result, as the 2-2 configuration was considered to be more robust than its 1-3 counterpart. Three different HIFU arrays were fabricated using this approach and importantly, good corroboration with the simulated results was demonstrated in Chapter 7. In each array configuration, poor electrical connectivity to the

centre electrode in the stacked configuration and bowing across the array aperture degraded the array performance and hence, it was not possible to generate a cavitating field with these devices.

Although, there were contrasting performances for both transducer configurations investigated in this Thesis, it is clear that the HIFU array transducer technology offers potential for use in the field of Sonochemistry. It was demonstrated that such arrays are capable of steering the focal region through an approximate $\pm 30^{o}$ angular range calculated from the 6dB points in the measured pressure fields. This could revolutionise the way in which high power ultrasonic systems are deployed in Sonochemistry applications and provide a mechanism for scale-up for industrial applications. Current transducer systems are typically resonant in nature and hence, efficiency reduces as the size of the reactor increases. Whereas, with an array based system the limitation for scale up depends on the ability of the array to generate a high pressure focal region at depth into the load medium. This work described in this Thesis has shown that this can be achieved over depths up to 100mm and angular steering of $\pm 30^{o}$. This is by no means the limit of the technology and there is considerable scope for extending this depth range through the manufacture of more efficient array configurations.

8.2 Potential future work concepts

8.2.1 Non-invasive ultrasonic technique for HTT product

The experimental characterization of HTT products can be improved by the introduction of a non-invasive approach. Importantly, the non-invasive methodology will increase the repeatability of the measurement and be closer to a practical technique for industrial use. There are many potential implementations of a non-invasive ultrasonic transduction system, but for this work the reception transducer will be located through a water path between the sample bottle and the transducer.

The repeatability/reliability is the most important issue for accurate characterisation of chemical products. The repeatability issues of the experiment described in this Thesis is mainly affected from two aspects: the sample preparation process; and the repeated insertion of the transducer into sample container. In the current experimental setup, the sample needs to be transferred from the original container into the experimental container, which introduces air bubbles. This will not be a problem in an industrial setting, as the product will already be in a sample bottle to undergo several quality checks. Whereas, the introduction of a transducer into the sample may also introduce air bubbles, which may be located on the transducer front face and degrade the 'contact' between the transducer and sample, and may be considered as a potential source of contaminant into the sample itself. If the receiving transducer is located within the water bath into which the sample bottle is placed, then each measured result will have consistency in the coupling between the various components and differences in the acquired signals will be directly relevant to the sample itself. One particular issue with this approach could be a reduction in received signal SNR due to the scattered signals having to propagate through the vessel wall and the water path. To mitigate against this, the number of receivers could be increased and placed radially around the sample bottle in the same axial plane as the transmitting device.

8.2.2 Utilization of PVDF as a reception device for HTT characterisation

Higher harmonic signals correspond to smaller wavelengths, which could contain information on the micro-structure of the scattering medium. In high power ultrasonic systems, it has been found that cavitation will scatter/radiate higher harmonic signals and these can be used to measure the intensity of a cavitating field. Although cavitation is not likely happen during the proposed high power approach discussed in this Thesis for HTT product monitoring, there is a possibility that higher harmonic signals may be generated through this active ultrasound monitoring process. Moreover, this effect may be enhanced if the excitation voltage level is increased.

Under the current experimental setup, only the fundamental and second harmonic signals can be detected. This is a limitation of the receiver device bandwidth. Hence, the use of a broadband reception device would be advantageous. One possibility is a PVDF device that exhibits a wide and flat frequency response. Due to the high attenuation of HTT product samples and low sensitivity of PVDF device, high voltage excitation and high signal amplification gain will need to be applied to enable detection of these higher harmonic signals.

8.2.3 Establishment of 2-2 stacked piezocomposite manufacture guidelines

In this Thesis, simulation using FEM was conducted during the design of 2-2 connectivity piezocomposite transducers for use in a HIFU array transducer. Unfortunately, successful manufacture of these HIFU array configurations was not achieved and guidelines for fabrication have not yet been established. There are several manufacturing issues that should improve the performance of the HIFU arrays incorporating a 2-2 stacked piezocomposite structure:

- Ensure high quality bonding between the two piezoelectric ceramic layers is maintained after the dicing process. This is critical to ensure that the electrical connection to the piezoceramic layers has low resistance to maximise electrical energy transfer into the piezoelectric material.

- Utilise thicker piezoceramic layers during the manufacturing process to provide a stable substrate/base for the support of the 2-2 piezocomposite structure during the dicing process.
- Refine the curing process for the filled polymer phase to ensure uniformity across the array aperture. This is key to prevent the structure curing into a bow shape, which introduces degradation at the extremities of the aperture.

Once the manufacturing guideline have been established and these issues have been addressed to produce HIFU arrays with consistent quality, it will be necessary to refine the design process through further simulation to optimise the array performance for HIFU applications. Here, it will be important to investigate the impact of plate width, piezoelectric ceramic volume faction, thickness, etc. on the performance of the piezocomposite material used within this structure for utilization in HIFU applications.

8.2.4 1.5-D HIFU phased array transducer

To increase the input power of the HIFU transducer, one way is to increase the number of array elements. However, further scale up of the transducer from current design would be difficult, because of the large lateral dimension of the transducer which would lead to difficulty in mounting such a device onto a Sonochemical reactor.

A 2-D array could massively increase the number of elements, but this is not appropriate for use with the proposed 2-2 piezocomposite structure. A compromise could be to use a 1.5-D configuration, which would require minimal machining of the 2-2 piezocomposite structure and effectively the transducer will be assembled using several 2-2 piezocomposites. There are 32 channels in the fabricated 2-2 piezocomposite (BII) in Chapter 7, and it is proposed to keep the number of elements in the lateral dimension and add an additional two rows of elements across the array width. This will produce a 32 x 3 array configuration and a total of 96 array elements. Obviously, a design exercise will have to be undertaken to determine the optimum size of the array elements, but it is envisaged that each array width will be less than in the current design (i.e > 20mm). It could be hypothesised that the increase in active array size will result in between a 2-3 times increase in acoustic power in the load medium. Moreover, the 1.5 D transducer

arrangement will not only increase the generated power, but will also improve the focusing ability in lateral axis which should greatly increase the pressure magnitude and steering ability of the transducer.

8.2.5 Multi-channel power amplifier

The OPEN (Lecoeur-technique Ltd) and Dynaray (Zetec Inc.) phased array controllers were used in this Thesis for high power excitation. However, both systems are mainly for NDT research purposes, which has limited the applicability of these instruments for the current work. For the OPEN system, its arbitrary function generator has a maximum peak output voltage of 50 V, at a maximum duty cycle of 20%. Whereas, the Dynaray only provides pulse excitation, with a maximum 200 V output level. Under both of these setups, it is difficult to achieve high power ultrasound and effectively generate a cavitation field.

The application of a power amplifier is one solution, but it is difficult and expensive to design and build a multi-channel power amplifier in a conventional way. Recently, Mutasa has built a multi-channel excitation system with phase control [148] for a multi-transducer high power reactor system. This system was controlled by a FPGA board and it combines a H-bridge circuit, transformer, and a resonant circuit for power amplification. Although this system has only 12 channels and an output frequency of 27 kHz, it should be possible to adapt this system for a larger number of channels and a higher operational frequency. By using such a bespoke system, it would be expected that more power could be used to excite the transducer array elements and ultimately produce higher ultrasonic energy levels in the load medium.

8.2.6 Evaluate HIFU approach on chemical reactions

Due to a combination of inefficient excitation of the array transducers from the available instrumentation (see Section 8.2.5) and the fabrication issues (discussed in Chapter 7), the proposed HIFU array approach has not been tested on a chemical reaction. This is an obvious next step in the continuation of this work, but the compatibility of the transducer materials with the constituent chemicals used will be a limiting factor. The

front face material used in an ultrasonic transducer may be damaged by contact with chemical load medium. This will require careful consideration of the chemical reaction to be used to evaluate this technique or a re-design of the HIFU transducer, as discussed in Section 8.2.7.

8.2.7 Non-invasive HIFU array approach

For industrial applications, the current HIFU approach with the transducer in direct contact with the load medium would be a limiting factor due to access and chemical compatibility issues. Hence, the HIFU transducer should be re-designed to operate through the wall structure of the reactor vessel. This is non-trivial as in many cases a jacketed wall configuration is used in reactor vessels and hence, the ultrasound would have to propagate through two solid wall materials and an additional (heat transfer) fluid, before focussing in the load medium of interest. Hence the transduction efficiency will be affected and the array design will require efficient energy transfer from the transducer into the outer wall material, typically glass or steel. In addition, calculation of the focal laws will be complicated by the multiple materials in the propagation path and the effects of refraction within the solid wall materials. Moreover, if the vessel is complex in shape, then interfacing the array to the outer wall will be problematic. Interestingly, if the vessel is cylindrical then there will be a natural focussing effect due to the curvature of the vessel walls which could be exploited in the array design process to improve the ultrasonic intensity in the focal region.

8.2.8 Integrated monitoring/intensification ultrasonic system

Ultrasound can be used for monitoring (or characterisation) of chemical reactions and to influence the progress of a chemical reaction. This Thesis has described novel approaches for both monitoring and intensification approaches. In an industrial environment, being able to combine these approaches would be the ideal solution. Hence, integrating the high frequency, low power capability with a low frequency, high power array would present a powerful instrument for industrial usage. This is not straightforward

to achieve as ensuring isolation of the two transduction approaches will be critical for efficient operation in both modes. But, one solution could be to integrate a PVDF layer onto the front face of the HIFU transducer. This should have a minimal impact on the high power operation and the PVDF would act as a broadband receiver to detect acoustic emission from the cavitating field.

References

[1] D. J. McClements, *Ultrasonics in Food Processing: Recent Developments*. Amsterdam,: Gaonkar,A. G., Ed., Elsevier, 1995.

[2] B. G. Lipták, *Process Measurement and Analysis*: CRC Press, 2003.

[3] L. C. Lynnworth, *Ultrasonic Measurements for Process Control*. San Diego: Academic Press, Inc.

[4] S. Samari, "Ultrasonic inspection methods for food products," *Lebensmittel Wissenschaft und Technologie,* vol. 27, pp. 210-213, 1994.

[5] D. J. McClements and M. J. W. Povey, "Scattering of ultrasound by emulsions," *Journal of Physics D-Applied Physics,* vol. 22, pp. 38-47, Jan 1989.

[6] D. J. McClements, "Particle sizing of food emulsions using ultrasonic spectrometry: principles, techniques and application," in *Ultrasound in Food Processing*, ed New York: Thomson Science, 1998, pp. 85-104.

[7] H. Günzler and H. U. Gremlich, *IR Spectroscopy: An Introduction*: Wiley, 2002.

[8] T. L. Szabo, "Nonlinear acoustics and imaging " in *Diagnostic Ultrasound Imaging: Inside Out: Inside Out*, ed: Elsevier Science, 2004, pp. 381-428.

[9] M. A. Averkiou, D. N. Roundhill, and J. E. Powers, "A new imaging technique based on the nonlinear properties of tissues," in *Ultrasonics Symposium, 1997. Proceedings., 1997 IEEE*, 1997, pp. 1561-1566 vol.2.

[10] B. Ward, A. C. Baker, and V. F. Humphrey, "Nonlinear propagation applied to the improvement of resolution in diagnostic medical ultrasound," *The Journal of the Acoustical Society of America,* vol. 101, pp. 143-154, 1997.

[11] P. N. Burns, "Ultrasound contrast agents in radiological diagnosis," *La Radiologia medica,* vol. 87, pp. 71-82, May 1994.

[12] ESC. (2014, 06/07/2014). *The physics of Contrast Imaging*. Available: http://www.escardio.org/communities/EACVI/education/echo-box/contrast-echo-box/Pages/introduction-physics.aspx#

[13] A. Shoh, "Industrial applications of ultrasound - a review I. High-power ultrasound," *IEEE Transactions on Sonics and Ultrasonics,* vol. 22, pp. 60-70, 1975.

[14] R. S. Tranter, R. Sivaramakrishnan, N. Srinivasan, and K. Brezinsky, "Calibration of reaction temperatures in a very high pressure shock tube using chemical thermometers," *International Journal of Chemical Kinetics,* vol. 33, pp. 722-731, 2001.

[15] T. J. Mason and J. P. Lorimer, *Sonochemistry: theory, applications and uses of ultrasound in chemistry*: Ellis Horwood, 1988.

[16] L. H. Thompson and L. K. Doraiswamy, "Sonochemistry: science and engineering," *Industrial & Engineering Chemistry Research,* vol. 38, pp. 1215-1249, Apr 1999.

[17] K. S. Suslick, J. J. Gawienowski, P. F. Schubert, and H. H. Wang, "Sonochemistry in non-aqueous liquids " *Ultrasonics,* vol. 22, pp. 33-36, 1984.

[18] M. A. Margulis, "Sonochemistry as a new promising area of high energy chemistry," *High Energy Chemistry,* vol. 38, pp. 135-142, May-Jun 2004.

[19] J. Klima, A. Frias-Ferrer, J. Gonzalez-Garcia, J. Ludvik, V. Saez, and J. Iniesta, "Optimisation of 20 kHz sonoreactor geometry on the basis of numerical simulation of local ultrasonic intensity and qualitative comparison with experimental results," *Ultrasonics Sonochemistry,* vol. 14, pp. 19-28, Jan 2007.

[20] L. Curiel, F. Chavrier, R. Souchon, A. Birer, and J. Y. Chapelon, "1.5-D high intensity focused ultrasound array for non-invasive prostate cancer surgery," *IEEE Transactions on Ultrasonics Ferroelectrics and Frequency Control,* vol. 49, pp. 231-242, Feb 2002.

[21] R. T. Held, V. Zderic, T. N. Nguyen, and S. Vaezy, "Annular phased-array high-intensity focused ultrasound device for image-guided therapy of uterine fibroids," *IEEE Transactions on Ultrasonics Ferroelectrics and Frequency Control,* vol. 53, pp. 335-348, Feb 2006.

[22] M. Carrera, B. Canas, D. Lopez-Ferrer, C. Pineiro, J. Vazquez, and J. M. Gallardo, "Fast monitoring of species-specific peptide biomarkers using high-intensity-focused-ultrasound-assisted tryptic digestion and selected MS/MS ion monitoring," *Analytical Chemistry,* vol. 83, pp. 5688-5695, Jul 2011.

[23] G. S. Chen, C. Y. Lin, J. S. Jeong, J. M. Cannata, W. L. Lin, H. Chang*, et al.*, "Design and characterization of dual-curvature 1.5-dimensional high-intensity focused ultrasound phased-array transducer," *IEEE Transactions on Ultrasonics Ferroelectrics and Frequency Control,* vol. 59, pp. 150-155, Jan 2012.

[24] Z. Xu, M. Raghavan, T. L. Hall, M. A. Mycek, J. B. Fowlkes, and C. A. Cain, "Evolution of bubble clouds induced by pulsed cavitational ultrasound therapy - Histotripsy," *IEEE Transactions on Ultrasonics Ferroelectrics and Frequency Control,* vol. 55, pp. 1122-1132, May 2008.

[25] T. L. Hall, C. R. Hempel, K. Wojno, Z. Xu, C. A. Cain, and W. W. Roberts, "Histotripsy of the prostate: dose effects in a chronic canine model," *Urology,* vol. 74, pp. 932-7, Oct 2009.

[26] A. M. Lake, T. L. Hall, K. Kieran, J. B. Fowlkes, C. A. Cain, and W. W. Roberts, "Histotripsy: Minimally invasive technology for prostatic tissue ablation in an in vivo canine model," *Urology,* vol. 72, pp. 682-686, Sep 2008.

[27] T. H. S. C. THS International, Ltd., "High Intensity Focused Ultrasound (HIFU)," ed: THS International, Takai Hospital Supply Co., Ltd., 2010.

[28] C. Wang, A. Gachagan, A. Nordon, A. Robin, and D. Littlejohn, "The characterization of HTT products using a combination linear and non-linear ultrasonic techniques," in *Ultrasonics Symposium (IUS), 2010 IEEE*, 2010, pp. 1160-1163.

[29] T. J. Mason, *Advances in Sonochemistry*. London: JAI PRESS LTD, 1991.

[30] G. J. Price, *Current Trends in Sonochemistry*: Royal Society of Chemistry, 1992.

[31] G. Carson, A. J. Mulholland, A. Nordon, M. Tramontana, A. Gachagan, and G. Hayward, "Particle sizing using passive ultrasonic measurement of particle-wall impact vibrations," *Journal of Sound and Vibration,* vol. 317, pp. 142-157, Oct 2008.

[32] M. Tramontana, A. Gachagan, G. Hayward, A. Nordon, D. Littlejohn, and Ieee, "Ultrasonic monitoring of heterogeneous chemical reactions," in *2006 IEEE Ultrasonics Symposium, Vols 1-5, Proceedings*, ed New York: Ieee, 2006, pp. 910-913.

[33] A. B. Pandit, J. Varley, R. B. Thorpe, and J. F. Davidson, "Measurement of bubble size distribution: an acoustic technique," *Chemical Engineering Science,* vol. 47, pp. 1079-1089, Apr 1992.

[34] A. B. Bhatia, *Ultrasonic Absorption: An Introduction to the Theory of Sound Absorption and Dispersion in Gases, Liquids and Solids*, clarendon press, 1967. includes ed.: Bibliographic references 1967.

[35] D. J. McClements, *Food Emulsions : Principles, Practice, and Techniques*. Boca Raton: CRC Press 1999.

[36] M. J. W. Povey, *Ultrasound in Food Processing* London Blackie Academic & Professional 1998.

[37] J. Sijl, H. J. Vos, T. Rozendal, N. de Jong, D. Lohse, and M. Versluis, "Combined optical and acoustical detection of single microbubble dynamics," *Journal of the Acoustical Society of America,* vol. 130, pp. 3271-3281, Nov 2011.

[38] P. S. Epstein and R. R. Carhart, "The Absorption of Sound in Suspensions and Emulsions. I. Water Fog in Air," *The Journal of the Acoustical Society of America,* vol. 25, pp. 553-565, 1953.

[39] P. C. Waterman and R. Truell, "Multiple sacttering of waves," *Journal of Mathematical Physics,* vol. 2, p. 512, 1961.

[40] J. R. Allegra and S. A. Hawley, "Attenuation of sound in suspensions and emulsions - theory and experiments," *Journal of the Acoustical Society of America,* vol. 51, p. 1545, 1972.

[41] D. Brill, G. Gaunaurd, and H. Uberall, "The response-surface in elastic wave scattering," *Journal of Applied Physics,* vol. 52, pp. 3205-3214, 1981.

[42] P. Havelka, T. Moucha, J. Sinkule, and V. Linek, "Chemical dynamic method for measuring k(L)a in gas-liquid dispersions," *Chemical Engineering Communications,* vol. 168, pp. 97-110, 1998.

[43] V. L. Koval'chuk, V. B. Fainerman, R. Miller, and S. S. Dukhin, "Bubble formation in maximum bubble pressure measuring systems employing a gas reservoir of limited volume," *Colloids and Surfaces a-Physicochemical and Engineering Aspects,* vol. 143, pp. 381-393, Dec 15 1998.

[44] C. Sieblist, A. Lübbert, and M. C. Flickinger, "Gas holdup in bioreactors," in *Encyclopedia of Industrial Biotechnology*, ed: John Wiley & Sons, Inc., 2009.

[45] T. G. Leighton, *The Acoustic Bubble*. New York: Academic Press, 1994.

[46] M. Minnaert, "On musical air-bubbles and the sounds of running water," *Philosophical Magazine Series 7,* vol. 16, pp. 235-248, Aug 1933.

[47] M. Strasberg, "Gas bubbles as sources of sound in liquids," *Journal of the Acoustical Society of America,* vol. 28, pp. 20-26, 1956.

[48] T. G. Leighton, K. J. Fagan, and J. E. Field, "Acoustic and photographic studies of injected bubbles," *European Journal of Physics,* vol. 12, pp. 77-85, 1991.

[49] R. Hsi, M. Tay, D. Bukur, G. Tatterson, and G. Morrison, "Sound spectra of gas dispersion in an agitated tank," *The Chemical Engineering Journal,* vol. 31, pp. 153-161, Dec 1985.

[50] L. S. De More, W. F. Pafford, and G. B. Tatterson, "Cavity sound resonance and mass transfer in aerated agitated tanks," *AIChE Journal,* vol. 34, pp. 1922-1926, 1988.

[51] J. W. R. Boyd and J. Varley, "Sound measurement as a means of gas-bubble sizing in aerated agitated tanks," *AIChE Journal,* vol. 44, pp. 1731-1739, 1998.

[52] M. F. Leach, G. A. Rubin, and J. C. Williams, "Particle size determination from acoustic emissions," *Powder Technology,* vol. 16, pp. 153-158, Mar 1977.

[53] M. F. Leach and G. A. Rubin, "Size analysis of particles of irregular shape from their acoustic emissions," *Powder Technology,* vol. 21, pp. 263-267, Nov 1978.

[54] J. A. C. Van Ooijen, E. Van Tooren, and J. Reedijk, "Acoustic emission during the preparation of dichloro(pyrazine)zinc(II)," *Journal of the American Chemical Society,* vol. 100, pp. 5569-5570, Aug 1978.

[55] M. R. Carlos, R. D. Finlayson, R. K. Miller, M. A. Friesel, and L. L. Klokus, *Acoustic emission on-line monitoring systems (AEOLMS)*. Lancaster: Technomic Publ Co Inc, 1999.

[56] W. Li, S. F. Wang, and X. Jia, "Acoustic emission monitoring of low carbon steel corrosion inside and outside the comparative study," in *2013 International Conference on Process Equipment, Mechatronics Engineering and Material Science*. vol. 331, ed Stafa-Zurich: Trans Tech Publications Ltd, 2013, pp. 246-249.

[57] O. Hunaidi and W. T. Chu, "Acoustical characteristics of leak signals in plastic water distribution pipes," *Applied Acoustics,* vol. 58, pp. 235-254, Nov 1999.

[58] T. J. Fowler, "Chemical - industry applications of acoustic - emission " *Materials Evaluation,* vol. 50, pp. 875-882, Jul 1992.

[59] L. Bjørnø, "Introduction to nonlinear acoustics," *Physics Procedia,* vol. 3, pp. 5-16, Jan 2010.

[60] L. Bjørnø, "Forty years of nonlinear ultrasound," *Ultrasonics,* vol. 40, pp. 11-17, May 2002.

[61] R. T. Beyer, "Parameter of nonlinearity in fluids," *Journal of Acoustic Society of America,* pp. 719-721, 1960.

[62] L. Bjørnø, "Characterization of biological media by means of their non-linearity," *Ultrasonics,* vol. 24, pp. 254-259, Sep 1986.

[63] Z. A. Gol'dberg, "On the propagation of plane waves of finite amplitude," *Soviet Phycis-Acoustics,* vol. 2, pp. 346-352, 1956.

[64] O. Reynolds, "An experimental investigation of the circumstances which determine whether the motion of water shall be direct or sinuous, and of the law of resistance in parallel channels," *Philosophical Transactions of the Royal Society,* vol. 174 pp. 935–982, 1883.

[65] E. L. Carstensen, W. K. Law, N. D. McKay, and T. G. Muir, "Demostration of nonlinear acoustical effects at biomedical frequencies and intensities," *Ultrasound in Med. & Biol,* vol. 6, pp. 359-368, 1980.

[66] D. R. Becon, "Finite amplitude distortion of the pulsed fields used in diagnostic ultrasound," *Ultrasound in Med. & Biol.,* vol. 10, pp. 189-195, 1984.

[67] P. J. Westervelt, "Parameteric acoustic array," *Journal of the Acoustical Society of America,* vol. 35, p. 535, 1963.

[68] M. J. Lighthill, "On Sound Generated Aerodynamically. I. General Theory," *Proceedings of the Royal Society of London. Series A. Mathematical and Physical Sciences,* vol. 211, pp. 564-587, Mar 1952.

[69] T. G. Muir and J. G. Willette, "Parametric Acoustic Transmitting Arrays," *The Journal of the Acoustical Society of America,* vol. 52, pp. 1481-1486, 1972.

[70] J. L. S. Bellin and R. T. Beyer, "Scattering of sound by sound," *Journal of the Acoustical Society of America,* vol. 32, pp. 339-341, 1960.

[71] R. A. Roy and J. Wu, "An experimental investigation of the nonlinear interaction of noncollinear sound beams," *The Journal of the Acoustical Society of America,* vol. 93, pp. 2383-2383, 1993.

[72] H. C. Woodsum, "Comparison of Nonlinear Acoustic Experiments with a Formal Theory for the Scattering of Sound by Sound," in *17th International Conference on Nonlinear Acoustics*, New York, 2006.

[73] "www.alicat.com," ed: Alicat Scientific, Incorporated, 2013.

[74] M. S. Greenwood, J. R. Skorpik, J. A. Bamberger, and R. V. Harris, "On-line ultrasonic density sensor for process control of liquids and slurries," *Ultrasonics,* vol. 37, pp. 159-171, Feb 1999.

[75] M. S. Greenwood and J. A. Bamberger, "Ultrasonic sensor to measure the density of a liquid or slurry during pipeline transport," *Ultrasonics,* vol. 40, pp. 413-417, May 2002.

[76] P. Shakkottai and S. P. Venkateshan, "System for temperature profile measurement in large furnances and kilns and method therefor," US Patent 4762425, 1988.

[77] M. J. W. Povey, "Rapid determination of food material properies," in *Ultrasound in Food Processing*, ed New York: Thomson Science, 1998, pp. 30-65.

[78] J. Stadler, T. Schmid, and R. Zenobi, "Developments in and practical guidelines for tip-enhanced Raman spectroscopy," *Nanoscale,* vol. 4, pp. 1856-1870, 2012.

[79] S. Samari, "Ultrasonic Inspection Methods for Food Products," *LWT - Food Science and Technology,* vol. 27, pp. 210-213, Jun 1994.

[80] Panetta and P. D., "Ultrasonic characterization of solid liquid suspensions " US Patent 39110756, 2006.

[81] L. C. Lynnworth, "Industrial applications of ultrasound: A review. II - Measurements, tests, and process control using low-intensity ultrasound," *IEEE Transactinos on Sonics and Ultrasonics,* pp. 71-101, 1975.

[82] L. C. Lynnworth and V. Mágori, "Industrial process control sensors and systems," in *Physical Acoustics*. vol. Volume 23, A. D. P. R.N. Thurston and P. P. Emmanuel, Eds., ed: Academic Press, 1999, pp. 275-470.

[83] K. H. Irwin, "Application of an active acoustic spectrometry procedure for the assessment of shampoos and conditioners," MSci, Chemistry department, University of Strathclyde, 2008.

[84] R. K. Johnson, "Sound scattering from a fluid sphere revistted " *Journal of the Acoustical Society of America,* vol. 61, pp. 375-377, 1977.

[85] C. R. Robbins, *Chemical and physical behavior of human hair*. New York: Springer, 1994.

[86] S. Mensah, E. Franceschini, and M. C. Pauzin, "Ultrasound mammography," *Nuclear Instruments & Methods in Physics Research Section a-Accelerators Spectrometers Detectors and Associated Equipment,* vol. 571, pp. 52-55, Feb 2007.

[87] W. A. Smith and B. A. Auld, "Modeling 1-3 composite piezoelectrics: thickness-mode oscillations," *IEEE Transactions on Ultrasonics Ferroelectrics and Frequency Control,* vol. 38, pp. 40-47, 1991.

[88] P. R. Gogate and A. B. Pandit, "A review and assessment of hydrodynamic cavitation as a technology for the future," *Ultrasonics Sonochemistry,* vol. 12, pp. 21-27, Jan 2005.

[89] G. T. N.H. Ince, R.K. Belen, & I.G. Apikyan, "Ultrasound as a catalyzer of aqueous reaction systems- the state of the art and environmental applications," *Applied Catalysis B: Environmental,* pp. 167–176, 2001.

[90] O. V. Abramov, *High-Intensity Ultrasonics- Theory and Industrial Applications*. Amsterdam: GORDON AND BREACH SCIENCE PUBLISHERS, 1998.

[91] V. A. Shutilov, *Fundamental physics of ultrasound*. Tokyo: Gordon and Breach Science Publishers, 1988.

[92] E. A. Neppiras and B. E. Noltingk, "Cavitation Produced by Ultrasonics: Theoretical Conditions for the Onset of Cavitation," *Proceedings of the Physical Society. Section B,* vol. 64, p. 1032, 1951.

[93] M. G. Sirotyuk, "Experimental studies of ultrasonic cavitation," in *Intense Ultrasonic Fields*, ed Moscow, 1968, pp. 167-220.

[94] M. Degrois and P. Baldo, "A new electrical hypothesis explaining sonoluminescence, chemical actions and other effects produced in gaseous cavitation," *Ultrasonics,* vol. 12, pp. 25-28, Jan 1974.

[95] H. G. Flynn, "Physics of acoustic cavitation in liquids.," in *Physical Acoustics*. vol. 1, W. Mason, Ed., ed New York: Academic Press, 1964, pp. 58-172.

[96] O. Wilson, *Introduction to Theory and Design of Sonar Transducers*. Los Altos: Peninsula Publishing, 1989.

[97] I. A. k. B. Zel′dovich, *Theory of Formation of a New Phase Cavitation*: U.S. Joint Publications Research Service, 1961.

[98] D. Y. Hsieh and M. S. Plesset, "Theory of rectified diffusion of mass into gas bubbles," *The Journal of the Acoustical Society of America,* vol. 33, pp. 206-215, 1961.

[99] W. E. Whybrew, G. D. Kinzer, and R. Gunn, "Electrification of small air bubbles in water," *Journal of Geophysical Research,* vol. 57, pp. 459-471, 1952.

[100] E. N. Harvey, A. H. Whiteley, W. D. McElroy, D. C. Pease, and D. K. Barnes, "Bubble formation in animals. II. Gas nuclei and their distribution in blood and tissues," *Journal of Cellular and Comparative Physiology,* vol. 24, pp. 23-34, 1944.

[101] E. Ackerman, "Pressure Thresholds for Biologically Active Cavitation," *Journal of Applied Physics,* vol. 24, pp. 1371-1373, 1953.

[102] M. Kornfeld, *Elasticity and strength of liquids(Russian translation)*. Moscow, Leningrad: GINTL, 1951.

[103] R. Cole, *Underwater Explosions*. Princeton: Princeton University Press, 1948.

[104] R. Koul, *Underwater Bursts(Russian translation)*. Moscow: Inostr. Liter, 1950.

[105] E. B. Flint and K. S. Suslick, "Sonoluminescence from nonaqueous liquids: emission from small molecules," *Journal of the American Chemical Society,* vol. 111, pp. 6987-6992, 1989/08/01 1989.

[106] R. Esche, "Investigation of vibration cavitation in liquids," *Akust. Beihefte,* vol. 4, p. 208, 1952.

[107] U. Parlitz, V. Englisch, C. Scheffczyk, and W. Lauterborn, "Bifurcation structure of bubble oscilators," *Journal of the Acoustical Society of America,* vol. 88, pp. 1061-1077, Aug 1990.

[108] D. Ensminger and L. J. Bond, *Ultrasonics: Fundamentals, Technologies, and Applications, Third Edition*: Taylor & Francis, 2011.

[109] L. Rayleigh, *Theory of Sound*. New York: Dover Pubns, 1900.

[110] S. K. R. S. Sankaranarayanan, R. Singh, and V. R. Bhethanabotla, "Acoustic streaming induced elimination of nonspecifically bound proteins from a surface acoustic wave biosensor: Mechanism prediction using fluid-structure interaction models," *Journal of Applied Physics,* vol. 108, p. 104507, Nov 15 2010.

[111] V. Zderic, "Ultrasound-enhanced drug and gene delivery: A review," in *30th Annual International Conference of the IEEE Engineering in Medicine and Biology Society*, Vancouver, 2008, pp. 4472-4472.

[112] R. W. Wood and A. L. Loomis, "The physical and biological effects of high-frequency sound-waves of great intensity," *Philosophical Magazine,* vol. 4, pp. 417-436, Sep 1927.

[113] T. J. Mason, *Sonochemistry* New York: Oxfor University Press Inc, 1999.

[114] A. Lifshitz, *Shock Wave in Chemistry*. New York: Dekker, 1981.

[115] M. A. Margulis, "Sonoluminescence and sonochemical reactions in cavitation fields. A review," *Ultrasonics,* vol. 23, pp. 157-169, 1985.

[116] K. S. Suslick, "Sonochemistry," *Science,* vol. 247, pp. 1439-1445, Mar 1990.

[117] S. E. Skrabalak, "Ultrasound-assisted synthesis of carbon materials," *Physical Chemistry Chemical Physics,* vol. 11, pp. 4930-4942, 2009.

[118] A. Vogel and W. Lauterborn, "Acoustic transient generation by laser‐produced cavitation bubbles near solid boundaries," *The Journal of the Acoustical Society of America,* vol. 84, pp. 719-731, 1988.

[119] A. Vogel, W. Lauterborn, and R. Timm, "Optical and acoustic investigations of the dynamics of laser-produced cavitation bubbles near a solid boundary," *Journal of Fluid Mechanics,* vol. 206, pp. 299-338, 1989.

[120] K. S. Suslick, S. J. Doktycz, and E. B. Flint, "On the origin of sonoluminescence and sonochemistry," *Ultrasonics,* vol. 28, pp. 280-290, Sep 1990.

[121] D. J. Casadonte Jr, J. D. Sweet, and M. S. Vedamuthu, "Sonochemical production of intermetallic coatings in heterogeneous media," *Ultrasonics,* vol. 32, pp. 477-480, Nov 1994.

[122] D. Rieke Reuben, P. Burns Timothy, M. Wehmeyer Richard, and E. Kahn Bruce, "Preparation of Highly Reactive Metal Powders: Some of Their Uses in Organic and Organometallic Synthesis," in *High-Energy Processes in Organometallic Chemistry*. vol. 333, ed: American Chemical Society, 1987, pp. 223-245.

[123] R. D. Rieke, "Preparation of organometallic compounds from highly reactive metal powders," *Science,* vol. 246, pp. 1260-1264, Dec 1989.

[124] G. Cahiez, C. Duplais, and J. Buendia, "Chemistry of Organomanganese(II) Compounds," *Chemical Reviews,* vol. 109, pp. 1434-1476, Mar 2009.

[125] T. Kitazume and N. Ishikawa, "Ultrasound-promoted selective perfluoroalkylation on the desired position of organic-molecules," *Journal of the American Chemical Society,* vol. 107, pp. 5186-5191, 1985.

[126] K. Chatakondu, M. L. H. Green, M. E. Thompson, and K. S. Suslick, "The enhancement of intercalation reactions by ultrasound " *Journal of the Chemical Society-Chemical Communications,* pp. 900-901, Jun 1987.

[127] B. W. Zeiger and K. S. Suslick, "Sonofragmentation of Molecular Crystals," *Journal of the American Chemical Society,* vol. 133, pp. 14530-14533, Sep 2011.

[128] D. Peters, "Ultrasound in materials chemistry," *Journal of Materials Chemistry,* vol. 6, pp. 1605-1618, 1996.

[129] G. Engdahl and L. Svensson, "Simulation of the magnetostrictive performance of terfenol-D in mechanical devices " *Journal of Applied Physics,* vol. 63, pp. 3924-3926, Apr 1988.

[130] D. G. Lord, V. Elliott, A. E. Clark, H. T. Savage, J. P. Teter, and O. D. McMasters, "Optical observation of closure domains in Terfenol-D single crystals," *IEEE Transactions on Magnetics,* vol. 24, pp. 1716-1718, Mar 1988.

[131] J. L. Butler, S. C. Butler, and A. E. Clark, "Unidirectional magnetostrictive piezoelectric-hybrid transducer," *Journal of the Acoustical Society of America,* vol. 88, pp. 7-11, Jul 1990.

[132] S. C. Butler and F. A. Tito, "A broadband hybrid magnetostrictive/piezoelectric transducer array," in *OCEANS 2000 MTS/IEEE Conference and Exhibition*, Providence, 2000, pp. 1469-1475.

[133] J. Hossack, Y. Gorfu, and G. Hayward, "The modeling and design of composite piezoelectric arrays," in *IEEE Ultrasonics Symposium*, Montreal, 1989, pp. 793-796.

[134] J. A. Hossack and G. Hayward, "Finite-element analysis of 1-3 composite transducers," *IEEE Transactions on Ultrasonics Ferroelectrics and Frequency Control,* vol. 38, pp. 618-629, Nov 1991.

[135] G. Hayward and J. Bennett, "Assessing the influence of pillar aspect ratio on the behavior of 1-3 connectivity composite transducers," *IEEE Transactions on Ultrasonics Ferroelectrics and Frequency Control,* vol. 43, pp. 98-108, Jan 1996.

[136] G. Hayward and J. Hyslop, "Determination of Lamb wave dispersion data in lossy anisotropic plates using time domain finite element analysis. Part II: Application to 2-2 and 1-3 piezoelectric composite transducer arrays," *IEEE Transactions on Ultrasonics Ferroelectrics and Frequency Control,* vol. 53, pp. 449-455, Feb 2006.

[137] J. Bennet and G. Hayward, "Design of monolithic 1-3 piezocomposite ultrasonic arrays using finite element modelling," in *IEEE Ultrasonics Symposium*, Seattle, 1995, pp. 925-928 vol.2.

[138] J. Bennett, R. Hamilton, and G. Hayward, "Finite element modelling of 1-3 composite transducers for underwater applications," in *IEEE Ultrasonics Symposium*, Baltimore, 1993, pp. 1113-1116 vol.2.

[139] E. W. Kellogg, "Design of non-distorting power amplifiers," *Transactions of the American Institute of Electrical Engineers,* vol. 44, pp. 490-498, 1925.

[140] I. Aoki, S. D. Kee, D. B. Rutledge, and A. Hajimiri, "Fully integrated CMOS power amplifier design using the distributed active-transformer architecture," *Ieee Journal of Solid-State Circuits,* vol. 37, pp. 371-383, Mar 2002.

[141] S. I. Ohashi, "Multi channel PWM power invertors integrated in a switching power supply circuit," *IEEE Transactions on Consumer Electronics,* vol. 35, pp. 43-49, 1989.

[142] S. I. Nikitenko, C. Le Naour, and P. Moisy, "Comparative study of sonochemical reactors with different geometry using thermal and chemical probes," *Ultrasonics Sonochemistry,* vol. 14, pp. 330-336, Mar 2007.

[143] O. Dahlem, J. Reisse, and V. Halloin, "The radially vibrating horn: A scaling-up possibility for sonochemical reactions," *Chemical Engineering Science,* vol. 54, pp. 2829-2838, Jul 1999.

[144] M. Lucas, A. Gachagan, and A. Cardoni, "Research applications and opportunities in power ultrasonics," *Proceedings of the Institution of Mechanical Engineers Part C-Journal of Mechanical Engineering Science,* vol. 223, pp. 2949-2965, Dec 2009.

[145] M. Romdhane, A. Gadri, F. Contamine, C. Gourdon, and G. Casamatta, "Experimental study of the ultrasound attenuation in chemical reactors," *Ultrasonics Sonochemistry,* vol. 4, pp. 235-243, Jul 1997.

[146] A. V. Prabhu, P. R. Gogate, and A. B. Pandit, "Optimization of multiple-frequency sonochemical reactors," *Chemical Engineering Science,* vol. 59, pp. 4991-4998, Nov-Dec 2004.

[147] V. S. Moholkar, "Mechanistic optimization of a dual frequency sonochemical reactor," *Chemical Engineering Science,* vol. 64, pp. 5255-5267, Dec 2009.

[148] T. Mutasa, A. Gachagan, A. Nordon, and R. L. O'Leary, "Ultrasonic wave propagation in cylindrical vessels and implications for ultrasonic reactor design," in *IEEE Ultrasonics Symposium*, San diego, 2010, pp. 1470-1473.

[149] A. Blana, F. J. Murat, B. Walter, S. Thuroff, W. F. Wieland, C. Chaussy*, et al.*, "First analysis of the long-term results with transrectal HIFU in patients with localised prostate cancer," *European Urology,* vol. 53, pp. 1194-1203, Jun 2008.

[150] E. A. Stewart, J. Rabinovici, C. M. C. Tempany, Y. Inbar, J. Hindley, L. Regan*, et al.*, "Clinical outcomes of focused ultrasound surgery for the treatment of uterine fibroids," *Fertility and Sterility,* vol. 85, pp. 22-29, Jan 2006.

[151] I. H. Rivens, R. L. Clarke, and G. R. terHaar, "Design of focused ultrasound surgery transducers," *IEEE Transactions on Ultrasonics Ferroelectrics and Frequency Control,* vol. 43, pp. 1023-1031, Nov 1996.

[152] W. S. Chen, C. C. Shen, J. C. Wang, C. T. Ko, H. L. Liu, M. C. Ho*, et al.*, "Single-element ultrasound transducer for combined vessel localization and ablation,"

IEEE Transactions on Ultrasonics Ferroelectrics and Frequency Control, vol. 58, pp. 766-775, Apr 2011.

[153] A. Gachagan, P. Reynolds, G. Hayward, and A. McNab, "Construction and evaluation of a new generation of flexible ultrasonic transducers," presented at the IEEE Ultrasonics Symposium, San Antonio, 1996.

[154] J. A. Ketterling, "Acoustic field of a wedge-shaped section of a spherical cap transducer," *The Journal of the Acoustical Society of America,* vol. 114, pp. 3065-3075, 2003.

[155] H. Azhari, "Acoustic lenses and mirrors " in *Basics of Biomedical Ultrasound for Engineers* ed: Wiley-IEEE Press 2010 pp. 133-152.

[156] K. Itsumi, Y. Hosono, N. Yamamoto, and Y. Yamashita, "Low acoustic attenuation silicone rubber lens for medical ultrasonic array probe," *IEEE Transactions on Ultrasonics Ferroelectrics and Frequency Control,* vol. 56, pp. 870-874, Apr 2009.

[157] W. L. Nastuk, *Physical Techniques in Biological Research: Special methods*: Academic Press, 1962.

[158] W. A. Smith, "The application of 1-3 piezocomposites in acoustic transducers," in *IEEE 7th International Symposium on Applications of Ferroelectrics*, Urbana-Champaign, 1990, pp. 145-152.

[159] W. A. Smith and B. A. Auld, "Modeling 1-3 composite piezoelectrics: thickness-mode oscillations," *Ultrasonics, Ferroelectrics and Frequency Control, IEEE Transactions on,* vol. 38, pp. 40-47, 1991.

[160] S. Sanchez and F. R. M. deEspinosa, "Modeling (2-2) piezocomposites partially sliced in the polymer phase," *IEEE Transactions on Ultrasonics Ferroelectrics and Frequency Control,* vol. 44, pp. 287-296, Mar 1997.

[161] S. Yongan and X. Qiang, "The piezoelectric coupling of 2-2 composite transducers," in *IEEE Ultrasonics Symposium*, Seattle, 1995, pp. 929-932 vol.2.

[162] D. Y. Xu, X. Cheng, S. F. Huang, and M. H. Jiang, "Electromechanical properties of 2-2 cement based piezoelectric composite," *Current Applied Physics,* vol. 9, pp. 816-819, Jul 2009.

[163] X. C. Geng and Q. M. Zhang, "Evaluation of piezocomposites for ultrasonic transducer applications - Influence of the unit cell dimensions and the properties of constituents on the performance of 2-2 piezocomposites," *IEEE Transactions on Ultrasonics Ferroelectrics and Frequency Control,* vol. 44, pp. 857-872, Jul 1997.

[164] R. Holland, "Representation of dielectric, elastic, and piezoelectric losses by complex coefficients," *IEEE Transactions on Sonics and Ultrasonics,* vol. 14, pp. 18-20, 1967.

[165] X. C. Geng and Q. M. Zhang, "Resonance modes and losses in 1-3 piezocomposites for ultrasonic transducer applications," *Journal of Applied Physics,* vol. 85, pp. 1342-1350, Feb 1999.

[166] R. L. O'Leary, G. Hayward, and V. Murray, "Finite element technique for the assessment of 3-1 and "Super 1-3" connectivity piezoelectric composite transducers," *IEEE Transactions on Ultrasonics Ferroelectrics and Frequency Control,* vol. 54, pp. 2024-2035, Oct 2007.

[167] R. L. O'Leary and G. Hayward, "A theoretical and experimental investigation into multilayered piezoelectric composite transducers," in *IEEE Ultrasonics Symposium*, Munich, 2002, pp. 1135-1138.

[168] W. A. Smith, "The role of piezocomposites in ultrasonic transducers," in *IEEE Ultrasonics Symposium*, Montreal, 1989, pp. 755-766 vol.2.

[169] A. J. Mulholland, N. Ramadas, R. L. O'Leary, A. C. S. Parr, G. Hayward, A. Troge*, et al.*, "Enhancing the performance of piezoelectric ultrasound transducers by the use of multiple matching layers," *IMA Journal of Applied Mathematics,* vol. 73, pp. 936-949, Dec 2008.

[170] J. Bennett, R. Hamilton, and G. Hayward, "Finite element modelling of 1-3 composite transducers for underwater applications," in *Ultrasonics Symposium, 1993. Proceedings., IEEE 1993*, 1993, pp. 1113-1116 vol.2.

[171] C. S. Desilets, J. D. Fraser, and G. S. Kino, "The design of efficient broad-band piezoelectric transducers," *IEEE Transactions on Sonics and Ultrasonics,* vol. 25, pp. 115-125, 1978.

[172] M. T. Buchanan and K. Hynynen, "Design and experimental evaluation of an intracavitary ultrasound phased array system for hyperthermia," *IEEE Transactions on Biomedical Engineering,* vol. 41, pp. 1178-1187, 1994.

[173] J. P. Dohuu and P. Hartemann, "Annular array transducer for deep acoustic hyperthermia," *IEEE Transactions on Sonics and Ultrasonics,* vol. 29, pp. 195-195, 1982.

[174] E. S. Ebbini and C. A. Cain, "A spherical-section ultrasound phased-array applicator for deep localized hyperthermia," *IEEE Transactions on Biomedical Engineering,* vol. 38, pp. 634-643, Jul 1991.

[175] S. A. Goss, L. A. Frizzell, J. T. Kouzmanoff, J. M. Barich, and J. M. Yang, "Sparse random ultrasound phased array for focal surgery," *IEEE Transactions on Ultrasonics, Ferroelectrics and Frequency Control,* vol. 43, pp. 1111-1121, 1996.

[176] C. A. Cain and S. Umemura, "Concentric-ring and sector-vortex phased-array applicators for ultrasound hyperthermia," *IEEE Transactions on Microwave Theory and Techniques,* vol. 34, pp. 542-551, May 1986.

[177] J. H. Song and K. Hynynen, "Feasibility of using lteral node coupling method for a large scale ultrasound phased array for noninvasive transcranial therapy," *IEEE Transactions on Biomedical Engineering,* vol. 57, pp. 124-133, Jan 2010.

[178] K. Hynynen, G. T. Clement, N. McDannold, N. Vykhodtseva, R. King, P. J. White, *et al.*, "500-element ultrasound phased array system for noninvasive focal surgery of the brain: A preliminary rabbit study with ex vivo human skulls," *Magnetic Resonance in Medicine,* vol. 52, pp. 100-107, Jul 2004.

[179] D. R. Daum, M. T. Buchanan, T. Fjield, and K. Hynynen, "Design and evaluation of a feedback based phased array system for ultrasound surgery," *IEEE Transactions on Ultrasonics Ferroelectrics and Frequency Control,* vol. 45, pp. 431-438, Mar 1998.

[180] A. Lovejoy, P. Pedrick, A. Doran, T. A. Delchar, J. A. Mills, and A. Stamm, "A novel 8-bit ultrasound phased-array controller for hyperthermia applications," *Ultrasonics,* vol. 33, pp. 69-73, Jan 1995.

[181] M. M. El-Desouki and K. Hynynen, "Driving circuitry for focused ultrasound noninvasive surgery and drug delivery applications," *Sensors,* vol. 11, pp. 539-556, Jan 2011.

[182] Y. Y. Botros, J. L. Volakis, P. VanBaren, and E. S. Ebbini, "A hybrid computational model for ultrasound phased-array heating in presence of strongly scattering obstacles," *IEEE Transactions on Biomedical Engineering,* vol. 44, pp. 1039-1050, Nov 1997.

[183] D. H. Li, G. F. Shen, J. F. Bai, and Y. Z. Chen, "Focus shift and phase correction in soft tissues during focused ultrasound surgery," *IEEE Transactions on Biomedical Engineering,* vol. 58, pp. 1621-1628, Jun 2011.

[184] E. S. Ebbini, "Multiple-focus ultrasound phased-array patern synthesis - optimal driving-signal distributions for hyperthermia," *IEEE Transactions on Ultrasonics Ferroelectrics and Frequency Control,* vol. 36, pp. 540-548, Sep 1989.

[185] H. L. Liu, N. McDannold, and K. Hynynen, "Focal beam distortion and treatment planning in abdominal focused ultrasound surgery," in *Therapeutic Ultrasound*. vol. 829, G. T. Clement, N. J. McDannold, and K. Hynynen, Eds., ed Melville: Amer Inst Physics, 2006, pp. 191-195.

[186] J. Sun and K. Hynynen, "Focusing of therapeutic ultrasound through a human skull: A numerical study," *Journal of the Acoustical Society of America,* vol. 104, pp. 1705-1715, Sep 1998.

[187] J. Gatcau, L. Marsac, M. Pernot, J. F. Aubry, M. Tanter, and M. Fink, "Transcranial ultrasonic therapy based on time reversal of acoustically induced cavitation bubble signature," *IEEE Transactions on Biomedical Engineering,* vol. 57, pp. 134-144, Jan 2010.

[188] M. Pernot, G. Montaldo, M. Tanter, and M. Fink, ""Ultrasonic stars" for time-reversal focusing using induced cavitation bubbles," *Applied Physics Letters,* vol. 88, p. 3, Jan 2006.

[189] O. Couture, J. F. Aubry, M. Tanter, and M. Fink, "Time-reversal focusing of therapeutic ultrasound on targeted microbubbles," *Applied Physics Letters,* vol. 94, p. 3, Apr 2009.

[190] F. Dupenloup, J. Y. Chapelon, D. Cathignol, and O. Sapozhnikov, "The use of broadband signals to reduce grating lobe effects in HIFU tissue ablation," in *IEEE Ultrasonics Symposium*, Cannes, 1994, pp. 1865-1868.

[191] Wikipedia. (2014, 7-January). *High-intensity focused ultrasound --- Wikipedia{,} The Free Encyclopedia*. Available: http://en.wikipedia.org/w/index.php?title=High-intensity_focused_ultrasound&oldid=589558476

[192] M. R. Bailey, V. A. Khokhlova, O. A. Sapozhnikov, S. G. Kargl, and L. A. Crum, "Physical mechanisms of the therapeutic effect of ultrasound (a review)," *Acoustical Physics,* vol. 49, pp. 369-388, Jul 2003.

[193] S. Vaezy, R. Martin, G. Keilman, P. Kaczkowski, E. Chi, E. Yazaji*, et al.*, "Control of splenic bleeding by using high intensity ultrasound," *Journal of Trauma-Injury Infection and Critical Care,* vol. 47, pp. 521-525, Sep 1999.

[194] I. H. Rivens, I. J. Rowland, M. Denbow, N. M. Fisk, G. R. ter Haar, and M. O. Leach, "Vascular occlusion using focused ultrasound surgery for use in fetal medicine," *European journal of ultrasound : official journal of the European Federation of Societies for Ultrasound in Medicine and Biology,* vol. 9, pp. 89-97, 1999.

[195] K. Hynynen, V. Colucci, A. Chung, and F. Jolesz, "Noninvasive arterial occlusion using MRI-guided focused ultrasound," *Ultrasound in Medicine and Biology,* vol. 22, pp. 1071-1077, 1996.

[196] X. Wang, H. R. Chen, Y. Chen, M. Ma, K. Zhang, F. Q. Li*, et al.*, "Perfluorohexane-encapsulated mesoporous silica nanocapsules as enhancement agents for highly efficient high intensity focused ultrasound (HIFU)," *Advanced Materials,* vol. 24, p. 785, Feb 2012.

[197] C. D. Arvanitis, M. Bazan-Peregrino, B. Rifai, L. W. Seymour, and C. C. Coussios, "Caitation-enhanced extravasation for drug delivery," *Ultrasound in Medicine and Biology,* vol. 37, pp. 1838-1852, Nov 2011.

[198] H. Cao, M. X. Wan, Y. Z. Qiao, S. S. Zhang, and R. X. Li, "Spatial distribution of sonoluminescence and sonochemiluminescence generated by cavitation bubbles in 1.2 MHz focused ultrasound field," *Ultrasonics Sonochemistry,* vol. 19, pp. 257-263, Mar 2012.

[199] L. Hallez, F. Touyeras, J. Y. Hihn, and J. Klima, "Energetic balance in an ultrasonic reactor using focused or flat high frequency transducers," *Ultrasonics Sonochemistry,* vol. 14, pp. 739-749, Sep 2007.

[200] D. Lopez-Ferrer, J. L. Capelo, and J. Vazquez, "Ultra fast trypsin digestion of proteins by high intensity focused ultrasound," *Journal of Proteome Research,* vol. 4, pp. 1569-1574, Sep-Oct 2005.

[201] S. Catarino, J. L. Capelo, A. S. Curvelo-Garcia, and R. B. De Sousa, "Evaluation of contaminant elements in portuguese wines and original musts by high intensity focused ultrasound combined with inductively coupled plasma mass spectrometry," *Journal International Des Sciences De La Vigne Et Du Vin,* vol. 40, pp. 91-100, Apr-Jun 2006.

[202] R. J. Carreira, F. M. Cordeiro, A. J. Moro, M. G. Rivas, R. Rial-Otero, E. M. Gaspar*, et al.*, "New findings for in-gel digestion accelerated by high-intensity focused ultrasound for protein identification by matrix-assisted laser desorption ionization time-of-flight mass spectrometry," *Journal of Chromatography A,* vol. 1153, pp. 291-299, Jun 2007.

[203] A. Gachagan, A. McNab, R. Blindt, M. Patrick, and C. Marriott, "A high power ultrasonic array based test cell," *Ultrasonics,* vol. 42, pp. 57-68, Apr 2004.

[204] Y. Asakura, T. Nishida, T. Matsuoka, and S. Koda, "Effects of ultrasonic frequency and liquid height on sonochemical efficiency of large-scale sonochemical reactors," *Ultrasonics Sonochemistry,* vol. 15, pp. 244-250, Mar 2008.

[205] D. N. Stephens, D. E. Kruse, A. S. Ergun, S. Barnes, X. M. Lu, and K. W. Ferrara, "Efficient array design for sonotherapy," *Physics in Medicine and Biology,* vol. 53, pp. 3943-3969, Jul 2008.

[206] J. E. Hyslop, J. T. Bennett, and G. Hayward, "An investigation into the design of high frequency two-dimensional arrays for ultrasonic imaging," in *IEEE Ultrasonics Symposium*, Cannes, 1994, pp. 1515-1518 vol.3.

[207] S.-C. Wooh and Y. Shi, "Influence of phased array element size on beam steering behavior," *Ultrasonics,* vol. 36, pp. 737-749, 4// 1998.

[208] N. N. Abboud, G. L. Wojcik, D. K. Vaughan, J. Mould, D. J. Powell, and L. Nikodym, "Finite element modeling for ultrasonic transducers," in *Ultrasonic Transducer Engineering: Medical Imaging 1998*. vol. 3341, K. K. Shung, Ed., ed Bellingham: Spie-Int Soc Optical Engineering, 1998, pp. 19-42.

[209] R. L. O'Leary, A. C. S. Parr, and G. Hayward, "Multilayered piezoelectric composite transducers," in *Ultrasonics, 2003 IEEE Symposium on*, 2003, pp. 1306-1309 Vol.2.

[210] A. Cochran, G. Hayward, and V. Murray, "Multilayer piezocomposite ultrasonic transducers operating below 50 kHz," in *Ultrasonics Symposium, 1999. Proceedings. 1999 IEEE*, 1999, pp. 953-956 vol.2.

[211] R. L. O'Leary and G. Hayward, "A theoretical and experimental investigation into multilayered piezoelectric composite transducers," in *Ultrasonics Symposium, 2002. Proceedings. 2002 IEEE*, 2002, pp. 1135-1138 vol.2.

[212] J. E. Hyslop and G. Hayward, "The study of Lamb wave dispersion in piezoelectric plate transducers," in *Ultrasonics Symposium, 1999. Proceedings. 1999 IEEE*, 1999, pp. 577-580 vol.1.

[213] J. Bennett and G. Hayward, "Design of 1-3 piezocomposite hydrophones using finite element analysis," *IEEE Transactions on Ultrasonics Ferroelectrics and Frequency Control,* vol. 44, pp. 565-574, May 1997.

[214] G. Hayward and J. A. Hossack, "Unidimensional modeling of 1-3 composite transducer," *Journal of the Acoustical Society of America,* vol. 88, pp. 599-608, Aug 1990.

[215] N. Lamberti, F. Montero de Espinosa, N. Perez, H. Gomez, and C. Negreira, "Optimization of acoustic matching layers for piezocomposite transducers," in *IEEE Ultrasonics Symposium*, San Juan-Puerto Rico, 2000, pp. 1105-1108 vol.2.

[216] A. Shoh, "Industrial applications of ultrasound -a review I. High-power ultrasound," *IEEE TRANSACTIONS ON SONICS AND ULTRASONICS,* pp. 60-71, 1975.

Appendix A

Epoxy material data sheet

Calcined Alumina 70% by wgt with Hard set (Vantico HY1300/CY1301) 13.133mm

IN WATER	FREQUENCY (MHz)		
	0.5	1.0	2.25
Vl(m/s)	3014.6	2999	2921.7
Vs(m/s)	1684.1	1686.1	1662.6
Density(kg/m^3)	2308	2308	2308
Poisson Ratio	0.2732	0.2689	0.2606
Young's Modulus E ($m \cdot s^{-2} kg$)	1.6668E+10	1.6652E+10	1.6084E+10
Impedance Z ($kg \cdot m^2 s^{-1}$)	6.9577E+06	6.9217E+06	6.7433E+06
Bulk Modulus B ($m \cdot s^{-2}.kg$)	1.2247E+10	1.2010E+10	1.1195E+10
Shear Modulus G ($m \cdot s^{-2} kg$)	6.5459E+09	6.5615E+09	6.3799E+09
c11	2.0975E+10	2.0758E+10	1.9702E+10
c44	6.5460E+09	6.5610E+09	6.3800E+09
s11	6.0000E-11	6.0100E-11	6.7200E-11
s44	1.5280E-10	1.5240E-10	1.5670E-10
Longitudinal Attenuation (dB/m)	182	321	678
Shear Attenuation (dB/m)		556	1364

Calcined Alumina 73% by wgt with Hard set (Vantico HY1300/CY1301) 13.133mm

IN WATER	FREQUENCY (MHz)
	0.5
Vl(m/s)	**2920.1**
Vs(m/s)	**1552.1**
Density(kg/m^3)	2170
Poisson Ratio	0.3031
Young's Modulus E ($m \cdot s^{-2}kg$)	1.3620E+10
Impedance Z ($kg \cdot m^2 s^{-1}$)	6.3366E+06
Bulk Modulus B ($m \cdot s^{-2}.kg$)	1.1530E+10
Shear Modulus G ($m \cdot s^{-2}kg$)	5.2280E+09
c11	1.8504E+10
c44	5.2280E+09
s11	7.3400E-11
s44	1.9130E-10
Longitudinal Attenuation (dB/m)	135
Shear Attenuation (dB/m)	

Medium Set (Vantico HY956EN/CY221) (3.103mm)

IN WATER	FREQUENCY (MHz)		
	0.5	1.0	2.25
Vl(m/s)	2364.1	2451.5	2440.9
Vs(m/s)	1064.6	1109.9	1084.5
Density(kg/m^3)	1134	1134	1134
Poisson Ratio	0.3728	0.3711	0.377
Young's Modulus E ($m \cdot s^{-2}kg$)	3.5288E+09	3.8307E+09	3.6732E+09
Impedance Z ($kg \cdot m^2 s^{-1}$)	2.6809E+06	2.7800E+06	2.7680E+06
Bulk Modulus B ($m \cdot s^{-2}.kg$)	4.6242E+09	4.9526E+09	4.9780E+09
Shear Modulus G ($m \cdot s^{-2}kg$)	1.2852E+09	1.3969E+09	1.3337E+09
c11	6.3379E+09	6.8152E+09	6.7564E+09
c44	1.2852E+09	1.3969E+09	1.3337E+09
s11	2.8340E-10	2.6110E-10	2.7220E-10
s44	7.7810E-10	7.1580E-10	7.4980E-10
Longitudinal Attenuation (dB/m)	208	895	1711
Shear Attenuation (dB/m)	2319	4108	8147

Soft Set (Vantico HY956/CY208) (3.692mm)

IN LOW VELOCITY OIL	FREQUENCY (MHz)		
	0.5	1.0	2.25
Vl(m/s)	2000.8	1989.2	1998.1
Vs(m/s)	747.8	762	779.8
Density(kg/m^3)	1165	1165	1165
Poisson Ratio	0.4188	0.414	0.4102
Young's Modulus E ($m \cdot s^{-2}kg$)	1.8486E+09	1.9130E+09	1.9980E+09
Impedance Z ($kg \cdot m^2 s^{-1}$)	2.3309E+06	2.3174E+06	2.3278E+06
Bulk Modulus B ($m \cdot s^{-2}.kg$)	3.7951E+09	3.7079E+09	3.7066E+09
Shear Modulus G ($m \cdot s^{-2}kg$)	6.5147E+08	6.7645E+08	7.0842E+08
c11	4.6637E+09	4.6098E+09	4.6512E+09
c44	6.5150E+08	6.7650E+08	7.0840E+08
s11	5.4100E-10	5.2300E-10	5.0100E-10
s44	1.5350E-09	1.4780E-09	1.4120E-09
Longitudinal Attenuation (dB/m)	825	1633	1694
Shear Attenuation (dB/m)	6063	11526	12638

Piezoelectric material data sheet

PZ26/PZT4D

Symbol	Unit	Pz26	Pz26, FEM use
$e_{1,r}^{s}$		1.19E+03	1.31E+03
$e_{3,r}^{s}$		1.33E+03	1.08E+03
$e_{1,r}^{S}$		8.28E+02	9.29E+02
$e_{3,r}^{S}$		7.00E+02	5.18E+02
tan d ($_3^s$)		0.003	
T_C >	ºC	330	
k_p		0.568	-0.575
k_t		0.471	0.525
k_{31}		0.327	-0.310
k_{33}		0.684	0.707
k_{15}		0.553	0.538
d_{31}	C/N	-1.28E-10	-1.06E-10
d_{33}	C/N	3.28E-10	2.77E-10
d_{15}	C/N	3.27E-10	3.50E-10
d_h	C/N	7.24E-11	
g_{31}	V m/N	-0.0109	-0.0111
g_{33}	V m/N	0.0280	0.0289
g_{15}	V m/N	0.0389	0.0303
e_{31}	C/m^2	-2.80	-5.48
e_{33}	C/m^2	14.7	13.6
e_{15}	C/m^2	9.86	9.55
h_{31}	V/m	-4.52E+08	-1.20E+09
h_{33}	V/m	2.37E+09	2.97E+09
h_{15}	V/m	1.34E+09	1.16E+09
N_p	m/s	2209.94	

Symbol	Unit	Pz26	Pz26, FEM use
N_t	m/s	2038	
N_{31}	m/s	1500	
N_{33}	m/s	1800	
N_{15}	m/s	1018	
$Q_{m,p}{}^E$		2.7E+03	
$Q_{m,t}{}^E$		3.3E+03	
r	kg/m^3	7.70E+03	7.65E+03
$n_{12}{}^E$		0.334	0.420
$s_{11}{}^E$	m^2/N	1.30E-11	1.22E-11
$s_{12}{}^E$	m^2/N	-4.35E-12	-5.13E-12
$s_{13}{}^E$	m^2/N	-7.05E-12	-5.13E-12
$s_{33}{}^E$	m^2/N	1.96E-11	1.60E-11
$s_{44}{}^E = s_{55}{}^E$	m^2/N	3.32E-11	3.67E-11
s_{66}	m^2/N	3.47E-11	
$s_{11}{}^D$	m^2/N	1.16E-11	1.11E-11
$s_{12}{}^D$	m^2/N	-5.74E-12	-6.31E-12
$s_{13}{}^D$	m^2/N	-3.47E-12	-6.31E-12
$s_{33}{}^D$	m^2/N	1.05E-11	8.00E-12
$s_{44}{}^D = s_{55}{}^D$	m^2/N	2.31E-11	8.80E-13
$c_{11}{}^E$	N/m^2	1.68E+11	1.55E+11
$c_{12}{}^E$	N/m^2	1.10E+11	9.41E+10
$c_{13}{}^E$	N/m^2	9.99E+10	7.99E+10
$c_{33}{}^E$	N/m^2	1.23E+11	1.10E+11
$c_{44}{}^E = c_{55}{}^E$	N/m^2	3.01E+10	2.73E+10
c_{66}	N/m^2	2.88E+10	
$c_{11}{}^D$	N/m^2	1.69E+11	1.62E+11
$c_{12}{}^D$	N/m^2	1.12E+11	1.01E+11
$c_{13}{}^D$	N/m^2	9.33E+10	8.64E+10

Symbol	Unit	Pz26	Pz26, FEM use
c_{33}^{D}	N/m^2	1.58E+11	1.51E+11
$c_{44}^{D} = c_{55}^{D}$	N/m^2	4.34E+10	1.14E+12
Y_{11}^{E}	GPa	7.69E+01	8.18E+01
Y_{33}^{E}	GPa	5.09E+01	6.25E+01
Y_{11}^{D}	GPa	8.62E+01	9.05E+01
Y_{33}^{D}	GPa	9.56E+01	1.25E+02

Appendix B

Piezocomposite housing dimension specification

Upper part of transducer case

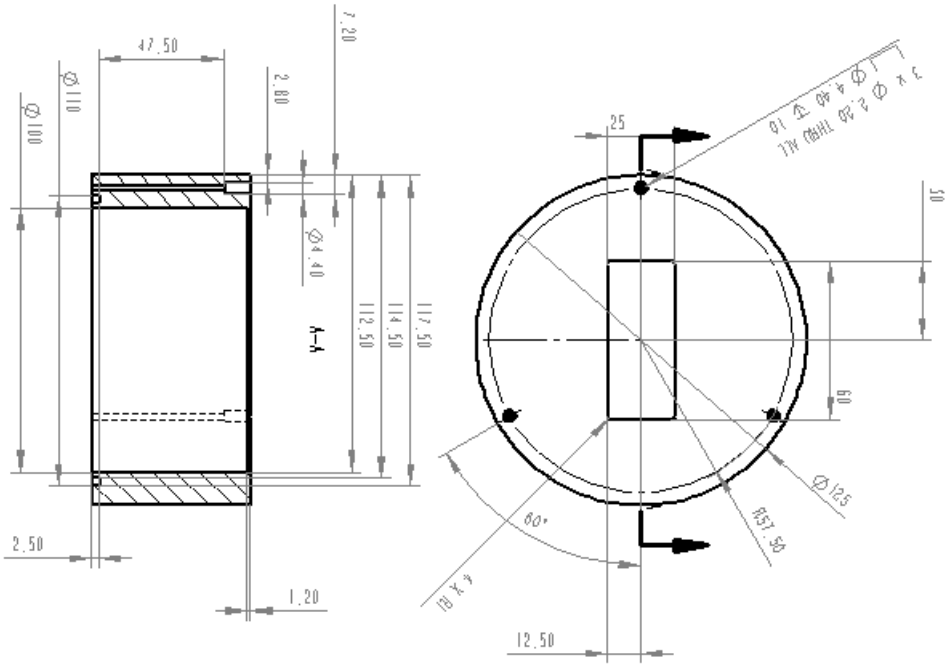

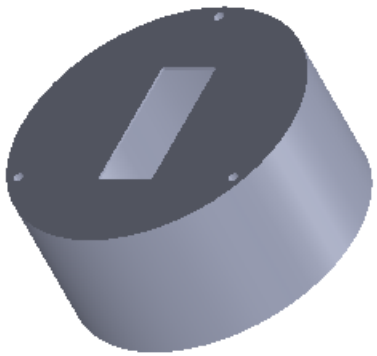

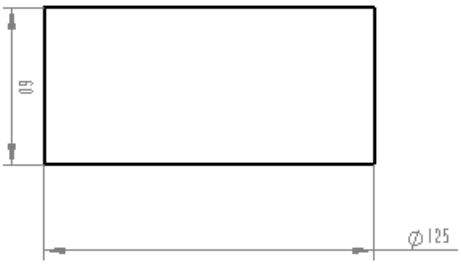

Lower part of transducer case